

**Molecular mechanisms of endomembrane trafficking in
*Arabidopsis thaliana***

by

Mina Vasileva

October, 2019

*A thesis presented to the
Graduate School
of the
Institute of Science and Technology Austria, Klosterneuburg, Austria
in partial fulfillment of the requirements
for the degree
of
Doctor of Philosophy*



Institute of Science and Technology

The dissertation of Mina Vasileva, titled *Molecular mechanisms of endomembrane trafficking in Arabidopsis thaliana*, is approved by:

Supervisor: Jiri Friml, IST Austria, Klosterneuburg, Austria

Signature: _____

Committee Member: Eva Benkova, IST Austria, Klosterneuburg, Austria

Signature: _____

Committee Member: Christian Luschnig, BOKU, Vienna, Austria

Signature: _____

Exam Chair: Florian Schur, IST Austria, Klosterneuburg, Austria

Signature: _____

signed page is on file

IST Austria Thesis, ISSN: 2663-337X

I hereby declare that this dissertation is my own work and that it does not contain other people's work without this being so stated; this thesis does not contain my previous work without this being stated, and the bibliography contains all the literature that I used in writing the dissertation.

I declare that this is a true copy of my thesis, including any final revisions, as approved by my thesis committee, and that this thesis has not been submitted for a higher degree to any other university or institution.

I certify that any republication of materials presented in this thesis has been approved by the relevant publishers and co-authors.

Signature: _____

Mina Vasileva

December 12, 2019

signed page is on file

Abstract

The development and growth of *Arabidopsis thaliana* is regulated by a combination of genetic programming and also by the environmental influences. An important role in these processes play the phytohormones and among them, auxin is crucial as it controls many important functions. It is transported through the whole plant body by creating local and temporal concentration maxima and minima, which have an impact on the cell status, tissue and organ identity. Auxin has the property to undergo a directional and finely regulated cell-to-cell transport, which is enabled by the transport proteins, localized on the plasma membrane. An important role in this process have the PIN auxin efflux proteins, which have an asymmetric/polar subcellular localization and determine the directionality of the auxin transport. During the last years, there were significant advances in understanding how the trafficking molecular machineries function, including studies on molecular interactions, function, subcellular localization and intracellular distribution. However, there is still a lack of detailed characterization on the steps of endocytosis, exocytosis, endocytic recycling and degradation. Due to this fact, I focused on the identification of novel trafficking factors and better characterization of the intracellular trafficking pathways. My PhD thesis consists of an introductory chapter, three experimental chapters, a chapter containing general discussion, conclusions and perspectives and also an appendix chapter with published collaborative papers.

The **first chapter** is separated in two different parts: I start by a general introduction to auxin biology and then I introduce the trafficking pathways in the model plant *Arabidopsis thaliana*. Then, I explain also the phosphorylation-signals for polar targeting and also the roles of the phytohormone strigolactone.

The **second chapter** includes the characterization of *bar1/sacsin* mutant, which was identified in a forward genetic screen for novel trafficking components in *Arabidopsis thaliana*, where by the implementation of an EMS-treated *pPIN1::PIN1-GFP* marker line and by using the established inhibitor of ARF-GEFs, Brefeldin A (BFA) as a tool to study trafficking processes, we identified a novel factor, which is mediating the adaptation of the plant cell to ARF-GEF inhibition. The mutation is in a previously uncharacterized gene, encoding a very big protein that we, based on its homologies, called SACSIN with domains suggesting roles as a molecular

chaperon or as a component of the ubiquitin-proteasome system. Our physiology and imaging studies revealed that SACSIN is a crucial plant cell component of the adaptation to the ARF-GEF inhibition.

The **third chapter** includes six subchapters, where I focus on the role of the phytohormone strigolactone, which interferes with auxin feedback on PIN internalization. Strigolactone moderates the polar auxin transport by increasing the internalization of the PIN auxin efflux carriers, which reduces the canalization related growth responses. In addition, I also studied the role of phosphorylation in the strigolactone regulation of auxin feedback on PIN internalization. In this chapter I also present my results on the MAX2-dependence of strigolactone-mediated root growth inhibition and I also share my results on the auxin metabolomics profiling after application of GR24.

In the **fourth chapter** I studied the effect of two small molecules ES-9 and ES9-17, which were identified from a collection of small molecules with the property to impair the clathrin-mediated endocytosis.

In the **fifth chapter**, I discuss all my observations and experimental findings and suggest alternative hypothesis to interpret my results.

In the **appendix** there are three collaborative published projects. In the first, I participated in the characterization of the role of ES9 as a small molecule, which is inhibitor of clathrin-mediated endocytosis in different model organisms. In the second paper, I contributed to the characterization of another small molecule ES9-17, which is a non-protonophoric analog of ES9 and also impairs the clathrin-mediated endocytosis not only in plant cells, but also in mammalian HeLa cells. Last but not least, I also attach another paper, where I tried to establish the grafting method as a technique in our lab to study canalization related processes.

Acknowledgments

Life is a wonderful mixture of coincidences and luck and it happened to me that I had the opportunity to become a member of Friml group and to join the PhD program at IST. In this section, I would like to acknowledge the people, who helped me and supported me during my time and “journey” at IST.

First of all, I would like to thank Jiří Friml for giving me the opportunity to be a member of his group and also for his support and guidance during my PhD. I learned a lot about science and also how to present in the best possible way. Then, I would also like to acknowledge my internal and external committee members for their time and efforts to read, to evaluate and to suggest improvements for my PhD thesis - Jiří Friml, Eva Benkova and Christian Luschnig, thank you very much.

Next, I appreciate the help of Maciek for all of his ideas, his careful guidance, for the inspiration he gave me and for his passion on science. I would also like to thank to the people, who were involved in the project – Yuliya, Mike, Petr and Lukasz, who shared their results, crosses and observations on the SACSIN project.

In addition, I would like to thank all of the group members, who helped me with their knowledge on different methods and techniques, for the nice working atmosphere and collegial environment, for the collaboration, criticism and suggestions. There are a couple of group members, who were next to me in good and bad days – Lanxin, Huibin, Madhu, Hana, Zuzana and Moni, thank you all. A special person, who I would also like to acknowledge is Jenny Russinova, who offered me collaboration projects and who helped me to publish my results and observations in high impact journals.

I also appreciate the help and support of the IST facilities – the Bioimaging facility, the media kitchen, the plant facility and all of the campus services, who made my PhD easier.

By joining IST I found a strong interdisciplinary, international research environment with some of the most interesting, clever and friendly scientists I ever met. Thanks to Stephan, Kristof, Feyza, Karla and Lenka for offering me their friendship, for giving me confidence and for helping me to look on the bright side of life.

Being abroad is a challenge and it is connected with missing your family and relatives. During my academic development I was dedicating every passed exam and every success to them, which was a small return for the time and moments we could have spent together by just

being on the same geographical location. It is a wonderful feeling to know that you are unconditionally loved and supported: from the bottom of my heart I say thanks to my parents – Valya and Krasimir and to my brother Boris. Thanks for giving me love, recognition, courage, support, example in life, for being always there for me, for making me smile, for helping me to keep going, for waiting for me and my news.

Thanks!

About the Author

Mina Vasileva completed a BSc in Molecular Biotechnology at the Dresden University of Technology and an MSc in Molecular Biology at the University of Vienna. She did her Master thesis at the Institute for Pharmacology and Physiology to the Medical University of Vienna where she worked on the project “Chemical derivatization and cellular imaging of immunosuppressive peptides” under the supervision of Dr. Christian Gruber and Dr. Gernot Schabbauer. Then she joined IST Austria in November 2014 as an intern in Friml group and in 2015 she became a member of the Graduate School of IST Austria, where she later affiliated with Friml group. She worked on the project “SACSIN mediates adaptation of plant cells to ARF-GEF inhibition” and also on side projects, which got successfully published in high impact journals like *Nature Communications* and *Nature Chemical Biology*. During her PhD studies, Mina has also presented her research results in the *ENPER* conference in Bordeaux in 2016 and in Prague in 2017.

List of Publications Appearing in Thesis

1. **Dejonghe, W. et al.** (2016). Mitochondrial uncouplers inhibit clathrin-mediated endocytosis largely through cytoplasmic acidification. *Nat. Commun.* **7**: 11710.
2. **Prát, T., Hajný, J., Grunewald, W., Vasileva, M., Molnár, G., Tejos, R., Schmid, M., Sauer, M., and Friml, J.** (2018). WRKY23 is a component of the transcriptional network mediating auxin feedback on PIN polarity. *PLOS Genet.* **14**: e1007177.
3. **Dejonghe, W. et al.** (2019). Disruption of endocytosis through chemical inhibition of clathrin heavy chain function. *Nat. Chem. Biol.* **15**: 641–649.
4. **Zhang, J.,..., Vasileva, M.,..., Friml, J.** Strigolactones inhibit the feed-back of auxin on PIN-dependent canalization. (in preparation)
5. **Baster, P.;...Vasileva, M.;Friml, J.** Putative regulator of PIN polarity identified by means of forward genetics screen using strigolactone analogue GR24. (in preparation)
6. **Vasileva, M.,...,Friml, J.** SACSIN is component of plant cell adaptation to ARF GEF inhibition. (in preparation)

Table of Contents

Abstract	v
Acknowledgments	vii
List of Figures	xiii
List of Abbreviations.....	xv
1 Introduction to auxin biology and endomembrane trafficking in <i>Arabidopsis thaliana</i>	1
1.1 INTRODUCTION TO AUXIN BIOLOGY	1
1.1.1 <i>Early experiments in auxin research</i>	1
1.1.2 <i>Auxin perception and signalling</i>	2
1.1.3 <i>Metabolism of the phytohormone auxin</i>	6
1.1.4 <i>Pathways of auxin transport</i>	6
1.1.5 <i>Discovery of PINs</i>	7
1.1.6 <i>The phytohormone strigolactone</i>	9
1.2 ENDOMEMBRANE TRAFFICKING IN ARABIDOPSIS THALIANA	12
1.2.1 <i>Secretion</i>	14
1.2.2 <i>Exocytosis</i>	14
1.2.3 <i>Endocytosis</i>	15
1.2.4 <i>Constitutive recycling</i>	16
1.2.5 <i>Degradation into vacuoles</i>	18
1.2.6 <i>Phosphorylation-related signals for polar targeting</i>	18
1.2.7 <i>Auxin feedback regulation of PIN-mediated auxin transport</i>	19
1.3 SUMMARY	20
1.4 REFERENCES.....	21
2 SACSIN mediates adaptation of plant cells to ARF-GEF inhibition.....	49
2.1 ABSTRACT.....	49
2.2 INTRODUCTION	49
2.3 RESULTS	51
2.3.1 <i>Forward genetic screening for Brefeldin A-resistant mutants</i>	52
2.3.2 <i>AT5G23110 encodes SACSIN protein</i>	54
2.3.3 <i>Plant growth and development in sacsins mutants</i>	56
2.3.4 <i>Endomembrane and subcellular trafficking in sacsins mutants</i>	58
2.3.5 <i>SACSIN role in BFA-sensitive trafficking</i>	60
2.3.6 <i>Roles of SACSIN and GNOM ARF-GEF in apical-basal PIN targeting</i>	61
2.3.7 <i>Genetic interaction of SACSIN and BIG3 encoding a BFA-resistant ARF-GEF</i>	63
2.3.8 <i>Genetic interaction of SACSIN and BIG/DOC1/TIR3 encoding a Callosin-like protein implicated in auxin action</i>	63
2.4 DISCUSSION AND CONCLUSION.....	66
2.5 SUPPLEMENTARY.....	70
2.6 MATERIALS AND METHODS.....	74
2.7 REFERENCE	77
3 The phytohormone strigolactone	82
3.1 INTRODUCTION.....	82
3.2 STRIGOLACTONE INTERFERES WITH AUXIN FEEDBACK ON PIN INTERNALIZATION.....	82
3.2.1 <i>Abstract</i>	83
3.2.2 <i>Introduction</i>	83
3.2.3 <i>Results</i>	84
3.2.4 <i>Discussion and conclusions</i>	86
3.3 WRKY23 IS A COMPONENT OF THE TRANSCRIPTIONAL NETWORK MEDIATING AUXIN FEEDBACK ON PIN POLARITY ..	87
3.3.1 <i>Introduction</i>	87

3.4	ROLE OF PHOSPHORYLATION IN THE STRIGOLACTONE REGULATION OF AUXIN FEEDBACK ON PIN INTERNALIZATION ..	87
3.4.1	<i>Abstract</i>	87
3.4.2	<i>Introduction</i>	88
3.4.3	<i>Results</i>	89
3.4.4	<i>Discussion and conclusions</i>	91
3.5	MAX2-DEPENDENCE OF STRIGOLACTONE-MEDIATED ROOT GROWTH INHIBITION.....	92
3.5.1	<i>Introduction</i>	92
3.5.2	<i>Results</i>	93
3.5.3	<i>Discussion and conclusions</i>	94
3.6	PUTATIVE REGULATOR OF PIN POLARITY IDENTIFIED BY MEANS OF FORWARD GENETICS SCREEN USING STRIGOLACTONE ANALOGUE GR24	95
3.6.1	<i>Abstract</i>	95
3.6.2	<i>Introduction</i>	95
3.6.3	<i>Results</i>	96
3.6.4	<i>Discussion and conclusions</i>	100
3.7	MATERIAL AND METHODS	101
3.8	REFERENCE	102
4	Endosidin 9 (ES9) and Endosidin 9-17 (ES9-17) are small molecules, inhibitors of clathrin-mediated endocytosis.....	112
4.1	INTRODUCTION	112
4.2	RESULTS	114
4.3	DISCUSSION AND CONCLUSIONS	115
4.4	MATERIAL AND METHODS	115
4.5	REFERENCE	116
5	General conclusions, discussion and perspectives.....	119
5.1	SACSIN MEDIATES ADAPTATION OF PLANT CELLS TO ARF-GEF INHIBITION	120
5.2	STRIGOLACTONE INTERFERES WITH AUXIN FEEDBACK ON PIN INTERNALIZATION.....	124
5.3	ROLE OF PHOSPHORYLATION IN THE STRIGOLACTONE REGULATION OF AUXIN FEEDBACK ON PIN INTERNALIZATION	125
5.4	MAX2-DEPENDENCE OF STRIGOLACTONE-MEDIATED ROOT GROWTH INHIBITION.....	127
5.5	PUTATIVE REGULATOR OF PIN POLARITY IDENTIFIED BY MEANS OF FORWARD GENETICS SCREEN USING STRIGOLACTONE ANALOGUE GR24	128
5.6	ENDOSIDIN 9 (ES9) AND ENDOSIDIN 9-17 (ES9-17) ARE SMALL MOLECULES, INHIBITORS OF CLATHRIN-MEDIATED ENDOCYTOSIS.....	128
5.7	REFERENCE	129
6	Appendix	133
6.1	APPENDIX A.....	133
6.2	APPENDIX B.....	145
6.3	APPENDIX C	161

List of Figures

Chapter 1: Introduction

Figure 1: Auxin perception and receptor systems.....	3
Figure 2: Strigolactone effects.....	10
Figure 3: Biosynthesis and signalling pathways of the phytohormone strigolactone and effect on PIN localization.....	11
Figure 4: Subcellular trafficking mechanisms controlling PIN polarity and degradation.....	13

Chapter 2: SACSIN mediates adaptation of plant cells to ARF-GEF inhibition

Figure 1: Outline of the forward genetic screen for the identification of novel trafficking components in <i>Arabidopsis thaliana</i>	52
Figure 2. <i>BAR1</i> gene and protein structure, gene expression and co-expression graph.....	55
Figure 3: Morphology phenotypes of <i>sacsin</i>	57
Figure 4: Non-BFA related cell phenotype of <i>sacsin</i>	58
Figure 5: <i>sacsin</i> is defective in exocytosis and transcytosis.....	60
Figure 6: Characterization of <i>gnom</i> ^{R5} cross.....	62
Figure 7: <i>SACSIN-BIG</i> genetic interaction on cellular level.....	64
Figure 8: <i>SACSIN-BIG</i> genetic interaction on morphology level.....	65
Suppl. Fig. 1: qRT-PCR analysis of the T-DNA insertional lines and the <i>bar1-2</i> expression in the isolated mutant lines.....	70
Suppl. Fig. 2: Evolutionary analysis of the <i>BAR1</i> protein and <i>SACSIN</i> protein structure in humans.....	70
Suppl. Fig. 3: Phenotypic analysis of <i>sacsin</i>	71
Suppl. Fig. 4: Non-BFA related cell phenotype of <i>sacsin</i>	72
Suppl. Fig. 5: <i>sacsin</i> is defective in exocytosis and transcytosis.....	73
Suppl. Fig. 6: <i>SACSIN-BIG3</i> genetic interaction.....	74

Chapter 3: The phytohormone strigolactone

Figure 1: Experimental setting to study the PIN1 localization in strigolactone signalling mutants after the application of GR24 and/or NAA and BFA.....	85
Figure 2: Role of phosphorylation in the strigolactone regulation of auxin feedback on PIN internalization.....	90
Figure 3: MAX2-dependence of strigolactone-mediated root growth inhibition.....	93
Figure 4: Putative pathways of IAA biosynthesis and metabolism in <i>Arabidopsis</i>	98
Figure 5: Tendencies and alterations of the auxin metabolites after application of strigolactone.....	100

Chapter 4: Endosidin 9 (ES9) and Endosidin 9-17 (ES 9-17) are small molecules, inhibitors of clathrin-mediated endocytosis

Figure 1: ES9 and ES91-17 as small molecules, inhibitors of clathrin-mediated endocytosis.....	114
---	-----

List of Abbreviations

ABCB	ATP-Binding Cassette B
ABCG36	ATP Binding Cassette subfamily G36
ABP1	auxin binding protein 1
AFB	Auxin signaling F-Box proteins
AM	abascular mycorrhizal
AM+/-	Arabidopsis Medium with/without sucrose
AP	Adaptor Protein
ARF	ADP-Ribosylation Factor
ARF	Auxin Response Factor
ARSACS	Autosomal recessive spastic ataxia of Charlevoix-Saguenay
ATP	Adenosine Triphosphate
ATPase	Adenosine Triphosphate hydrolase
AUX1	Auxin Resistant 1
AuxRE	Auxin Responsive Elements
BAR	BFA Alternative Response
BEN	BFA-visualized endocytic trafficking defective
BEX	BFA-visualized exocytic trafficking defective
BFA	Brefeldin A
BLAST	Basic Local Alignment Search Tool
Bp	base pair
C	Celsius degree
CBP1	C-terminal peptide binding protein 1
CCCP	carbonyl cyanide m-chlorophenyl hydrazine
CCD	carotenoid cleavage dioxygenase
cDNA	complementary DNA
CDS	coding sequences
CHC	Clathrin Heavy Chain
CME	Clathrin-Mediated Endocytosis
CO ₂	Carbon dioxide
CoA	coenzyme A
Col-0	Columbia ecotype
COPI	Coat protein I
COPII	Coat protein II
CRISPR	Clustered Regularly Interspaced Short Palindromic Repeats
D6PK	D6 Protein Kinase
D6PKL	D6 Protein Kinase Like
DA	dihydrolipoyl acetyltransferase
DD	dihydrolipoyl dehydrogenase
dH ₂ O	deionized water
DMEM	Dulbecco's Modified Eagle's Medium
DMSO	Dimethyl Sulfoxide
DNA	Deoxyribonucleic Acid
DPB	Dimerization Partner of E2Fs B
EE	Early Endosomes

EMS	Ethyl MethaneSulfonate
ER	Endoplasmic Reticulum
ERES	ER Exit Site
ES9	endosidin 9
ES9-17	endosidin 9-17
EXO	EXOCYST subunit
Fig	figure
Flg22	flagellin 22
FM4-64	Fei-Mao 4-64 Styryl Dye
FRAP	fluorescence recovery after photobleaching
GAP	GTPase-activating protein
GDP	guanosine diphosphate
GEF	Guanine-nucleotide Exchange Factor
GFP	Green Fluorescent Protein
GNL1	GNOM Like 1 protein
GPI	glycosylphosphatidylinositol
GTP	Guanosine TriPhosphate
GTPase	Guanosine TriPhosphate hydrolase
GUS	beta-glucuronidase gene
h	hour(s)
HSP	heat shock protein
IAA	Indole-3-Acetic Acid
IAA-CoA	indole-3-acetyl-CoA
IAAId	indole-3-acetaldehyde
IAAsp	IAA-aspartate
IAGlu	IAA-glutamate
IAM	indole-3-acetamide
IAN	indole-3-acetonitrile
IAOx	indole-3-acetaldoxime
IBA	Indole-3-butyric acid
IPA	indole-3-pyruvate
IPyA	indole-3-pyruvic acid
kDa	kiloDalton
LAX	Like Auxin Resistant1 Auxin Permeases
LC-MS	Liquid chromatography–mass spectrometry
Ler	Landsberg erecta ecotype
LR	Lateral Root
LSM	Light Scanning Microscopy
MAX	more axillary growth
MDR	Multi-Drug Resistance
min	minute(s)
MIN7	HOPM interactor 7
MS	Murashige and Skoog
MT	microtubule
mtPD	mitochondrial pyruvate dehydrogenase
MVB	multivesicular bodies
NAA	naphthaleneacetic acid

NAD	Nicotinamide adenine dinucleotide
NGS	Next Generation Sequencing
NLS	nuclear localized signal
NPA	1-N-naphthylphthalamic acid
NRT1	nitrate permease 1
nTD	N-terminal domain
oxIAA	2-oxindole-3-acetic acid
oxIAA-glc	oxIAA-glucose
PAT	Polar Auxin Transport
PD E1- β	pyruvate dehydrogenase E1- β subunit
PDC	pyruvate dehydrogenase complex
PDR8	Pleiotropic Drug Resistance 8
PEN3	Penetration 3
PGP	P-Glycoprotein
PID	PINOID
pig1	PIN localization resistant to GR24 1
PILS	PIN Likes
PIN	PIN-FORMED auxin transport protein
PI(4,5)P2	phosphatidylinositol 4,5-bisphosphate
PIS1	Polar Auxin Transport Inhibitor 1
pIPDC	plastid pyruvate dehydrogenase complex
PM	Plasma Membrane
PP2A	Protein Phosphatase 2A
PP6	protein phosphatase 6
PVC	prevacuolar compartment
qPCR	quantitative Polymerase Chain Reaction
RAB	RAS protein from rat Brain
Ras	Rat sarcoma
RBR	RetinoBlastoma Related
RCN1	Roots Curl in Naphthylphthalamic acid1
RFP	Red Fluorescent Protein
RING	Really Interesting New Gene
RNA	RiboNucleic Acid
ROP	Rho of plants
qRT-PCR	quantitative Real-Time quantitative Polymerase Chain Reaction
SAL	SAPS domain like
SAR	Secretion-Associated RAS-related proteins
SCF	Skp, Cullin, F-box containing complex
SD	standard deviation
SEC	Secretory domain
SKP1	S-phase kinase associated protein 1
SKP2a	S-Phase Kinase-Associated Protein 2A
SL	strigolactone
SMAX1	suppressor of max2
SMXL	SMAX like
SNARE	SNAP receptor protein
SNX	sorting nexin

Suppl	supplementary
TAA	tryptophan amino transferase
TCP	teosinte branched 1 cycloidea
T-DNA	Transfer DNA
TGN	Trans-Golgi Network
TIR1	Transport Inhibitor Response 1
TMK	transmembrane kinase
TPC	TPLATE adaptor complex
TRA	tryptamine
Trp	Tryptophan
TyrA23	tyrphostinA23
UBL	ubiquitin-like domain
VAN	VAscular Network defective
V-ATPase	Vacuolar ATPase
VHA-a1	Vacuolar H(+)-ATPase 1
VPS	Vacuolar Protein Sorting
v/v	volume per volume
WAT1	Walls Are Thin 1
X-Gluc	5-bromo-4-chloro-3-indolyl- β -d-glucuronic acid

1 Introduction to auxin biology and endomembrane trafficking in *Arabidopsis thaliana*

Plants are sessile and they need to adapt to the changing environment. Their ability to survive is based on the remodeling of growth and dynamic responses to the biological changes. Many of these responses and developmental processes are regulated by the plant hormone auxin. In comparison to other phytohormones, it has the property to undergo a directional and finely regulated cell-to-cell transport, which is enabled by the transport proteins, localized on the plasma membrane. An important role in this process have the PIN auxin efflux proteins, which have an asymmetric and polar subcellular localization and determine the directionality of the auxin transport. In this chapter we focus on the auxin-regulated development through cellular responses, we describe the evolutionary perspective and we discuss the PIN function and endomembrane trafficking processes in *Arabidopsis thaliana*.

1.1 Introduction to auxin biology

1.1.1 Early experiments in auxin research

First insights into the biology of the phytohormone auxin came with the observations of Charles Darwin in 1880 that there is a mobile signal, which is effecting the plant tropisms (Darwin, 2009). Later Went and Thimann did the first plant physiology experiments with auxinic molecules (Thimann, 1939). This signal was suggested to be transported through the plant tissues in a controlled manner and it has the property to create concentration gradients between the shaded and the illuminated side of a phototropically responding coleoptile (Went, 1974).

The distribution of auxin in the plant body is regulated by a fast and nondirectional flow in the phloem with photosynthetic assimilates or by a directional cell-to-cell polar auxin transport (PAT), which is critical for the formation of auxin maxima in the developing tissues. This fine-tuned polar auxin transport can be explained by the chemiosmotic hypothesis (Goldsmith, 1977). The indole-3-acetic acid can exist predominantly in its protonated (IAAH) form in the acidic pH of the apoplast, which is allowing it to pass to the plasma membrane by

diffusion. However, while in the cytosol where the pH is of around 7, the auxin molecule dissociates into its ionic form and cannot exit the cell passively. For this, there are the plasma membrane localized auxin efflux carriers, which export auxin out of the cell and direct the auxin movement between the cells.

1.1.2 Auxin perception and signalling

The phytohormone auxin is a trigger for the cell growth and differentiation through its interaction with the molecular machinery of a cell. One of the best studied mechanism for its perception and its response includes the role of a co-receptor, which influences the degradation of proteins and the control of transcription. This co-receptor system is the Transport Inhibitor Response 1/Auxin F-Box (TIR1/AFB) where auxin is perceived, forming the S-Phase Kinase Protein 1 (SKP1)-Cullin-F-box (SCF)-type E-type ubiquitin ligase nuclear complex (Dharmasiri et al., 2005; Kepinski and Leyser, 2004; Calderón Villalobos et al., 2012; Gray et al., 2001). When the hormone is not present, then the AUXin/Indole-3-Acetic Acid (AUX/IAA) repressor proteins interact with the transcription factors of the auxin response factor (ARF) family, blocking the gene transcription (Ulmasov et al., 1997; Wu et al., 2012) (Figure 1A). They are bound in homodimers on genomic Auxin Responsive Elements (AuxRE) sequences, upstream of the auxin regulated genes (Shimizu-Mitao and Kakimoto, 2014; Ulmasov et al., 1997; Boer et al., 2014; Nanao et al., 2014; Korasick et al., 2014). When auxin is present in the system, then it binds to the TIR1/AFB and it promotes the recognition and poly-ubiquitination of Aux/IAA transcriptional repressors by the SCF^{TIR1} machinery, which is followed by proteasome-based degradation and release of auxin-regulated transcription (Figure 1A). All of this multiple levels of control result in the broad spectrum of auxin responses. The different sensitivities of interaction and specificity of the Aux/IAA transcriptional mediators, either with the TIR1/AFB complex or with the ARFs, regulate the starting steps of this signalling. There is also a second checkpoint for the alteration in the gene expression and this is the specificity of the different ARFs on various AuxRE in the gene promoter sequences. In summary, the co-receptor system, which governs the transcriptional responses consists of TIR1/AFB receptors, AUX/IAA repressors, ARF transcription factors and AuxRE promoter sequences.

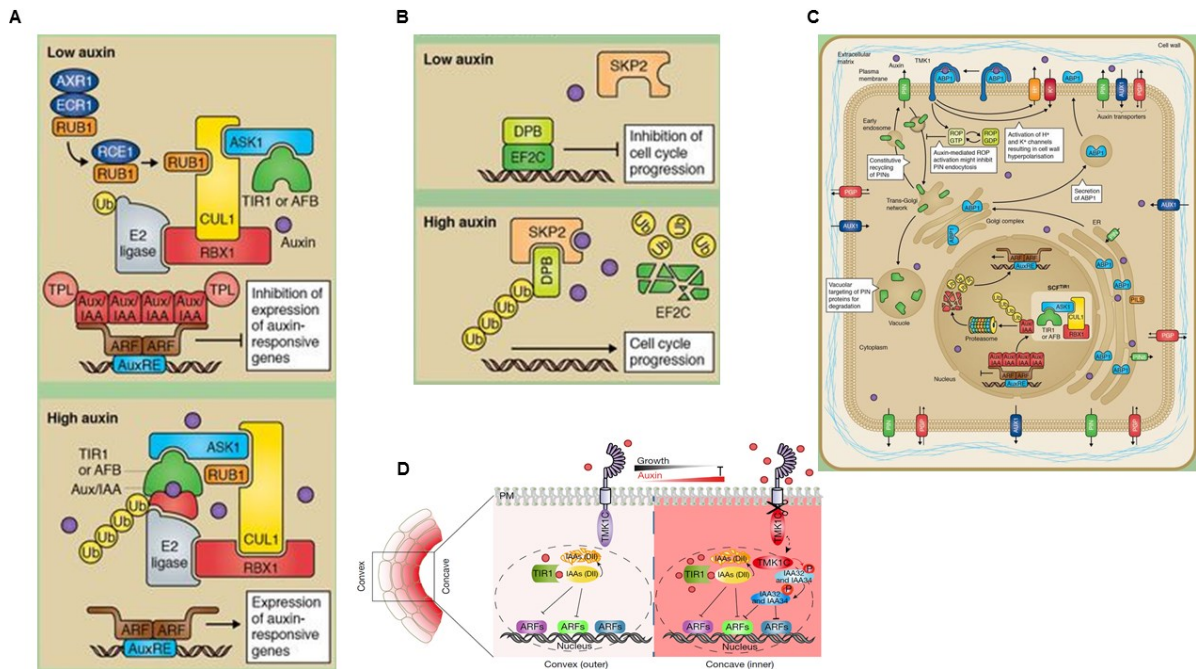


Figure 1: Auxin perception and receptor systems. (A) Auxin mediated transcriptional regulation by TIR1 (Grones and Friml, 2015). **(B)** SKP2, an atypical auxin binding protein (Grones and Friml, 2015). **(C)** Proposed model of auxin–TMK1–IAA32 and IAA34 signalling in apical hook development (Cao et al., 2019). **(D)** Overview of the auxin cellular machinery (Grones and Friml, 2015).

In addition, there is also another complex, which can bind auxin in the nucleus similar to the TIR1/AFB and it is the S-phase Kinase Protein, SKP2a (Jurado et al., 2010) (Figure 1B). The binding of auxin mediates the SKP2a interaction with the Dimerization Partner of E2Fs B (DPB), promoting its ubiquitination and degradation (Jurado et al., 2010). There is a transcriptional repressor, which is known as DPB, which binds and inhibits the RetinoBlastoma Related/E2Fc (RBR/E2Fc) transcriptional factor (del Pozo et al., 2006). The auxin-activated SKP2a interacts with DPB, which promotes its ubiquitination and degradation from the proteasome, releasing the E2Fc transcriptional factors for targeted gene expression. The SKP2a-DPB-E2Fc module has an influence on the development of cotyledons, leaves and lateral roots and the action is through regulation of the cell cycle balance between the G2 to M transition (del Pozo et al., 2006; Del Pozo et al., 2007).

The sensing of auxin is also potentially achieved by pathways outside of nucleus, such as the auxin binding protein (ABP1) (Figure 1C). It was discovered in maize by the investigations aiming for proteins with *in vitro* auxin binding properties from coleoptiles. By the implementation of biochemical methods it was shown that the ABP1 can bind auxin (Cross and Briggs, 1978; Löbner and Klämbt, 1985; Shimomura et al., 1999) and that the protein confirmation forms an auxin binding pocket (Brown and Jones, 1994; Grones et al., 2015). By

using bioinformatics tools and running protein modelling and auxin binding simulations, it was predicted that ABP1 forms a dimer, which undergoes conformational changes upon auxin binding (Grandits and Oostenbrink, 2014). In addition, auxin stabilizes ABP1 and alters the interactions with other proteins (Shimomura et al., 1986; Bertosa et al., 2008). It was also predicted that the protein is localized in the endoplasmic reticulum (ER) (Cross and Briggs, 1979; Inohara et al., 1989), where the pH is of around 7, which differs from the optimal binding affinity, which was shown to be at a pH of 5-5.5 (Chen et al., 2014). Additionally, by the implementation of electron microscopy imaging it was observed that a small fraction of the ABP1 protein is localized in the space between the plasma membrane and the cell wall, in the apoplast (Löbner and Klämbt, 1985; Jones and Herman, 1993) or in clusters at the plasma membrane (Diekmann et al., 1995). The ABP1 protein potentially interacts on the cell surface with the C-terminal peptide binding protein 1 (CBP1), which anchors to the plasma membrane through glycosylphosphatidylinositol (GPI) (Shimomura, 2006). Moreover, the functional role and localization of ABP1 on the plasma membrane was shown through direct interaction experiments with TransMembrane receptor-like Kinase (TMK), which forms an auxin perception complex at the cell surface (Xu et al., 2014). The auxin signalling, which is mediated by ABP1, is going further through the ABP1's intracellular genetic interactors, which are the Rho like GTPase 2 and 6 (ROP2 and ROP6) and their downstream effectors, ROP-interactive CRIB motif-containing protein 1 and 4 (RIC1 and RIC4) (Chen et al., 2012). The ROP/RIC machinery results in remodelling the cytoskeleton through effects on actin filaments (AF) and microtubules (MT) (Nagawa et al., 2010; Lin et al., 2012). Moreover, the ABP1/ROP/RIC signalling module inhibits the endocytosis of clathrin-coated vesicles by auxin (Robert et al., 2010; Wang et al., 2013; Čovanová et al., 2013). In conclusion, the auxin binding protein 1 (ABP1) mediates auxin responses from the cell surface, affecting the cell cytoskeleton and endocytosis.

Another branch of the ABP1 signalling is connected with the nuclear TIR1/AFB auxin signalling pathway on the basis of transcription regulation of auxin responsive genes. Thus, the ABP1 stabilizes the Aux/IAA transcriptional repressors or acts negatively on TIR1/AFB auxin receptors, which results in an altered gene expression (Tomas et al., 2013). Moreover, the binding of auxin to ABP1 interferes with the clathrin-mediated endocytosis of auxin transporters from the plasma membrane (Robert et al., 2010; Chen et al., 2012). All of this

has an influence on the auxin homeostasis and results in altered gene expression through the TIR1/AFB auxin sensing and signalling complex (Tomas et al., 2013).

Recently, a new auxin signalling mechanism was identified, which acts in parallel to the canonical auxin pathway, based on the transport inhibitor response1 (TIR1) and other auxin receptor F-box (AFB) family proteins (TIR1/AFB receptors) (Salehin et al., 2015; Weijers and Wagner, 2016) and which mediates differential growth during apical-hook development (Cao et al., 2019) (Figure 1D). There is an asymmetrical accumulation of auxin at the concave side of the hook during the formation state (Liao et al., 2015), which leads to bending of the hook due to the inhibition of cell elongation (Li et al., 2004; Žádníková et al., 2016). This process represents a model that involves differential auxin concentrations, which comprises three sequential steps: formation, maintenance and openings (Raz and Ecker, 1999; Žádníková et al., 2010). The newly introduced signalling mechanism operates at the concave side of the apical hook, and involves auxin-mediated C-terminal cleavage of transmembrane kinase 1 (TMK1). The C-terminus of TMK1, which is translocated to the cytosol and nucleus, interacts with two non-canonical transcriptional repressors of the Aux/IAA family – IAA32 and IAA34 and also phosphorylates them. These two transcriptional repressors are stabilized and like this they can regulate expression and also inhibit growth, which is a difference to the canonical pathway, where Aux/IAA transcriptional repressors are degraded (Cao et al., 2019). High levels of auxin trigger the auxin-TMK1 signalling pathway, which originates at the cell surface, which also shares transcriptional factors with the TIR1/AFB signalling pathway (Cao et al., 2019). Like this different concentrations of auxin are generated and complex developmental outcomes can be mediated (Cao et al., 2019).

The role of ABP1 in plant development is characterized on experiments with *abp1* mutants. It was shown that ABP1 affects the cell cycle progression (Chen et al., 2001; Robinson et al., 2007; Braun et al., 2008; Tomas et al., 2009) and cell expansion (Jones et al., 1998; Baully et al., 2000; Chen et al., 2001; Braun et al., 2008; Tomas et al., 2009), by transcriptional regulation or cell wall modelling (Paque et al., 2014), cytoskeleton reorganization (Chen et al., 2014; Lin et al., 2012), changes in the cytoplasmic pH (Gehring et al., 1998) and K⁺ currents (Baully et al., 2000). Unfortunately, there were mistakes in the original characterization of the *abp1* mutants (Chen et al., 2001) (Habets and Offringa, 2015). The misunderstandings came from the fact that the embryo lethality of *abp1-1* is due to a mutation in a gene different than the *abp1* (Gao et al., 2015; Dai et al., 2015; Michalko et al., 2015), while the new null mutants

generated by CRISPR/Cas9 technology did not significantly differ in their growth from the wild type. Another mutant with a point mutation in the auxin binding pocket *abp1-5* (Enders et al., 2015) was re-sequenced and there were thousands of additional mutations, which might be the reason for the described phenotypes. Thus careful re-evaluation of the ABP1 physiological roles is essential and the development of the new molecular biology techniques and methods is a good starting point for further research on auxin binding, signal mediation and auxin response by the ABP1 pathways.

1.1.3 Metabolism of the phytohormone auxin

Tryptophan is a precursor of auxin and the tryptophan amino transferase (TAA) converts it into Indole-3-Pyruvic acid (IPyA), which is later converted into Indole-3-Acetic Acid (IAA) by the family of Yucca enzymes. In addition, there are four additional IAA precursors, formed from tryptophan – indole-3-acetaldoxime (IAOx), indole-3-acetonitrile (IAN), indole-3-acetamide (IAM) and indole-3-acetaldehyde (IAAld), which can be directly converted to IAA, which is the naturally occurring auxin molecule. These precursors have a biological activity depending on the tissue and also species (Mano and Nemoto, 2012; Vernoux et al., 2010). Moreover, the auxin related processes are supported by free, active IAA, which can be further converted to inactive forms such as glucose, conjugates of amino acids or Indole-3-butyric acid (IBA).

Important tools for assessing auxin levels are the artificial auxin responsive promoters, which give indirect measure of the auxin concentration in plant cells (Ulmasov et al., 1997). In addition, an auxin metabolomics profiling can be implemented to analyse the amount of auxinic compounds, with which the active and the inactive forms can be evaluated. This type of analysis is useful for the investigation of tissue patterning, developmental dynamics and physiological responsiveness (Efroni and Birnbaum, 2016; Bargmann et al., 2013).

1.1.4 Pathways of auxin transport

Auxin has an important role in nearly every aspect of plant development throughout the whole plant. Majority of the hormone is synthesized in apical and lateral shoot meristems,

young leaves (Ljung et al., 2001) and in meristems of primary and lateral roots (Vernoux et al., 2010). In the plant body, there are the auxin minima and maxima, which are areas, differing from the synthesis locations. The auxin transport from cell-to-cell has been connected with venation (Sieburth, 1999), cotyledon shape (Koizumi et al., 2000), apical hook curvature (Žádníková et al., 2010; Vandenbussche et al., 2010), hypocotyl elongation (Zheng et al., 2016), root hair, lateral root formation (Petrášek and Friml, 2009), growth (Overvoorde et al., 2010), altered gravitropism (Rashotte et al., 2000; Rahman et al., 2010; Geisler et al., 2014; Sato et al., 2015), leaf epinasty, salt avoidance, stress tolerance and others (Adamowski and Friml 2015).

For the active transport there are the influx and efflux carrier, which enable the directed cell-to-cell transport. There are four classes of auxin transporters - the PIN exporters (Zazimalová et al., 2010; Adamowski and Friml, 2015), the PILS ER-localized transporters (Barbez et al., 2012; Feraru et al., 2012b), the ATP-Binding Cassette subfamily-B/P-GlycoProtein Transporter / Multi-Drug Resistance (ABCB/PGP/MDR), which are transporting inward or outwards (Cho and Cho, 2013) and AUXin Resistant 1/Like AUX1 (AUX/LAX), which act as auxin importers (Swarup and Péret, 2012; Péret et al., 2012). There are also other transporters, which were shown to participate in the transfer of auxin: transporters nitrate permease 1 (NRT1) (Krouk et al., 2010), Penetration 3/Pleiotropic Drug Resistance 8/ATP Binding Cassette subfamily G36 (PEN3/PDR8/ABCG36) (Stein et al., 2006; Strader and Bartel, 2009) and Polar Auxin Transport Inhibitor 1/PLEIOTROPIC DRUG RESISTANCE 9/ATP Binding Cassette subfamily G37 (PIS1/PDR9/ABCG37) (Ruzicka et al., 2010). Interestingly, the Walls Are Thin 1 (WAT1) in *Arabidopsis* exports auxin from the vacuole into the cytoplasm (Ranocha et al., 2013) adding an additional complexity to the regulation of cellular auxin homeostasis.

1.1.5 Discovery of PINs

In our lab we concentrate on the PIN proteins, which are represented by eight members in *Arabidopsis thaliana*. PIN1, PIN2, PIN3, PIN4 and PIN7 are the once with a long hydrophilic loop, located at the PM, while PIN5, PIN6 and PIN8 are located also on the ER, presumably importing auxin in the lumen and are the once with a shorter hydrophilic loop (Nisar et al., 2014; Bosco et al., 2012; Ding et al., 2012; Mravec et al., 2009). The PIN proteins are auxin

efflux carriers, which export the phytohormone from the cytoplasm towards the ER or apoplast and in this way they regulate the cellular auxin homeostasis. The founding member of the PIN family is the PIN1 protein, which is characterized by a phenotype, reminding the form of a pin: it consists of stem and missing organs of leaves or flowers due to the fact that primordia failed to form at the shoot apical meristem (Okada et al., 1991). In addition, the molecular cloning of the *PIN1* gene revealed that the PIN protein encodes a transmembrane protein with carrier properties (Gälweiler et al., 1998) and a localization to the basal side of the stele cells. Another protein of this family is the PIN2 protein, which has a gravitropic phenotype (Chen et al., 1998; Luschnig et al., 1998; Müller et al., 1998; Utsuno et al., 1998). The role of a component in polar auxin transport of root gravitropic response was assigned to the identified protein. In transport assays in different systems it was shown that the PIN proteins have an auxin efflux capacity (Petrášek et al., 2006; Yang and Murphy, 2009; Barbez et al., 2013; Zourelidou et al., 2009).

Moreover, the PIN expression and localization is detectable from the very first stages of embryo development. There are four genes, which are expressed in the embryos – *PIN1,3,4* and *7* and in the single mutants *pin4* (Friml et al., 2002a) and *pin7* (Friml et al., 2003) early embryogenesis defects can be found with increasing severity in the multiple mutants (Friml et al., 2003; Blilou et al., 2005; Vieten et al., 2005). The auxin accumulation occurs for the first time in the apical cell, which originates after the division of the zygote and auxin remains in the apical part of the embryo until a switch occurs around the 32-cell stage, where the auxin maximum is detected in the basal parts of the embryo, as well as the uppermost suspensor cell (Friml et al., 2003). The polarity of the localization of the PIN proteins corresponds to the auxin fluxes as the PIN7 is expressed in the basal domains of the embryo and then it is polarized toward the apical cells, while later PIN7 in the suspensor and PIN1 in the stele cells of the embryo show basal polarity (Friml et al., 2003). Recent research showed that due to the feedback regulation by auxin sources, the PIN polarity switches during embryogenesis and in this case the auxin is produced in the suspensor cell and in the maternal tissues and later in the apical end of the embryo and like this the apical-basal axis is defined (Robert et al., 2013; Wabnik et al., 2013; Robert et al., 2018). With the progression of the embryo development, there are additional maxima of auxin response in the sites of cotyledon formation. The polarity of the PIN1 protein in the epidermal layer faces the auxin maxima, while a canal of cells, expressing the PIN1 protein on the basal side of the inner embryo body

is formed, where the future vascular strands are formed by driving auxin away from the primordium (Benkova et al., 2003). In the *pin* mutants, there are cotyledon developmental defects, which are pronounced as single, triple fused or improperly shaped cotyledons (Benkova et al., 2003; Friml et al., 2003).

In the later stages of development, the auxin transporters are expressed progressively (Robert et al., 2015). Through the coordination of importers and exporters, the flow of auxin through tissues and cells can be coordinated and these phytohormone is transported from the shoot to the root. The lateral roots emerge from the pericycle layer at the primary root at the sites, where the amount of auxin response is elevated (Benkova et al., 2003; Dubrovsky et al., 2008). In the case of lateral root primordia, the PIN proteins are redistributed, which marks the lateral root initiation and the generation of new auxin maxima (Marhavý et al., 2013). Another process, which is connected with rearrangement of PIN proteins is the phototropic bending, where the polarity in the hypocotyl changes, which re-alter the auxin flow from basipetal to lateral direction (Ding et al., 2011). The auxin morphogens allow the plant to adapt to the changing environment by polar auxin transport, which enables plasticity and capacity to develop in agreement with the surrounding conditions. In all of the mentioned cases, auxin is transported in direction of the tip, which is a stream supplying the root-derived organs with auxin, while it depletes the apical organs. The complementary flux through the outer layer has opposite directions in apical and basal organs. These two patterns of auxin flow through tissues are defined as “fountain” and “reverse fountain” (Benkova et al., 2003).

1.1.6 The phytohormone strigolactone

Next to auxin there are other phytohormones, which participate in the regulation of plant growth and development. The strigolactones and karrikins are butenolide compounds, which play an important role in those processes (Soundappan et al., 2015). The strigolactones were first identified as compounds, which are stimulating the germination of parasitic weeds from the family of *Orobanche* and *Striga spp* (Cook et al., 1966) (Figure 2). In addition, when the nutrients are limited, then SLs promote the symbiosis with arbuscular mycorrhizal (AM) fungi,

which permit the exchange of carbon for nitrogen, phosphorus and water (Akiyama et al., 2005)(Figure 2). Another property of the strigolactones is connected with the inhibition of shoot branching, regulating of the root architecture, leaf senescence and secondary growth (Gomez-Roldan et al., 2008; Umehara et al., 2008; Agusti et al., 2011; Kapulnik et al., 2011; Ruyter-Spira et al., 2011; Rasmussen et al., 2014).

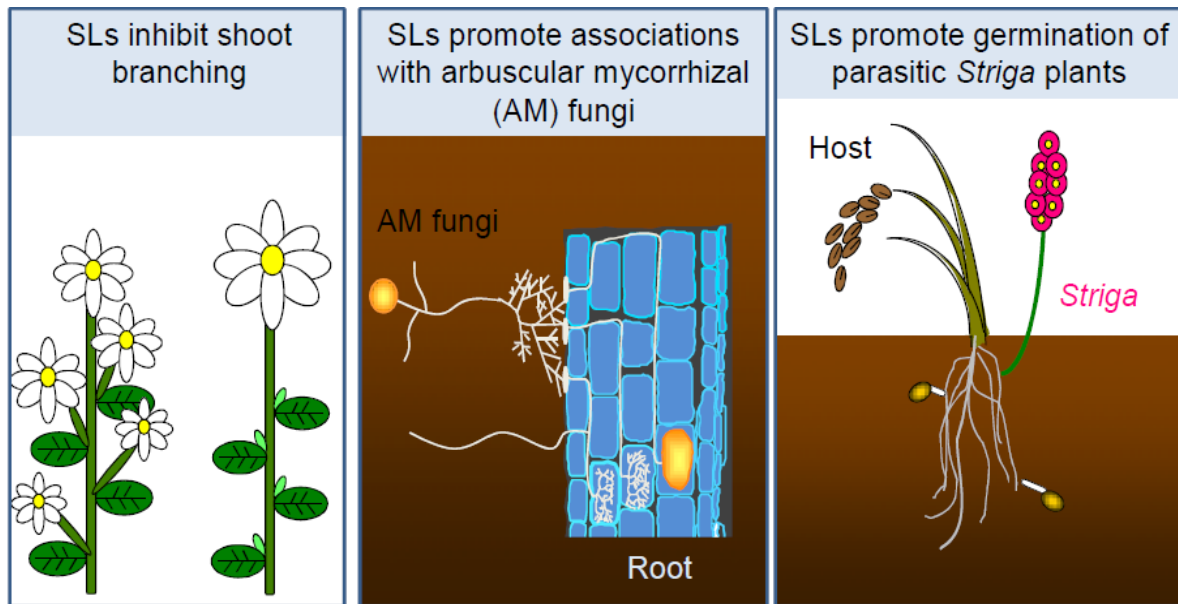


Figure 2: Strigolactone effects (Figure adapted from Plant cell)

The biosynthesis of strigolactones is derived from the carotenoid pathway (Matusova et al., 2005) with the activity of various oxygenases (Gomez-Roldan et al., 2008; Umehara et al., 2008). In *Arabidopsis thaliana* there are the carotenoid dioxygenase MAX3 (MORE AXILLARY GROWTH3) and MAX4 (AtCCD8) and also MAX1 (cytochrome P450), which are participating in the biosynthesis of this phytohormone (Turnbull et al., 2002; Sorefan et al., 2003; Booker et al., 2005) (Figure 3A). There are more than 20 naturally occurring strigolactone derivatives, which play essential roles in the plant growth and development (reviewed by (Lopez-Obando et al., 2015)).

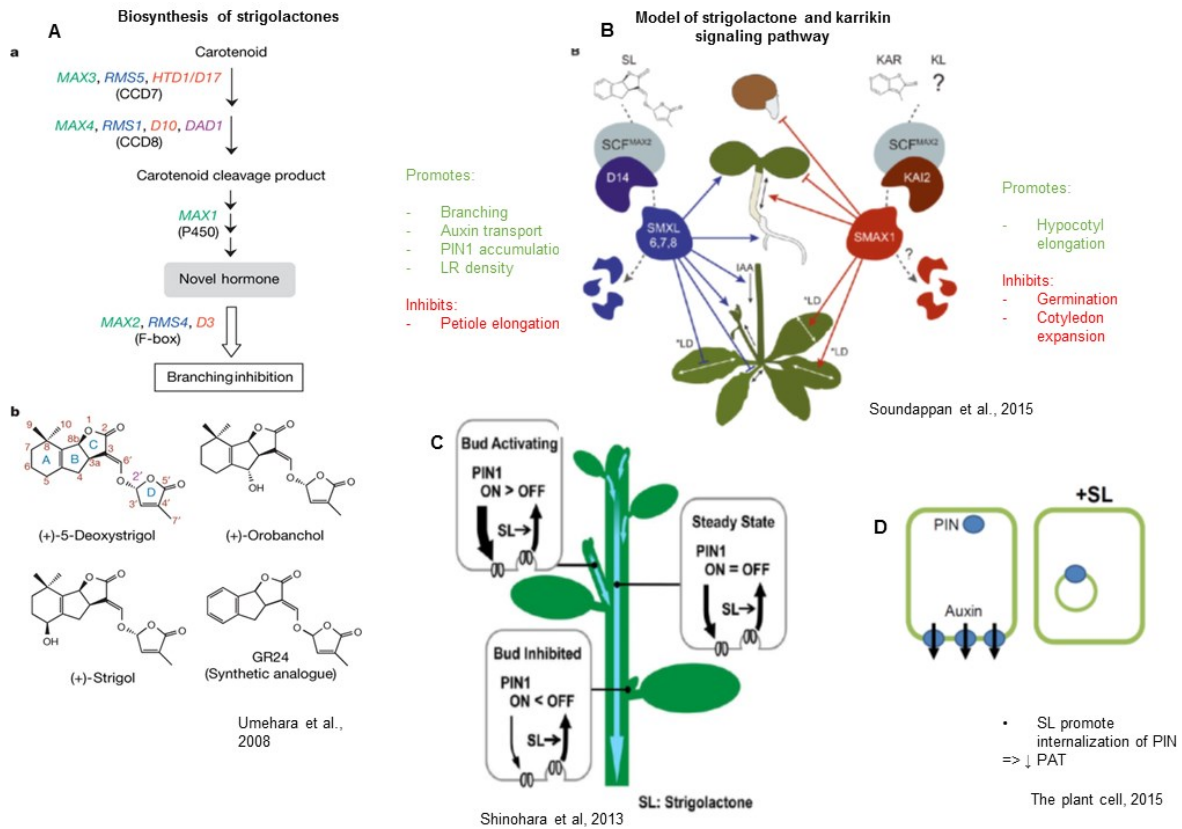


Figure 3: Biosynthesis and signalling pathways of the phytohormone strigolactone and effect on PIN localization. (A) Biosynthesis pathway of strigolactones. **(B)** Model of strigolactones and karrikin signalling pathways. **(C)** Representation of PIN1 protein regulation by strigolactones and its effect on bud activity. **(D)** Strigolactones' effect on the polar auxin transport.

The strigolactone signalling includes the hormone-mediated interaction between receptor and F-box protein, degradation of suppressor proteins and activation of transcription factors. In the Figure 3B there is a model, which illustrates this signalling cascade. A known receptor for strigolactone is the D14 receptor, which is an alpha/beta hydrolase and it does not recognize karrikin (Waters et al., 2012). The karrikins are chemical signals, which were found in smoke and which promote seed germination (Flematti et al., 2004; Nelson et al., 2009, 2012). In *Arabidopsis thaliana* this molecule can enhance the seedling response to light (Jain et al., 2006; Kulkarni et al., 2006; van Staden et al., 2006; Nelson et al., 2010). It is suggested that the karrikins mimic a butenolide molecule (KAI2 ligand), which is different than strigolactone (Flematti et al., 2013; Waters et al., 2014). Moreover, in the presence of strigolactone or karrikin, the corresponding receptor recognizes the molecules and hydrolyses them. Then the receptor alters its conformation and is able to bind to the F-box protein (MAX2), which is a component of the SCF complex, and also to the transcription repressors. The next step in the signalling pathway is the degradation of the transcription repressors

(*smax* and *smxl*) in the proteasome. *SMAX1* (*suppressor of max2*) has seven *SMAX-like* (*SMXL2-8*) homologs and all 8 genes are members of a gene family with similarity to *AtHSP101* (thermotolerance) (reviewed in (Stanga et al., 2013)). The role of *SMAX1* is in repression of the germination and the responses of the seedling to light by reduction of the expansion of the cotyledons and promotion of the hypocotyl elongation. In addition, *SMXL6, 7, 8* stimulate the branching, the transport of the phytohormone auxin and the PIN1 accumulation at the basal plasma membrane and also the density of the lateral roots. But on the other hand, they inhibit the petiole elongation (Soundappan et al., 2015).

One of the roles of strigolactone is in the shoot branching inhibition and in Figure 3C there is a model, which represents the action of it together with auxin in this process. There are two putative scenarios for the regulation of this process. The first one is that auxin regulates the synthesis of strigolactone (Shinohara et al., 2013). The activity of the bud is inhibited by auxin by the elevation of strigolactone biosynthetic genes. The second putative model is connected with the auxin transport canalization to connect the bud to the stem. In this process the role of strigolactone is to reduce the accumulation of PIN1 on the plasma membrane (Shinohara et al., 2013). If the bud is activated, then the canalization takes place and the PIN1 protein is localized mostly on the plasma membrane. However, when the outgrowth is inhibited, then the PIN1 protein is internalized (Shinohara et al., 2013). On a cellular level, strigolactone promotes the internalization of the PIN1 protein, which leads to a decrease in the polar auxin transport (Figure 3D).

1.2 Endomembrane trafficking in *Arabidopsis thaliana*

The cell structure and function is largely determined by the presence of intracellular organelles and the cytosol. Both have specific properties, which navigate their function and role in specialized mechanisms. The PIN proteins, are transmembrane proteins, which regulate developmental processes, environmental responses and cellular auxin homeostasis. These auxin efflux carriers traffic through intracellular compartments such as the ER, Golgi apparatus, TGN, vacuole and the plasma membrane and this trafficking is enabled by the small trafficking vesicles (Figure 4). The secretion of the newly synthesized proteins, their cycling between the subcellular domains and also the targeting to the lytic vacuole are strictly

regulated trafficking processes. In the next paragraphs I will focus on these subcellular trafficking mechanisms.

The small GTPases, such as Secretion-Associated RAS-related proteins (SARs), Ras genes from rat brain (RAB) and ADP-Ribosylation Factor (ARFs), are activated upon the switch of GDP with GTP and they act as regulators of the endomembrane trafficking (Rutherford and Moore, 2002; Yorimitsu et al., 2014; Nielsen et al., 2008). These proteins are inactive and soluble when they are bound to GDP. However, when the GDP exchanges to GTP (a process, regulated by the GTP exchange factor (GEF)), then they are active and hydrophobic and this enables their interaction with lipid layers of membranes, which initiates the mechanisms for vesicle formation (Yorimitsu et al., 2014; Cevher-Keskin, 2013; Shin and Nakayama, 2004). The GEF proteins are targeted by the fungal toxin Brefeldin A (BFA), which is thus an important tool for trafficking manipulations (Figure 4). Moreover, the small GTP proteins become again soluble when the bound GTP is hydrolysed to GDP by a specific protein, which is defined as GTPase activating protein (GAP) (Spang et al., 2010). The vesicle is formed and released by the synchronized action of the GTPases, GEFs and GAPs.

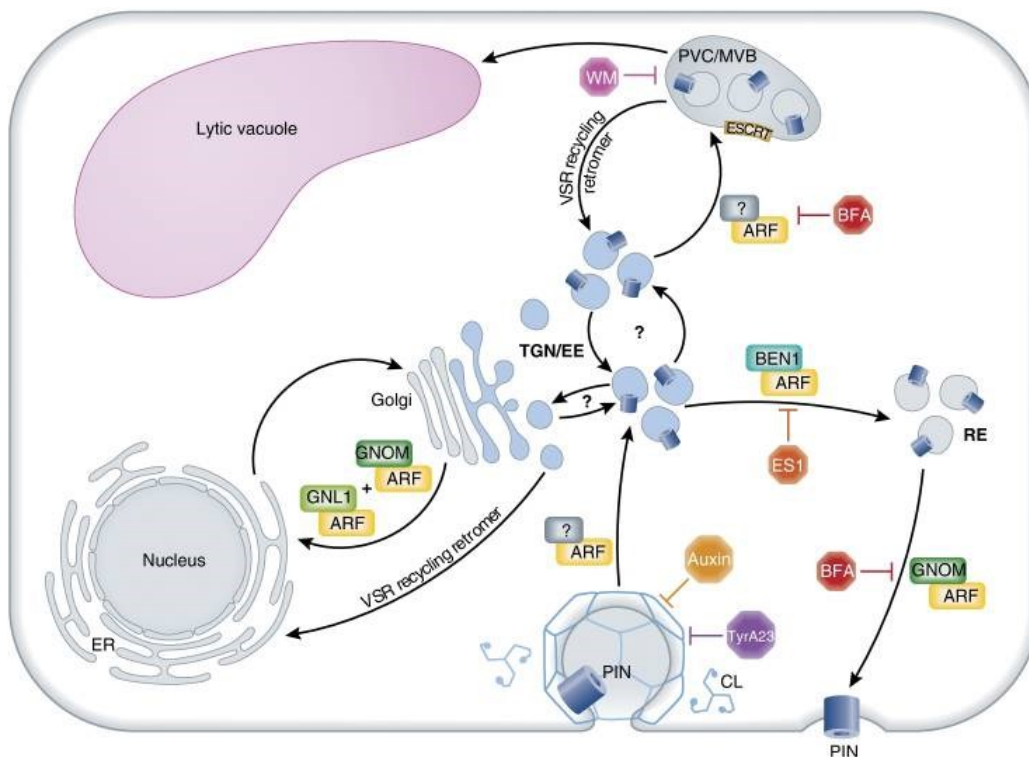


Figure 4: Subcellular trafficking mechanisms controlling PIN polarity and degradation.

In the next paragraphs the anterograde trafficking events from the ER to the Golgi and from the Golgi to the TGN and the plasma membrane will be explained.

1.2.1 Secretion

The proteins are synthesized in the endoplasmic reticulum (ER) and then they are co-translationally imported in the ER membrane via the translocon machinery (Mothes et al., 1997; Skach, 2009; Vitale and Denecke, 1999). Later, the sorting process into coat protein II (COPII) membrane vesicles takes place and the cargos are transferred to the *cis* side of the Golgi apparatus (Ding et al., 2012; Kang and Staehelin, 2008; Bar-Peled et al., 1995; Brandizzi and Barlowe, 2013). Next to the COPII complex, there are vesicles, budding from the ER and delivered to the Golgi and this process is regulated by SAR1, SEC12, Soluble N-ethylmaleimide-sensitive factor Attachment protein Receptors (SNAREs), MAIGO5 (MAG5) and p24 membrane proteins (Takagi et al., 2013; Montesinos et al., 2013). In the protein secretion pathway the SAR1 GTPase is activated by the ER integral protein SEC12, which stimulates the interaction of the SAR12 with COPII heterodimer subunits (Hanton et al., 2009; Cevher-Keskin, 2013; Osterrieder et al., 2009). Through interaction with COPII subunits there are the MAG5 and p24 proteins which are needed for the formation and budding of vesicle in ER Exit Site (ERES). In addition, the SNARE proteins are important for the recognition and tethering of the vesicle (vSNARE) to the targeted organelle (tSNARE) (Lipka et al., 2007; Uemura and Ueda, 2014). The further transport mechanisms are characterized either by a sorting back to the ER, which is a process, regulated by the COPI-coated vesicles or another option is that the proteins are targeted further to the TGN in the anterograde pathway.

1.2.2 Exocytosis

In the process of association of the cargo and tethering with the early endosome layer, there is the Exocyst complex, which regulates this process. It is evolutionary conserved among animals, fungi and plants and it has an octameric ultrastructure of six Sec and two Exo proteins, which have sequence similarities (Munson and Novick, 2006; Elias et al., 2003). In *Arabidopsis thaliana* there are two genes, which are encoding each of the following proteins:

Sec3, Sec5, Sec10 and Sec15 proteins and three genes encoding Exo84 proteins and 23 genes coding for Exo70 proteins (Elias et al., 2003; Cvrčková et al., 2012). For the assembly and tethering, there are the Exocyst subunits, which interact with each other, but there is also interaction with SNAREs, Rab and Rho GTPase (Nagawa et al., 2010; Hála et al., 2008; Fendrych et al., 2013). By the implementation of BFA as a tool to study vesicle trafficking it was observed that Exocyst 70 has a role in the polar delivery of the PIN1 and PIN2 proteins with the Exocyst complex regulating the last step of the anterograde trafficking of PIN proteins to the plasma membrane (Tan et al., 2016; Drdová et al., 2013).

1.2.3 Endocytosis

As mentioned earlier, plants have extraordinary adaptation skills, which largely depend on the ability of plant cells to maintain and to keep a particular homeostasis of plasma membrane proteins including different transporters or receptors. As we explained in the last paragraphs, the exocytosis is controlled by a large number of factors, which are targeting the transport towards the plasma membrane. On the other hand, there is the process of endocytosis, where cargos are internalized, which results in mediation of signals from the extracellular space and also plasma membrane rearrangement. The process of endocytosis is mediated by small vesicles, which bud from the plasma membrane and are transferred towards the cytosol, where they can be united into endosomes. The whole process of initiation of the endocytosis is mediated by clathrin, which is a protein, responsible for the recruitment of endocytic vesicles (Dannhauser and Ungewickell, 2012; Baisa et al., 2013; Chen et al., 2011). The structure of the protein is defined by a heavy and by a light chain, which builds a specialized structure of a triskelion (Kirchhausen, 2009). The clathrin triskelion is localized on the plasma membrane and supports the formation of the emerging bud, which has the shape of a ball (Kirchhausen, 2009; Dannhauser and Ungewickell, 2012). It is known that the PIN proteins in *Arabidopsis thaliana* undergo clathrin-mediated endocytosis (Dhonukshe et al., 2007). Through the analysis of the clathrin mutants it was shown that this protein plays essential roles in many crucial developmental processes, efficient auxin transport, PIN endocytosis and proper PIN polar distribution (Kitakura et al., 2011; Dhonukshe et al., 2007; Wang and Ruan, 2013). In our model organism there is no well-defined mechanism for clathrin-independent

mechanism for uptake of auxin transporters (Onelli et al., 2008; Bandmann and Homann, 2012; Li et al., 2012; Baral et al., 2015; Fan et al., 2015).

In the past studies on polar auxin transport, mutants like *Transport Inhibitor Response 3/BIG* (*TIR3/BIG*) were identified (Ruegger et al., 1997). Through the implementation of BFA as a tool to study trafficking processes it was observed that a mutation in the TIR3/BIG protein impairs the regulation of PIN1 endocytosis by auxin identifying TIR3/BIG is important auxin transport regulator (Paciorek et al., 2005). A role of both clathrin and BIG protein in the endocytosis of PIN1 was thus established, however still no direct connection was identified.

1.2.4 Constitutive recycling

In plants the TGN is a hub where the re-direction of many trafficking processes takes place (Ito et al., 2012; Groen et al., 2014). It is interconnecting the vesicle communication between the plasma membrane, Golgi apparatus and vacuole, but it is also indirectly connected with the nucleus and ER through the Golgi apparatus. Towards the PM the transport is enabled through endosomes and towards the vacuole through MultiVesicular Bodies/PreVacuolar Compartment (MVB/PVC). The regulation of the sorting into specific trafficking pathways is defined by different GTPases and their regulatory GEFs and GAPs.

The PIN proteins are not statically localized on the plasma membrane, but continuously cycle between their polar domain at the plasma membrane and the endosomes. This conclusion was made from the observation that the fungal toxin BFA causes the accumulation of the PIN1 protein into BFA bodies, which is a reversible process after the removal of BFA (Geldner et al., 2001). BFA acts on the subset of the ARF-GEFs, which are the activators of ARFs, being important for the formation of coated vesicles mediating trafficking processes of the endomembrane system. GNOM is an ARF-GEF, which regulates the endocytic recycling and the polar localization of the PIN proteins. There are severe phenotypes of the *gnom* mutants, such as shorter root length, fused or cup-shaped cotyledons and also inhibited development (Geldner et al., 2004; Richter et al., 2010; Anders and Jürgens, 2008; Koizumi et al., 2000). Through the phenotypic characterization of the *gnom^{R5}* mutant, it was shown that GNOM has an important role for the meristem maintenance (Geldner et al., 2004). In addition, through immunolocalization studies it was observed that the embryo axis formation is defective and

there is a defective PIN1 delivery to the plasma membrane in the *gnom* mutant embryos (Steinmann et al., 1999). Further research on the role of GNOM in the basal delivery of the PIN1 protein was performed by the implementation of BFA (Nebenführ et al., 2002; Geldner et al., 2003). By treatments with different BFA concentrations, it was observed that the polarity of the PIN1 protein is GNOM-dependent (Geldner et al., 2001, 2003). When prolonging the incubation time with BFA, the PIN1 protein moves from the basal to the apical site of the cell in a process known as transcytosis (Kleine-Vehn et al., 2008a). Additionally, there are two other proteins, which are similar to GNOM and they play important role in the early or late protein trafficking. One of them is GNOM LIKE1 (GNL1), which is BFA insensitive and is essential for the endocytosis of the PIN proteins. It is also important for the Golgi apparatus integrity and is a regulator of the trafficking from Golgi to the ER (Teh and Moore, 2007). Another ARF-GEF from GNOM-type is GNOM-LIKE2 (GNL2), which is active in the polar growth of the root hairs and pollen tubes and is able to substitute for GNOM in the process of PIN1 polar recycling (Jia et al., 2009). By the implementation of BFA as a tool to study GNOM-mediated trafficking, we discovered new components of trafficking processes. In the past, there were forward genetic screens, which were based on microscopy of altered sensitivity of PIN localization to BFA, where the role of additional trafficking components was established (Tanaka et al., 2009; Zwiewka and Friml, 2012). In those screens trafficking factors as BFA-visualized endocytic trafficking defective 1 and 2 (BEN1 and BEN2) proteins, which are described as components of the endocytic recycling and vacuolar targeting, were identified (Tanaka et al., 2009, 2013). Moreover, by the implementation of a similar experimental setting, the role of membrane trafficking factors like BFA-visualized EXocytic trafficking defective 1, which plays a role in the endocytic recycling and BEX5, which is a member of the RAB protein family was elucidated (Tanaka et al., 2014; Feraru et al., 2012a). Both factors are regulators of exocytic events and both factors show higher sensitivity to the vesicle trafficking inhibitor BFA and are involved in the process of exocytosis of early endosomes or anterograde vesicles, which are budding from the TGN to the PM.

Another important trafficking regulator is the VAN3 (Vascular Network) protein, which is another member of the GTPase machinery (Koizumi et al., 2000). VAN3 is an ARF-GAP, which activity is pronounced in TGN/EE and the plasma membrane (Koizumi et al., 2005; Naramoto et al., 2009, 2010).

1.2.5 Degradation into vacuoles

On the way to the lytic vacuole, there are the PVC/MVB, known as the late endosomes, which are a sorting hub for receptors and ligands on their way to the vacuole. The trafficking pathway was characterized with the help of chemical inhibitors like wortmannin, which is an inhibitor of phosphatidylinositol 3-kinase (Emans et al., 2002) targeting the PVC-based trafficking (Jaillais et al., 2006). Another compound is BFA, which also affects the vacuolar targeting as the amount of some cargo proteins after treatments is reduced in the lytic vacuole (Kleine-Vehn et al., 2008c). The results show that there is an ARF-GEF mediated, BFA-sensitive trafficking from endosomes to the vacuole (Kleine-Vehn et al., 2008c). Next to this pathway, there is also the requirement for vacuolar-sorting receptors (VSRs), which are recycled (Seaman, 2005) a process, mediated by the retromer, a heteropentameric complex consisting of a dimer of sorting nexin proteins (SNX) and a trimer composed of vacuolar protein sorting (VPS) 26, VPS29 and VPS35 proteins (Seaman, 2005; Bonifacino and Hurley, 2008; Collins, 2008). SNX1 and VPS29 participate in the recycling of PIN2 (Jaillais et al., 2006) and PIN1 (Jaillais et al., 2007) at the plasma membrane.

Another role of SNX1 and VPS29 is in a pathway that retrieves PIN proteins from the PVC back to the recycling pathways, thus keeping the balance between vacuolar targeting and recycling of PIN proteins (Jürgens and Geldner, 2007; Kleine-Vehn et al., 2008c). To enable the incorporation of the PVC/MVB with the lumen for the lytic degradation in the vacuole, there is the endosomal-sorting complex, required for transport (ESCRT) machinery (Piper and Katzmann, 2007), which counteracts the function of the retromer. The retromer transports transmembrane proteins from the endosomal membrane and returns them to the TGN, on the other hand, there are ESCRT proteins, which sort the target proteins from the membrane into the lumen of the endosomes.

1.2.6 Phosphorylation-related signals for polar targeting

The mutant *pinoid* (*pid*) was identified in a screen for mutants that have lost their ability to build flower primordia (Bennett et al., 1995). The protein encodes a member of the AGCVIII family of protein kinases (Christensen et al., 2000) and it has a function in auxin transport (Benjamins et al., 2001). When overexpressing the protein, the main root collapsed, which was correlated with the loss of local auxin maximum in the root apex (Benjamins et al., 2001; Friml et al., 2004). In the shoot apical meristem of the *pid* mutant, there is the apical-to-basal polarity switch of the PIN1 protein (Friml et al., 2004), which confirms the function of the PID protein in the PIN apical versus basal polarity determination. The action of PID and its homologs is to phosphorylate the PIN protein hydrophilic loops at three highly conserved motifs (Michniewicz et al., 2007; Huang et al., 2010; Zhang et al., 2010). Next to the PID activity, there is the phosphatase activity of the protein phosphatase 2A (PP2A), which is essential for the PIN polarity regulation. In the PP2AA-deficient plants, there is a basal-to-apical polarity shift of PIN1, PIN2 and PIN4, which indicates that the dephosphorylation of the PINs promotes basal localization (Michniewicz et al., 2007). In summary, the PID-mediated phosphorylation promotes the PIN localization to the apical cell side and the dephosphorylation by PP2A leads to basal PIN polarity (Adamowski and Friml, 2015).

There is also another group of proteins from the same family of protein kinases, which includes D6 protein kinase (D6PK) and D6 protein kinase-likes (D6PKL), which are also important factors for the polar auxin transport. Loss of the activity resulted in phenotypes, which correspond to phenotypes, typical for the reduced PAT rates (Zourelidou et al., 2014; Willige et al., 2013). D6PK phosphorylates the PIN proteins, but does not affect their polar localization (Willige et al., 2013) and it activates the auxin efflux activity of the PINs.

1.2.7 Auxin feedback regulation of PIN-mediated auxin transport

Tsvi Sachs proposed a self-organizing property for polar auxin transport on the level of organs and tissues, which is known as the canalization hypothesis (Sachs, 1981). If there is a source and a sink of auxin, then the cells polarize their auxin transport activities towards neighbors, which already transport auxin. Thus, the local flow of auxin affects the cells to alter the

direction of the flow and strength, which forms a narrow and well-defined canal of cells, which efficiently transport auxin to connect the source with the sink. The canalization hypothesis is important for processes like *de novo* vascular tissue formation or its regeneration. The parts of the plant body will be connected by the cells, forming the canals for polar auxin transport, which will differentiate into stele cells. As a result, auxin has the property to influence the directionality and capacity of a cell's auxin transport. (Sauer et al., 2006) designed experiments on wounded pea epicotyls (*Pisum sativum*) to study the auxin flow on the example of the PIN1 protein, which polarized around the wound, which later differentiated to reconnect the vascular strand. The PIN proteins are good candidates as target for the canalization mechanism as auxin is regulating their localization and expression (Adamowski and Friml, 2015).

1.3 Summary

A large spectrum of developmental processes are regulated by auxin (Friml et al., 2003). The auxin efflux carriers of the PIN family have a polar, plasma membrane localization and they determine the direction of the auxin flow, which modulates different aspects of development, including gravitropism, phototropism, embryogenesis, organogenesis, vascular tissue formation and regeneration as well as others (Vanneste and Friml, 2009). For the fulfillment of their diverse roles, the PIN proteins are regulated by different factors at the levels of transcription as well as cellular polar, subcellular localization, which results from trafficking processes like secretion, endocytosis, recycling, and vacuolar trafficking. Endogenous signals, including auxin and other hormones, like strigolactone, have impact on the regulatory steps in order to fine-tune PIN localization and function (Shinohara et al., 2013). In summary, plants have developed specific mechanisms, in which endogenous and exogenous signals, regulate the PIN trafficking and the auxin distribution, which provides guidelines for many aspects of growth and development (Adamowski and Friml, 2015).

1.4 References

- Adamowski, M. and Friml, J.** (2015). PIN-dependent auxin transport: action, regulation, and evolution. *Plant Cell* **27**: 20–32.
- Adamowski, M., Narasimhan, M., Kania, U., Glanc, M., De Jaeger, G., and Friml, J.** (2018). A Functional Study of AUXILIN-LIKE1 and 2, Two Putative Clathrin Uncoating Factors in Arabidopsis. *Plant Cell* **30**: 700 LP – 716.
- Agusti, J., Herold, S., Schwarz, M., Sanchez, P., Ljung, K., Dun, E.A., Brewer, P.B., Beveridge, C.A., Sieberer, T., Sehr, E.M., and Greb, T.** (2011). Strigolactone signaling is required for auxin-dependent stimulation of secondary growth in plants. *Proc. Natl. Acad. Sci.* **108**: 20242 LP – 20247.
- Akiyama, K., Matsuzaki, K., and Hayashi, H.** (2005). Plant sesquiterpenes induce hyphal branching in arbuscular mycorrhizal fungi. *Nature* **435**: 824–827.
- Anders, N. and Jürgens, G.** (2008). Large ARF guanine nucleotide exchange factors in membrane trafficking. *Cell. Mol. Life Sci.* **65**: 3433–3445.
- Baisa, G.A., Mayers, J.R., and Bednarek, S.Y.** (2013). Budding and braking news about clathrin-mediated endocytosis. *Curr. Opin. Plant Biol.* **16**: 718–725.
- Balla, J., Kalousek, P., Reinöhl, V., Friml, J., and Procházka, S.** (2011). Competitive canalization of PIN-dependent auxin flow from axillary buds controls pea bud outgrowth. *Plant J.* **65**: 571–577.
- Banbury, D.N., Oakley, J.D., Sessions, R.B., and Banting, G.** (2003). Tyrphostin A23 Inhibits Internalization of the Transferrin Receptor by Perturbing the Interaction between Tyrosine Motifs and the Medium Chain Subunit of the AP-2 Adaptor Complex. *J. Biol. Chem.* **278**: 12022–12028.
- Bandmann, V. and Homann, U.** (2012). Clathrin-independent endocytosis contributes to uptake of glucose into BY-2 protoplasts. *Plant J.* **70**: 578–584.
- Bar-Peled, M., Conceicao, A., Frigerio, L., and Raikhel, N. V** (1995). Expression and Regulation of aERD2, a Gene Encoding the KDEL Receptor Homolog in Plants, and Other Genes Encoding Proteins Involved in ER-Golgi Vesicular Trafficking. *Plant Cell* **7**: 667 LP – 676.
- Baral, A., Irani, N.G., Fujimoto, M., Nakano, A., Mayor, S., and Mathew, M.K.** (2015). Salt-Induced Remodeling of Spatially Restricted Clathrin-Independent Endocytic Pathways in

- Arabidopsis Root. *Plant Cell* **27**: 1297 LP – 1315.
- Barbez, E. et al.** (2012). A novel putative auxin carrier family regulates intracellular auxin homeostasis in plants. *Nature* **485**: 119.
- Barbez, E., Laňková, M., Pařezová, M., Maizel, A., Zařímalová, E., Petrášek, J., Friml, J., and Kleine-Vehn, J.** (2013). Single-cell-based system to monitor carrier driven cellular auxin homeostasis. *BMC Plant Biol.* **13**: 20.
- Bargmann, B.O.R., Vanneste, S., Krouk, G., Nawy, T., Efroni, I., Shani, E., Choe, G., Friml, J., Bergmann, D.C., Estelle, M., and Birnbaum, K.D.** (2013). A map of cell type-specific auxin responses. *Mol. Syst. Biol.* **9**: 688.
- Bauly, J.M., Sealy, I.M., Macdonald, H., Brearley, J., Dröge, S., Hillmer, S., Robinson, D.G., Venis, M.A., Blatt, M.R., Lazarus, C.M., and Napier, R.M.** (2000). Overexpression of auxin-binding protein enhances the sensitivity of guard cells to auxin. *Plant Physiol.* **124**: 1229–1238.
- Benjamins, R., Quint, A., Weijers, D., Hooykaas, P., and Offringa, R.** (2001). The PINOID protein kinase regulates organ development in *Arabidopsis* by enhancing polar auxin transport. *Development* **128**: 4057 LP – 4067.
- Benkova, E., Michniewicz, M., Sauer, M., Teichmann, T., and Pflanz, M.** (2003). Local, Efflux-Dependent Auxin Gradients as a Common Module for Plant Organ Formation. *Plant Cell* **15**: 591–602.
- Bennett, S.R.M., Alvarez, J., Bossinger, G., and Smyth, D.R.** (1995). Morphogenesis in pinoid mutants of *Arabidopsis thaliana*. *Plant J.* **8**: 505–520.
- Bennett, T. and Leyser, O.** (2014). Strigolactone signalling: standing on the shoulders of DWARFs. *Curr. Opin. Plant Biol.* **22**: 7–13.
- Bennett, T., Liang, Y., Seale, M., Ward, S., Müller, D., and Leyser, O.** (2016). Strigolactone regulates shoot development through a core signalling pathway. *Biol. Open* **5**: 1806 LP – 1820.
- Bertosa, B., Kojić-Prodić, B., Wade, R.C., and Tomić, S.** (2008). Mechanism of auxin interaction with Auxin Binding Protein (ABP1): a molecular dynamics simulation study. *Biophys. J.* **94**: 27–37.
- Bhalerao, R.P., Eklöf, J., Ljung, K., Marchant, A., Bennett, M., and Sandberg, G.** (2002). Shoot-derived auxin is essential for early lateral root emergence in *Arabidopsis* seedlings. *Plant J.* **29**: 325–332.

- Blilou, I., Xu, J., Wildwater, M., Willemsen, V., Paponov, I., Friml, J., Heidstra, R., Aida, M., Palme, K., and Scheres, B.** (2005). The PIN auxin efflux facilitator network controls growth and patterning in Arabidopsis roots. *Nature* **433**: 39–44.
- Boer, D.R., Freire-Rios, A., van den Berg, W.A.M., Saaki, T., Manfield, I.W., Kepinski, S., López-Vidrieo, I., Franco-Zorrilla, J.M., de Vries, S.C., Solano, R., Weijers, D., and Coll, M.** (2014). Structural Basis for DNA Binding Specificity by the Auxin-Dependent ARF Transcription Factors. *Cell* **156**: 577–589.
- Bonifacio, J.S. and Hurley, J.H.** (2008). Retromer. *Curr. Opin. Cell Biol.* **20**: 427–436.
- Bonifacio, J.S. and Lippincott-Schwartz, J.** (2003). Coat proteins: shaping membrane transport. *Nat. Rev. Mol. Cell Biol.* **4**: 409–414.
- Booker, J., Sieberer, T., Wright, W., Williamson, L., Willett, B., Stirnberg, P., Turnbull, C., Srinivasan, M., Goddard, P., and Leyser, O.** (2005). MAX1 Encodes a Cytochrome P450 Family Member that Acts Downstream of MAX3/4 to Produce a Carotenoid-Derived Branch-Inhibiting Hormone. *Dev. Cell* **8**: 443–449.
- Borden, K.L.** (2000). RING domains: master builders of molecular scaffolds? *J. Mol. Biol.* **295**: 1103–1112.
- Bosco, C.D. et al.** (2012). The endoplasmic reticulum localized PIN8 is a pollen-specific auxin carrier involved in intracellular auxin homeostasis. *Plant J.* **71**: 860–870.
- Bradshaw, T.Y., Romano, L.E.L., Duncan, E.J., Nethisinghe, S., Abeti, R., Michael, G.J., Giunti, P., Vermeer, S., and Chapple, J.P.** (2016). A reduction in Drp1-mediated fission compromises mitochondrial health in autosomal recessive spastic ataxia of Charlevoix Saguenay. *Hum. Mol. Genet.* **25**: 3232–3244.
- Brandizzi, F. and Barlowe, C.** (2013). Organization of the ER-Golgi interface for membrane traffic control. *Nat. Rev. Mol. Cell Biol.* **14**: 382–392.
- Braun, N., Wyrzykowska, J., Muller, P., David, K., Couch, D., Perrot-Rechenmann, C., and Fleming, A.J.** (2008). Conditional repression of AUXIN BINDING PROTEIN1 reveals that it coordinates cell division and cell expansion during postembryonic shoot development in Arabidopsis and tobacco. *Plant Cell* **20**: 2746–2762.
- Brown, J.C. and Jones, A.M.** (1994). Mapping the auxin-binding site of auxin-binding protein 1. *J. Biol. Chem.* **269**: 21136–21140.
- Calderón Villalobos, L.I.A. et al.** (2012). A combinatorial TIR1/AFB-Aux/IAA co-receptor system for differential sensing of auxin. *Nat. Chem. Biol.* **8**: 477–485.

- Camp, P.J. and Randall, D.D.** (1985). Purification and Characterization of the Pea Chloroplast Pyruvate Dehydrogenase Complex : A Source of Acetyl-CoA and NADH for Fatty Acid Biosynthesis. *Plant Physiol.* **77**: 571–577.
- Cao, M. et al.** (2019). TMK1-mediated auxin signalling regulates differential growth of the apical hook. *Nature* **568**: 240–243.
- Casimiro, I., Beeckman, T., Graham, N., Bhalerao, R., Zhang, H., Casero, P., Sandberg, G., and Bennett, M.J.** (2003). Dissecting Arabidopsis lateral root development. *Trends Plant Sci.* **8**: 165–171.
- Casimiro, I., Marchant, A., Bhalerao, R.P., Beeckman, T., Dhooge, S., Swarup, R., Graham, N., Inzé, D., Sandberg, G., Casero, P.J., and Bennett, M.** (2001). Auxin transport promotes Arabidopsis lateral root initiation. *Plant Cell* **13**: 843–852.
- Cevher-Keskin, B.** (2013). ARF1 and SAR1 GTPases in endomembrane trafficking in plants. *Int. J. Mol. Sci.* **14**: 18181–18199.
- Chen, J.G., Ullah, H., Young, J.C., Sussman, M.R., and Jones, A.M.** (2001). ABP1 is required for organized cell elongation and division in Arabidopsis embryogenesis. *Genes Dev.* **15**: 902–911.
- Chen, R., Hilson, P., Sedbrook, J., Rosen, E., Caspar, T., and Masson, P.H.** (1998). The arabidopsis thaliana AGRVITROPIC 1 gene encodes a component of the polar-auxin-transport efflux carrier. *Proc. Natl. Acad. Sci. U. S. A.* **95**: 15112–15117.
- Chen, X., Grandont, L., Li, H., Hauschild, R., Paque, S., Abuzeineh, A., Rakusová, H., Benkova, E., Perrot-Rechenmann, C., and Friml, J.** (2014). Inhibition of cell expansion by rapid ABP1-mediated auxin effect on microtubules. *Nature* **516**: 90–93.
- Chen, X., Irani, N.G., and Friml, J.** (2011). Clathrin-mediated endocytosis: the gateway into plant cells. *Curr. Opin. Plant Biol.* **14**: 674–682.
- Chen, X., Naramoto, S., Robert, S., Tejos, R., Löffke, C., Lin, D., Yang, Z., and Friml, J.** (2012). ABP1 and ROP6 GTPase Signaling Regulate Clathrin-Mediated Endocytosis in Arabidopsis Roots. *Curr. Biol.* **22**: 1326–1332.
- Cheng, Y., Dai, X., and Zhao, Y.** (2006). Auxin biosynthesis by the YUCCA flavin monooxygenases controls the formation of floral organs and vascular tissues in Arabidopsis. *Genes Dev.* **20**: 1790–1799.
- Cho, M. and Cho, H.-T.** (2013). The function of ABCB transporters in auxin transport. *Plant Signal. Behav.* **8**: e22990–e22990.

- Christensen, S.K., Dagenais, N., Chory, J., and Weigel, D.** (2000). Regulation of Auxin Response by the Protein Kinase PINOID. *Cell* **100**: 469–478.
- Clough, S.J. and Bent, A.F.** (1998). Floral dip: a simplified method for *Agrobacterium* - mediated transformation of *Arabidopsis thaliana*. *Plant J.* **16**: 735–743.
- Collins, B.M.** (2008). The Structure and Function of the Retromer Protein Complex. *Traffic* **9**: 1811–1822.
- Cook, C.E., Whichard, L.P., Turner, B., Wall, M.E., and Egley, G.H.** (1966). Germination of Witchweed (*Striga lutea* Lour.): Isolation and Properties of a Potent Stimulant. *Science* (80-). **154**: 1189 LP – 1190.
- Čovanová, M., Sauer, M., Rychtář, J., Friml, J., Petrášek, J., and Zažímalová, E.** (2013). Overexpression of the Auxin Binding PROTEIN1 Modulates PIN-Dependent Auxin Transport in Tobacco Cells. *PLoS One* **8**: e70050.
- Crawford, S., Shinohara, N., Sieberer, T., Williamson, L., George, G., Hepworth, J., Müller, D., Domagalska, M.A., and Leyser, O.** (2010). Strigolactones enhance competition between shoot branches by dampening auxin transport. *Development* **137**: 2905 LP – 2913.
- Cross, J.W. and Briggs, W.R.** (1978). Auxin receptors of maize coleoptile membranes do not have ATPase activity. *Plant Physiol.* **61**: 581–584.
- Cross, J.W. and Briggs, W.R.** (1979). *Planta*. **270**: 263–264.
- Crump, C.M., Williams, J.L., Stephens, D.J., and Banting, G.** (1998). Inhibition of the Interaction between Tyrosine-based Motifs and the Medium Chain Subunit of the AP-2 Adaptor Complex by Specific Tyrostatins. *J. Biol. Chem.* **273**: 28073–28077.
- Cvrčková, F., Grunt, M., Bezdová, R., Hála, M., Kulich, I., Rawat, A., and Zárský, V.** (2012). Evolution of the land plant exocyst complexes. *Front. Plant Sci.* **3**: 159.
- Dai, M. et al.** (2012). A PP6-Type Phosphatase Holoenzyme Directly Regulates PIN Phosphorylation and Auxin Efflux in *Arabidopsis*. *Plant Cell* **24**: 2497 LP – 2514.
- Dai, X., Zhang, Y., Zhang, D., Chen, J., Gao, X., Estelle, M., and Zhao, Y.** (2015). Embryonic lethality of *Arabidopsis* *abp1-1* is caused by deletion of the adjacent *BSM* gene. *Nat. Plants* **1**: 15183.
- Dannhauser, P.N. and Ungewickell, E.J.** (2012). Reconstitution of clathrin-coated bud and vesicle formation with minimal components. *Nat. Cell Biol.* **14**: 634.

- Darwin, C.** (2009). *The Power of Movement in Plants* (Cambridge University Press: Cambridge).
- Dejonghe, W. et al.** (2019). Disruption of endocytosis through chemical inhibition of clathrin heavy chain function. *Nat. Chem. Biol.* **15**: 641–649.
- Dejonghe, W. et al.** (2016). Mitochondrial uncouplers inhibit clathrin-mediated endocytosis largely through cytoplasmic acidification. *Nat. Commun.* **7**: 11710.
- Dettmer, J., Hong-Hermesdorf, A., Stierhof, Y.-D., and Schumacher, K.** (2006). Vacuolar H⁺-ATPase activity is required for endocytic and secretory trafficking in Arabidopsis. *Plant Cell* **18**: 715–730.
- Dharmasiri, N., Dharmasiri, S., and Estelle, M.** (2005). The F-box protein TIR1 is an auxin receptor. *Nature* **435**: 441–445.
- Dhonukshe, P., Aniento, F., Hwang, I., Robinson, D.G., Mravec, J., Stierhof, Y.-D., and Friml, J.** (2007). Clathrin-Mediated Constitutive Endocytosis of PIN Auxin Efflux Carriers in Arabidopsis. *Curr. Biol.* **17**: 520–527.
- Diekmann, W., Venis, M.A., and Robinson, D.G.** (1995). Auxins induce clustering of the auxin-binding protein at the surface of maize coleoptile protoplasts. *Proc. Natl. Acad. Sci. U. S. A.* **92**: 3425–3429.
- Ding, Z. et al.** (2012). ER-localized auxin transporter PIN8 regulates auxin homeostasis and male gametophyte development in Arabidopsis. *Nat. Commun.* **3**: 941.
- Ding, Z., Galván-Ampudia, C.S., Demarsy, E., Łangowski, Ł., Kleine-Vehn, J., Fan, Y., Morita, M.T., Tasaka, M., Fankhauser, C., Offringa, R., and Friml, J.** (2011). Light-mediated polarization of the PIN3 auxin transporter for the phototropic response in Arabidopsis. *Nat. Cell Biol.* **13**: 447.
- Drdová, E.J., Synek, L., Pečenková, T., Hála, M., Kulich, I., Fowler, J.E., Murphy, A.S., and Žárský, V.** (2013). The exocyst complex contributes to PIN auxin efflux carrier recycling and polar auxin transport in Arabidopsis. *Plant J.* **73**: 709–719.
- Du, Y., Tejos, R., Beck, M., Himschoot, E., Li, H., Robatzek, S., Vanneste, S., and Friml, J.** (2013). Salicylic acid interferes with clathrin-mediated endocytic protein trafficking. *Proc. Natl. Acad. Sci. U. S. A.* **110**: 7946–7951.
- Dubrovsky, J.G., Sauer, M., Napsucialy-Mendivil, S., Ivanchenko, M.G., Friml, J., Shishkova, S., Celenza, J., and Benková, E.** (2008). Auxin acts as a local morphogenetic trigger to specify lateral root founder cells. *Proc. Natl. Acad. Sci. U. S. A.* **105**: 8790–8794.

- Efroni, I. and Birnbaum, K.D.** (2016). The potential of single-cell profiling in plants. *Genome Biol.* **17**: 65.
- Elias, M., Drdova, E., Ziak, D., Bavlnka, B., Hala, M., Cvrckova, F., Soukupova, H., and Zarsky, V.** (2003). The exocyst complex in plants. *Cell Biol. Int.* **27**: 199–201.
- Elkin, S.R., Oswald, N.W., Reed, D.K., Mettlen, M., MacMillan, J.B., and Schmid, S.L.** (2016). Ikarugamycin: A Natural Product Inhibitor of Clathrin-Mediated Endocytosis. *Traffic* **17**: 1139–1149.
- Emans, N., Zimmermann, S., and Fischer, R.** (2002). Uptake of a fluorescent marker in plant cells is sensitive to brefeldin A and wortmannin. *Plant Cell* **14**: 71–86.
- Enders, T.A., Oh, S., Yang, Z., Montgomery, B.L., and Strader, L.C.** (2015). Genome Sequencing of *Arabidopsis* *abp1-5* Reveals Second-Site Mutations That May Affect Phenotypes. *Plant Cell* **27**: 1820–1826.
- Fan, L., Li, R., Pan, J., Ding, Z., and Lin, J.** (2015). Endocytosis and its regulation in plants. *Trends Plant Sci.* **20**: 388–397.
- Fendrych, M., Synek, L., Pecenková, T., Drdová, E.J., Sekeres, J., de Rycke, R., Nowack, M.K., and Zársky, V.** (2013). Visualization of the exocyst complex dynamics at the plasma membrane of *Arabidopsis thaliana*. *Mol. Biol. Cell* **24**: 510–520.
- Feraru, E., Feraru, M.I., Asaoka, R., Paciorek, T., De Rycke, R., Tanaka, H., Nakano, A., and Friml, J.** (2012a). BEX5/RabA1b regulates trans-Golgi network-to-plasma membrane protein trafficking in *Arabidopsis*. *Plant Cell* **24**: 3074–3086.
- Feraru, E., Vosolsobě, S., Feraru, M.I., Petrášek, J., and Kleine-Vehn, J.** (2012b). Evolution and Structural Diversification of PILS Putative Auxin Carriers in Plants. *Front. Plant Sci.* **3**: 227.
- Flematti, G.R., Ghisalberti, E.L., Dixon, K.W., and Trengove, R.D.** (2004). A Compound from Smoke That Promotes Seed Germination. *Science* (80-.). **305**: 977 LP – 977.
- Flematti, G.R., Waters, M.T., Scaffidi, A., Merritt, D.J., Ghisalberti, E.L., Dixon, K.W., and Smith, S.M.** (2013). Karrikin and Cyanohydrin Smoke Signals Provide Clues to New Endogenous Plant Signaling Compounds. *Mol. Plant* **6**: 29–37.
- Freemont, P.S., Hanson, I.M., and Trowsdale, J.** (1991). A novel cysteine-rich sequence motif. *Cell* **64**: 483–484.
- Friml, J. et al.** (2004). A PINOID-Dependent Binary Switch in Apical-Basal PIN Polar Targeting Directs Auxin Efflux. *Science* (80-.). **306**: 862 LP – 865.

- Friml, J., Benková, E., Blilou, I., Wisniewska, J., Hamann, T., Ljung, K., Woody, S., Sandberg, G., Scheres, B., Jürgens, G., and Palme, K.** (2002a). AtPIN4 Mediates Sink-Driven Auxin Gradients and Root Patterning in *Arabidopsis*. *Cell* **108**: 661–673.
- Friml, J., Vieten, A., Sauer, M., Weijers, D., Schwarz, H., Hamann, T., Offringa, R., and Jürgens, G.** (2003). Efflux-dependent auxin gradients establish the apical–basal axis of *Arabidopsis*. *Nature* **426**: 147–153.
- Friml, J., Wiśniewska, J., Benková, E., Mendgen, K., and Palme, K.** (2002b). Lateral relocation of auxin efflux regulator PIN3 mediates tropism in *Arabidopsis*. *Nature* **415**: 806–809.
- Gadeyne, A. et al.** (2014). The TPLATE Adaptor Complex Drives Clathrin-Mediated Endocytosis in Plants. *Cell* **156**: 691–704.
- Gälweiler, L., Guan, C., Müller, A., Wisman, E., Mendgen, K., Yephremov, A., and Palme, K.** (1998). Regulation of Polar Auxin Transport by AtPIN1 in *Arabidopsis* Vascular Tissue. *Science* (80-.). **282**: 2226 LP – 2230.
- Gao, Y., Zhang, Y., Zhang, D., Dai, X., Estelle, M., and Zhao, Y.** (2015). Auxin binding protein 1 (ABP1) is not required for either auxin signaling or *Arabidopsis* development. *Proc. Natl. Acad. Sci. U. S. A.* **112**: 2275–2280.
- Garbers, C., DeLong, A., Deruère, J., Bernasconi, P., and Söll, D.** (1996). A mutation in protein phosphatase 2A regulatory subunit A affects auxin transport in *Arabidopsis*. *EMBO J.* **15**: 2115–2124.
- Gehring, C., Mcconchie, R., A. Venis, M., and Parish, R.** (1998). Auxin-binding-protein antibodies and peptides influence stomatal opening and alter cytoplasmic pH.
- Geisler, M., Wang, B., and Zhu, J.** (2014). Auxin transport during root gravitropism: transporters and techniques. *Plant Biol.* **16**: 50–57.
- Geldner, N., Anders, N., Wolters, H., Keicher, J., Kornberger, W., Muller, P., Delbarre, A., Ueda, T., Nakano, A., and Jürgens, G.** (2003). The *Arabidopsis* GNOM ARF-GEF Mediates Endosomal Recycling, Auxin Transport, and Auxin-Dependent Plant Growth. *Cell* **112**: 219–230.
- Geldner, N., Friml, J., Stierhof, Y.-D., Jürgens, G., and Palme, K.** (2001). Auxin transport inhibitors block PIN1 cycling and vesicle trafficking. *Nature* **413**: 425–428.
- Geldner, N., Richter, S., Vieten, A., Marquardt, S., Torres-Ruiz, R.A., Mayer, U., and Jürgens, G.** (2004). Partial loss-of-function alleles reveal a role for GNOM in auxin transport-related, post-embryonic development of *Arabidopsis*. *Development* **131**: 389–400.

- Gil, P., Dewey, E., Friml, J., Zhao, Y., Snowden, K.C., Putterill, J., Palme, K., Estelle, M., and Chory, J.** (2001). BIG: a calossin-like protein required for polar auxin transport in *Arabidopsis*. *Genes Dev.* **15**: 1985–1997.
- Goldsmith, M.H.M.** (1977). The Polar Transport of Auxin. *Annu. Rev. Plant Physiol.* **28**: 439–478.
- Gomez-Roldan, V. et al.** (2008). Strigolactone inhibition of shoot branching. *Nature* **455**: 189.
- Grandits, M. and Oostenbrink, C.** (2014). Molecular dynamics simulations of the auxin-binding protein 1 in complex with indole-3-acetic acid and naphthalen-1-acetic acid. *Proteins Struct. Funct. Bioinforma.* **82**: 2744–2755.
- Gray, W.M., Kepinski, S., Rouse, D., Leyser, O., and Estelle, M.** (2001). Auxin regulates SCFTIR1-dependent degradation of AUX/IAA proteins. *Nature* **414**: 271–276.
- Grigoriev, A. and Biotech, G.P.C.** (2001). A relationship between gene expression and protein interactions on the proteome scale : analysis of the bacteriophage T7 and the yeast *Saccharomyces cerevisiae*. **29**: 3513–3519.
- Groen, A.J., Sancho-Andrés, G., Breckels, L.M., Gatto, L., Aniento, F., and Lilley, K.S.** (2014). Identification of trans-golgi network proteins in *Arabidopsis thaliana* root tissue. *J. Proteome Res.* **13**: 763–776.
- Grones, P., Chen, X., Simon, S., Kaufmann, W.A., De Rycke, R., Nodzyński, T., Zažímalová, E., and Friml, J.** (2015). Auxin-binding pocket of ABP1 is crucial for its gain-of-function cellular and developmental roles. *J. Exp. Bot.* **66**: 5055–5065.
- Grones, P. and Friml, J.** (2015). Auxin transporters and binding proteins at a glance. *J. Cell Sci.* **128**: 1 LP – 7.
- Grosshans, B.L., Ortiz, D., and Novick, P.** (2006). Rabs and their effectors: achieving specificity in membrane traffic. *Proc. Natl. Acad. Sci. U. S. A.* **103**: 11821–11827.
- Grunewald, W. and Friml, J.** (2010). The march of the PINs: developmental plasticity by dynamic polar targeting in plant cells. *EMBO J.* **29**: 2700–2714.
- Habets, M.E.J. and Offringa, R.** (2015). Auxin Binding Protein 1: A Red Herring After All? *Mol. Plant* **8**: 1131–1134.
- Hála, M., Cole, R., Synek, L., Drdová, E., Pečenková, T., Nordheim, A., Lamkemeyer, T., Madlung, J., Hochholdinger, F., Fowler, J.E., and Žárský, V.** (2008). An Exocyst Complex Functions in Plant Cell Growth in *Arabidopsis* and Tobacco. *Plant Cell* **20**: 1330 LP – 1345.

- Hanton, S.L., Matheson, L.A., Chatre, L., and Brandizzi, F.** (2009). Dynamic organization of COPII coat proteins at endoplasmic reticulum export sites in plant cells. *Plant J.* **57**: 963–974.
- Hayward, A., Stirnberg, P., Beveridge, C., and Leyser, O.** (2009). Interactions between Auxin and Strigolactone in Shoot Branching Control. *Plant Physiol.* **151**: 400 LP – 412.
- Hicks, G.R. and Raikhel, N. V** (2012). Small Molecules Present Large Opportunities in Plant Biology. *Annu. Rev. Plant Biol.* **63**: 261–282.
- Hruz, T., Laule, O., Szabo, G., Wessendorp, F., Bleuler, S., Oertle, L., Widmayer, P., Gruissem, W., and Zimmermann, P.** (2008). Genevestigator V3: A Reference Expression Database for the Meta-Analysis of Transcriptomes. *Adv. Bioinformatics* **2008**: 1–5.
- Huang, F., Kemel Zago, M., Abas, L., van Marion, A., Galván-Ampudia, C.S., and Offringa, R.** (2010). Phosphorylation of Conserved PIN Motifs Directs *Arabidopsis* PIN1 Polarity and Auxin Transport. *Plant Cell* **22**: 1129 LP – 1142.
- Inohara, N., Shimomura, S., Fukui, T., and Futai, M.** (1989). Auxin-binding protein located in the endoplasmic reticulum of maize shoots: molecular cloning and complete primary structure. *Proc. Natl. Acad. Sci. U. S. A.* **86**: 3564–3568.
- Ito, E., Fujimoto, M., Ebine, K., Uemura, T., Ueda, T., and Nakano, A.** (2012). Dynamic behavior of clathrin in *Arabidopsis thaliana* unveiled by live imaging. *Plant J.* **69**: 204–216.
- Jaillais, Y., Fobis-Loisy, I., Miège, C., Rollin, C., and Gaude, T.** (2006). AtSNX1 defines an endosome for auxin-carrier trafficking in *Arabidopsis*.
- Jaillais, Y., Santambrogio, M., Rozier, F., Fobis-Loisy, I., Miège, C., and Gaude, T.** (2007). The Retromer Protein VPS29 Links Cell Polarity and Organ Initiation in Plants. *Cell* **130**: 1057–1070.
- Jain, N., Kulkarni, M.G., and van Staden, J.** (2006). A butenolide, isolated from smoke, can overcome the detrimental effects of extreme temperatures during tomato seed germination. *Plant Growth Regul.* **49**: 263–267.
- Jander, G.** (2006). Gene Identification and Cloning by Molecular Marker Mapping. In *Arabidopsis Protocols*, J. Salinas and J.J. Sanchez-Serrano, eds (Humana Press: Totowa, NJ), pp. 115–126.
- Jelínková, A., Malínská, K., Simon, S., Kleine-Vehn, J., Pařezová, M., Pejchar, P., Kubeš, M.,**

- Martinec, J., Friml, J., Zažímalová, E., and Petrášek, J.** (2010). Probing plant membranes with FM dyes: tracking, dragging or blocking? *Plant J.* **61**: 883–892.
- Jia, D.-J., Cao, X., Wang, W., Tan, X.-Y., Zhang, X.-Q., Chen, L.-Q., and Ye, D.** (2009). GNOM-LIKE 2, Encoding an Adenosine Diphosphate-Ribosylation Factor-Guanine Nucleotide Exchange Factor Protein Homologous to GNOM and GNL1, is Essential for Pollen Germination in Arabidopsis. *J. Integr. Plant Biol.* **51**: 762–773.
- Jones, A.M. and Herman, E.M.** (1993). KDEL-Containing Auxin-Binding Protein Is Secreted to the Plasma Membrane and Cell Wall. *Plant Physiol.* **101**: 595–606.
- Jones, A.M., Im, K.-H., Savka, M.A., Wu, M.-J., DeWitt, N.G., Shillito, R., and Binns, A.N.** (1998). Auxin-Dependent Cell Expansion Mediated by Overexpressed Auxin-Binding Protein 1. *Science* (80-.). **282**: 1114 LP – 1117.
- Jurado, S., Abraham, Z., Manzano, C., López-Torrejón, G., Pacios, L.F., and Del Pozo, J.C.** (2010). The Arabidopsis cell cycle F-box protein SKP2A binds to auxin. *Plant Cell* **22**: 3891–3904.
- Jürgens, G. and Geldner, N.** (2007). The High Road and the Low Road: Trafficking Choices in Plants. *Cell* **130**: 977–979.
- Kai, K., Horita, J., Wakasa, K., and Miyagawa, H.** (2007). Three oxidative metabolites of indole-3-acetic acid from Arabidopsis thaliana. *Phytochemistry* **68**: 1651–1663.
- Kang, B.-H. and Staehelin, L.A.** (2008). ER-to-Golgi transport by COPII vesicles in Arabidopsis involves a ribosome-excluding scaffold that is transferred with the vesicles to the Golgi matrix. *Protoplasma* **234**: 51–64.
- Kania, U. et al.** (2018). The Inhibitor Endosidin 4 Targets SEC7 Domain-Type ARF GTPase Exchange Factors and Interferes with Subcellular Trafficking in Eukaryotes. *Plant Cell* **30**: 2553 LP – 2572.
- Kapulnik, Y. et al.** (2011). Strigolactones affect lateral root formation and root-hair elongation in Arabidopsis. *Planta* **233**: 209–216.
- Kasahara, H.** (2016). Current aspects of auxin biosynthesis in plants. *Biosci. Biotechnol. Biochem.* **80**: 34–42.
- Kepinski, S. and Leyser, O.** (2004). Auxin-induced SCFTIR1-Aux/IAA interaction involves stable modification of the SCFTIR1 complex. *Proc. Natl. Acad. Sci. U. S. A.* **101**: 12381–12386.
- Kirchhausen, T.** (2009). Imaging endocytic clathrin structures in living cells. *Trends Cell Biol.* **19**: 596–605.

- Kitakura, S., Adamowski, M., Matsuura, Y., Santuari, L., Kouno, H., Arima, K., Hardtke, C.S., Friml, J., Kakimoto, T., and Tanaka, H.** (2017). BEN3/BIG2 ARF GEF is Involved in Brefeldin A-Sensitive Trafficking at the trans-Golgi Network/Early Endosome in *Arabidopsis thaliana*. *Plant Cell Physiol.* **58**: 1801–1811.
- Kitakura, S., Vanneste, S., Robert, S., Löffke, C., Teichmann, T., Tanaka, H., and Friml, J.** (2011). Clathrin mediates endocytosis and polar distribution of PIN auxin transporters in *Arabidopsis*. *Plant Cell* **23**: 1920–1931.
- Kleine-Vehn, J., Dhonukshe, P., Sauer, M., Brewer, P.B., Wiśniewska, J., Paciorek, T., Benková, E., and Friml, J.** (2008a). ARF GEF-Dependent Transcytosis and Polar Delivery of PIN Auxin Carriers in *Arabidopsis*. *Curr. Biol.* **18**: 526–531.
- Kleine-Vehn, J., Ding, Z., Jones, A.R., Tasaka, M., Morita, M.T., and Friml, J.** (2010). Gravity-induced PIN transcytosis for polarization of auxin fluxes in gravity-sensing root cells. *Proc. Natl. Acad. Sci. U. S. A.* **107**: 22344–22349.
- Kleine-Vehn, J. and Friml, J.** (2008). Polar targeting and endocytic recycling in auxin-dependent plant development. *Annu. Rev. Cell Dev. Biol.* **24**: 447–473.
- Kleine-Vehn, J., Huang, F., Naramoto, S., Zhang, J., Michniewicz, M., Offringa, R., and Friml, J.** (2009). PIN Auxin Efflux Carrier Polarity Is Regulated by PINOID Kinase-Mediated Recruitment into GNOM-Independent Trafficking in *Arabidopsis*. *Plant Cell* **21**: 3839 LP – 3849.
- Kleine-Vehn, J., Łangowski, Ł., Wiśniewska, J., Dhonukshe, P., Brewer, P.B., and Friml, J.** (2008b). Cellular and Molecular Requirements for Polar PIN Targeting and Transcytosis in Plants. *Mol. Plant* **1**: 1056–1066.
- Kleine-Vehn, J., Leitner, J., Zwiewka, M., Sauer, M., Abas, L., Luschnig, C., and Friml, J.** (2008c). Differential degradation of PIN2 auxin efflux carrier by retromer-dependent vacuolar targeting. *Proc. Natl. Acad. Sci. U. S. A.* **105**: 17812–17817.
- Koga, J.** (1995). Structure and function of indolepyruvate decarboxylase, a key enzyme in indole-3-acetic acid biosynthesis. *Biochim. Biophys. Acta - Protein Struct. Mol. Enzymol.* **1249**: 1–13.
- Koizumi, K., Naramoto, S., Sawa, S., Yahara, N., Ueda, T., Nakano, A., Sugiyama, M., and Fukuda, H.** (2005). VAN3 ARF–GAP-mediated vesicle transport is involved in leaf vascular network formation. *Development* **132**: 1699 LP – 1711.
- Koizumi, K., Sugiyama, M., and Fukuda, H.** (2000). A series of novel mutants of *Arabidopsis*

thaliana that are defective in the formation of continuous vascular network: calling the auxin signal flow canalization hypothesis into question. *Development* **127**: 3197 LP – 3204.

Koltai, H. (2015). Cellular events of strigolactone signalling and their crosstalk with auxin in roots. *J. Exp. Bot.* **66**: 4855–4861.

Koltai, H., LekKala, S.P., Bhattacharya, C., Mayzlish-Gati, E., Resnick, N., Winger, S., Dor, E., Yoneyama, K., Yoneyama, K., Hershenhorn, J., Joel, D.M., and Kapulnik, Y. (2010). A tomato strigolactone-impaired mutant displays aberrant shoot morphology and plant interactions. *J. Exp. Bot.* **61**: 1739–1749.

Korasick, D.A., Westfall, C.S., Lee, S.G., Nanao, M.H., Dumas, R., Hagen, G., Guilfoyle, T.J., Jez, J.M., and Strader, L.C. (2014). Molecular basis for AUXIN RESPONSE FACTOR protein interaction and the control of auxin response repression. *Proc. Natl. Acad. Sci.* **111**: 5427 LP – 5432.

Kosarev, P., Mayer, K.F.X., and Hardtke, C.S. (2002). Evaluation and classification of RING-finger domains encoded by the Arabidopsis genome. *Genome Biol.* **3**: RESEARCH0016.

Kowalczyk, M. and Sandberg, G. (2001). Quantitative analysis of indole-3-acetic acid metabolites in Arabidopsis. *Plant Physiol.* **127**: 1845–1853.

Krouk, G. et al. (2010). Nitrate-Regulated Auxin Transport by NRT1.1 Defines a Mechanism for Nutrient Sensing in Plants. *Dev. Cell* **18**: 927–937.

Kulkarni, M.G., Sparg, S.G., Light, M.E., and Van Staden, J. (2006). Stimulation of Rice (*Oryza sativa* L.) Seedling Vigour by Smoke-water and Butenolide. *J. Agron. Crop Sci.* **192**: 395–398.

LeClere, S., Rampey, R.A., and Bartel, B. (2004). IAR4, a gene required for auxin conjugate sensitivity in Arabidopsis, encodes a pyruvate dehydrogenase E1alpha homolog. *Plant Physiol.* **135**: 989–999.

Lee, M.H., Min, M.K., Lee, Y.J., Jin, J.B., Shin, D.H., Kim, D.H., Lee, K.-H., and Hwang, I. (2002). ADP-ribosylation factor 1 of Arabidopsis plays a critical role in intracellular trafficking and maintenance of endoplasmic reticulum morphology in Arabidopsis. *Plant Physiol.* **129**: 1507–1520.

Lernmark, U. and Gardestrom, P. (1994). Distribution of Pyruvate Dehydrogenase Complex Activities between Chloroplasts and Mitochondria from Leaves of Different Species. *Plant Physiol.* **106**: 1633–1638.

- Li, R., Liu, P., Wan, Y., Chen, T., Wang, Q., Mettbach, U., Baluška, F., Šamaj, J., Fang, X., Lucas, W.J., and Lin, J.** (2012). A Membrane Microdomain-Associated Protein, *Flot1*, Is Involved in a Clathrin-Independent Endocytic Pathway and Is Required for Seedling Development. *Plant Cell* **24**: 2105 LP – 2122.
- Lin, D. et al.** (2012). A ROP GTPase-dependent auxin signaling pathway regulates the subcellular distribution of PIN2 in *Arabidopsis* roots. *Curr. Biol.* **22**: 1319–1325.
- Lipka, V., Kwon, C., and Panstruga, R.** (2007). SNARE-Ware: The Role of SNARE-Domain Proteins in Plant Biology. *Annu. Rev. Cell Dev. Biol.* **23**: 147–174.
- Ljung, K.** (2013). Auxin metabolism and homeostasis during plant development. *Development* **140**: 943 LP – 950.
- Ljung, K., Bhalerao, R.P., and Sandberg, G.** (2001). Sites and homeostatic control of auxin biosynthesis in *Arabidopsis* during vegetative growth. *Plant J.* **28**: 465–474.
- Löbler, M. and Klämbt, D.** (1985). Auxin-binding protein from coleoptile membranes of corn (*Zea mays* L.). I. Purification by immunological methods and characterization. *J. Biol. Chem.* **260**: 9848–9853.
- Lopez-Obando, M., Ligerot, Y., Bonhomme, S., Boyer, F.-D., and Rameau, C.** (2015). Strigolactone biosynthesis and signaling in plant development. *Development* **142**: 3615 LP – 3619.
- Lorick, K.L., Jensen, J.P., Fang, S., Ong, A.M., Hatakeyama, S., and Weissman, A.M.** (1999). RING fingers mediate ubiquitin-conjugating enzyme (E2)-dependent ubiquitination. *Proc. Natl. Acad. Sci. U. S. A.* **96**: 11364–11369.
- Lucas, M., Guédon, Y., Jay-Allemand, C., Godin, C., and Laplaze, L.** (2008). An Auxin Transport-Based Model of Root Branching in *Arabidopsis thaliana*. *PLoS One* **3**: e3673.
- Ludwig-Müller, J.** (2011). Auxin conjugates: their role for plant development and in the evolution of land plants. *J. Exp. Bot.* **62**: 1757–1773.
- Luethy, M.H., Miernyk, J.A., and Randall, D.D.** (1995). The mitochondrial pyruvate dehydrogenase complex: nucleotide and deduced amino-acid sequences of a cDNA encoding the *Arabidopsis thaliana* E1 α -subunit. *Gene* **164**: 251–254.
- Luschnig, C., Gaxiola, R.A., Grisafi, P., and Fink, G.R.** (1998). EIR1, a root-specific protein involved in auxin transport, is required for gravitropism in *Arabidopsis thaliana*. *Genes Dev.* **12**: 2175–2187.

- Macia, E., Ehrlich, M., Massol, R., Boucrot, E., Brunner, C., and Kirchhausen, T. (2006).** Dynasore, a Cell-Permeable Inhibitor of Dynamin. *Dev. Cell* **10**: 839–850.
- Mangnus, E.M., Dommerholt, F.J., De Jong, R.L.P., and Zwanenburg, B. (1992).** Improved synthesis of strigol analog GR24 and evaluation of the biological activity of its diastereomers. *J. Agric. Food Chem.* **40**: 1230–1235.
- Mano, Y. and Nemoto, K. (2012).** The pathway of auxin biosynthesis in plants. *J. Exp. Bot.* **63**: 2853–2872.
- Marhavý, P., Duclercq, J., Weller, B., Feraru, E., Bielach, A., Offringa, R., Friml, J., Schwechheimer, C., Murphy, A., and Benková, E. (2014).** Cytokinin Controls Polarity of PIN1-Dependent Auxin Transport during Lateral Root Organogenesis. *Curr. Biol.* **24**: 1031–1037.
- Marhavý, P., Vanstraelen, M., De Rybel, B., Zhaojun, D., Bennett, M.J., Beeckman, T., and Benková, E. (2013).** Auxin reflux between the endodermis and pericycle promotes lateral root initiation. *EMBO J.* **32**: 149–158.
- Marzec, M. (2016).** Perception and Signaling of Strigolactones. *Front. Plant Sci.* **7**: 1260.
- Matusova, R., Rani, K., Verstappen, F.W.A., Franssen, M.C.R., Beale, M.H., and Bouwmeester, H.J. (2005).** The strigolactone germination stimulants of the plant-parasitic *Striga* and *Orobancha* spp. are derived from the carotenoid pathway. *Plant Physiol.* **139**: 920–934.
- Mayzlish-Gati, E. et al. (2012).** Strigolactones are involved in root response to low phosphate conditions in *Arabidopsis*. *Plant Physiol.* **160**: 1329–1341.
- McCluskey, A. et al. (2013).** Building a better dynasore: the dyngo compounds potently inhibit dynamin and endocytosis. *Traffic* **14**: 1272–1289.
- McMahon, H.T. and Boucrot, E. (2011).** Molecular mechanism and physiological functions of clathrin-mediated endocytosis. *Nat. Rev. Mol. Cell Biol.* **12**: 517.
- Michalko, J., Dravecká, M., Bollenbach, T., and Friml, J. (2015).** Embryo-lethal phenotypes in early *abp1* mutants are due to disruption of the neighboring *BSM* gene. *F1000Research* **4**: 1104.
- Michniewicz, M. et al. (2007).** Antagonistic Regulation of PIN Phosphorylation by PP2A and PINOID Directs Auxin Flux. *Cell* **130**: 1044–1056.
- Montesinos, J.C., Langhans, M., Sturm, S., Hillmer, S., Aniento, F., Robinson, D.G., and Marcote, M.J. (2013).** Putative p24 complexes in *Arabidopsis* contain members of the

delta and beta subfamilies and cycle in the early secretory pathway. *J. Exp. Bot.* **64**: 3147–3167.

Mooney, B.P., Miernyk, J.A., and Randall, D.D. (2002). THE COMPLEX FATE OF α -KETOACIDS. *Annu. Rev. Plant Biol.* **53**: 357–375.

Moorhead, G.B.G., Trinkle-Mulcahy, L., and Ulke-Lemée, A. (2007). Emerging roles of nuclear protein phosphatases. *Nat. Rev. Mol. Cell Biol.* **8**: 234.

Mossessova, E., Bickford, L.C., and Goldberg, J. (2003). SNARE Selectivity of the COPII Coat. *Cell* **114**: 483–495.

Mothes, W., Heinrich, S.U., Graf, R., Nilsson, I., von Heijne, G., Brunner, J., and Rapoport, T.A. (1997). Molecular Mechanism of Membrane Protein Integration into the Endoplasmic Reticulum. *Cell* **89**: 523–533.

Movafeghi, A., Happel, N., Pimpl, P., Tai, G.H., and Robinson, D.G. (1999). Arabidopsis Sec21p and Sec23p homologs. Probable coat proteins of plant COP-coated vesicles. *Plant Physiol.* **119**: 1437–1446.

Mravec, J. et al. (2009). Subcellular homeostasis of phytohormone auxin is mediated by the ER-localized PIN5 transporter. *Nature* **459**: 1136.

Müller, A., Guan, C., Gälweiler, L., Tänzler, P., Huijser, P., Marchant, A., Parry, G., Bennett, M., Wisman, E., and Palme, K. (1998). AtPIN2 defines a locus of Arabidopsis for root gravitropism control. *EMBO J.* **17**: 6903–6911.

Munson, M. and Novick, P. (2006). The exocyst defrocked, a framework of rods revealed. *Nat. Struct. Mol. Biol.* **13**: 577–581.

Nagawa, S., Xu, T., and Yang, Z. (2010). RHO GTPase in plants: Conservation and invention of regulators and effectors. *Small GTPases* **1**: 78–88.

Nanao, M.H. et al. (2014). Structural basis for oligomerization of auxin transcriptional regulators. *Nat. Commun.* **5**: 3617.

Naramoto, S., Kleine-Vehn, J., Robert, S., Fujimoto, M., Dainobu, T., Paciorek, T., Ueda, T., Nakano, A., Van Montagu, M.C.E., Fukuda, H., and Friml, J. (2010). ADP-ribosylation factor machinery mediates endocytosis in plant cells. *Proc. Natl. Acad. Sci. U. S. A.* **107**: 21890–21895.

Naramoto, S., Otegui, M.S., Kutsuna, N., de Rycke, R., Dainobu, T., Karampelias, M., Fujimoto, M., Feraru, E., Miki, D., Fukuda, H., Nakano, A., and Friml, J. (2014). Insights into the Localization and Function of the Membrane Trafficking Regulator GNOM ARF-

GEF at the Golgi Apparatus in *Arabidopsis*. *Plant Cell* **26**: 3062–3076.

- Naramoto, S., Sawa, S., Koizumi, K., Uemura, T., Ueda, T., Friml, J., Nakano, A., and Fukuda, H.** (2009). Phosphoinositide-dependent regulation of VAN3 ARF-GAP localization and activity essential for vascular tissue continuity in plants. *Development* **136**: 1529 LP – 1538.
- Nebenführ, A., Ritzenthaler, C., and Robinson, D.G.** (2002). Brefeldin A: deciphering an enigmatic inhibitor of secretion. *Plant Physiol.* **130**: 1102–1108.
- Nelson, D.C., Flematti, G.R., Ghisalberti, E.L., Dixon, K.W., and Smith, S.M.** (2012). Regulation of Seed Germination and Seedling Growth by Chemical Signals from Burning Vegetation. *Annu. Rev. Plant Biol.* **63**: 107–130.
- Nelson, D.C., Flematti, G.R., Riseborough, J.-A., Ghisalberti, E.L., Dixon, K.W., and Smith, S.M.** (2010). Karrikins enhance light responses during germination and seedling development in *Arabidopsis thaliana*; *Proc. Natl. Acad. Sci.* **107**: 7095 LP – 7100.
- Nelson, D.C., Riseborough, J.-A., Flematti, G.R., Stevens, J., Ghisalberti, E.L., Dixon, K.W., and Smith, S.M.** (2009). Karrikins discovered in smoke trigger *Arabidopsis* seed germination by a mechanism requiring gibberellic acid synthesis and light. *Plant Physiol.* **149**: 863–873.
- Nielsen, E., Cheung, A.Y., and Ueda, T.** (2008). The regulatory RAB and ARF GTPases for vesicular trafficking. *Plant Physiol.* **147**: 1516–1526.
- Nisar, N., Cuttriss, A.J., Pogson, B.J., and Cazzonelli, C.I.** (2014). The promoter of the *Arabidopsis* PIN6 auxin transporter enabled strong expression in the vasculature of roots, leaves, floral stems and reproductive organs. *Plant Signal. Behav.* **9**: e27898–e27898.
- Novák, O., Pěňčík, A., and Ljung, K.** (2014). Identification and Profiling of Auxin and Auxin Metabolites BT - Auxin and Its Role in Plant Development. In E. Zažímalová, J. Petrášek, and E. Benková, eds (Springer Vienna: Vienna), pp. 39–60.
- Okada, K., Ueda, J., Komaki, M.K., Bell, C.J., and Shimura, Y.** (1991). Requirement of the Auxin Polar Transport System in Early Stages of *Arabidopsis* Floral Bud Formation. *Plant Cell* **3**: 677 LP – 684.
- Onelli, E., Precianotto-Baschong, C., Caccianiga, M., and Moscatelli, A.** (2008). Clathrin-dependent and independent endocytic pathways in tobacco protoplasts revealed by

- labelling with charged nanogold. *J. Exp. Bot.* **59**: 3051–3068.
- Osterrieder, A., Hummel, E., Carvalho, C.M., and Hawes, C.** (2009). Golgi membrane dynamics after induction of a dominant-negative mutant Sar1 GTPase in tobacco. *J. Exp. Bot.* **61**: 405–422.
- Ostin, A., Kowalyczk, M., Bhalerao, R.P., and Sandberg, G.** (1998). Metabolism of indole-3-acetic acid in *Arabidopsis*. *Plant Physiol.* **118**: 285–296.
- Overvoorde, P., Fukaki, H., and Beeckman, T.** (2010). Auxin control of root development. *Cold Spring Harb. Perspect. Biol.* **2**: a001537–a001537.
- Paciorek, T., Zažímalová, E., Ruthardt, N., Petrášek, J., Stierhof, Y.-D., Kleine-Vehn, J., Morris, D.A., Emans, N., Jürgens, G., Geldner, N., and Friml, J.** (2005). Auxin inhibits endocytosis and promotes its own efflux from cells. *Nature* **435**: 1251–1256.
- Paque, S., Mouille, G., Grandont, L., Alabadí, D., Gaertner, C., Goyallon, A., Muller, P., Primard-Brisset, C., Sormani, R., Blázquez, M.A., and Perrot-Rechenmann, C.** (2014). AUXIN BINDING PROTEIN1 Links Cell Wall Remodeling, Auxin Signaling, and Cell Expansion in *Arabidopsis*. *Plant Cell* **26**: 280 LP – 295.
- Park, R.J., Shen, H., Liu, L., Liu, X., Ferguson, S.M., and De Camilli, P.** (2013). Dynamin triple knockout cells reveal off target effects of commonly used dynamin inhibitors. *J. Cell Sci.* **126**: 5305–5312.
- Paul, M.J. and Frigerio, L.** (2007). Coated vesicles in plant cells. *Semin. Cell Dev. Biol.* **18**: 471–478.
- Pencík, A. et al.** (2013). Regulation of auxin homeostasis and gradients in *Arabidopsis* roots through the formation of the indole-3-acetic acid catabolite 2-oxindole-3-acetic acid. *Plant Cell* **25**: 3858–3870.
- Pencík, A., Casanova-Sáez, R., Pilarová, V., Žukauskaite, A., Pinto, R., Micol, J.L., Ljung, K., and Novák, O.** (2018). Ultra-rapid auxin metabolite profiling for high-throughput mutant screening in *Arabidopsis*. *J. Exp. Bot.* **69**: 2569–2579.
- Péret, B. et al.** (2012). *AUX/LAX* Genes Encode a Family of Auxin Influx Transporters That Perform Distinct Functions during *Arabidopsis* Development. *Plant Cell* **24**: 2874 LP – 2885.
- Petrášek, J. et al.** (2006). PIN Proteins Perform a Rate-Limiting Function in Cellular Auxin Efflux. *Science* (80-.). **312**: 914 LP – 918.
- Petrášek, J. and Friml, J.** (2009). Auxin transport routes in plant development. *Development*

136: 2675 LP – 2688.

- Piper, R.C. and Katzmann, D.J.** (2007). Biogenesis and function of multivesicular bodies. *Annu. Rev. Cell Dev. Biol.* **23**: 519–547.
- Porfírio, S., Gomes da Silva, M.D.R., Peixe, A., Cabrita, M.J., and Azadi, P.** (2016). Current analytical methods for plant auxin quantification – A review. *Anal. Chim. Acta* **902**: 8–21.
- Powers, E.T. and Balch, W.E.** (2013). Diversity in the origins of proteostasis networks--a driver for protein function in evolution. *Nat. Rev. Mol. Cell Biol.* **14**: 237–248.
- del Pozo, J.C., Diaz-Trivino, S., Cisneros, N., and Gutierrez, C.** (2006). The balance between cell division and endoreplication depends on E2FC-DPB, transcription factors regulated by the ubiquitin-SCFSKP2A pathway in Arabidopsis. *Plant Cell* **18**: 2224–2235.
- Del Pozo, J.C., Diaz-Trivino, S., Cisneros, N., and Gutierrez, C.** (2007). The E2FC-DPB Transcription Factor Controls Cell Division, Endoreplication and Lateral Root Formation in a SCF-Dependent Manner. *Plant Signal. Behav.* **2**: 273–274.
- Prát, T., Hajný, J., Grunewald, W., Vasileva, M., Molnár, G., Tejos, R., Schmid, M., Sauer, M., and Friml, J.** (2018). WRKY23 is a component of the transcriptional network mediating auxin feedback on PIN polarity. *PLOS Genet.* **14**: e1007177.
- Prusinkiewicz, P., Crawford, S., Smith, R.S., Ljung, K., Bennett, T., Ongaro, V., and Leyser, O.** (2009). Control of bud activation by an auxin transport switch. *Proc. Natl. Acad. Sci. U. S. A.* **106**: 17431–17436.
- Quint, M., Barkawi, L.S., Fan, K.-T., Cohen, J.D., and Gray, W.M.** (2009). Arabidopsis IAR4 modulates auxin response by regulating auxin homeostasis. *Plant Physiol.* **150**: 748–758.
- Rahman, A., Takahashi, M., Shibasaki, K., Wu, S., Inaba, T., Tsurumi, S., and Baskin, T.I.** (2010). Gravitropism of Arabidopsis thaliana roots requires the polarization of PIN2 toward the root tip in meristematic cortical cells. *Plant Cell* **22**: 1762–1776.
- Rakusová, H., Abbas, M., Han, H., Song, S., Robert, H.S., and Friml, J.** (2016). Termination of Shoot Gravitropic Responses by Auxin Feedback on PIN3 Polarity. *Curr. Biol.* **26**: 3026–3032.
- Rakusová, H., Gallego-Bartolomé, J., Vanstraelen, M., Robert, H.S., Alabadí, D., Blázquez, M.A., Benková, E., and Friml, J.** (2011). Polarization of PIN3-dependent auxin transport for hypocotyl gravitropic response in Arabidopsis thaliana. *Plant J.* **67**: 817–826.
- Randall, D.D., Miernyk, J.A., David, N.R., Gemel, J., and Luethy University of Missouri, Columbia, Missouri 65211 (USA)), M.H. (Interdisciplinary P.G.** (1996). Regulation of leaf

- mitochondrial pyruvate dehydrogenase complex activity by reversible phosphorylation.
- Ranocha, P. et al.** (2013). Arabidopsis WAT1 is a vacuolar auxin transport facilitator required for auxin homeostasis. *Nat. Commun.* **4**: 2625.
- Rao, V.S., Srinivas, K., Sujini, G.N., and Kumar, G.N.S.** (2014). Protein-protein interaction detection: methods and analysis. *Int. J. Proteomics* **2014**: 147648.
- Rashotte, A.M., Brady, S.R., Reed, R.C., Ante, S.J., and Muday, G.K.** (2000). Basipetal Auxin Transport Is Required for Gravitropism in Roots of Arabidopsis. *Plant Physiol.* **122**: 481 LP – 490.
- Rashotte, A.M., DeLong, A., and Muday, G.K.** (2001). Genetic and chemical reductions in protein phosphatase activity alter auxin transport, gravity response, and lateral root growth. *Plant Cell* **13**: 1683–1697.
- Rasmussen, A., Hosseini, S.A., Hajirezaei, M.-R., Druge, U., and Geelen, D.** (2014). Adventitious rooting declines with the vegetative to reproductive switch and involves a changed auxin homeostasis. *J. Exp. Bot.* **66**: 1437–1452.
- Reynolds, G.D., Wang, C., Pan, J., and Bednarek, S.Y.** (2018). Inroads into Internalization: Five Years of Endocytic Exploration. *Plant Physiol.* **176**: 208 LP – 218.
- Richter, S., Anders, N., Wolters, H., Beckmann, H., Thomann, A., Heinrich, R., Schrader, J., Singh, M.K., Geldner, N., Mayer, U., and Jürgens, G.** (2010). Role of the GNOM gene in Arabidopsis apical-basal patterning - From mutant phenotype to cellular mechanism of protein action. *Eur. J. Cell Biol.* **89**: 138–144.
- Richter, S., Geldner, N., Schrader, J., Wolters, H., Stierhof, Y.D., Rios, G., Koncz, C., Robinson, D.G., and Jürgens, G.** (2007). Functional diversification of closely related ARF-GEFs in protein secretion and recycling. *Nature* **448**: 488–492.
- Richter, S., Kientz, M., Brumm, S., Nielsen, M.E., Park, M., Gavidia, R., Krause, C., Voss, U., Beckmann, H., Mayer, U., Stierhof, Y.-D., and Jürgens, G.** (2014). Delivery of endocytosed proteins to the cell–division plane requires change of pathway from recycling to secretion. *Elife* **3**: 1–16.
- Robert, H., Grunewald, W., Sauer, M., Cannoot, B., Soriano Castán, M., Swarup, R., Weijers, D., J. Bennett, M., Boutilier, K., and Friml, J.** (2015). Plant embryogenesis requires AUX/LAX-mediated auxin influx.
- Robert, H.S., Grones, P., Stepanova, A.N., Robles, L.M., Lokerse, A.S., Alonso, J.M., Weijers, D., and Friml, J.** (2013). Local Auxin Sources Orient the Apical-Basal Axis in

- Arabidopsis* Embryos. *Curr. Biol.* **23**: 2506–2512.
- Robert, S. et al.** (2010). ABP1 mediates auxin inhibition of clathrin-dependent endocytosis in *Arabidopsis*. *Cell* **143**: 111–121.
- Robinson, D.G., Herranz, M.-C., Bubeck, J., Pepperkok, R., and Ritzenthaler, C.** (2007). Membrane Dynamics in the Early Secretory Pathway. *CRC. Crit. Rev. Plant Sci.* **26**: 199–225.
- Ruegger, M., Dewey, E., Hobbie, L., Brown, D., Bernasconi, P., Turner, J., Muday, G., and Estelle, M.** (1997). Reduced naphthylphthalamic acid binding in the *tir3* mutant of *Arabidopsis* is associated with a reduction in polar auxin transport and diverse morphological defects. *Plant Cell* **9**: 745–757.
- Rutherford, S. and Moore, I.** (2002). The *Arabidopsis* Rab GTPase family: another enigma variation. *Curr. Opin. Plant Biol.* **5**: 518–528.
- Ruyter-Spira, C., Kohlen, W., Charnikhova, T., van Zeijl, A., van Bezouwen, L., de Ruijter, N., Cardoso, C., Lopez-Raez, J.A., Matusova, R., Bours, R., Verstappen, F., and Bouwmeester, H.** (2011). Physiological effects of the synthetic strigolactone analog GR24 on root system architecture in *Arabidopsis*: another belowground role for strigolactones? *Plant Physiol.* **155**: 721–734.
- Ruzicka, K. et al.** (2010). *Arabidopsis* PIS1 encodes the ABCG37 transporter of auxinic compounds including the auxin precursor indole-3-butyric acid. *Proc. Natl. Acad. Sci. U. S. A.* **107**: 10749–10753.
- Sabatini, S., Beis, D., Wolkenfelt, H., Murfett, J., Guilfoyle, T., Malamy, J., Benfey, P., Leyser, O., Bechtold, N., Weisbeek, P., and Scheres, B.** (1999). An Auxin-Dependent Distal Organizer of Pattern and Polarity in the *Arabidopsis* Root. *Cell* **99**: 463–472.
- Sachs, T.** (2000). Integrating Cellular and Organismic Aspects of Vascular Differentiation. *Plant Cell Physiol.* **41**: 649–656.
- Sachs, T.** (1981). The Control of the Patterned Differentiation of Vascular Tissues. In H.W.B.T.-A. in B.R. Woolhouse, ed (Academic Press), pp. 151–262.
- Salanenko, Y., Verstraeten, I., Löffke, C., Tabata, K., Naramoto, S., Glanc, M., and Friml, J.** (2018). Gibberellin DELLA signaling targets the retromer complex to redirect protein trafficking to the plasma membrane. *Proc. Natl. Acad. Sci. U. S. A.* **115**: 3716–3721.
- Sang, D. et al.** (2014). Strigolactones regulate rice tiller angle by attenuating shoot gravitropism through inhibiting auxin biosynthesis. *Proc. Natl. Acad. Sci.* **111**: 11199 LP –

11204.

- Sato, E.M., Hijazi, H., Bennett, M.J., Vissenberg, K., and Swarup, R.** (2015). New insights into root gravitropic signalling. *J. Exp. Bot.* **66**: 2155–2165.
- Sauer, M., Balla, J., Luschnig, C., Wisniewska, J., Reinöhl, V., Friml, J., and Benková, E.** (2006). Canalization of auxin flow by Aux/IAA-ARF-dependent feedback regulation of PIN polarity. *Genes Dev.* **20**: 2902–2911.
- Sauer, M. and Friml, J.** (2010). Immunolocalization of Proteins in Plants. In *Plant Developmental Biology: Methods and Protocols*, L. Hennig and C. Köhler, eds (Humana Press: Totowa, NJ), pp. 253–263.
- Scarpella, E., Marcos, D., Friml, J., and Berleth, T.** (2006). Control of leaf vascular patterning by polar auxin transport. *Genes Dev.* **20**: 1015–1027.
- Schlereth, A., Möller, B., Liu, W., Kientz, M., Flipse, J., Rademacher, E.H., Schmid, M., Jürgens, G., and Weijers, D.** (2010). MONOPTEROS controls embryonic root initiation by regulating a mobile transcription factor. *Nature* **464**: 913.
- Seaman, M.N.J.** (2005). Recycle your receptors with retromer. *Trends Cell Biol.* **15**: 68–75.
- Serafini, T., Orci, L., Amherdt, M., Brunner, M., Kahn, R.A., and Rothmant, J.E.** (1991). ADP-Ribosylation factor is a subunit of the coat of Golgi-derived COP-coated vesicles: A novel role for a GTP-binding protein. *Cell* **67**: 239–253.
- Shimizu-Mitao, Y. and Kakimoto, T.** (2014). Auxin Sensitivities of All Arabidopsis Aux/IAs for Degradation in the Presence of Every TIR1/AFB. *Plant Cell Physiol.* **55**: 1450–1459.
- Shimomura, S.** (2006). Identification of a Glycosylphosphatidylinositol-anchored Plasma Membrane Protein Interacting with the C-terminus of Auxin-binding Protein 1: A Photoaffinity Crosslinking Study. *Plant Mol. Biol.* **60**: 663–677.
- SHIMOMURA, S., SOTOBAYASHI, T., FUTAI, M., and FUKUI, T.** (1986). Purification and Properties of an Auxin-Binding Protein from Maize Shoot Membranes¹. *J. Biochem.* **99**: 1513–1524.
- Shimomura, S., Watanabe, S., and Ichikawa, H.** (1999). Characterization of auxin-binding protein 1 from tobacco: Content, localization and auxin-binding activity. *Planta* **209**: 118–125.
- Shin, H.-W. and Nakayama, K.** (2004). Dual control of membrane targeting by PtdIns(4)P and ARF. *Trends Biochem. Sci.* **29**: 513–515.
- Shinohara, N., Taylor, C., and Leyser, O.** (2013). Strigolactone Can Promote or Inhibit Shoot

- Branching by Triggering Rapid Depletion of the Auxin Efflux Protein PIN1 from the Plasma Membrane. *PLOS Biol.* **11**: e1001474.
- Sieburth, L.E.** (1999). Auxin is required for leaf vein pattern in Arabidopsis. *Plant Physiol.* **121**: 1179–1190.
- Sigismund, S., Confalonieri, S., Ciliberto, A., Polo, S., Scita, G., and Di Fiore, P.P.** (2012). Endocytosis and signaling: cell logistics shape the eukaryotic cell plan. *Physiol. Rev.* **92**: 273–366.
- Singh, M.K. et al.** (2018). A single class of ARF GTPase activated by several pathway-specific ARF-GEFs regulates essential membrane traffic in Arabidopsis. *PLOS Genet.* **14**: e1007795.
- Singh, V., Davidson, A.C., Hume, P.J., Humphreys, D., and Koronakis, V.** (2017). Arf GTPase interplay with Rho GTPases in regulation of the actin cytoskeleton. *Small GTPases*: 1–8.
- Skach, W.R.** (2009). Cellular mechanisms of membrane protein folding. *Nat. Struct. Mol. Biol.* **16**: 606–612.
- De Smet, I.** (2012). Lateral root initiation: one step at a time. *New Phytol.* **193**: 867–873.
- Smith, J.M., Salamango, D.J., Leslie, M.E., Collins, C.A., and Heese, A.** (2014). Sensitivity to Flg22 Is Modulated by Ligand-Induced Degradation and de Novo Synthesis of the Endogenous Flagellin-Receptor FLAGELLIN-SENSING2. *Plant Physiol.* **164**: 440 LP – 454.
- Sorefan, K., Booker, J., Haurogné, K., Goussot, M., Bainbridge, K., Foo, E., Chatfield, S., Ward, S., Beveridge, C., Rameau, C., and Leyser, O.** (2003). MAX4 and RMS1 are orthologous dioxygenase-like genes that regulate shoot branching in Arabidopsis and pea. *Genes Dev.* **17**: 1469–1474.
- Sorefan, K., Girin, T., Liljegren, S.J., Ljung, K., Robles, P., Galván-Ampudia, C.S., Offringa, R., Friml, J., Yanofsky, M.F., and Østergaard, L.** (2009). A regulated auxin minimum is required for seed dispersal in Arabidopsis. *Nature* **459**: 583.
- Soundappan, I., Bennett, T., Morffy, N., Liang, Y., Stanga, J.P., Abbas, A., Leyser, O., and Nelson, D.C.** (2015). SMAX1-LIKE/D53 Family Members Enable Distinct MAX2-Dependent Responses to Strigolactones and Karrikins in Arabidopsis. *Plant Cell* **27**: 3143–3159.
- Spang, A., Shiba, Y., and Randazzo, P.A.** (2010). Arf GAPs: gatekeepers of vesicle generation. *FEBS Lett.* **584**: 2646–2651.
- van Staden, J., Sparg, S.G., Kulkarni, M.G., and Light, M.E.** (2006). Post-germination effects

of the smoke-derived compound 3-methyl-2H-furo[2,3-c]pyran-2-one, and its potential as a preconditioning agent. *F. Crop. Res.* **98**: 98–105.

Stanga, J.P., Smith, S.M., Briggs, W.R., and Nelson, D.C. (2013). SUPPRESSOR OF MORE AXILLARY GROWTH2 1 controls seed germination and seedling development in *Arabidopsis*. *Plant Physiol.* **163**: 318–330.

Stein, M., Dittgen, J., Sánchez-Rodríguez, C., Hou, B.-H., Molina, A., Schulze-Lefert, P., Lipka, V., and Somerville, S. (2006). *Arabidopsis* PEN3/PDR8, an ATP binding cassette transporter, contributes to nonhost resistance to inappropriate pathogens that enter by direct penetration. *Plant Cell* **18**: 731–746.

Steinmann, T., Geldner, N., Grebe, M., Mangold, S., Jackson, C.L., Paris, S., Gälweiler, L., Palme, K., and Jürgens, G. (1999). Coordinated polar localization of auxin efflux carrier PIN1 by GNOM ARF GEF. *Science* (80-.). **286**: 316–318.

Stone, S.L., Hauksdóttir, H., Troy, A., Herschleb, J., Kraft, E., and Callis, J. (2005). Functional analysis of the RING-type ubiquitin ligase family of *Arabidopsis*. *Plant Physiol.* **137**: 13–30.

Strader, L.C. and Bartel, B. (2009). The *Arabidopsis* PLEIOTROPIC DRUG RESISTANCE8/ABCG36 ATP binding cassette transporter modulates sensitivity to the auxin precursor indole-3-butyric acid. *Plant Cell* **21**: 1992–2007.

Swarup, R. and Péret, B. (2012). AUX/LAX family of auxin influx carriers-an overview. *Front. Plant Sci.* **3**: 225.

Szklarczyk, D., Morris, J.H., Cook, H., Kuhn, M., Wyder, S., Simonovic, M., Santos, A., Doncheva, N.T., Roth, A., Bork, P., Jensen, L.J., and von Mering, C. (2017). The STRING database in 2017: quality-controlled protein-protein association networks, made broadly accessible. *Nucleic Acids Res.* **45**: D362–D368.

Takagi, J., Renna, L., Takahashi, H., Koumoto, Y., Tamura, K., Stefano, G., Fukao, Y., Kondo, M., Nishimura, M., Shimada, T., Brandizzi, F., and Hara-Nishimura, I. (2013). MAIGO5 Functions in Protein Export from Golgi-Associated Endoplasmic Reticulum Exit Sites in *Arabidopsis*. *Plant Cell* **25**: 4658 LP – 4675.

Tam, Y.Y., Epstein, E., and Normanly, J. (2000). Characterization of auxin conjugates in *Arabidopsis*. Low steady-state levels of indole-3-acetyl-aspartate, indole-3-acetyl-glutamate, and indole-3-acetyl-glucose. *Plant Physiol.* **123**: 589–596.

Tan, X., Feng, Y., Liu, Y., and Bao, Y. (2016). Mutations in exocyst complex subunit SEC6 gene

- impaired polar auxin transport and PIN protein recycling in Arabidopsis primary root. *Plant Sci.* **250**: 97–104.
- Tanaka, H., Kitakura, S., Rakusová, H., Uemura, T., Feraru, M.I., De Rycke, R., Robert, S., Kakimoto, T., and Friml, J.** (2013). Cell Polarity and Patterning by PIN Trafficking through Early Endosomal Compartments in Arabidopsis thaliana. *PLOS Genet.* **9**: e1003540.
- Tanaka, H., Kitakura, S., De Rycke, R., De Groot, R., and Friml, J.** (2009). Fluorescence Imaging-Based Screen Identifies ARF GEF Component of Early Endosomal Trafficking. *Curr. Biol.* **19**: 391–397.
- Tanaka, H., Nodzyński, T., Kitakura, S., Feraru, M.I., Sasabe, M., Ishikawa, T., Kleine-Vehn, J., Kakimoto, T., and Friml, J.** (2014). BEX1/ARF1A1C is required for BFA-sensitive recycling of PIN auxin transporters and auxin-mediated development in Arabidopsis. *Plant Cell Physiol.* **55**: 737–749.
- Tarkowská, D., Novák, O., Floková, K., Tarkowski, P., Turečková, V., Grúz, J., Rolčík, J., and Strnad, M.** (2014). Quo vadis plant hormone analysis? *Planta* **240**: 55–76.
- Teh, O.-K. and Moore, I.** (2007). An ARF-GEF acting at the Golgi and in selective endocytosis in polarized plant cells. *Nature* **448**: 493–496.
- Terol, J., Bagues, M., Carrasco, P., Pérez-Alonso, M., and Paricio, N.** (2002). Molecular characterization and evolution of the protein phosphatase 2A B' regulatory subunit family in plants. *Plant Physiol.* **129**: 808–822.
- THIMANN, K. V.** (1939). AUXINS AND THE INHIBITION OF PLANT GROWTH. *Biol. Rev.* **14**: 314–337.
- Tomas, A., Braun, N., Muller, P., Khodus, T., Paponov, I.A., Palme, K., Ljung, K., Lee, J.-Y., Benfey, P., Murray, J.A.H., Scheres, B., and Perrot-Rechenmann, C.** (2009). The AUXIN BINDING PROTEIN 1 is required for differential auxin responses mediating root growth. *PLoS One* **4**: e6648–e6648.
- Tomas, A., Paque, S., Stierlé, V., Quettier, A.-L., Muller, P., Lechner, E., Genschik, P., and Perrot-Rechenmann, C.** (2013). Auxin-Binding Protein 1 is a negative regulator of the SCFTIR1/AFB pathway. *Nat. Commun.* **4**: 2496.
- Turnbull, C.G.N., Booker, J.P., and Leyser, H.M.O.** (2002). Micrografting techniques for testing long-distance signalling in Arabidopsis. *Plant J.* **32**: 255–262.
- Uemura, T. and Ueda, T.** (2014). Plant vacuolar trafficking driven by RAB and SNARE proteins. *Curr. Opin. Plant Biol.* **22**: 116–121.

- Ulmasov, T., Murfett, J., Hagen, G., and Guilfoyle, T.J.** (1997). Aux/IAA proteins repress expression of reporter genes containing natural and highly active synthetic auxin response elements. *Plant Cell* **9**: 1963 LP – 1971.
- Umehara, M., Hanada, A., Yoshida, S., Akiyama, K., Arite, T., Takeda-Kamiya, N., Magome, H., Kamiya, Y., Shirasu, K., Yoneyama, K., Kyojuka, J., and Yamaguchi, S.** (2008). Inhibition of shoot branching by new terpenoid plant hormones. *Nature* **455**: 195.
- Utsuno, K., Shikanai, T., Yamada, Y., and Hashimoto, T.** (1998). AGR, an Agravitropic Locus of *Arabidopsis thaliana*, Encodes a Novel Membrane-Protein Family Member. *Plant Cell Physiol.* **39**: 1111–1118.
- Vandenbussche, F., Petrášek, J., Žádníková, P., Hoyerová, K., Pešek, B., Raz, V., Swarup, R., Bennett, M., Zažímalová, E., Benková, E., and Van Der Straeten, D.** (2010). The auxin influx carriers AUX1 and LAX3 are involved in auxin-ethylene interactions during apical hook development in *Arabidopsis thaliana* seedlings. *Development* **137**: 597 LP – 606.
- Vanneste, S. and Friml, J.** (2009). Auxin: A Trigger for Change in Plant Development. *Cell* **136**: 1005–1016.
- Vernoud, V., Horton, A.C., Yang, Z., and Nielsen, E.** (2003). Analysis of the Small GTPase Gene Superfamily of *Arabidopsis*. *Plant Physiol.* **131**: 1191 LP – 1208.
- Vernoux, T., Besnard, F., and Traas, J.** (2010). Auxin at the shoot apical meristem. *Cold Spring Harb. Perspect. Biol.* **2**: a001487–a001487.
- Vieten, A., Vanneste, S., Wiśniewska, J., Benková, E., Benjamins, R., Beeckman, T., Luschnig, C., and Friml, J.** (2005). Functional redundancy of PIN proteins is accompanied by auxin-dependent cross-regulation of PIN expression. *Development* **132**: 4521 LP – 4531.
- Vitale, A. and Denecke, J.** (1999). The endoplasmic reticulum-gateway of the secretory pathway. *Plant Cell* **11**: 615–628.
- von Kleist, L. et al.** (2011). Role of the Clathrin Terminal Domain in Regulating Coated Pit Dynamics Revealed by Small Molecule Inhibition. *Cell* **146**: 471–484.
- Wabnik, K., Robert, H.S., Smith, R.S., and Friml, J.** (2013). Modeling Framework for the Establishment of the Apical-Basal Embryonic Axis in Plants. *Curr. Biol.* **23**: 2513–2518.
- Waldie, T., McCulloch, H., and Leyser, O.** (2014). Strigolactones and the control of plant development: lessons from shoot branching. *Plant J.* **79**: 607–622.
- Wang, C., Yan, X., Chen, Q., Jiang, N., Fu, W., Ma, B., Liu, J., Li, C., Bednarek, S.Y., and Pan,**

- J. (2013). Clathrin light chains regulate clathrin-mediated trafficking, auxin signaling, and development in Arabidopsis. *Plant Cell* **25**: 499–516.
- Wang, L. and Ruan, Y.-L.** (2013). Regulation of cell division and expansion by sugar and auxin signaling. *Front. Plant Sci.* **4**: 163.
- Waters, M.T., Nelson, D.C., Scaffidi, A., Flematti, G.R., Sun, Y.K., Dixon, K.W., and Smith, S.M.** (2012). Specialisation within the DWARF14 protein family confers distinct responses to karrikins and strigolactones in *Arabidopsis*; *Development* **139**: 1285 LP – 1295.
- Waters, M.T., Scaffidi, A., Sun, Y.K., Flematti, G.R., and Smith, S.M.** (2014). The karrikin response system of Arabidopsis. *Plant J.* **79**: 623–631.
- Weigel, D. and Glazebrook, J.** (2006). Forward Genetics in Arabidopsis: Finding Mutations that Cause Particular Phenotypes. *Cold Spring Harb. Protoc.* **2006**: pdb.top1.
- Went, F.W.** (1974). Reflections and Speculations. *Annu. Rev. Plant Physiol.* **25**: 1–27.
- Willige, B.C., Ahlers, S., Zourelidou, M., Barbosa, I.C.R., Demarsy, E., Trevisan, M., Davis, P.A., Roelfsema, M.R.G., Hangarter, R., Fankhauser, C., and Schwechheimer, C.** (2013). D6PK AGCVIII kinases are required for auxin transport and phototropic hypocotyl bending in Arabidopsis. *Plant Cell* **25**: 1674–1688.
- Willige, B.C., Isono, E., Richter, R., Zourelidou, M., and Schwechheimer, C.** (2011). Gibberellin regulates PIN-FORMED abundance and is required for auxin transport-dependent growth and development in Arabidopsis thaliana. *Plant Cell* **23**: 2184–2195.
- Willox, A.K., Sahraoui, Y.M.E., and Royle, S.J.** (2014). Non-specificity of Pitstop 2 in clathrin-mediated endocytosis. *Biol. Open* **3**: 326–331.
- Wiśniewska, J., Xu, J., Seifertová, D., Brewer, P.B., Růžička, K., Blilou, I., Rouquié, D., Benková, E., Scheres, B., and Friml, J.** (2006). Polar PIN Localization Directs Auxin Flow in Plants. *Science* (80-.). **312**: 883 LP – 883.
- WOODWARD, A.W. and BARTEL, B.** (2005). Auxin: Regulation, Action, and Interaction. *Ann. Bot.* **95**: 707–735.
- Wu, X., Cheng, Y., Li, T., Wang, Z., and Liu, J.-Y.** (2012). In vitro identification of DNA-binding motif for the new zinc finger protein AtYY1. *Acta Biochim. Biophys. Sin. (Shanghai)*. **44**: 483–489.
- Xu, J. and Scheres, B.** (2005). Dissection of Arabidopsis ADP-RIBOSYLATION FACTOR 1 function in epidermal cell polarity. *Plant Cell* **17**: 525–536.

- Xu, T. et al.** (2014). Cell surface ABP1-TMK auxin-sensing complex activates ROP GTPase signaling. *Science* **343**: 1025–1028.
- Yaish, P., Gazit, A., Gilon, C., and Levitzki, A.** (1988). Blocking of EGF-dependent cell proliferation by EGF receptor kinase inhibitors. *Science* (80-.). **242**: 933 LP – 935.
- Yang, H. and Murphy, A.S.** (2009). Functional expression and characterization of Arabidopsis ABCB, AUX 1 and PIN auxin transporters in *Schizosaccharomyces pombe*. *Plant J.* **59**: 179–191.
- Yorimitsu, T., Sato, K., and Takeuchi, M.** (2014). Molecular mechanisms of Sar/Arf GTPases in vesicular trafficking in yeast and plants. *Front. Plant Sci.* **5**: 1–12.
- Žádníková, P. et al.** (2010). Role of PIN-mediated auxin efflux in apical hook development of *Arabidopsis thaliana*. *Development* **137**: 607 LP – 617.
- Zazimalová, E., Murphy, A.S., Yang, H., Hoyerová, K., and Hosek, P.** (2010). Auxin transporters—why so many? *Cold Spring Harb. Perspect. Biol.* **2**: a001552–a001552.
- Zerial, M. and McBride, H.** (2001). Rab proteins as membrane organizers. *Nat. Rev. Mol. Cell Biol.* **2**: 107.
- Zhang, J., Nodzynski, T., Pencík, A., Rolcík, J., and Friml, J.** (2010). PIN phosphorylation is sufficient to mediate PIN polarity and direct auxin transport. *Proc. Natl. Acad. Sci. U. S. A.* **107**: 918–922.
- Zheng, Z., Guo, Y., Novák, O., Chen, W., Ljung, K., Noel, J.P., and Chory, J.** (2016). Local auxin metabolism regulates environment-induced hypocotyl elongation. *Nat. plants* **2**: 16025.
- Zourelidou, M. et al.** (2014). Auxin efflux by PIN-FORMED proteins is activated by two different protein kinases, D6 PROTEIN KINASE and PINOID. *Elife* **3**: e02860.
- Zourelidou, M., Müller, I., Willige, B.C., Nill, C., Jikumaru, Y., Li, H., and Schwechheimer, C.** (2009). The polarly localized D6 PROTEIN KINASE is required for efficient auxin transport in *Arabidopsis thaliana*. *Development* **136**: 627 LP – 636.
- Zwiewka, M. and Friml, J.** (2012). Fluorescence imaging-based forward genetic screens to identify trafficking regulators in plants. *Front. Plant Sci.* **3**: 97.

2 SACSIN mediates adaptation of plant cells to ARF-GEF inhibition

2.1 Abstract

Similar to all eukaryotes, the plant cells, are structurally and metabolically divided into different compartments, where the communication between them is enabled by vesicle trafficking. Due to the changing environment, the endomembrane trafficking needs also to adapt to the alterations. This process depends on the vesicle budding where important regulators are the ARF GTPases, acting as molecular switches. Thus, their activators ARF-GEFs, such as GNOM, are essential for many cellular processes including the polar targeting of PIN transporters for the plant hormone auxin. We used the established inhibitor of ARF-GEFs, Brefeldin A (BFA) and designed a morphology-based forward genetic screen on EMS mutagenized PIN1-GFP population of *Arabidopsis*. We identified *bar1*, which shows BFA-insensitive growth but on the subcellular level, it fails to adapt to BFA-mediated inhibition of trafficking. The mutation is in a previously uncharacterized gene, encoding a very large protein called SACSIN with domains suggesting roles as a molecular chaperon or as a component of the ubiquitin-proteasome system. Our physiology and imaging studies revealed that SACSIN is a crucial plant cell component of the adaptation to the ARF-GEF inhibition.

2.2 Introduction

The model organism *Arabidopsis thaliana* has a complex endomembrane system, which has a lot of specialized intracellular trafficking pathways (Paul and Frigerio, 2007). For the membrane protein trafficking, the cargo proteins have to be packed into membrane vesicles, which bud from a donor compartment and later fuse with an acceptor compartment by releasing the cargo. This process of vesicle formation requires ARF GTPases, which mediate the recruitment of vesicle coats at the donor membrane (Singh et al., 2018). ARFs act as nucleotide-dependent molecular switches regulating cell processes by action on effectors (Singh et al., 2017). For this process to take place the small GTPases of the ARF class are activated or inactivated by the binding or hydrolysis of GTP. The GTPase-activating proteins (GAPs) stimulating the release of phosphate, whereas the exchange of GDP to GTP is

mediated by guanine nucleotide exchange factors (GEFs). They constitutively cycle between a membrane-associated and active GTP-bound form and a mainly cytosolic and inactive GDP-bound conformation (Vernoud et al., 2003; Grosshans et al., 2006). After being activated, the ARF proteins are able to recruit cytosolic coat proteins Coat Protein Complex I (COPI), COPII, and clathrin to the vesicle budding site at the Golgi apparatus, *trans*-Golgi network (TGN), plasma membrane (PM), and endosomal compartments (Serafini et al., 1991; Bonifacino and Lippincott-Schwartz, 2003) and they regulate diverse processes such as vesicle budding (Zerial and McBride, 2001; Vernoud et al., 2003; Rutherford and Moore, 2002). The studies of the ARF-GEFs and their cellular and developmental roles have been greatly aided by the implementation of BrefeldinA (BFA), a fungal toxin specifically targeting the ARF-GEFs (Mossessova et al., 2003).

In *Arabidopsis thaliana* there are eight large ARF-GEFs, which can be split into two different subfamilies: the GGG class, which includes GNOM, GNOM-LIKE1 (GNL1) and GNL2 and in the BIG class, which contains five members – from BIG1 to BIG5. Moreover, in this model organism, two of the ARF-GEFs are BFA insensitive – GNL1 and BIG3 (Anders and Jürgens, 2008). Additional proteins, which participate in the GTPase machinery are the ARF-GAPs. The family consists of 15 members, which can be grouped in 7 classes (Singh et al., 2018). Among the known ARF-GAPs there is the VAN3/SCARFACE protein, which is active in TGN/EE and plasma membrane and is participating as trafficking regulator on the plasma membrane and appears to play a crucial role in auxin-related patterning (Koizumi et al., 2005; Naramoto et al., 2009, 2010).

The phytohormone auxin participates in many crucial developmental processes and regulates various cellular responses in plants (Adamowski and Friml, 2015). There, the plasma membrane proteins can recycle from between the plasma membrane and the endosomes (Geldner et al., 2001). This endocytic recycling allows the regulation of the protein amount at the plasma membrane as well as the changes in the polar distribution of the PIN auxin efflux carriers, which defines the cell-to-cell auxin transport and mediates the directionality of it. This is crucial for the embryogenesis, organogenesis and also during gravitropic and phototropic response in plants (Friml et al., 2003; Benkova et al., 2003; Rakusová et al., 2016). The PIN auxin transporters undergo constitutive clathrin-mediated endocytosis and subsequent recycling to different polar domains. This vesicle trafficking process, requires GNOM ARF-GEF (Geldner et al., 2003; Mossessova et al., 2003; Kleine-Vehn and Friml, 2008;

Naramoto et al., 2014; Anders and Jürgens, 2008) and other ARF GEFs (Tanaka et al., 2009, 2013; Kitakura et al., 2017; Kania et al., 2018).

The inhibition of the recycling of the PIN proteins through the endomembrane compartments results in the formation of so called BFA bodies after short treatment (Geldner et al., 2001). After prolonged treatment, the cells gradually adapt to BFA; BFA bodies dissipate but PIN proteins transcytose from the basal to the apical side of the cell (Kleine-Vehn and Friml, 2008; Kleine-Vehn et al., 2008b). Nonetheless, the mechanism, by which cells adapt to the compromised ARF-GEF activity, is unknown.

Previously, microscopy-based genetic approaches using *PIN1pro::PIN1-GFP* line led to identification of trafficking mutants such as *ben1* (*bfa-visualized endocytic trafficking defective1*), which mediates endosomal trafficking and encodes AtMIN7/BIG5; *ben3*, which encodes a member of BIG family ARF GEFs, BIG2 and confers BFA sensitivity to the TGN/EE; or *bex5* (for *BFA-visualized exocytic trafficking defective*), which has defects in the exocytosis trafficking small GTPase, RAS GENES FROM RAT BRAINA1b (RabA1b) (Tanaka et al., 2009; Feraru et al., 2012; Kitakura et al., 2017). Whereas the *ben* mutants show less sensitivity to the BFA treatment, *bex1* (Tanaka et al., 2013) and *bex5* (Feraru et al., 2012) show higher sensitivity to BFA and form more pronounced BFA bodies. The listed examples are an evidence that screens in *Arabidopsis thaliana* based on alterations in the localization or intensity of the fluorescent marker and involving pharmacological treatment represent a good tool for the identification of novel trafficking components (Zwiewka and Friml, 2012).

Here we took advantage of the morphological defects induced by BFA and screened for mutants developing better on medium supplemented with BFA. We identified a recessive mutant *bar1* (*bfa altered response 1*), which grows better on a BFA-containing medium but is unable to adapt its subcellular trafficking to a prolonged BFA exposition. Mapping of the causative mutation and analysis of additional alleles identified *SACSIN* gene coding for a large, protein of an unknown function as a first component of a so far elusive mechanism of vesicle trafficking adaptation to adversary conditions.

2.3 Results

2.3.1 Forward genetic screening for Brefeldin A-resistant mutants

We designed a forward genetic screen for the identification of novel trafficking components in *Arabidopsis thaliana*. For this, we made use of a well-established inhibitor of vesicle trafficking, Brefeldin A (BFA), which causes accumulation of plasma membrane proteins, such as basal localized PIN1, into intracellular aggregates, which are known as BFA bodies. We used an EMS-mutagenized *PIN1pro::PIN1-GFP Arabidopsis* population and we screened for mutant candidates, which are growing better in a BFA-supplemented *in vitro* culture (Figure 1A).

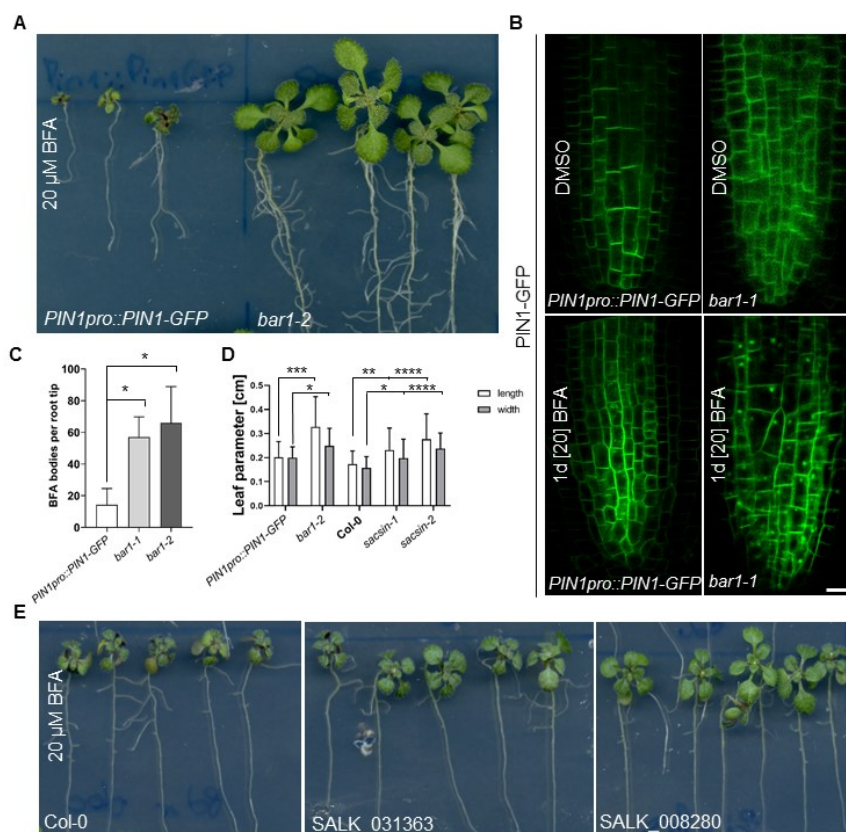


Figure 1: Outline of the forward genetic screen for the identification of novel trafficking components in *Arabidopsis thaliana*. (A): Morphology based screen for mutants with altered developmental response on 20 μM BFA-supplemented medium. *Bar1-2* is growing better on BFA supplemented media in comparison to the parental *PIN1pro::PIN1-GFP* line. (B) Confocal imaging of the selected mutant candidates, which grow better upon inhibited ARF-GEF by the fungal toxin BFA. In the vasculature cells PIN1:GFP is localized in the basal side of the cell in wild type and in the mutant. Upon longer incubation with BFA containing solution (1 day), this lead to apicalization and few small BFA bodies in *PIN1pro::PIN1-GFP*, while the mutant preserves aggregates of internalized PIN1:GFP. (C) Graph, which represents the quantification of BFA bodies remaining in the *bar 1-1* and *bar 1-2* mutants after treatment with 20 μM BFA for 1 day. (D) Graph, which represents the leaf parameters of the point mutant, the T-DNA insertional lines and the corresponding controls on a plate, containing 20 μM BFA. The mutant has longer and wider leaves, compared to the control. (E) Better growth and development of the *SALK_031363* and *SALK_008280* T-DNA insertional lines on BFA supplemented medium compared to the *Col-0* control.

We screened approximately 36.000 seeds (87 pools) for altered growth sensitivity on half strength Murashige and Skoog medium with 1% sucrose ($\frac{1}{2}$ MS) supplemented with 20 μ M BFA, compared to non-mutagenized *PIN1pro::PIN1-GFP* seeds grown in the same conditions. We retained 120 seedlings, which were grown to maturity and their offspring were rescreened both for insensitive growth on 20 μ M BFA supplemented $\frac{1}{2}$ MS. We selected 48 lines with variable growth insensitivity on 20 μ M BFA-supplemented solid medium. After the selection for morphology phenotypes, we performed cell biology characterization where we screened for the altered PIN1 protein accumulation in BFA bodies after long treatment with BFA (1d of 20 μ M BFA) (Figure 1B). From this approach we identified *bar1* (*bfa altered response 1*) which shows growth resistance on an $\frac{1}{2}$ MS supplemented with 20 μ M BFA and which is characterized by persisting PIN1-GFP BFA bodies after 1d treatment with 20 μ M BFA (Figure 1C). In order to identify the causal mutation for the *bar1* phenotypes, we implemented the classical mapping with markers and a Next Generation Sequencing (NGS) approach (Jander, 2006; Weigel and Glazebrook, 2006). For this we generated mapping populations by backcrossing the *bar1* mutant to *PIN1pro::PIN1:GFP* parental plants or to *Landsberg erecta* ecotype. The F2 seedlings were screened for PIN1:GFP accumulation after 1 day incubation on 20 μ M BFA containing $\frac{1}{2}$ MS *in vitro* cultures on solid medium. By the implementation of rough mapping with genomic markers, we found that the mutation is located on the 5th chromosome between the markers T6114 and nga139. For the NGS, we isolated high quality genomic DNA from around 60 plants, which were backcrossed to the parental line. This approach revealed a mutation in a gene on chromosome 5, At5G23110, which encodes a predicted, unusually large protein of unknown function. In *bar1-1*, there is a G to A substitution at the position 1173, which causes an early stop codon that impairs the translation after 390 amino acids of a 4706 amino acids long protein. Independently, we found an allelic mutant, which we named *bar1-2* and it also shows a growth resistance on a BFA supplemented medium and it has bigger leaves in comparison to the parental line (Figure 1A and 1C). It has a C to T mutation at the position 6964 of the AT5G23110 locus. The mutation causes a premature stop codon after 2153 amino acids (Figure 2A). Similar to *bar1-1*, this allele preserves BFA aggregates following prolonged BFA treatment (1d 20 μ M BFA) (Figure 1B and 1C).

To confirm that the mutations in AT5G23110 are responsible for the phenotype, we analysed two T-DNA insertion alleles, SALK_031363 and SALK_008280 (Figure 1E). The homozygous

mutants show similar phenotype to *bar1-1* and *bar1-2* regarding the growth resistance to BFA (bigger leaves and cotyledons) (Figure 1D and 1E) and the increased sensitivity to prolonged BFA treatment on cellular level (persisting BFA bodies after the long treatment with BFA). We also did qRT-PCR analysis of the T-DNA insertional lines and of the *bar1-2* point mutant and we verified that there is none or very less gene expression compared to the corresponding controls (Suppl. Fig. 1).

Thus our morphological BFA screen was instrumental to identify that mutation in AT5G23110 confers changed growth and trafficking sensitivity to ARF-GEF inhibition by BFA.

2.3.2 AT5G23110 encodes SACSIN protein

The AT5G23110 gene has a size of 17576 bp, where the coding sequence is 14121 bp (Figure 2A). It is a single copy gene, which is ubiquitously expressed (Hruz et al., 2008). By cloning a 2300 bp promoter region controlling the GUS expression, we observed the GUS staining in the vasculature cells of the root tip, in the hypocotyl, in the vasculature of cotyledons and leaves (Figure 2B). In addition, we verified that the gene expression in the root tip by a promoter fusion with NLS-GFP (Figure 2C). Moreover, in the genevestigator data (Figure 2D), the highest gene expression is observed in the chalazal endosperm, in the root protophloem and in the giant cell.

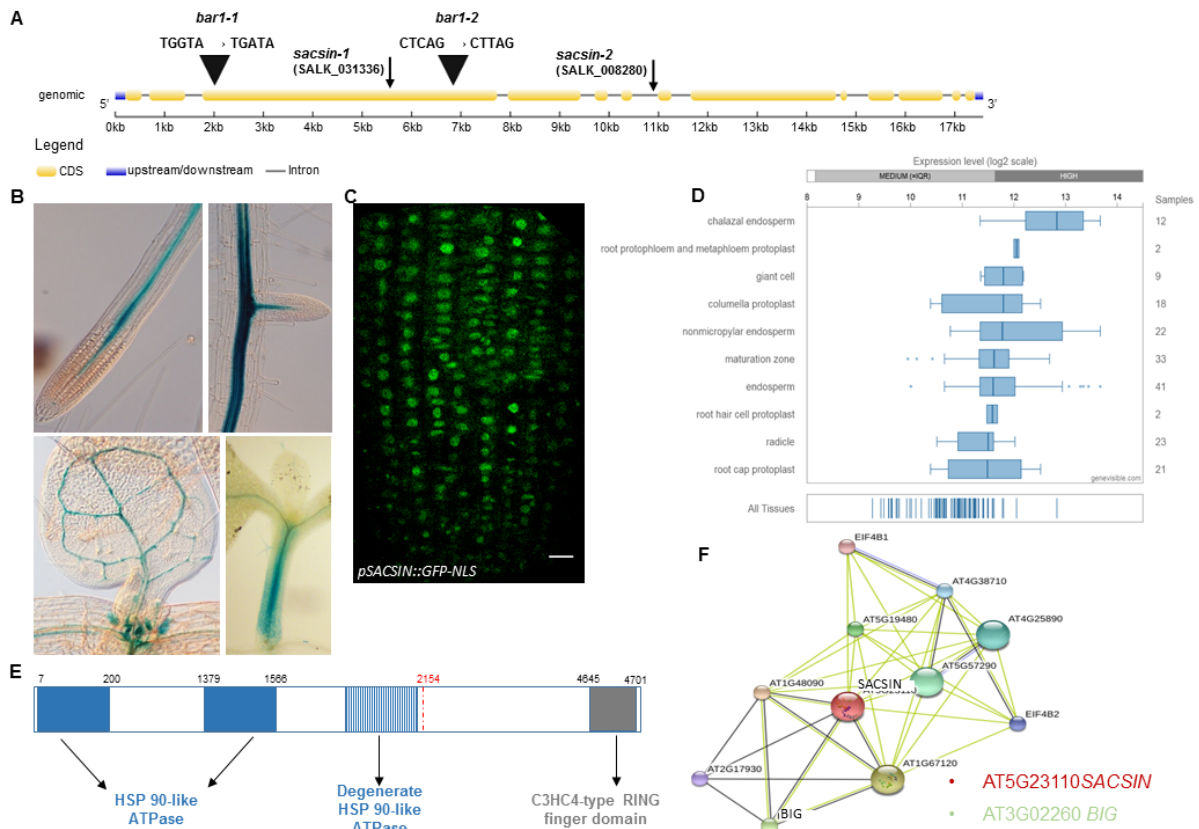


Figure 2. *BAR1* gene and protein structure, gene expression and co-expression graph. (A) Schematic representation of the *bar1* locus. Exons are represented by boxes, while introns are shown as lines. Coding regions are filled with yellow. Exact locations of the T-DNA insertions are depicted by arrows and the exact location of the point mutations are illustrated by triangles. **(B)** Expression of pSACSIN::GUS in the stele cells of the root, in the vasculature of the leaf and in the hypocotyl. **(C)** Expression of pSACSIN::NLS-GFP in the root tip. **(D)** Genevestigator data on the gene expression of the gene AT5G23110. **(E)** Domain organization of the BAR1 protein. The predicted domains are illustrated as rectangular. In blue these are the HSP 90-like ATPase domains, in striped blue there is the degenerate HSP 90-like ATPase domain and in grey there is the C3HC4-type RING finger domain. The stop codon and the corresponding amino acid number are illustrated in red. **(F)** STRING co-expression graph of SACSIN and BIG.

The protein motif prediction suggests two large repeat regions that have a HSP90-like ATPase function and one degenerate domain with the same function, as well as a C3HC4 RING-finger domain at the carboxyl terminus (Figure 2E). Based on the presence of these conserved domains, some of which are present in molecular chaperons and components of the ubiquitin-proteasome system. Moreover, the protein is a member of the Zinc-finger family, possessing a C3HC4 domain in a RING conformation (Kosarev et al., 2002), which is a motif encoded by the *Really Interesting New Gene* (Freemont et al., 1991). In addition, it is known that those class of proteins participate in a large number of cellular processes such as recombination, transduction and transcription (Stone et al., 2005) and play important roles in various physiological processes of plant life. Other functions are linked to protein-protein interaction and a key role in the ubiquitination pathway (Lorick et al., 1999; Borden, 2000).

Thus, this protein is prone to interact with other proteins and presumably to regulate proteostasis (Powers and Balch, 2013). In addition, our evolutionary analysis showed the AT5G23110 protein is conserved and is present in the genome of some of the very early diverging plant species like the green algae, *Marchantia* or *Physcomitrella patens* (Suppl. Fig 2A).

In humans, the *SACS* gene encodes a similar protein with a ubiquitin-like (UBL) domain, which has a role in the proteasome binding, three large domains with an HSP90-like chaperone function, a DnaJ and a HEPN domain, which can dimerize (Bradshaw et al., 2016) (Suppl. Fig. 2B). Mutations in this gene lead to a neurodegenerative disease ARSACS, which causes a defect in the mitochondria fission (Bradshaw et al., 2016). Due to the homology with the protein encoded by AT5G23110, which is pronounced in the similarity in the HSP 90-like ATPase domains, we named the AT5G23110 gene *AtSACSIN* and the corresponding predicted protein AtSACSIN.

In addition, functional protein association network predicted by STRING (Figure 2F) (Szkarczyk et al., 2017) found several possible associated proteins including translation factors, as well as the BIG/Callosin-like protein, which is known to have a role in trafficking of auxin transporters (Gil et al., 2001). The connection to the BIG protein is of a particular interest, as *big* loss-of-function alleles show, similar to *bar* mutants, defects in BFA-sensitive PIN trafficking (Paciorek et al., 2005).

2.3.3 Plant growth and development in *sacsin* mutants

To gain insight into possible developmental roles of AtSACSIN, we utilized *bar1-2*, SALK_031363 (*sacsin-1*) and SALK_008280 (*sacsin-2*) mutant alleles and analysed their seedling development. We grew seedlings for 6 days on a ½ MS plate and then transferred them to a 20 µM BFA containing ½ MS plates, where *bar1-2* had a more resistant phenotype in comparison to the control seedlings (*PIN1pro:PIN1-GFP*) (Figure 1A and 1E) .

We also characterized the *sacsin* phenotype in normal conditions (on a ½ MS solid medium). The original *bar1* allele showed slightly longer primary root length (Figure 3A and 3B) and an increased density of the initiated lateral roots (Figure 3A and 3C).

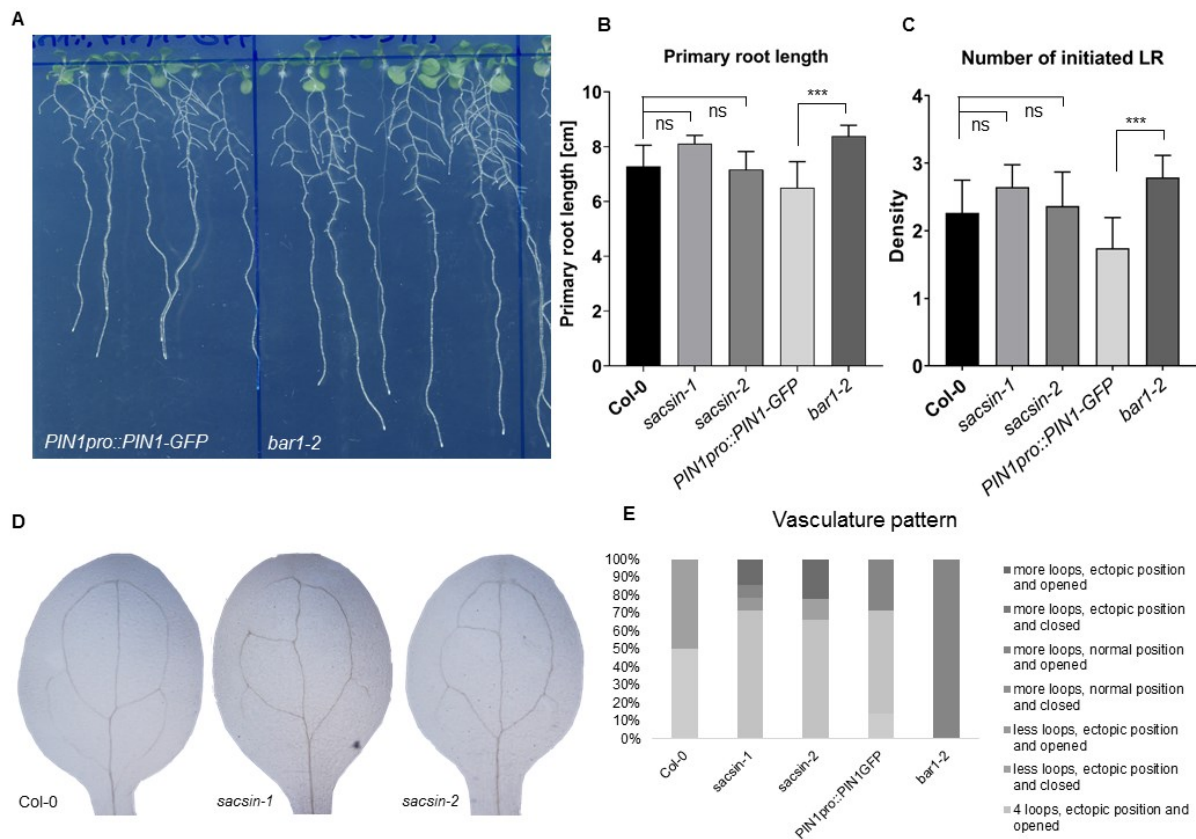


Figure 3. Morphology phenotypes of *saccsin* (A) Representative image of the *PIN1pro::PIN1-GFP* and *bar1-2* seedlings growth and development on ½ MS solid medium. (B) Primary root length in cm in the *bar1-2* and *saccsin* and in the corresponding controls. *Bar1-2* has a significantly longer and the *saccsin* T-DNA insertional alleles have slightly longer, but not significant, primary root. (C) Density of the initiated lateral roots in *saccsin* and in the corresponding controls. *Bar1-2* has a significantly increased density of lateral roots and the *saccsin* T-DNA insertional lines have slightly increased density of LR, but not significant. (D) Representative images of analysed vasculature defects. (E) Quantification of the observations on the vasculature phenotype in the corresponding genotype. The *saccsin* mutant has a more complex vasculature pattern.

We also analysed the vasculature formation during leaf venation. After clearing of the cotyledons, we noticed venation alterations in *saccsin* mutants (Figure 3D), manifested by increased number of loops, ectopic position of loops and open veins (Figure 3E). Next, we characterized the role of *saccsin* in the gravitropic response. We performed a kinetic study of the root bending after gravistimulation and did not observe any obvious defects (Suppl. Fig. 3D). We also analysed other growth parameters such as hypocotyl elongation and bending in the dark (Suppl. Fig. 3A and 3B), apical hook opening (Suppl. Fig. 3C) and seed length and seed width (Suppl. Fig. 3E and 3F).

With exception of more irregular leaf venation pattern, *saccsin* mutants do not show any obvious developmental aberrations when grown under standard conditions.

2.3.4 Endomembrane and subcellular trafficking in *sacsin* mutants

Next, we analysed a role of SACSIN in subcellular trafficking by quantitatively assessing various trafficking processes in *sacsin* mutants. First, we assessed endocytosis rate and endomembrane dynamics by monitoring uptake of the lipophilic dye FM4-64, which is internalized with the endocytic vesicles and as a result stains the early endosomes (Jelínková et al., 2010). This analysis did not reveal any significant differences in the endocytosis rate between *sacsin* mutants and control lines (Suppl. Fig. 4A).

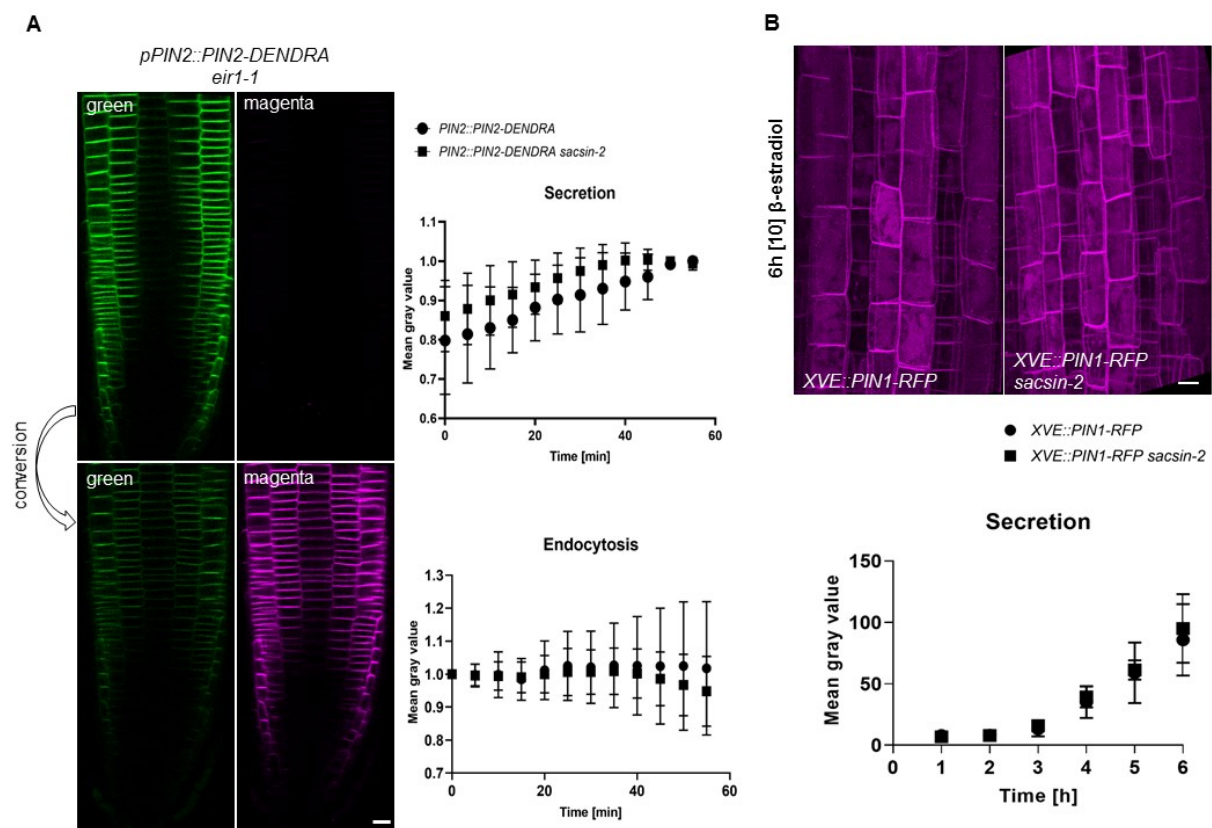


Figure 4: Non-BFA related cell phenotype of *sacsin*. (A) Before the photoconversion, there is green signal, but no magenta signal. After the photoconversion the old pool of PIN2 protein can be visualized in the magenta channel and there is a decrease in PIN2-Dendra magenta signal and increase in the green signal over time, reflecting the rate of endocytosis and exocytosis and secretion, respectively. The mean gray value was quantified and normalized for a time period of 55 min after the photoconversion. There is no significant change in the rate of endocytosis and secretion or exocytosis in the signal when comparing the mutant background to the control. (B) Secretion of the PIN1-RFP protein to the plasma membrane for a time frame of 6h after induction with 10 μ M β -estradiol. There is no significant change in the amount of secreted PIN1-RFP protein after the induction.

Next, we used the photoconvertible *pPIN2::PIN2-Dendra* line (Salanenka et al., 2018). After irreversible Dendra photoconversion from green to red, we examined the fate of the already

present PIN2 (magenta) and of the newly synthesized PIN2 protein (green). We quantified the depletion of the magenta signal from the plasma membrane over time corresponding to the PIN2 endocytosis. On the other hand, we monitored the recovery of the green signal, which corresponds to the newly synthesized PIN2 at the plasma membrane. Again, we did not observe any significant alterations in PIN2 endocytosis and secretion in the *sacsin* mutant (Figure 4A). To confirm the PIN2-Dendra observations, we performed the fluorescence recovery after photobleaching (FRAP) and live imaging of the parental *PIN1pro::PIN1-GFP* and *bar1-2* lines (Suppl. Fig. 4B). A region of interest of the PIN1-GFP fluorescence was almost completely bleached in the whole cell, so that the signal recovery indicated predominantly the delivery of the *de novo* synthesized PIN1. Again there was no obvious difference between the FRAP kinetics in the parental and mutant line. Next, we used the estradiol-inducible PIN1-RFP line to analyse the fate of the newly synthesized PIN1 protein. We did a kinetic study on the secretion of the newly synthesized PIN1 protein to the plasma membrane by quantifying the mean grey value of the plasma membrane in the *sacsin* mutant after induction with 10 μ M β -estradiol (Figure 4B). We did not observe a significant difference in the amount of the secreted PIN1-RFP over a period of 6h. However, after the simultaneous induction of PIN1-RFP expression by 10 μ M β -estradiol and treatment with 25 μ M BFA for 6h, we observed bigger and more BFA bodies in the *sacsin* mutant, compared to its control (Suppl. Fig. 4C). This confirms the previous observation that the *sacsin* mutant is more sensitive to BFA in terms of PIN trafficking (see Figure 1B).

As next we examined vacuolar targeting of the GFP-fused proteins as visualized by a dark treatment experiment (Kleine-Vehn et al., 2010). After 4h in the dark, we observed that in both the wild type and the *sacsin* mutant, PIN2-GFP was targeted to the lytic vacuole (Suppl. Fig. 4D). From this experimental setting we conclude that the *sacsin* mutation does not visibly interfere with the degradation pathway.

In summary, the FM4-64 uptake experiments, the *PIN2::PIN2-Dendra* photoconversion, the FRAP experiments, the β -estradiol inducible PIN1-RFP line and the dark treatment revealed that SACSIN is not essential for basic trafficking processes, at least under optimal growth conditions, nonetheless, it may be involved in reaction of endocytic trafficking to inhibition by BFA.

2.3.5 SACSIN role in BFA-sensitive trafficking

Next, we analysed in detail the role of SACSIN in subcellular dynamics and trafficking processes in presence of BFA. Our immunolocalization studies revealed no alterations in the PIN1 or PIN2 localization in the *sacsin* mutant lines under standard conditions (Figure 5A and Figure 5B). After a treatment for 90 min with 50 μ M BFA, the number of PIN1 BFA bodies in the mutant was comparable to the one in wild type (Figure 5A) but slightly increased in the mutant for the PIN2 cargo (Figure 5B). In conclusion, these results indicate that *sacsin* is inducing a comparable or slightly increased number of BFA bodies for PIN1 and PIN2 proteins after short treatment with the compound.

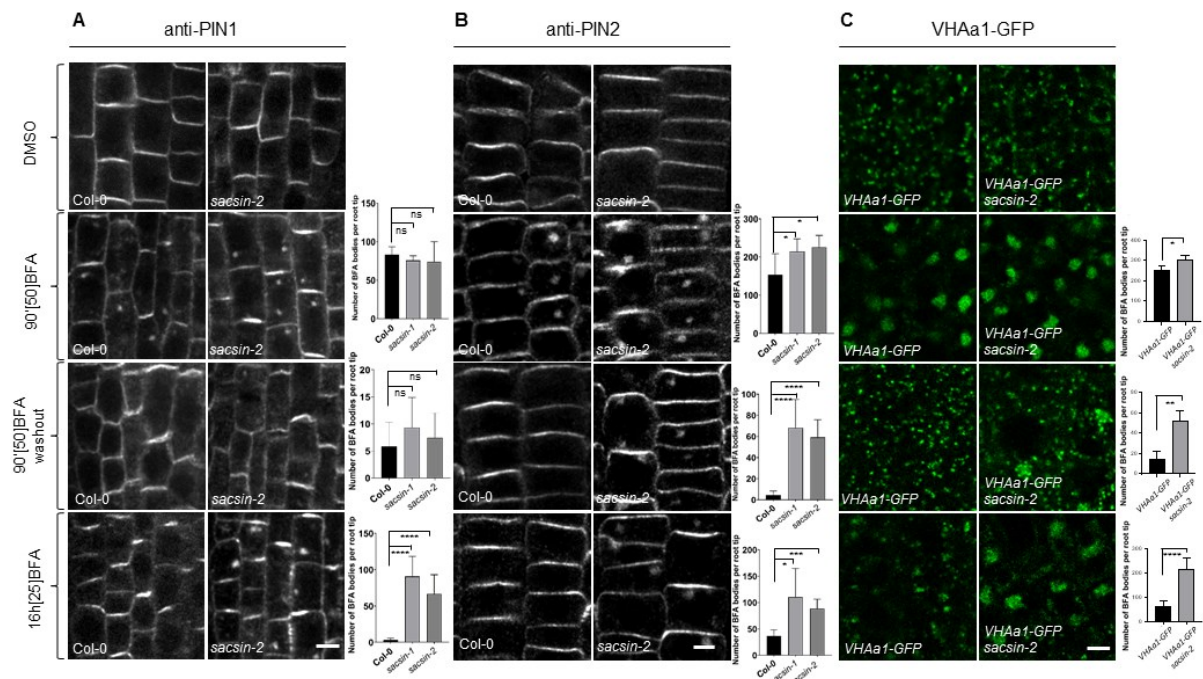


Figure 5: *sacsinn* is defective in exocytosis and transcytosis
(A) Immunolocalization of PIN1 protein (vasculature cells). **(B)** Immunolocalization of PIN2 (epidermis cells). **(C)** Life imaging of the VHAa1-GFP protein (TGN marker). A 90 min treatment with 50 μ M BFA causes increased intracellular protein accumulation in the *sacsinn* mutant. A 1.5-h treatment with 50 μ M followed by a 1.5-h wash out with liquid medium led to almost complete disappearance of PIN1 and PIN2, but also of VHAa1-GFP from the bodies in wild type, but in the *sacsinn* mutant there were more BFA bodies, which remained in the cells. No or very less intracellular PIN1, PIN2 or TGN marker accumulation could be observed in the wild type cells treated for 16 h with 25 μ M BFA. In contrast, pronounced intracellular protein accumulation persisted in the *sacsinn* cells. Data is means \pm SD; ≥ 8 roots were analysed for each genotype.

To further investigate the protein trafficking in *sacsinn* mutants, we did a 90 min treatment with 50 μ M BFA followed by a 90 min washout in $\frac{1}{2}$ MS liquid medium (Figure 5A and Figure 5B). In the wild type, we observed that the proteins, which accumulated into a BFA body,

localized almost completely back to their polar domain (Geldner et al., 2001). In contrast, in the *sacsin* mutant many BFA bodies persisted, which remained in the cell.

Prolonged treatment with BFA causes that PIN1, normally localized at the basal cell side in the stele cells of the *Arabidopsis thaliana* root, first accumulates into BFA bodies and later it transcytose to the apical side of the cells (Kleine-Vehn et al., 2010). In the wild type situation there are none or very little BFA bodies, which remain in the cells after a 16h treatment with 25 μ M BFA (Figure 5A and 5B). In contrast, in the *sacsin* mutants there are a lot and bigger BFA body accumulations, which persist in the cells (Figure 5A and 5B). These results support the hypothesis that in *sacsin* mutants the cells are not able to efficiently recover from BFA treatment.

Next, we analysed directly the BFA effect on the endomembrane system using the early endosome marker VHAa1-GFP (Figure 5C) and of the Golgi apparatus marker Sec21 (Suppl. Fig 5B). Both endomembrane markers showed similar cell biology phenotypes as with PIN1 and PIN2 (Figure 5A and 5B). In control situation there were multiple Golgis and TGNs dispersed in the cytosol. Treatments with BFA lead to their aggregation into bodies and the washout experiments lead to their disaggregation. In the *sacsin* mutants, there was no altered localization of these markers indicating that the Golgi apparatus and the early endosome morphology are not affected (Figure 5C and Suppl.Fig. 5B). After a short BFA treatment, the endomembrane compartments aggregate normally into BFA bodies and after a washout, they still remain in the cells of the *sacsin* mutant. Also after the long treatment with BFA, these markers remain aggregated into BFA bodies and do not recover as seen in the controls (Figure 5).

Our observations, using immunolocalization and live imaging, show that in the *sacsin* mutants, the recovery of cells from the inhibition of the ARF GEF function is defective. PM markers such as PIN auxin transporters as well as Golgi apparatus and TGNs in *sacsin* root cells aggregate in response to BFA normally but they do not adapt to this inhibition and also their recovery after BFA removal is dramatically delayed.

2.3.6 Roles of SACSIN and GNOM ARF-GEF in apical-basal PIN targeting

Long-term adaptation of cells to BFA does not involve only the dissolution of BFA body but also a shift of basally localized PIN proteins from the basal to the apical cell side (Kleine-Vehn et al., 2008a). PIN basal targeting is dependent on GNOM, and in the weak *gnom*^{R5} allele, PIN1 in the stele is often missorted to the apical cell side (Kleine-Vehn et al., 2008a)(Figure 6A and 6B). The degree of apicalization in the *gnom*^{R5} mutant is further enhanced by the BFA treatment (Figure 6A and 6C). Apart from analysing the basic trafficking processes and reactions of the endomembrane system to BFA, we also investigated the effect of *sacsin* mutation on native and BFA-induced apical-to-basal transcytosis. We found that the *sacsin* mutant had normal, basally localized PIN1 (Figure 6B) and after a long BFA treatment, the degree of PIN1 apicalization appeared normal (Figure 6C). In the double mutant *sacsin gnom*^{R5}, we found that the *sacsin* mutation did not influence (neither increase nor decrease) the effect of *gnom*^{R5} on basal-to-apical transcytosis whether undisturbed or after a long BFA treatment (Figure 6B and 6C). However, in the double mutant, we still observed the *sacsin* cellular phenotype, namely, that the BFA bodies persisted in cells after long BFA treatment (Figure 6D).

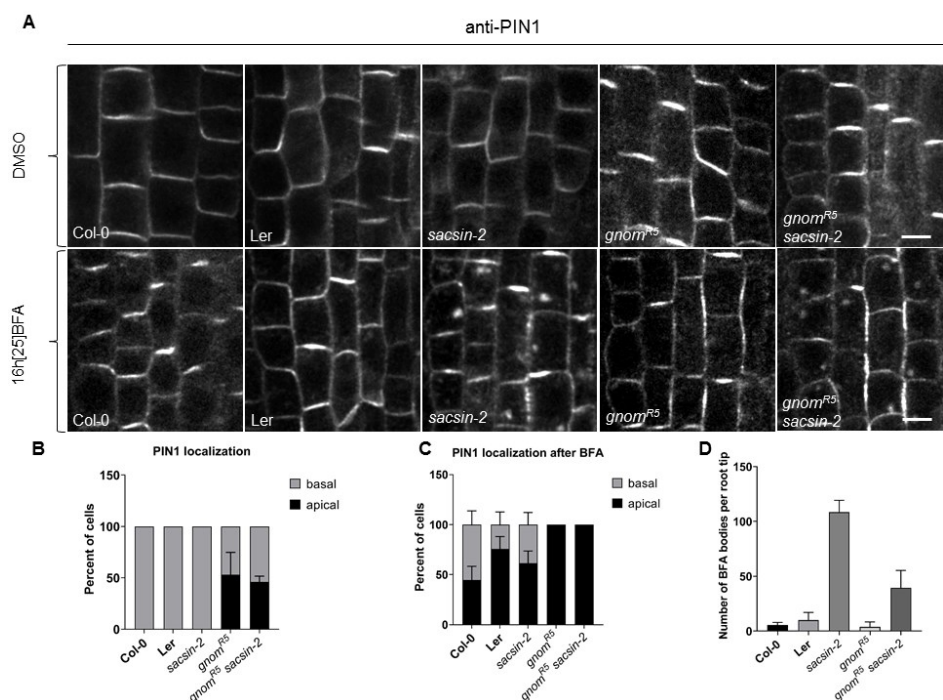


Figure 6: Characterization of *gnom*^{R5} cross (A) PIN1 immunolocalization in non treated cells and after a treatment for 16h with 25 μ M BFA. (B) and (C) Graphs, representing the observations of the polarity of the PIN1 protein to the basal or to the apical cell side in the stele cells of the *Arabidopsis thaliana* root tip. The quantification was done in non treated cells (B) and also after a treatment for 16h with 25 μ M BFA (C). (D) A graph, representing the number of BFA bodies per root tip after the treatment for 16h with 25 μ M BFA.

These results suggest that SACSIN does not play a direct role in the apical/basal PIN sorting. It also shows that the aggregation or disaggregation of the BFA bodies and PIN1 presence in them occurs independently from the apical/basal PIN sorting.

2.3.7 Genetic interaction of *SACSIN* and *BIG3* encoding a BFA-resistant ARF-GEF

BIG3 is a BFA-insensitive ARF-GEF, which together with other BIG ARF-GEFs is regulating the process of late secretion from the TGN, but not recycling of endocytosed proteins to the plasma membrane (Richter et al., 2014). Due to its insensitivity to BFA, it plays a major role in conditions of trafficking inhibited by BFA - as shown by the very strong reaction of *big3* to BFA, namely, arrest of seed germination (Richter et al., 2014). Therefore, we tested possible common roles of SACSIN and BIG3 by crossing the corresponding mutants.

In the undisturbed situation, the parental genotypes and the double mutant showed a normal, polar plasma membrane PIN localization with no aggregations of any type (Suppl. Fig. 6A). In the *big3* mutant, 16h treatments with 25 μ M BFA caused the accumulation of the PIN1 protein in intracellular aggregates, similar as seen in *sacsin* (Suppl. Fig. 6B). However, these intracellular bodies in *big3* had a bit different appearance; they appeared fuzzier, like clusters with a less defined structure in comparison with the round, well defined typical BFA bodies (Suppl.Fig. 6B). In the *sacsin big3* double mutant, the BFA bodies morphologically appeared more like in *big3* (Suppl.Fig. 6B).

Whereas subcellular reaction of *big3* and *sacsin* mutants to BFA treatment was not that different, the growth sensitivities to BFA were opposite: the *sacsin* mutant is BFA-resistant while *big3* is highly sensitive to BFA. In the double mutant, the phenotype is that of *big3* (Suppl.Fig. 6C). In conclusion, in terms of BFA reactions, the effects of *sacsin* mutation were masked by the dominant effects of *big3* mutation, suggesting that formally BIG3 acts downstream of SACSIN.

2.3.8 Genetic interaction of *SACSIN* and *BIG/DOC1/TIR3* encoding a Callosin-like protein implicated in auxin action

The bioinformatics tool STRING ((Szkarczyk et al., 2017); Figure 2E), suggested that the genes *SACSIN* and *BIG* are co-expressed. Independently identified mutations in *BIG*, called *doc1* and *tir3* have similar defects related to multiple signalling pathways including auxin (Ruegger et al., 1997; Gil et al., 2001). Previous research showed, that *doc1* does not form normal lateral roots due to reduced auxin transport to the root, however, if the seedlings were transferred to auxin, the LR are induced (Ruegger et al., 1997); it has a reduced sensitivity to synthetic auxin NAA in terms of BFA-sensitive PIN trafficking (Paciorek et al., 2005) and also sometimes accumulates PIN1 aggregates inside the cell on auxin transport inhibitor NPA (Gil et al., 2001). In addition, both genes *SACSIN* and *BIG* encode very large proteins and both have a relationship to auxin-mediated development and to BFA action. Therefore, we tested genetic interaction between *sacsin* and *doc1*.

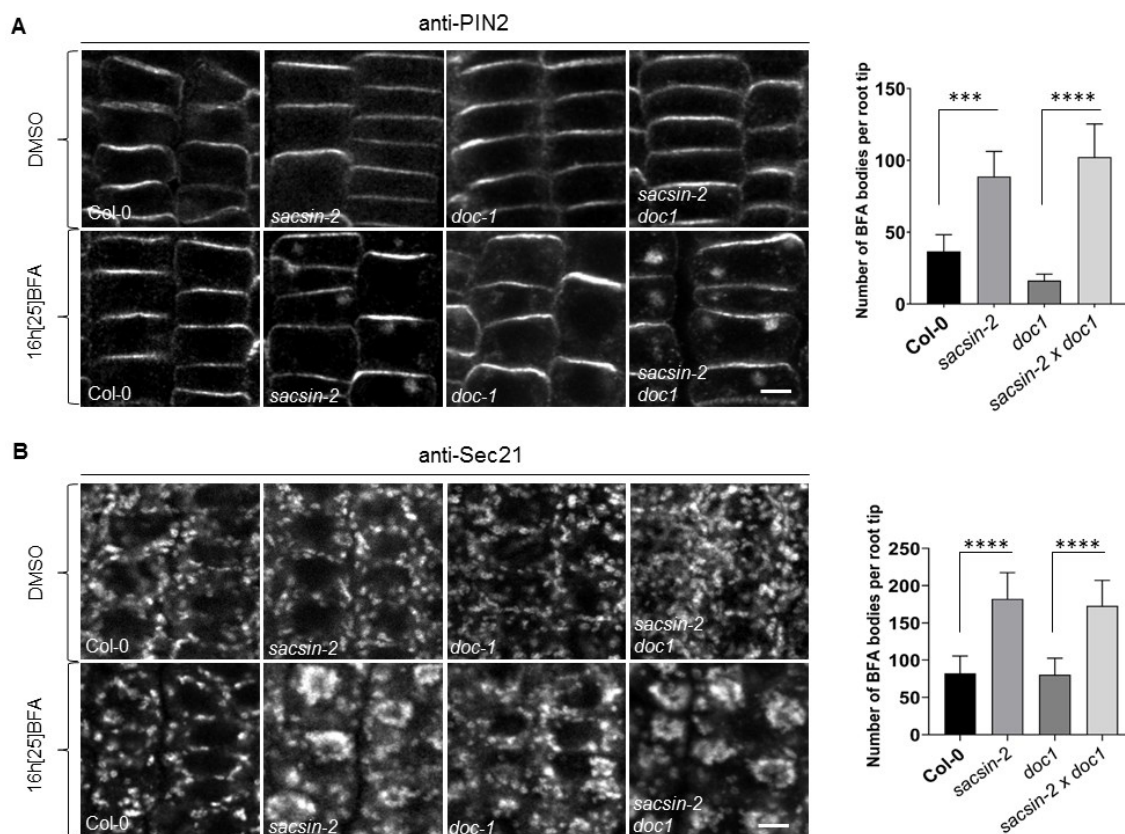


Figure 7: *SACSIN-BIG* genetic interaction on cellular level (A) Immunolocalization of PIN2 in the epidermis cells of wild type, *sacsin-2*, *doc1* and *sacsin-2 doc1* and after treatment for 16h with 25 μ M BFA. There are significantly more BFA bodies in *sacsin-2* and *sacsin-2 doc1*. **(B)** Immunolocalization of Sec21 in wild type, *sacsin-2*, *doc1* and *sacsin-2 doc1* in non treated cells and after treatment for 16h with 25 μ M BFA. There are significantly more BFA bodies in *sacsin-2* and *sacsin-2 doc1*.

In an undisturbed situation, *sacsin* and *doc1* have a normal, apical localization of PIN2 protein in the epidermis cells and there are no obvious alterations in the endomembrane system (Figure 7). After a 16h treatment with 25 μ M BFA, the PIN2 protein in the *sacsin* mutant persists in BFA bodies (Figure 7A). On the other hand, in the *doc1* allele, none or much less BFA bodies persist (Figure 7A). Nevertheless, the *sacsin doc* double mutant shows phenotype very much comparable to *sacsin* single mutant. The same also applies for the Sec21 golgi marker (Figure 7B). In conclusion, the characterization of the cell biology phenotypes is showing epistasis of *sacsin* over the *doc1*.

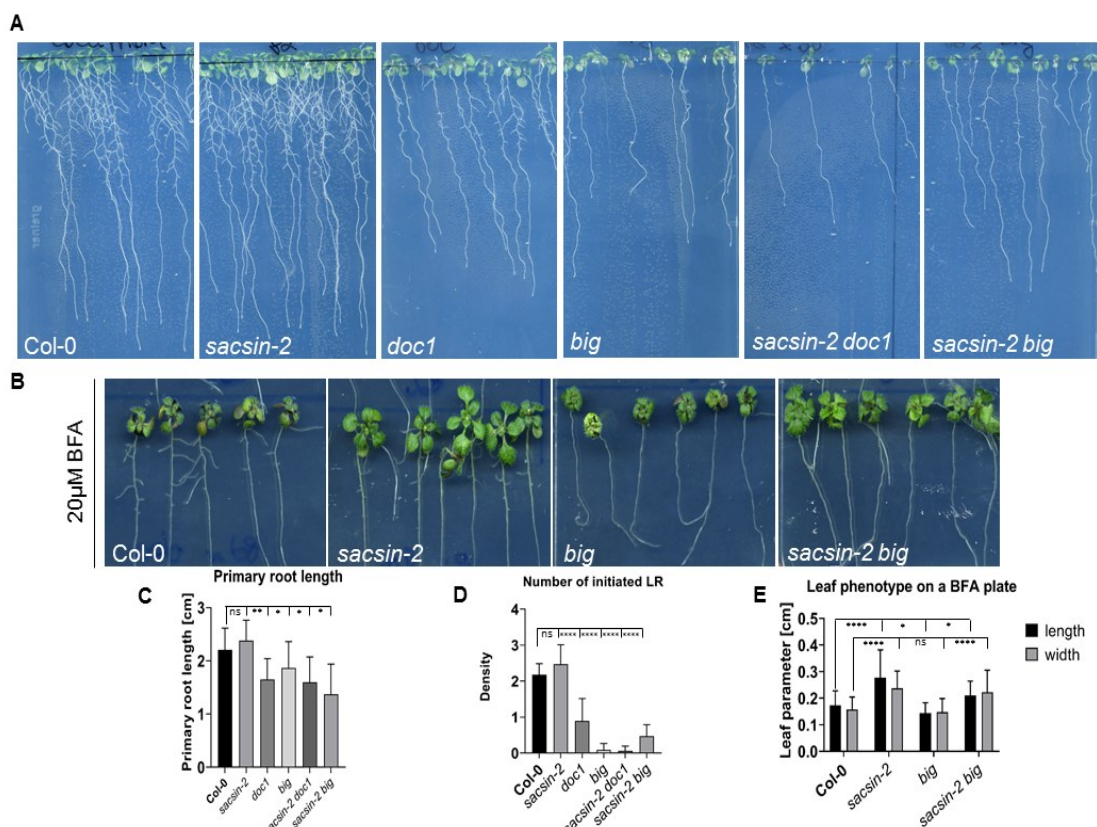


Figure 8: SAC SIN-BIG genetic interaction on morphology level. (A) Morphology phenotype when grown for 10 days on $\frac{1}{2}$ MS medium **(B)** Seedlings, which were grown for 6 days on $\frac{1}{2}$ MS medium and then transferred to 20 μ M BFA supplemented $\frac{1}{2}$ MS medium and grown for 2 weeks. Better growth and development of *sacsin-2* on BFA supplemented medium compared to wild type and to *big* mutant. The *sacsin-2 big* double mutant has a phenotype, which is partly epistatic to *sacsin-2*. **(C)** *sacsin-2* has not significantly longer primary root length in cm in comparison to wild type, *big* and *doc1*. **(D)** Number of initiated lateral roots of *sacsin-2*, *big*, *doc1*, the double mutants and the corresponding control. *sacsin-2* has slightly higher density of lateral roots in comparison to Col-0 and much higher density, compared to *big* or *doc1*. The double mutant has less initiated LR in comparison to Col-0 or *sacsin-2*. **(E)** The morphology phenotype of the double mutant is in between *sacsin-2* and *big* or *doc1*. **(E)** The morphology phenotype of *sacsin-2* on a BFA plate is characterized by larger leaf parameters in comparison to Col-0 and to *big*. The *sacsin-2 big* double mutant has a phenotype, which is comparable to the *sacsin-2* phenotype.

In terms of developmental phenotypes, *doc1* and *big* showed no or strongly decreased initiation of lateral roots (Gil et al., 2001). In contrast, *sacsin* is characterized by a normal or, if anything, a slightly increased lateral root density under normal conditions. In the double mutant, the primary root length of the double mutant was somewhat in between *sacsin* and *big* (Figure 8A and 8C). Moreover, while growing on a 20 μ M BFA containing $\frac{1}{2}$ MS medium, the *sacsin* mutant develops better than wild type (as discussed in Figure 1) and *big* and *doc1* mutants are smaller. Notably, the *sacsin-2 big* double mutant shows a partial resistance to the compound, which is again in between the phenotypes described for the single mutants (Figure 8B and 8E). Thus, the genetic interaction between *sacsin* and *big* can be best described in terms of a mutual partial rescue of two genes with antagonistic effects.

2.4 Discussion and conclusion

An essential functional hub between the cell and the surrounding environment is the plasma membrane of eukaryotic cells (Sigismund et al., 2012). During trafficking, the cargo proteins are packed into membrane vesicles which bud from a donor compartment and later fuse with an acceptor compartment, thus releasing the cargo. The process of vesicle formation requires ARF GTPases, which mediate the recruitment of vesicle coats at the donor membrane (Singh et al., 2018). The general model of ARF function describes them as nucleotide-dependent molecular switches that shift between active, membrane-bound states and inactive cytosolic forms (Vernoud et al., 2003; Grosshans et al., 2006). The membrane-bound form regulates cellular processes by the recruitment of effectors, such as vesicle coats (Singh et al., 2017). For this process to take place, the ARF proteins are activated or inactivated by the binding or hydrolysis of GTP. The GTPase-activating proteins (GAPs) stimulate the release of phosphate, deactivating ARFs, whereas the exchange of GDP to GTP is mediated by guanine nucleotide exchange factors (GEFs), and leading to ARF activation. The known sites of action of the ARF machinery is the Golgi apparatus, *trans*-Golgi network, and the plasma membrane, where ARFs recruit, among others, the cytosolic coat proteins Coat Protein Complex I (COPI) and adaptors for clathrin coats (Serafini et al., 1991; Bonifacino and Lippincott-Schwartz, 2003). The studies of ARFs have been greatly aided by the implementation of Brefeldin A (BFA), a fungal toxin specifically targeting a complex between an ARF and an ARF-GEF (Mossessova et

al., 2003). The inhibition of ARF-GEF function by BFA partially blocks the ARF-mediated trafficking pathways and leads, in *Arabidopsis thaliana*, to the formation of so-called BFA bodies, or BFA compartments, which are aggregates of multiple TGN/EE compartments and Golgi apparatus. Concomitantly, the inhibition of the exocytic step of PIN recycling results in the accumulation of the PIN proteins in the BFA body (Geldner et al., 2001). After a prolonged BFA treatment, the cells gradually adapt to BFA; BFA bodies dissipate and PIN proteins transcytose from the basal to the apical side of the cell (Kleine-Vehn and Friml, 2008; Kleine-Vehn et al., 2008b). Nonetheless, the mechanism, by which cells adapt to the compromised ARF-GEF activity, is unknown.

We took advantage of the morphological defects induced by BFA and screened for mutants developing better on medium supplemented with BFA. We identified a recessive mutant *bar1* (*bfa altered response 1*), which grows better on a BFA-containing medium but is unable to fully adapt its subcellular trafficking to a prolonged BFA exposition. Mapping of the causative mutation and analysis of additional alleles identified a novel *SACSIN* gene coding for a large, protein of an unknown function with similarity to the human protein Sacsin, and whose domain composition suggests a role as a molecular chaperon, or in the ubiquitin-proteasome system. Our morphology analysis shows that there are no developmental defects in the *sacsin* mutant with the exception that there is a more complex vasculature patterning in the mutant alleles. Additionally, after performing a large spectrum of experimental settings to study the subcellular trafficking role of *SACSIN*, we conclude that *SACSIN* is not involved in the trafficking mechanisms under normal conditions, but it is important for the BFA-sensitive trafficking, which we show by immunolocalization studies of PIN proteins and life imaging of the VHAa1-GFP protein. Our results revealed that in the cells of the mutant there are sustaining BFA bodies after washout of the compound, but also after long incubation with BFA. Thus, *sacsin* mutation has a specific effect on BFA reactions, both in the seedling growth and in the cellular reactions of the endomembrane system, observable by a defect in the recovery of the BFA treatment.

Due to the observation that the adaptation of the cell to the long treatment with BFA is characterized by a dissolution of the BFA body and by a shift of the PIN1 protein from the basal to the apical cell side, we wanted to characterize, if the *SACSIN* gene is involved in the basal-apical sorting. For these we studied the genetic interaction between *SACSIN* and *GNOM*^{R5}. *GNOM* is regulating the targeting of the PIN protein to the basal cell side and an

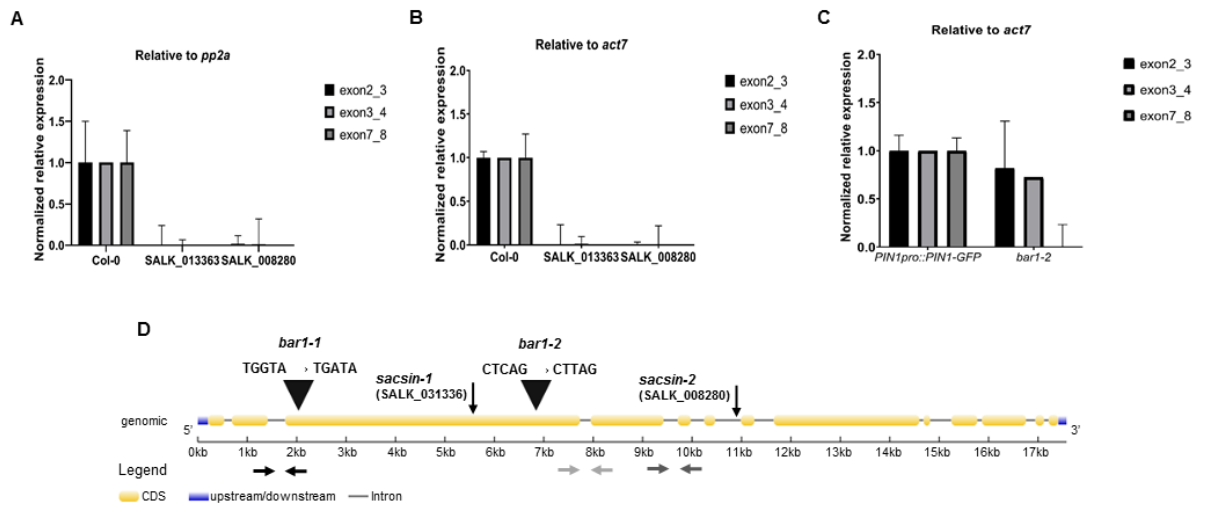
interference with the *GNOM* gene function leads to apicalization of the PIN1 protein in normal conditions (Kleine-Vehn et al., 2008a). On the other hand, after long treatment with BFA, the degrees of apicalization of the PIN1 protein were higher. Moreover, in *sacsin* the PIN1 protein is localized to the basal cell side in the stele cells of the root and after a long treatment with BFA, the levels of apicalization also look normal. However, in the *sacsin gnom^{R5}* double mutant, the *sacsin* mutation does not have an effect on the cellular phenotype of *gnom^{R5}*, neither in normal condition, nor after the long treatment with BFA. Our results suggest that SACSIN does not play a direct role in the apical/basal PIN sorting, and does not influence the polarity-related aspect of BFA action. It also highlights that the aggregation or disaggregation of the BFA bodies, and PIN1 presence in them, occur independently from the apical/basal PIN1 sorting decisions.

In *Arabidopsis thaliana* there are eight large ARF-GEFs, which can be separated into two classes: the GGG class, which includes GNOM, GNOM-LIKE1 (GNL1) and GNL2 that act at the Golgi apparatus, and the BIG class, which contains five members – BIG1 to BIG5 – and acts at the TGN/EE (*trans*-Golgi network/early endosome). Most of these ARF-GEFs are sensitive to BFA, while two of them - GNL1 and BIG3 - are BFA-insensitive due to a natural variation in SEC7 domain sequences (Anders and Jürgens, 2008). BIG3 is an ARF-GEF, which is mediating the late secretion, but not the recycling of the endocytosed proteins (Richter et al., 2014). Additionally, it plays an important role in the BFA sensitive trafficking, which is pronounced by the phenotype of arrested seed germination on solid BFA medium (Richter et al., 2014). Due to this fact, we wanted to characterize in detail the genetic interaction between *SACSIN* and *BIG3*. Whereas the subcellular reaction of *big3* and *sacsin* mutants to BFA treatment was not that different, the growth sensitivities to BFA were opposite: the *sacsin* mutant is BFA-resistant, while *big3* is highly sensitive to BFA. In the double mutant, the phenotype is that of *big3*. In conclusion, in terms of BFA reactions, the effects of *sacsin* mutation were masked by the dominant effects of *big3* mutation, suggesting that formally BIG3 acts downstream of SACSIN. The dominant effects of the *big3* mutation, as well as the particular morphology of *big3* cells after long BFA treatments, can be understood on the basis of BIG3's essential function for ARF activation in the conditions where other BIG ARF-GEFs are chemically inhibited. In contrast, the role of SACSIN appears more as a modifier, rather than a key component of the normal ARF cycle.

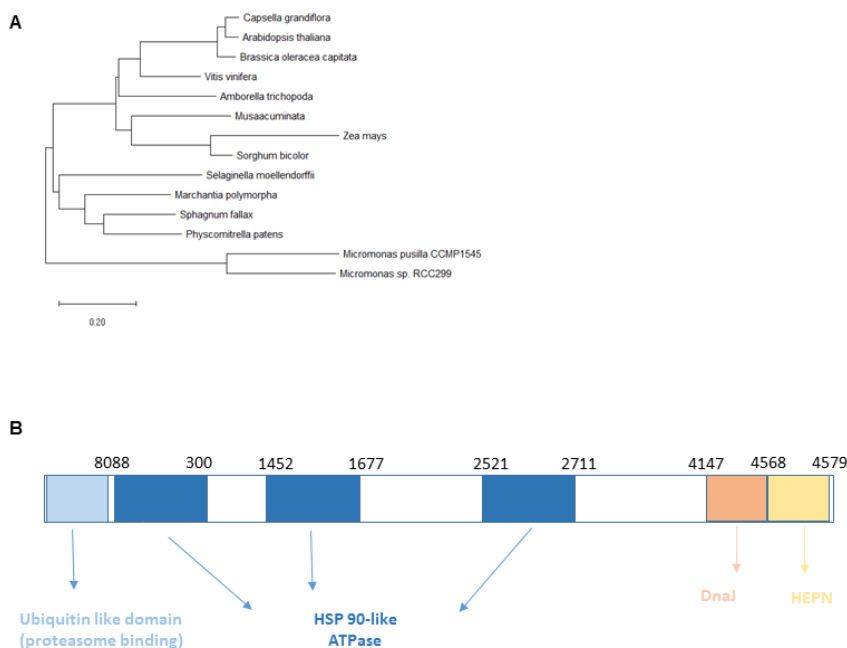
Previous research showed that genes, which are co-expressed are more likely to interact with each other than proteins, which belong to different clusters (Grigoriev and Biotech, 2001). By using STRING as a bioinformatics tools for co-expressions, we identified that *SACSIN* is correlated with *BIG*, which is a regulator of auxin transport (Paciorek et al., 2005). *Doc1* and *tir3* are alleles from the same gene, which is known as *BIG* (Gil et al., 2001). They have less basipetal auxin transport and due to this fact, they develop less lateral roots (Gil et al., 2001). Additionally, it was shown that a higher concentration of auxin is required to block the PIN1 endocytosis upon the implementation of BFA as a membrane trafficking inhibitor (Paciorek et al., 2005). Due to these data and due to our observations that *sacsin* has a better survival on a BFA solid medium, we examined the genetic interaction between *SACSIN* and *BIG*. On a cellular level *sacsin* is epistatic to *doc1* as there are a similar number of remaining BFA bodies in the cells after the long treatment with BFA, which is a phenotype, observed in *sacsin*. In terms of developmental phenotypes, *doc1* and *big* showed no or strongly decreased density of emerged lateral roots (Gil et al., 2001). In contrast, *sacsin* is characterized by a normal lateral root density under normal conditions. Moreover, while growing on a 20 μ M BFA containing $\frac{1}{2}$ MS medium, the *sacsin* mutant develops better than wild type and *big* mutants are smaller. Notably, the *sacsin-2 big* double mutant shows a partial resistance to the compound, which is again in between the phenotypes described for the single mutants. Based on this observation, the genetic interaction between *SACSIN* and *BIG/DOC1/TIR3* can be described in terms of additive phenotypes.

In these project we identify a novel component of intracellular trafficking in *Arabidopsis thaliana*. We show that a morphology based screen is a good method for the identification of novel components of endomembrane trafficking. We identify *BAR1/SACSIN*, which grows and develops better on BFA solid medium. *SACSIN* has a role in multiple *GNOM* regulated trafficking processes and plays a specific role in the adaptation to chemically induced inhibition, while apparently it does not exhibit a significant influence on normal cell function and development.

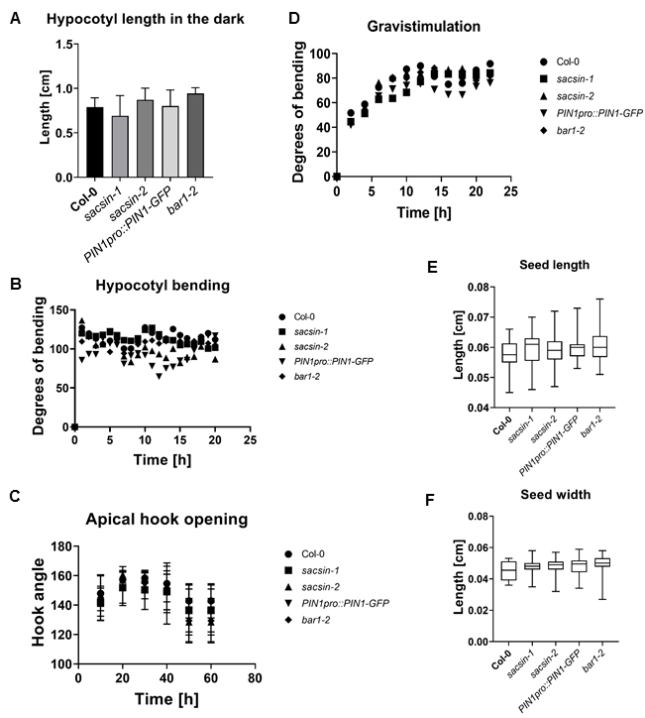
2.5 Supplementary



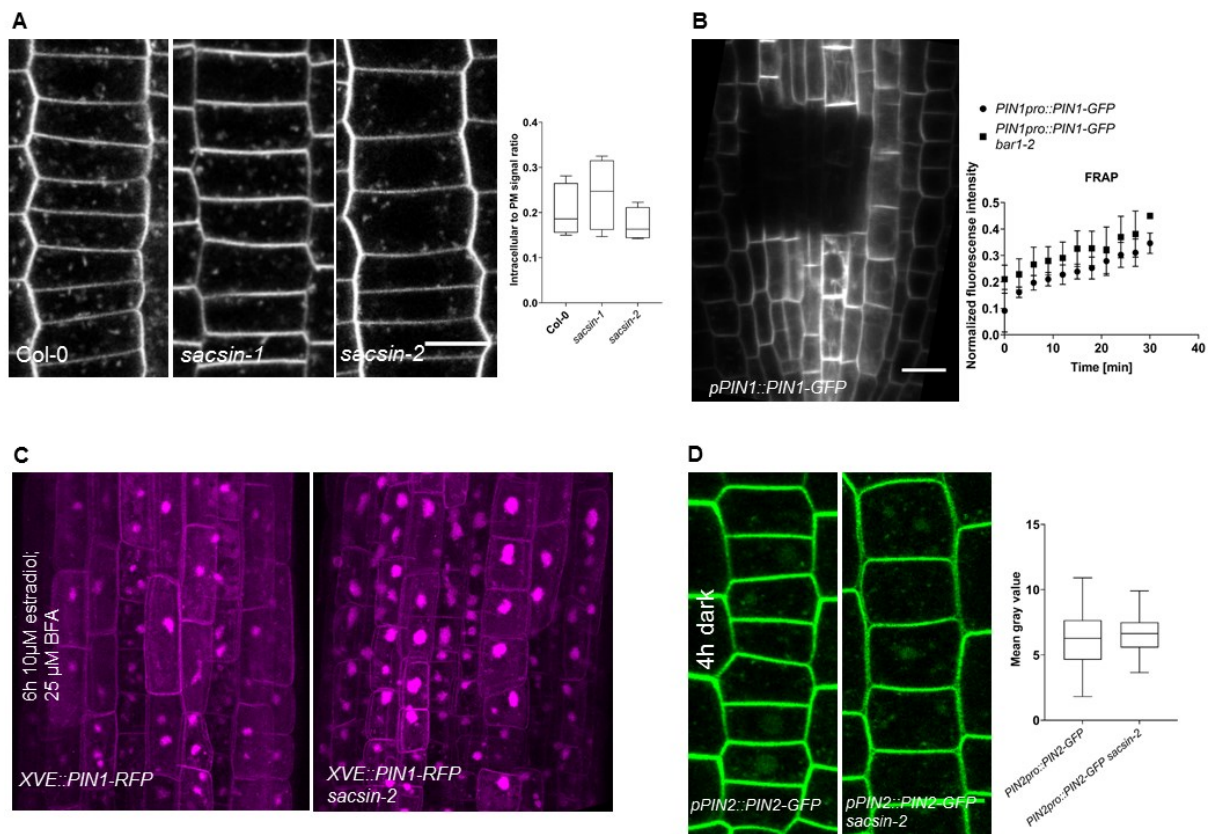
Suppl. Fig. 1: qRT-PCR analysis of the T-DNA insertional lines and the *bar1-2* expression in the isolated mutant lines. (A) Normalized relative expression to *pp2a*. **(B)** Normalized relative expression to *act7*. **(C)** Normalized relative expression to *act7*. **(D)** Schematic representation of the *bar1* locus. Exons are represented by boxes, while introns are shown as lines. Coding regions are filled with yellow. Exact locations of the T-DNA insertions are depicted by arrows and the exact location of the point mutations are illustrated by triangles. The different set of primers for the qRT-PCR analysis are shown by arrows and the colour of the arrows corresponds to the colour of the column in the charts.



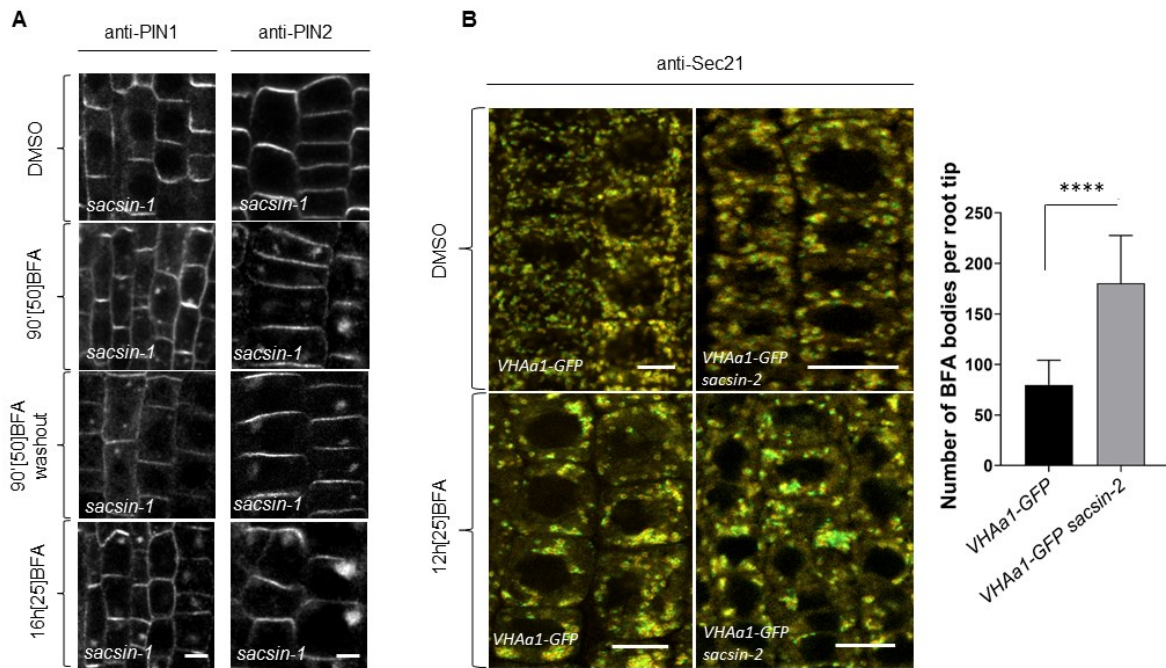
Suppl. Fig. 2: Evolutionary analysis of the BAR1 protein and SACSIN protein structure in humans. (A) Evolutionary tree, which represents that the BAR1 protein is conserved and is present in the genome of the very early diverging plant species like green algae, *Marchantia polymorpha* and *Physcomitrella patens*. **(B)** Domain organization of the SACSIN protein in humans. The predicted domains are illustrated as rectangular. In blue these are the HSP 90-like ATPase domains, in light blue there is the ubiquitin-like domain, in orange there is the DnaJ domain and in yellow the HEPN domain. The corresponding amino acid numbers are illustrated in black.



Suppl. Fig. 3: Phenotypic analysis of *saccsin*. (A) Hypocotyl length in the dark. (B) Hypocotyl bending. (C) Apical hook opening. (D) Gravistimulation. (E) Seed length. (H) Seed width.

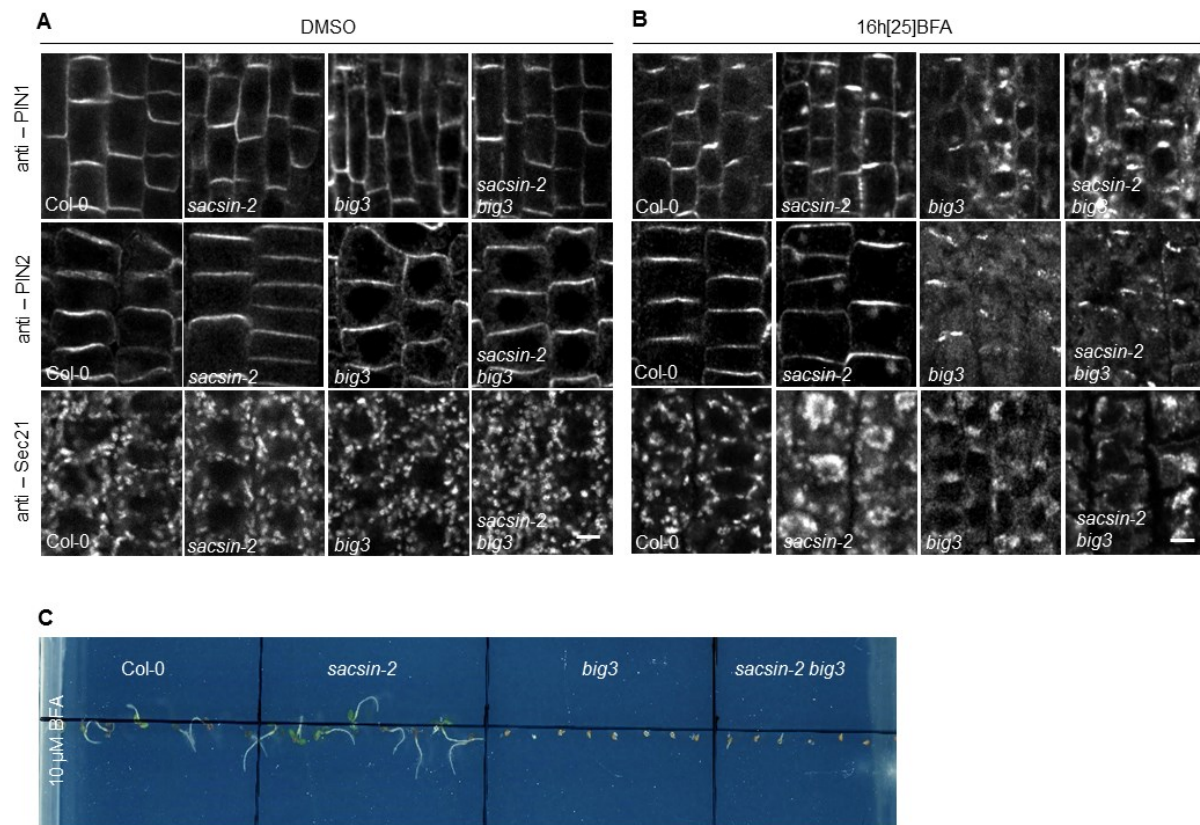


Suppl. Fig. 4: Non-BFA related cell phenotype of *saccsin* (A) Live imaging of FM4-64 (10 min; 2 μ M). There is no significant change in the amount of internalized clathrin-mediated endocytosis marker in *saccsin* and the corresponding control. (B) Fluorescence recovery after photobleaching (FRAP) in seedlings expressing PIN1-GFP. Root vasculature cells were imaged pre-bleach, after bleaching with the 488nm argon laser, and then the recovery of the signal was followed over time. Data is means \pm SD, $n \geq 3$ roots per genotype. No significant differences in the rate of fluorescence recovery was observed between *PIN1pro::PIN1-GFP* and *bar1-2*. (C) Fate of the newly synthesized PIN1-RFP protein after induction with 10 μ M β -estradiol and simultaneous treatment with 25 μ M BFA for 6h in the *XVE::PIN1-RFP* line in wild type and *saccsin* mutant background. (D) Trafficking to the vacuole is not affected in *saccsin* mutant. A 4h dark treatment results in PIN2-GFP accumulation into vacuoles of both wild type and *saccsin* epidermal cells.



Suppl. Fig. 5: *saccsin* is defective in exocytosis and transcytosis

(A) Immunolocalization of PIN1 protein (vasculature cells) and of PIN2 (epidermis cells) for the *saccsin-1* allele (SALK_031336). A 90 min treatment with 50 μ M BFA causes intracellular protein accumulation in the *saccsin* mutant. A 1.5-h treatment with 50 μ M BFA followed by a 1.5-h wash out with liquid medium led to remaining BFA bodies in the cells of the *saccsin-1* mutant. Pronounced intracellular protein accumulation persisted in the *saccsin* cells also after a long treatment for 16h with 25 μ M BFA. Data is means \pm SD; \geq 8 roots were analysed for each genotype. **(B)** Colocalization study of the SEC21 protein (ER marker) and the VHAa1-GFP protein (TGN marker). In the control situation there were multiple Golgis and TGNs dispersed in the cytosol. Treatments with 25 μ M BFA for 12h lead to an increased number of remaining aggregated BFA bodies in the *saccsin* mutant, which recover less as seen in the controls.



Suppl. Fig. 6: *SACSIN-BIG3* genetic interaction (A) Immunolocalization of PIN1, PIN2 and SEC21 (golgi marker) in the control (DMSO) treatment. (B) Immunolocalization of PIN1, PIN2 and SEC21 (golgi marker) after treatment for 16h with 25 μM BFA. The mutant *big3* is epistatic to *saccsin* as after long treatment with BFA there are atypical aggregates in the *big3 saccsin* double mutant of the immunolocalized protein, which is a phenotype observed in *big3*. (C) BFA treatment did not prevent seed germination in wild type and *saccsin-2*, but did so in *big3* mutants and in *saccsin-2 big3* double mutant.

2.6 Materials and Methods

Plant material and growth conditions

All *Arabidopsis thaliana* lines were in Columbia-0 (Col-0) background except of *PIN2::PIN2-Dendra*, which was in *eir 1-1* background and *gnom^{R5}*, which is in *Landsberg* background. The insertional mutants *saccsin-1* (SALK_000313) and *saccsin-2* (SALK_00082) were obtained from NASC. The *PIN1pro::PIN1-GFP* transgenic line was described previously (Benkova et al., 2003), *PIN2pro::PIN2-GFP* (Xu and Scheres, 2005), *VHAa1pro::VHAa1-GFP* (Dettmer et al., 2006), *XVE::PIN1-RFP* (Richter et al., 2014). The seeds were surface-sterilized overnight by chlorine gas, sown on solid *Arabidopsis* medium (½ MS, 1% [w/v] sucrose, and 0.8% [w/v] phytoagar, pH 5.7), and stratified at 4°C for at least 2 days prior to transfer to a growth room with a 16-

h light/8-h dark regime at 21°C. The seedlings were grown vertically for 4 or 8 days, depending on the assay.

Arabidopsis seedlings were treated with chemicals in liquid ½ MS at 21°C in a growth room with the following concentrations and times: 25 µM or 50 µM BFA for different time points; 10 µM β-Estradiol for an assay up to 6h. Mock treatments were done with equivalent amounts of DMSO.

Generation of constructs for the gene expression study

To clone the *sacsin* promoter, we designed primers to cover from -1 to -2333 bp upstream of the gene's ATG codon and PCR amplified, by implementing the iPROOF DNA polymerase (Bio-Rad), and recombined the products using the Gateway BP Clonase II Enzyme Mix (Invitrogen) into the entry vector pDONRP4P1r. Moreover, the GUS gene was recombined into the entry vector pDONR221 using the Gateway BP Clonase II Enzyme Mix. Then we recombined these plasmids with the respective promoter cloned in the entry vector pDONRP4P1r (described above) and the destination vector pB7m24GW,3 using the Gateway LR Clonase II Enzyme Mix (Invitrogen). All plasmids were sequenced to confirm the absence of point mutations in the PCR-amplified sequences prior to transformation into *Arabidopsis* Columbia using the floral dip method (Clough and Bent, 1998).

RNA extraction, cDNA synthesis, and quantitative RT-PCR and analysis

RNA extraction, cDNA synthesis, and quantitative qRT-PCR were done as described in Prat et al., 2018. Selected candidate gene transcript levels were quantified with qRT-PCR with specific primer pairs. Expression levels were normalized to *SERINE/THREONINE PHOSPHATASE 2A* (*PP2A*; AT1G69960) and to *ACTIN7* (*ACT7*), which was constitutively expressed across samples. All PCRs were run in three biological replicates. The data were processed with a qRT-PCR analysis software (Frederik Coppens, Ghent University-VIB, Ghent, Belgium). For quantitative RT-PCR, poly(dT) cDNA was prepared from 1 µg of total RNA with Superscript III (Invitrogen). Quantitative RT-PCR was done with LightCycler 480 SYBR Green I Master reagents (Roche Diagnostics) and a LightCycler 480 Real-Time PCR System (Roche Diagnostics). PCR was run on 384-well reaction plates that were heated for 10 min to 95°C,

followed by 45 denaturation cycles of 10 s at 95°C, annealing for 15 s at 60°C, and extension for 15 s at 72°C.

Protein immunolocalizations

Immunolocalizations were performed on 4-days old seedlings using the Intavis in situ pro robot, as described by (Sauer et al., 2006). The antibodies were used as follows: anti-PIN1 rabbit, 1:1000 (Paciorek et al., 2005), anti-PIN2 rabbit, 1:1000 (Paciorek et al., 2005), anti-Sec21 rabbit 1:800 (Movafeghi et al., 1999). For the secondary antibodies, goat anti-rabbit antibody coupled to Cy3 (Sigma-Aldrich) was diluted 1:600.

For live imaging, seedlings at 4 days after germination were mounted in ½ MS broth medium and visualized immediately using a Zeiss 800 confocal microscope. Root cells were imaged using a C-Apochromat 40×/1.20 water-immersion objective (Zeiss). YFP was excited using a 514-nm argon ion laser line, fluorescence was detected using a 540/20-nm bandpass filter, and each scan was the result of averaging 4 frames to produce low-noise images. The surface of the cells was carefully acquired when observing the root epidermal cells, whereas a middle section of the cells was used when imaging all other cell types.

Phenotypic analysis

All measurements were done with Fiji (Fiji is just ImageJ (<https://fiji.sc/>)). For the root length analysis 5-day-old seedlings were scanned and root lengths were measured. For the lateral roots analysis 10-day-old seedlings were scanned and lateral root density was calculated from ratio number of LR/root length. For the gravitropism experiments we grew the seedlings for 4 days and then we turned the plate to 90 degrees and followed the gravitropic response at a scanner for a time of 24h. The phenotypic analysis in the dark was recorded at 1h interval for 3 days at 18°C with an infrared light source (880 nm LED; Velleman, Belgium) by a spectrum-enhanced camera (EOS035 Canon Rebel Xti, 400DH) with built-in clear wideband-multicoated filter and standard accessories (Canon) and operated by the EOS utility software.

Histological analyses and microscopy

To detect β-glucuronidase (GUS) activity, seedlings were incubated in reaction buffer containing 0.1 M sodium phosphate buffer (pH 7), 5 mM ferricyanide, 5 mM ferrocyanide,

0.1% Triton X-100, and 1 mg/ml X-Gluc for 24 h in the dark at 37°C. Afterward, chlorophyll was removed by destaining in 70% ethanol and seedlings were cleared.

Tissues (seedlings, cotyledons and lateral roots) were cleared in a solution containing 4% HCl and 20% methanol for 15 min at 65°C, followed by a 15 min incubation in 7% NaOH and 60% ethanol at room temperature. Next, seedlings were rehydrated by successive incubations in 70%, 40%, 20% and 10% for 10 min, followed by incubation in a solution containing 25% glycerol and 5% ethanol. Finally, seedlings were mounted in 50% glycerol and monitored by differential interference contrast microscopy DIC (Olympus BX51).

Softwares

Sequences were analysed with CLC main workbench 7. Confocal images were analysed using the Fiji ImageJ program. Images were further processed using Adobe Illustrator CS3.

2.7 Reference

Adamowski, M. and Friml, J. (2015). PIN-dependent auxin transport: action, regulation, and evolution. *Plant Cell* **27**: 20–32.

Anders, N. and Jürgens, G. (2008). Large ARF guanine nucleotide exchange factors in membrane trafficking. *Cell. Mol. Life Sci.* **65**: 3433–3445.

Benkova, E., Michniewicz, M., Sauer, M., Teichmann, T., and Pflanz, M. Der (2003). Local , Efflux-Dependent Auxin Gradients as a Common Module for Plant Organ Formation. *115*: 591–602.

Bonifacio, J.S. and Lippincott-Schwartz, J. (2003). Coat proteins: shaping membrane transport. *Nat. Rev. Mol. Cell Biol.* **4**: 409–414.

Borden, K.L. (2000). RING domains: master builders of molecular scaffolds? *J. Mol. Biol.* **295**: 1103–1112.

Bradshaw, T.Y., Romano, L.E.L., Duncan, E.J., Nethisinghe, S., Abeti, R., Michael, G.J., Giunti, P., Vermeer, S., and Chapple, J.P. (2016). A reduction in Drp1-mediated fission compromises mitochondrial health in autosomal recessive spastic ataxia of Charlevoix Saguenay. *Hum. Mol. Genet.* **25**: 3232–3244.

- Feraru, E., Feraru, M.I., Asaoka, R., Paciorek, T., De Rycke, R., Tanaka, H., Nakano, A., and Friml, J.** (2012). BEX5/RabA1b regulates trans-Golgi network-to-plasma membrane protein trafficking in Arabidopsis. *Plant Cell* **24**: 3074–3086.
- Freemont, P.S., Hanson, I.M., and Trowsdale, J.** (1991). A novel gysteine-rich sequence motif. *Cell* **64**: 483–484.
- Friml, J., Vieten, A., Sauer, M., Weijers, D., Schwarz, H., Hamann, T., Offringa, R., and Jürgens, G.** (2003). Efflux-dependent auxin gradients establish the apical–basal axis of Arabidopsis. *Nature* **426**: 147–153.
- Geldner, N., Anders, N., Wolters, H., Keicher, J., Kornberger, W., Muller, P., Delbarre, A., Ueda, T., Nakano, A., and Jürgens, G.** (2003). The Arabidopsis GNOM ARF-GEF Mediates Endosomal Recycling, Auxin Transport, and Auxin-Dependent Plant Growth. *Cell* **112**: 219–230.
- Geldner, N., Friml, J., Stierhof, Y.-D., Jürgens, G., and Palme, K.** (2001). Auxin transport inhibitors block PIN1 cycling and vesicle trafficking. *Nature* **413**: 425–428.
- Gil, P., Dewey, E., Friml, J., Zhao, Y., Snowden, K.C., Putterill, J., Palme, K., Estelle, M., and Chory, J.** (2001). BIG: a calossin-like protein required for polar auxin transport in Arabidopsis. *Genes Dev.* **15**: 1985–1997.
- Grosshans, B.L., Ortiz, D., and Novick, P.** (2006). Rabs and their effectors: achieving specificity in membrane traffic. *Proc. Natl. Acad. Sci. U. S. A.* **103**: 11821–11827.
- Hruz, T., Laule, O., Szabo, G., Wessendorp, F., Bleuler, S., Oertle, L., Widmayer, P., Gruissem, W., and Zimmermann, P.** (2008). Genevestigator V3: A Reference Expression Database for the Meta-Analysis of Transcriptomes. *Adv. Bioinformatics* **2008**: 1–5.
- Jander, G.** (2006). Gene Identification and Cloning by Molecular Marker Mapping. In *Arabidopsis Protocols*, J. Salinas and J.J. Sanchez-Serrano, eds (Humana Press: Totowa, NJ), pp. 115–126.
- Jelínková, A., Malínská, K., Simon, S., Kleine-Vehn, J., Pařezová, M., Pejchar, P., Kubeš, M., Martinec, J., Friml, J., Zažímalová, E., and Petrášek, J.** (2010). Probing plant membranes with FM dyes: tracking, dragging or blocking? *Plant J.* **61**: 883–892.
- Kania, U. et al.** (2018). The Inhibitor Endosidin 4 Targets SEC7 Domain-Type ARF GTPase Exchange Factors and Interferes with Subcellular Trafficking in Eukaryotes. *Plant Cell* **30**: 2553 LP – 2572.
- Kitakura, S., Adamowski, M., Matsuura, Y., Santuari, L., Kouno, H., Arima, K., Hardtke, C.S.,**

- Friml, J., Kakimoto, T., and Tanaka, H.** (2017). BEN3/BIG2 ARF GEF is Involved in Brefeldin A-Sensitive Trafficking at the trans-Golgi Network/Early Endosome in *Arabidopsis thaliana*. *Plant Cell Physiol.* **58**: 1801–1811.
- Kleine-Vehn, J., Dhonukshe, P., Sauer, M., Brewer, P.B., Wiśniewska, J., Paciorek, T., Benková, E., and Friml, J.** (2008a). ARF GEF-Dependent Transcytosis and Polar Delivery of PIN Auxin Carriers in *Arabidopsis*. *Curr. Biol.* **18**: 526–531.
- Kleine-Vehn, J., Ding, Z., Jones, A.R., Tasaka, M., Morita, M.T., and Friml, J.** (2010). Gravity-induced PIN transcytosis for polarization of auxin fluxes in gravity-sensing root cells. *Proc. Natl. Acad. Sci. U. S. A.* **107**: 22344–22349.
- Kleine-Vehn, J. and Friml, J.** (2008). Polar targeting and endocytic recycling in auxin-dependent plant development. *Annu. Rev. Cell Dev. Biol.* **24**: 447–473.
- Kleine-Vehn, J., Łangowski, Ł., Wiśniewska, J., Dhonukshe, P., Brewer, P.B., and Friml, J.** (2008b). Cellular and Molecular Requirements for Polar PIN Targeting and Transcytosis in Plants. *Mol. Plant* **1**: 1056–1066.
- Koizumi, K., Naramoto, S., Sawa, S., Yahara, N., Ueda, T., Nakano, A., Sugiyama, M., and Fukuda, H.** (2005). VAN3 ARF–GAP-mediated vesicle transport is involved in leaf vascular network formation. *Development* **132**: 1699 LP – 1711.
- Kosarev, P., Mayer, K.F.X., and Hardtke, C.S.** (2002). Evaluation and classification of RING-finger domains encoded by the *Arabidopsis* genome. *Genome Biol.* **3**: RESEARCH0016.
- Lorick, K.L., Jensen, J.P., Fang, S., Ong, A.M., Hatakeyama, S., and Weissman, A.M.** (1999). RING fingers mediate ubiquitin-conjugating enzyme (E2)-dependent ubiquitination. *Proc. Natl. Acad. Sci. U. S. A.* **96**: 11364–11369.
- Mosesso, E., Bickford, L.C., and Goldberg, J.** (2003). SNARE Selectivity of the COPII Coat. *Cell* **114**: 483–495.
- Naramoto, S., Kleine-Vehn, J., Robert, S., Fujimoto, M., Dainobu, T., Paciorek, T., Ueda, T., Nakano, A., Van Montagu, M.C.E., Fukuda, H., and Friml, J.** (2010). ADP-ribosylation factor machinery mediates endocytosis in plant cells. *Proc. Natl. Acad. Sci. U. S. A.* **107**: 21890–21895.
- Naramoto, S., Otegui, M.S., Kutsuna, N., de Rycke, R., Dainobu, T., Karampelias, M., Fujimoto, M., Feraru, E., Miki, D., Fukuda, H., Nakano, A., and Friml, J.** (2014). Insights into the Localization and Function of the Membrane Trafficking Regulator GNOM ARF-GEF at the Golgi Apparatus in *Arabidopsis*. *Plant Cell* **26**: 3062–3076.

- Naramoto, S., Sawa, S., Koizumi, K., Uemura, T., Ueda, T., Friml, J., Nakano, A., and Fukuda, H.** (2009). Phosphoinositide-dependent regulation of VAN3 ARF-GAP localization and activity essential for vascular tissue continuity in plants. *Development* **136**: 1529 LP – 1538.
- Paciorek, T., Zažímalová, E., Ruthardt, N., Petrášek, J., Stierhof, Y.-D., Kleine-Vehn, J., Morris, D.A., Emans, N., Jürgens, G., Geldner, N., and Friml, J.** (2005). Auxin inhibits endocytosis and promotes its own efflux from cells. *Nature* **435**: 1251–1256.
- Paul, M.J. and Frigerio, L.** (2007). Coated vesicles in plant cells. *Semin. Cell Dev. Biol.* **18**: 471–478.
- Powers, E.T. and Balch, W.E.** (2013). Diversity in the origins of proteostasis networks--a driver for protein function in evolution. *Nat. Rev. Mol. Cell Biol.* **14**: 237–248.
- Rakusová, H., Abbas, M., Han, H., Song, S., Robert, H.S., and Friml, J.** (2016). Termination of Shoot Gravitropic Responses by Auxin Feedback on PIN3 Polarity. *Curr. Biol.* **26**: 3026–3032.
- Richter, S., Kientz, M., Brumm, S., Nielsen, M.E., Park, M., Gavidia, R., Krause, C., Voss, U., Beckmann, H., Mayer, U., Stierhof, Y.-D., and Jürgens, G.** (2014). Delivery of endocytosed proteins to the cell–division plane requires change of pathway from recycling to secretion. *Elife* **3**: 1–16.
- Ruegger, M., Dewey, E., Hobbie, L., Brown, D., Bernasconi, P., Turner, J., Muday, G., and Estelle, M.** (1997). Reduced naphthylphthalamic acid binding in the tir3 mutant of Arabidopsis is associated with a reduction in polar auxin transport and diverse morphological defects. *Plant Cell* **9**: 745–757.
- Rutherford, S. and Moore, I.** (2002). The Arabidopsis Rab GTPase family: another enigma variation. *Curr. Opin. Plant Biol.* **5**: 518–528.
- Salanenko, Y., Verstraeten, I., Löffke, C., Tabata, K., Naramoto, S., Glanc, M., and Friml, J.** (2018). Gibberellin DELLA signaling targets the retromer complex to redirect protein trafficking to the plasma membrane. *Proc. Natl. Acad. Sci. U. S. A.* **115**: 3716–3721.
- Serafini, T., Orci, L., Amherdt, M., Brunner, M., Kahn, R.A., and Rothmant, J.E.** (1991). ADP-Ribosylation factor is a subunit of the coat of Golgi-derived COP-coated vesicles: A novel role for a GTP-binding protein. *Cell* **67**: 239–253.
- Singh, M.K. et al.** (2018). A single class of ARF GTPase activated by several pathway-specific ARF-GEFs regulates essential membrane traffic in Arabidopsis. *PLOS Genet.* **14**:

e1007795.

- Singh, V., Davidson, A.C., Hume, P.J., Humphreys, D., and Koronakis, V.** (2017). Arf GTPase interplay with Rho GTPases in regulation of the actin cytoskeleton. *Small GTPases*: 1–8.
- Stone, S.L., Hauksdóttir, H., Troy, A., Herschleb, J., Kraft, E., and Callis, J.** (2005). Functional analysis of the RING-type ubiquitin ligase family of Arabidopsis. *Plant Physiol.* **137**: 13–30.
- Szklarczyk, D., Morris, J.H., Cook, H., Kuhn, M., Wyder, S., Simonovic, M., Santos, A., Doncheva, N.T., Roth, A., Bork, P., Jensen, L.J., and von Mering, C.** (2017). The STRING database in 2017: quality-controlled protein-protein association networks, made broadly accessible. *Nucleic Acids Res.* **45**: D362–D368.
- Tanaka, H., Kitakura, S., Rakusová, H., Uemura, T., Feraru, M.I., De Rycke, R., Robert, S., Kakimoto, T., and Friml, J.** (2013). Cell Polarity and Patterning by PIN Trafficking through Early Endosomal Compartments in Arabidopsis thaliana. *PLOS Genet.* **9**: e1003540.
- Tanaka, H., Kitakura, S., De Rycke, R., De Groodt, R., and Friml, J.** (2009). Fluorescence Imaging-Based Screen Identifies ARF GEF Component of Early Endosomal Trafficking. *Curr. Biol.* **19**: 391–397.
- Vernoud, V., Horton, A.C., Yang, Z., and Nielsen, E.** (2003). Analysis of the Small GTPase Gene Superfamily of Arabidopsis. *Plant Physiol.* **131**: 1191 LP – 1208.
- Weigel, D. and Glazebrook, J.** (2006). Forward Genetics in Arabidopsis: Finding Mutations that Cause Particular Phenotypes. *Cold Spring Harb. Protoc.* **2006**: pdb.top1.
- Zerial, M. and McBride, H.** (2001). Rab proteins as membrane organizers. *Nat. Rev. Mol. Cell Biol.* **2**: 107.
- Zwiewka, M. and Friml, J.** (2012). Fluorescence imaging-based forward genetic screens to identify trafficking regulators in plants. *Front. Plant Sci.* **3**: 97.

3 The phytohormone strigolactone

3.1 Introduction

The growth and development of *Arabidopsis thaliana* is regulated not only by auxin, but also by other phytohormones. Strigolactones are compounds, which participate in this processes (Soundappan et al., 2015). In its presence, the D14 receptor binds it, then the receptor changes its confirmation and binds to the MAX2 protein from the SCF complex. As a result, the transcription repressors are degraded in the proteasome and the receptor is destabilized. After this signal transduction pathway, the expression of the transcription factors of the TCP family can take place (Marzec, 2016). In xylem parenchyma cells of the stem, strigolactones cause depletion of PIN1 from the plasma membrane (Shinohara et al., 2013). Those phytohormones regulate the amount of PIN1 at the plasma membrane and influences the capacity of bud-derived auxin to canalize toward the stem, which alters the bud activity and shoot architecture (Shinohara et al., 2013).

In this chapter we investigate the action of strigolactone and auxin in the model of the *Arabidopsis thaliana* root tip and we characterize the role of the strigolactones in the canalization and in the polar auxin transport. For this we implement a system of treatments and co-treatments with both hormones and also BrefeldinA as a tool to study the membrane protein trafficking. As auxin inhibits the PIN internalization, which is a requirement for the polar auxin transport and canalization, auxin, when under the influence of strigolactones, becomes less likely to induce canalization-related growth responses. Additionally, I characterize the role of phosphorylation in the strigolactone regulation of auxin feedback on PIN internalization. I also discuss the MAX2-dependence of strigolactone-mediated root growth inhibition and also the auxin metabolomics profiling after application of strigolactone. The results from our study are described in the following section. I include my contribution to that manuscripts and I use the text from it as a basis for rephrasing of my observations.

3.2 Strigolactone interferes with auxin feedback on PIN internalization

3.2.1 Abstract

The canalization hypothesis is connected with polar auxin transport and proposes a feedback effect of auxin on the directionality of intracellular auxin flow (Sauer et al., 2006). The application of auxin, wounding or auxin accumulation during *de novo* organ formation leads to rearrangement in the subcellular polar localization of PIN auxin transport components (Sauer et al., 2006). The phytohormone strigolactone regulates many different plant developmental processes, which can be related to polar auxin transport and canalization. In addition, this phytohormone alters the phenotypic output of the PIN auxin efflux carriers by participating and regulating growth and developmental responses by moderating the polar auxin transport (Shinohara et al., 2013). As the phytohormone auxin reduces the internalization of the PIN proteins, which increases the polar auxin transport and the canalization, auxin, when under the influence of strigolactone, becomes less likely to induce canalization related growth responses.

3.2.2 Introduction

In the canalization process, the transporting routes for the phytohormone auxin are established between plant cells and tissues where the auxin concentration is higher (source) in direction to locations, where the auxin concentration is lower (sink) (Sachs, 1981; Sauer et al., 2006; Bennett et al., 2016). Important for this process is the polar auxin transport (PAT), where the phytohormone auxin promotes the expression of the *PIN* genes in channels and this leads to an increase of the amount of PIN proteins on the plasma membrane at the side of the cell towards the sink (Sauer et al., 2006; Balla et al., 2011). This process enables the transport of the hormone auxin outside of the cell and towards the sink (Bennett and Leyser, 2014). The process of canalization is very obvious when new vasculature connections along the channel routes form, for example after wounding or in the formation of venation in leaves (Sachs, 1981; Cheng et al., 2006; Scarpella et al., 2006). Moreover, there are cases where the polar auxin transport is redirected by developmentally regulated changes in PIN polarity, such in the cases of lateral root formation or leaf initiation or by environmental cues, such as during gravitropic responses (Friml et al., 2002).

The PIN proteins are cycling between the endosomes and the plasma membrane and the mechanism of uptake is enabled through clathrin-mediated endocytosis (Dhonukshe et al., 2007) and PINs may be relocated by vesicle movement to other membranes (Kleine-Vehn et al., 2008b). In addition, there are compounds and genetic factors, which were implemented to study more in detail PIN trafficking and the polar auxin transport mechanisms (Adamowski and Friml, 2015). One tool, which was used is the fungal toxin Brefedin A (BFA), which is a vesicle trafficking inhibitor that causes aggregates in cells by repressing GNOM ARF-GEF dependent vesicle movement (Geldner et al., 2001).

In addition, the effect of auxin is that more of the PIN proteins are localized to the plasma membrane so that the auxin canalization towards the sink can be enabled. In addition, there are other hormones, which have an effect on the PAT such as cytokinins (Marhavý et al., 2014), gibberellins (Willige et al., 2011; Salanenka et al., 2018), salicylic acid (Du et al., 2013) and strigolactones (SLs) (Crawford et al., 2010). The strigolactones can reduce the auxin transport by inhibition of the localization of the PIN proteins on the plasma membrane, which influences processes like shoot branching (Waldie et al., 2014), shoot gravitropism (Sang et al., 2014), secondary growth (Agusti et al., 2011), adventitious rooting (Rasmussen et al., 2014), and lateral rooting and root hair elongation (Koltai, 2015). Recent research showed that the canalization from the buds becomes less likely, if strigolactones inhibit the PAT in the stem and as a result there is inhibition of bud growth (Shinohara et al., 2013). To further characterize the role of strigolactone on PAT, we investigated the influence of this hormone on the auxin-PIN interaction in root cells. We observed that strigolactones inhibit the feedback of auxin on the PIN internalization.

3.2.3 Results

The feedback mechanisms between auxin and PIN polarity can be estimated by the auxin-mediated reorganization of the PIN polarity in *Arabidopsis thaliana* root (Sauer et al., 2006). In the primary root, the PIN1 protein is localized to the basal side of the stele cells (Kleine-Vehn et al., 2008a).

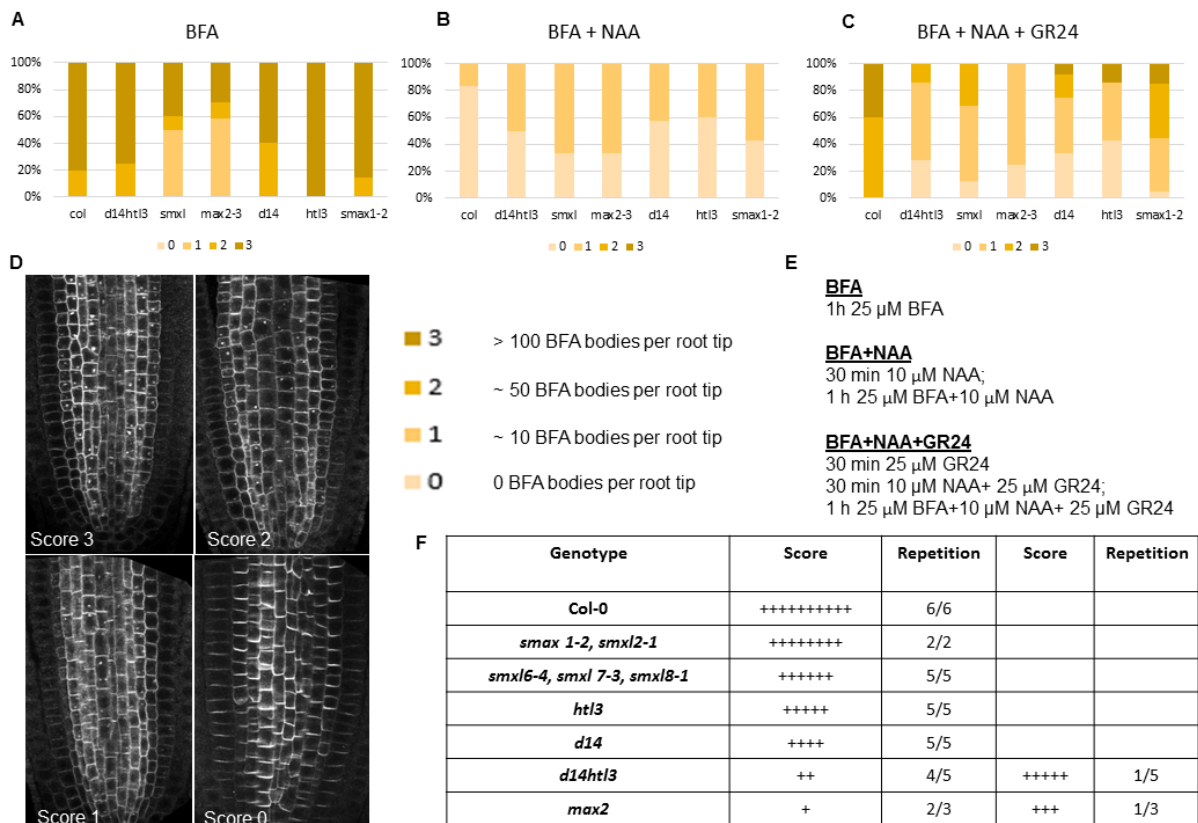


Figure 1: Experimental setting to study the PIN1 localization in strigolactone signalling mutants after the application of GR24 and/or NAA and BFA. (A) Example for the BFA treatment and scoring of the results. **(B)** Example for the BFA/NAA treatment and scoring of the results. **(C)** Example for the BFA/NAA/GR24 treatment and scoring of the result. **(D)** Scores, given to the amount of BFA bodies, observed in the images, compared to the corresponding control. **(E)** Concentrations and treatment times, used for the experiment. **(F)** Scheme, representing the score for the different transgenic lines and also number of repetitions of the particular cell phenotype.

To study the vesicle trafficking processes, we implemented BFA for a short time treatment, where membrane proteins and also endomembrane system compartments accumulate into BFA bodies (Figure 1A). To estimate the degree of BFA body formation we blindly gave scores to our optical observation after immunolocalization assays. A score of 3 was given when there were a lot of BFA bodies, a score of 2 correspond to many BFA bodies, a score of 1 to a few of them and 0 is the score given to observations when there are no BFA bodies (Figure 1D). Treatments with auxin (synthetic 1-naphthaleneacetic acid, NAA) lead to rearrangements of the PIN1 protein to the plasma membrane (Figure 1B). When co-treated with exogenous NAA and GR24, the effect of auxin was counteracted (Figure 1C). Notably, in comparison with wild type, the inhibitory effect of GR24 on auxin-mediated PIN lateralization was significantly impaired in *max2-3* (Figure 1F). These results suggest that SLs, through the MAX2-dependent pathway, regulate negatively the canalization processes at the organ and tissue levels, but also regulate the auxin-mediated polarization of the PIN transporters at the level of individual

cells. Next, we examined, if the action of SLs in regulating PIN trafficking also depends on SL signalling components. When GR24 was not applied, BFA-induced PIN1 internalization or NAA-mediated inhibition was similar in the *d14* SL signaling mutant or the *max2* SL/karrikin signalling mutant (Figure 1A and B). However, these mutants showed insensitivity to GR24 with respect of counteracting NAA action on PIN endocytic trafficking (Figure 1C). Moreover, in Figure 3F the observations after the treatments with SL, NAA and BFA are visualized. In the less sensitive to strigolactone mutant *d14htl3*, there were less BFA bodies formed after the simultaneous treatment with the hormones. In addition, in the single receptor mutants, the effect of strigolactone was slightly more pronounced and in the repressor mutants, the effect of strigolactone on the auxin feedback on PIN internalization was even more pronounced. Our conclusion is that the synthetic GR24 interferes with auxin-mediated feedback on BFA-visualized PIN1 intracellular accumulation, acting through D14- and MAX2-dependent strigolactone signalling.

3.2.4 Discussion and conclusions

Next to auxin, there is the phytohormone strigolactone, which participates in many developmental processes and also in the regulation of the polar auxin transport and canalization (Shinohara et al., 2013). The internalization of the PIN proteins is reduced by NAA, however on the other hand, strigolactone decreases the polar auxin transport and the canalization related growth responses are impaired (Shinohara et al., 2013).

Our main aim was to study through which signalling pathway the effect of strigolactone occurs. For this we used as a model system the primary root of *Arabidopsis thaliana* where the PIN1 protein is localized to the basal side of the vasculature cells (Kleine-Vehn et al., 2008). We examined the localization of the PIN1 protein after treatments with NAA and/or GR24 in the presence of BFA, which is a vesicle trafficking inhibitor, used as a tool for studies on GNOM-regulated trafficking mechanisms. Our results show that *max2* when compared to wild type has a lower sensitivity to the effect of GR24 as there were much less BFA bodies after the simultaneous treatment with NAA, GR24 and BFA. Moreover, the receptor mutant *d14* showed also much less BFA bodies compared to wild type in the same experimental condition.

We show that the synthetic GR24 interferes with auxin-mediated feedback on PIN internalization through the D14 receptor and MAX2-dependent pathway.

3.3 WRKY23 is a component of the transcriptional network mediating auxin feedback on PIN polarity

3.3.1 Introduction

Auxin is a phytohormone, which regulates many aspects of the plant development. The polarly localized PIN auxin efflux carriers regulate the flow of it (Adamowski and Friml, 2015). The canalization hypothesis suggests that there is the formation of self-organizing patterns due to the formation of narrow auxin transport channels caused by the polarized auxin carriers (Sauer et al., 2006). This process is important for a bright spectra of developmental processes like new vasculature formation, regeneration after wounding and control of apical dominance (Prát et al., 2018).

My contribution to this manuscript is in the examination of the hypothesis that the canalization process, through polar auxin transport, regulates the vasculature reconnection and patterning in the hypocotyls after grafting. By designing different experimental settings, I studied and tried to develop a method, which can be used to study the canalization properties after cutting the hypocotyls and then reconnecting them.

(Paper is attached to the supplementary of the PhD thesis)

3.4 Role of phosphorylation in the strigolactone regulation of auxin feedback on PIN internalization

3.4.1 Abstract

The phosphorylation status and the polar localization of the PIN proteins regulates the directional transport of auxin (Dai et al., 2012). The PINIOD (PID) kinase is responsible for the phosphorylation of the PIN proteins and their dephosphorylation is assured by the PP6

holoenzyme complex (Dai et al., 2012). In the case of a double mutant *fypp1 fypp3*, which is homologous and encode the catalytic subunit of protein phosphatase 6 (PP6), there is higher amount of phosphorylated PIN proteins, which causes a basal-to-apical shift in the subcellular localization of the PIN proteins (Dai et al., 2012). This alters the polarity of the PIN proteins and causes an increased basipetal flow of the phytohormone auxin, which leads to defects, pronounced in shorter roots, fewer lateral roots, root meristem collapse, abnormal cotyledons and altered leaf venation (Dai et al., 2012). It was shown that FyPP1/3, SAL (for SAPS DOMAIN-LIKE), and PP2AA proteins (RCN1 [for ROOTS CURL IN NAPHTHYLPHTHALAMIC ACID1] or PP2AA1, PP2AA2, and PP2AA3) physically interact and the results is the formation of a PP6-type heterotrimeric holoenzyme complex (Dai et al., 2012). Another interaction is between FyPP1/3, SAL, and PP2AA and the PIN proteins, which depends on the phosphorylation status of the auxin efflux carriers. As a summary, the *Arabidopsis* PP6-type phosphatase holoenzyme acts antagonistically with PID, which has an effect on the directional flow of the phytohormone auxin and consequently on the plant development by regulating the phosphorylation status of the PINs (Dai et al., 2012). In this chapter we study the localization of the PIN1 protein after using the experimental setting from the previous section.

3.4.2 Introduction

Many aspects of plant development are regulated by auxin (Grunewald and Friml, 2010). This phytohormone is transported from its site of synthesis towards the root tip by the directed cell-to-cell transport through the PIN auxin efflux carriers in a process known as polar auxin transport, which is subsequently also regulating the plant development (Wiśniewska et al., 2006).

The previous research showed that the phosphorylation status of the PIN proteins is important for the auxin transport polarity (Benjamins et al., 2001; Friml et al., 2004; Zhang et al., 2010; Huang et al., 2010). The Ser/Thr kinase PINOID (PID) was shown to directly phosphorylate the PIN proteins and this gives it a role as a regulator of the polar targeting of the PIN proteins. Moreover, the loss of that kinase activity causes an apical-to-basal shift in the PIN polarity and the gain of function results in a basal-to-apical shift in the PIN polarity (Friml et al., 2004; Michniewicz et al., 2007; Huang et al., 2010). With the altered activity of

the PID, the auxin flow is also altered, which causes defects in multiple developmental processes (Christensen et al., 2000; Benjamins et al., 2001; Friml et al., 2004).

Based on the sequence, structure and catalytic mechanism, the phosphatases can be classified into different groups (Moorhead et al., 2007). The PP2A heterotrimeric holoenzyme consists of a type A regulatory subunit, a type B regulatory subunit and a C subunit, which is a catalytic subunit (Terol et al., 2002). The role of the regulatory subunit A (hereafter, PP2AAs, including PP2AA1, also known as RCN1 [for ROOTS CURL IN NAPHTHYLPHTHALAMIC ACID1], PP2AA2, and PP2AA3) is connected with the regulation of the PIN phosphorylation state and auxin transport (Garbers et al., 1996; Rashotte et al., 2001; Michniewicz et al., 2007). Dai et al., 2012 showed that FyPP1 and FyPP3 interact with a pool of the PIN proteins and they regulate the PIN protein phosphorylation. Those two proteins directly interact with SAL and PP2AAs to form the PP6 heterotrimeric holoenzyme complex. In additions, mutations, which disrupt the function of four SAL genes also show developmental phenotypes, which are similar to the *fypp1fypp3* and *pp2a* higher order mutants. This data is an evidence that PP6 acts antagonistically with PID and participates in the regulation of the reversible phosphorylation of PIN and polar targeting, which has an influence on the polar auxin transport and on the plant development.

3.4.3 Results

To study the vesicle trafficking processes, we implemented the compound BFA for short time, where membrane proteins and also endomembrane system compartments accumulate into BFA bodies (Figure 2A). To estimate the degree of BFA body formation we gave scores to our optical observation after immunolocalization assays. A score of 3 was given when there were a lot of BFA bodies, a score of 2 correspond to many BFA bodies, a score of 1 to a few of them and 0 is scoring the observation when there are no BFA bodies. Treatments with auxin (synthetic 1-naphthaleneacetic acid, NAA) lead to rearrangements of the PIN1 proteins to the plasma membrane. When co-treated with exogenous NAA and GR24, the effect of auxin was counteracted.

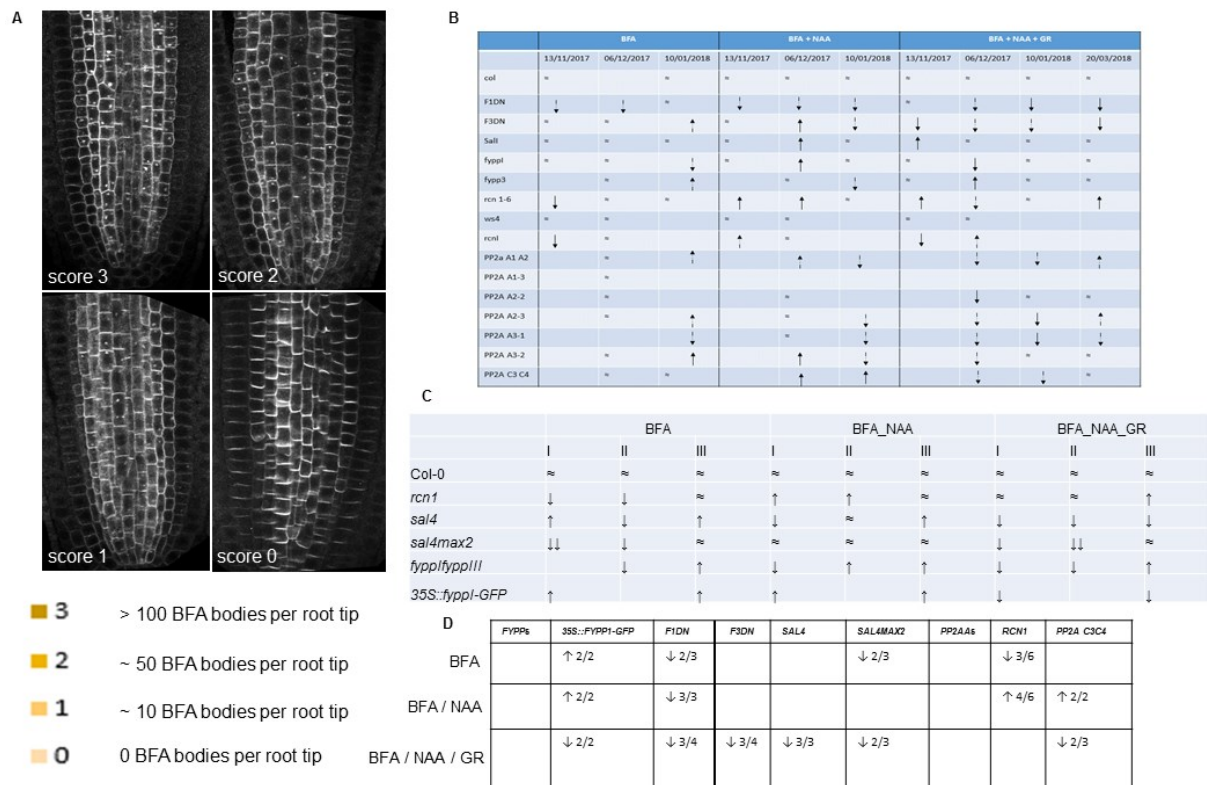


Figure 4: Role of phosphorylation in the strigolactone regulation of auxin feedback on PIN internalization. (A) Example for the quantification of the number of BFA bodies per root tip by giving scores to the optical estimation of the BFA aggregates after treatments with BFA; BFA and NAA or BFA, NAA and GR24. **(B)** and **(C)** Tables with results on the different experiments and their summary. **(D)** Final summary on the particular pattern and cell phenotype, which appears frequently.

Our results are summarized in Table 2B, 2C and the summary is shown in Table 2D.

For the BFA treatments there is a tendency for an increased number of BFA bodies in the *35S::FYPP1-GFP* line. On the other hand, a decreased PIN1 internalization was observed in *F1DN*, which also appeared with high frequency in *RCN1* and *SAL4MAX2*. The rest of the lines show internalization of PIN1, which is comparable to their control or the internalization fluctuates and no conclusion can be reached.

For the BFA+NAA treatment: there is a tendency for a decreased PIN1 internalization in *F1DN*. Additionally, there is increased PIN1 internalization in the *35S::FYPP1-GFP*, *rcn1-6* and *pp2a C3-C4*. The rest of the lines show internalization of PIN1, which is comparable to their control or the internalization fluctuates and no conclusion can be reached.

For the BFA/NAA/GR treatment: there is a tendency for a decreased PIN1 internalization in *35S::FYPP1-GFP*, *F1DN*, *F3DN*, *SAL4* and *SAL4MAX2* and also in *pp2a C3C4*. The rest of the lines show internalization of PIN1, which is comparable to their control or the internalization fluctuates and no conclusion can be reached.

3.4.4 Discussion and conclusions

The phytohormone strigolactone has the property to modify the basipetal auxin flow (Prusinkiewicz et al., 2009). It also regulates the canalization events by influencing the auxin feedback on PIN internalization (Sachs, 2000; Sauer et al., 2006). Other regulators of the PIN polar delivery are the Ser/Thr protein kinase PINOID (PID) and the protein phosphatase 2A (PP2A) (Kleine-Vehn et al., 2009). They determine the apical/basal targeting of the PIN proteins by modifying the phosphorylation status of the PIN proteins (Friml et al., 2004; Michniewicz et al., 2007). The PP6 holoenzyme complex is formed by the physical interaction of *FyPPs*, *SAL* genes, and *PP2AAs*, and the phosphorylation status of the PIN proteins determines the strength of their interaction (Dai et al., 2012). PP6 consists of the three subunits (regulatory subunits A and B and a catalytic subunit C) and it regulates the PIN phosphorylation, auxin transport, polar targeting and plant developmental processes (Dai et al., 2012). The basal targeting of the PIN proteins is promoted by PP6-mediated dephosphorylation, while the apical PIN localization is promoted by PID-dependent phosphorylation where both molecular mechanisms regulate the polar auxin transport and also the plant development. The catalytic subunit of PP6 is encoded by *FyPP1* and *FyPP3* genes and they regulate the polar PIN localization to the basal side of the vasculature cells. Moreover, loss of their function leads to shift in the PIN polar targeting from the basal to the apical cell side (Dai et al., 2012).

Our aim was to characterize the role of phosphorylation in the strigolactone regulation of auxin feedback on PIN internalization. For this we used PIN1 protein immunolocalization assays after NAA and/or GR24 treatment, where we used also the known vesicle trafficking inhibitor - BFA. In Col-0 roots, PIN1 is localized to the basal side of the vasculature cells, whereas in *f1f3*, *F1DN* and *F3DN* roots, there is a switch from the basal to the apical side in the vasculature cells of the untreated roots (Dai et al., 2012). Additionally, the NAA treatment leads to a reduced number of BFA bodies in the cells, where strigolactone counteracts these effect and there is a higher number of BFA bodies after simultaneous treatment with GR24, NAA and BFA in wild type. Our results show a reduction of the PIN1 internalization after GR24/NAA/BFA treatment in the cases of *35S::FyPP1-GFP* and also in the dominant negative

line *F1DN* (*35S:YFP-FyPP1^{D81N}/Col-0*; hereafter, *F1DN*). These results could be explained by the fact that the mutant phosphatase *F1DN* lost almost all activity, which means that even this weak activity will be enough to dephosphorylate. Additionally, our results show less sensitivity of *SAL4* to GR24 with respect of counteracting NAA action on PIN endocytic trafficking. In conclusion, the phosphorylation might be directly or indirectly involved in the strigolactone regulation of auxin feedback on PIN internalization.

3.5 MAX2-dependence of strigolactone-mediated root growth inhibition

3.5.1 Introduction

The phytohormone strigolactone participates in shaping the root architecture (Ruyter-Spira et al., 2011). When the growth conditions are optimal, the lateral root formation is repressed by strigolactone (Kapulnik et al., 2011; Ruyter-Spira et al., 2011) and the root hair prolongation is promoted (Kapulnik et al., 2011). In the formation of lateral roots, auxin plays an essential role and it determines the positioning of lateral roots, their initiation and elongation (De Smet, 2012). There is a crosstalk with strigolactone as it affects the formation of lateral roots by changes of the auxin efflux in the root. When SL is applied exogenously, it interferes with the PIN auxin efflux carriers and leads to a decreased PIN1-GFP intensity in lateral root primordia (Koltai et al., 2010). By the implementation of auxin signalling mutants, it was shown that strigolactones act upstream (Kapulnik et al., 2011; Mayzlish-Gati et al., 2012). The balance between strigolactones and auxin plays a crucial role in shaping the *Arabidopsis thaliana* root architecture. Also during the process of shoot branching the interaction between both hormones plays an important role.

In the past it has been also shown that the exogenous application of GR24 reduces the polar auxin transport (Crawford et al., 2010). Moreover, the phytohormones auxin and strigolactone interact and they regulate each other's levels through a feedback mechanism (Hayward et al., 2009) in the root growth and root branching. The lateral root initiation is triggered by the local accumulation of auxin in root pericycle cells (Casimiro et al., 2001; De Smet, 2012; Dubrovsky et al., 2008; Lucas et al., 2008). From this and the regulated cell division, LR primordia develop and finally the young LR emerge. Later, for the further LR

development, the auxin comes from the aerial part of the plant (Bhalerao et al., 2002). As the root system architecture is tightly regulated by auxin and auxin transport, it was suggested that strigolactone plays a role in regulating the auxin fluxes (Ruyter-Spira et al., 2011). For this we studied and further characterized the effect of GR24 on primary root and LR development.

3.5.2 Results

We examined, whether the application of GR24 leads to a MAX2-dependent or MAX2-independent effect of strigolactone on the primary root length and on the density of lateral roots.

We quantified the growth and development of roots of 8 days old *Arabidopsis thaliana* seedlings, which were germinated and grown on plates containing different concentrations of the synthetic analogue GR24.

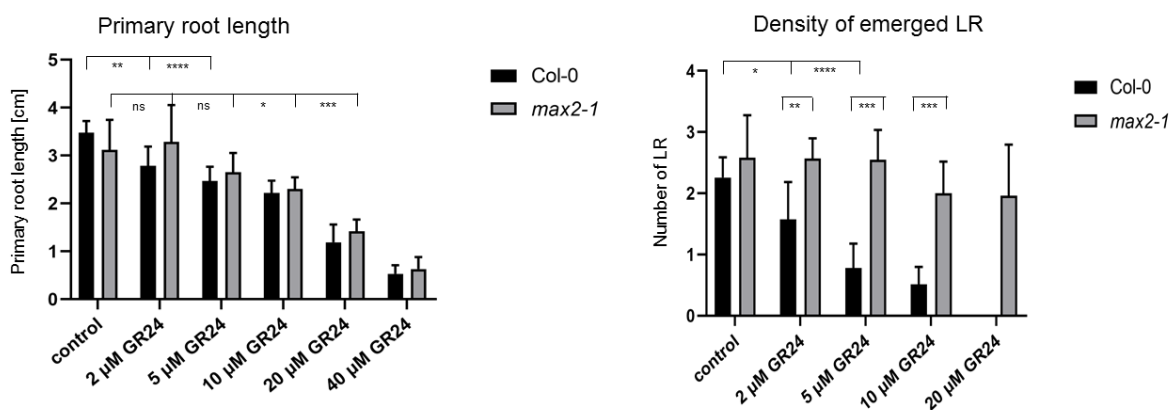


Figure 3: MAX2-dependence of strigolactone-mediated root growth inhibition. Quantification of the primary root length and of the number of initiated lateral roots in Col-0 and *max2-1*, when germinated on a control plate (1/2 MS, supplemented with acetone) or on 1/2 MS, supplemented with different concentrations of GR24.

In wild type the lowest concentration, at which GR24 starts having an effect on the inhibition of the primary root length and on the lateral root density is at the lowest tested concentration of 2 μM GR24 (Figure 3). We observe a resistance of the growth of the primary root length in *max2-1* and the concentration at which GR24 has an effect on the primary root length is at 10 μM GR24 (Figure 3). Additionally, when comparing the effect of GR24 on the primary root length in Col-0 and *max2-1* there is no significant difference in the length between the control and the mutant at the different GR24 concentrations.

On the other hand, the resistance of *max2-1* was very pronounced in the lateral root density and we did not observe a significant decrease in the amount of initiated LR even at a concentration of 20 μ M GR24. Wild type showed a significant reduction in the lateral root density, but not the *max2-1* mutant. This suggests that MAX2 is involved in strigolactone signalling for lateral root formation but possibly not for root growth regulation.

3.5.3 Discussion and conclusions

The root architecture is defined by the phytohormones auxin and strigolactone, which act in a regulated feedback mechanism. It was shown that *Arabidopsis* plants, grown in the presence of low levels of GR24 (1,25 and 2,5 μ M) have an increase in the primary root length (Ruyter-Spira et al., 2011). These phenotype is due to the fact that lower concentrations of GR24 lead to an increase in the auxin levels (Ruyter-Spira et al., 2011). When the concentrations of strigolactone are increased, the levels of auxin are reduced, which affects the whole seedling appearance (Ruyter-Spira et al., 2011).

Additionally, the density of the emerged lateral roots is reduced by GR24, which is also a process, dependent on the auxin concentration (Lucas et al., 2008). The delivery of auxin into the developing lateral root is enabled by the repolarization of the PIN1 protein (Ruyter-Spira et al., 2011). On the other hand, GR24 modulates this process by modulating and reducing the auxin levels in the aerial parts and then the amount of auxin, which reaches the LR, is not sufficient respectively (Ruyter-Spira et al., 2011).

Our aim was to study the MAX2-dependence of strigolactone-mediated root growth inhibition. We show that the application of strigolactones affects and impairs both the primary root length and the density of the emerged lateral roots. High concentrations of GR24 inhibits the growth of the primary root length in both wild type and *max2-1*. Moreover, *max2* is showing a resistance in the density of lateral roots compared to the control, which means that the inhibitory effect of strigolactones on the lateral root development is MAX2-dependent.

3.6 Putative regulator of PIN polarity identified by means of forward genetics screen using strigolactone analogue GR24

3.6.1 Abstract

In eukaryotic organisms, the establishment of cell polarity, which is a generation of asymmetry in the cell structure, is very important to multicellular existence. In plants this seems to be even more crucial as plants typically adapt to the changing environment by reshaping development. Auxin plays an important role in this process and regulates the shape and direction of organ growth and development (Friml et al., 2003). There is a cell-to-cell transport of it, performed by the auxin efflux carriers from the PIN family, which have a polar localization. In the presence of the strigolactone-analog GR24, the PINs are depleted from the basal plasma membrane and as a result, in the presence of GR24, the root growth is inhibited and the roots are agravitropic. These properties were a basis of a forward genetic screen, where GR24 was used as a tool to identify novel regulators of polar PIN localization. The EMS mutant *pig1* (*PIN localization resistant to GR24 1*) has a proper root growth, gravitropism and normal PIN polarization in the presence of GR24.

3.6.2 Introduction

Many events in the plant life are controlled by the phytohormone auxin, including processes at embryonic (Friml et al., 2003; Schlereth et al., 2010) and postembryonic level (Sabatini et al., 1999; Friml et al., 2002). In addition, responses to the changes in the environment like gravitropism or phototropism are regulated by auxin (Ding et al., 2011; Rakusová et al., 2011). Within plant tissues there are the auxin concentration gradients, which regulate many processes and also trigger downstream signalling cascades (Benkova et al., 2003; Sorefan et al., 2009). It was also reported that strigolactones can act as signalling molecules in the context of regulation of the shoot branching (Gomez-Roldan et al., 2008; Umehara et al., 2008).

In this study, we observe the effect of the exogenous application of strigolactone on the PIN1 localization and internalization. By the implementation of GR24, which is a synthetic

strigolactone analogue, we did a forward genetic screen to identify the regulators of PIN polarity, which led to the identification of *PIG1*, which modulates intracellular auxin and auxin-conjugate levels. It regulates the plasma membrane abundance of PIN and modulates the protein vacuolar targeting.

3.6.3 Results

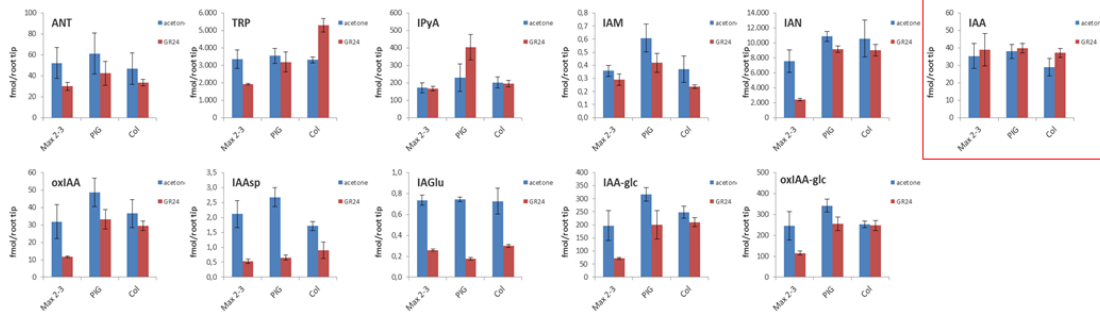
The *pPIN1::PIN1-GFP* expressing line showed an inhibited root growth and the gravitropism was disturbed upon transfer to 50 μ M GR24 containing $\frac{1}{2}$ MS medium. In contrast, the roots of *pig1-1* maintained growth and showed more normal gravitropic response in the same conditions. Moreover, *pig1-1* did not show alterations in the PIN1 polar localization upon GR24 treatment, which was observed in the control seedlings (Baster et al., unpublished). The mutation, which was responsible for the phenotype of *pig1* is a substitution of single nucleotide in the coding region of At5G50850, which is a gene coding for pyruvate dehydrogenase E1- β subunit (PD E1- β) (Luethy et al., 1995). In addition, the pyruvate dehydrogenase complex (PDC) in plants consists of three main components: E1 – pyruvate dehydrogenase (PD), E2 – dihydrolipoyl acetyltransferase (DA) and E3 – dihydrolipoyl dehydrogenase (DD), which catalyze three sequential reactions. Moreover, the E1 part of the PDC forms heterotetramer of two α and two β subunits. In plants the PDCs are special as they exist in two spatially and functionally separated forms (Mooney et al., 2002). The mitochondrial PDC participates in the reaction of catalyzing the oxidative decarboxylation of pyruvate, which is derived from glycolysis in the cytoplasm, to acetyl-CoA, which is used as a carbon source for the energy production and reducing agent NADH during Krebs cycle (Lernmark and Gardestrom, 1994; Randall et al., 1996). Additionally, there is the other pool of plastid form (pPDC), which provides the same substrate Acetyl-CoA for *de novo* fatty acid biosynthesis (Camp and Randall, 1985). The role of the PDC is to catalyze the oxidative decarboxylation of pyruvate to CoenzymeA, which is acetylated to form acetyl-CoA (Mooney et al., 2002). One possibility for the effect of mtPD on the resistance of root growth to auxin amino-acid conjugates is that the metabolism of auxin could be indirectly affected by reduced levels of acetyl-CoA, which is the result of defective or delayed pyruvate conversion. Another suggestion for its activity was that mtPD could interact with other subunits of PDC during the

conversion of indole-3-pyruvate (IPA) to indole-3-acetyl-CoA (IAA-CoA), which can be hydrolyzed to release free IAA or act as a precursor IAA conjugates (Koga, 1995; LeClere et al., 2004) and in this case certain tissues might have altered levels of auxin and auxin conjugates. As a support of this claim there is a recent evidence that the abundance of IAA-amino acid conjugates in tissues of PD E1- α mutant was doubled relatively to wild type plants (Quint et al., 2009).

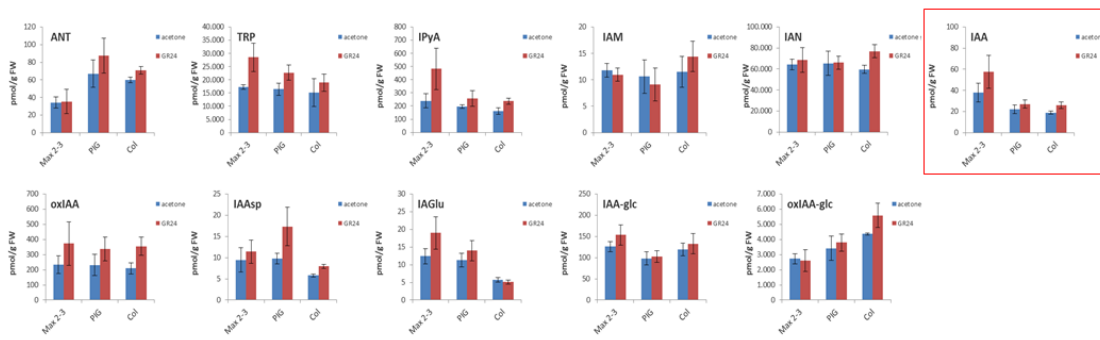
To further characterize the role of the *pig1* gene, we applied 50 μ M GR24 for 12h or 24h and we studied the auxin metabolomics profiling of the *pig1*, *max2* mutants and mock. We collected the root tips and the shoots of the samples (see Materials and Methods) and we send them for analysis to the Labor of Ales Pencik, having the equipment and protocols for the profiling of plant hormones and their metabolites.

The levels of L-Tryptophan (Trp), which is an amino acid generated by the shikimate pathway, is the key precursor of four major auxin biosynthesis pathways in plants: the indole-3-acetamide (IAM), indole-3-acetaldoxime (IAOx), tryptamine (TRA), and indole-3-pyruvic acid (IPyA) pathways, named according to the major intermediate (Mano and Nemoto, 2012; Ljung, 2013; Kasahara, 2016; Pencík et al., 2018) (Figure 4). After the biosynthesis and the transport of auxin, this hormone can be degraded by oxidation and subsequent conjugation, producing the major metabolites 2-oxindole-3-acetic acid (oxIAA) and oxIAA-glucose (oxIAA-glc) (Ostin et al., 1998; Kai et al., 2007; Pencík et al., 2013, 2018). In addition, the auxin can be inactivated by the mechanism of formation of conjugates with amino acids or sugars (Tam et al., 2000; Kowalczyk and Sandberg, 2001; Pencík et al., 2018). After the hydrolyzation of some of this conjugates, then free auxin is released, which indicates that they play the role of temporary storage forms for the inactive hormone (reviewed by (Ludwig-Müller, 2011) (Pencík et al., 2018)). However, conjugates like IAA-aspartate (IAA_{asp}) and IAA-glutamate (IAA_{glu}), are not reversibly converted to IAA, and might have a role as degradation intermediates (Kowalczyk and Sandberg, 2001; Woodward and Bartel, 2005; Pencík et al., 2018).

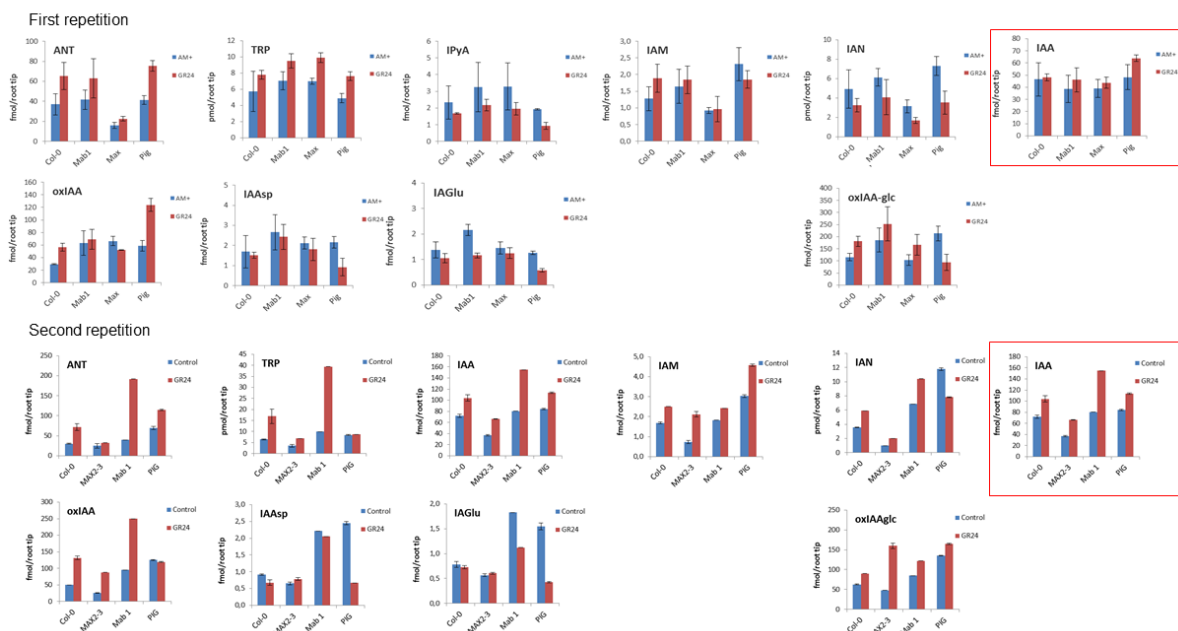
Roots [50]GR24 12h



Shoots [50]GR24 12h



Root tips [50]GR24 24h



Shoots [50]GR24 24h

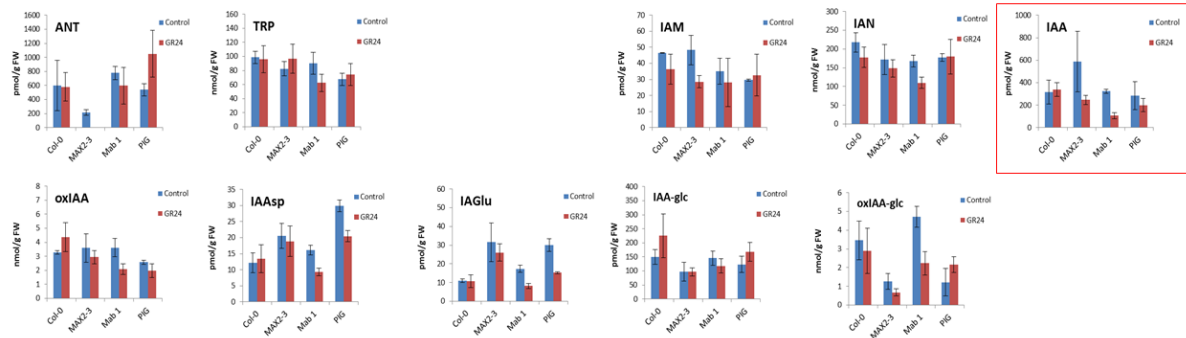


Figure 5: Tendencies and alterations of the auxin metabolites after application of strigolactone. The auxin metabolomics profiling after application of GR24 for 12h or for 24h was done on root tips and shoots. The graphs represent the concentrations of the different conjugates in the control situation or after application of strigolactone. The data in every chart is based on the quantification from three independent biological samples.

The application of strigolactone had an effect on the amount of free IAA in the wild type situation. By comparing the results, there is always an elevation in the amount of free IAA after the application of strigolactone (Figure 5). Additionally, we wanted to observe how the mutation in the *At5G50850* gene, coding for pyruvate dehydrogenase E1- β subunit (PD E1- β) influences the levels of auxin conjugates. Unfortunately, there were no particular, repetitive trends in the concentrations of conjugates in the mock situation and after strigolactone treatment. To further investigate the role of this mutation and also the role of the *max2* gene on the auxin conjugates, once should do further repetitions or design a better experimental setting. Regardless of the technical shortcomings, there is a clear trend that strigolactone increased levels of free auxin/IAA.

3.6.4 Discussion and conclusions

Our aim was to analyze the auxin metabolites in the root tips and in the shoots in normal condition and after treatment with GR24 in wild type, *pig1*, *max2* and *mab1*. For this we did the sampling of the root tips and of the shoots in normal condition and after treatment with 50 μ M GR24 for 12 or 24h. Our results show that there is a tendency of increased amounts of free IAA in wild type after application of strigolactone. Due to technical shortcomings in the sampling and in the analysis, we could not make any conclusion about the tendencies for the other auxin conjugates and for the other genotypes.

3.7 Material and methods

Plant material and growth conditions

All *Arabidopsis thaliana* mutants and transgenic lines used in this study are in the Columbia (Col-0) background and have been described previously. Surface-sterilized seeds were sown on half-strength Murashige and Skoog (1/2 MS) agar plates and stratified for 2 days at 4°C. Plants were grown on vertically oriented plates under 16h light/ 8h dark photoperiod at 18°C for 4-10 days.

Drug application and experimental condition for the BFA/NAA/GR experimental setting

Exogenous drugs were applied as following: GR24 (rac-GR24; 50 mM stock in acetone made freshly; StrigoLab; working concentrations of 25 µM and 50 µM GR24), 1-naphthalenacetic acid (NAA; 10 mM stock in DMSO; Sigma; working concentration of 5 µM or 10 µM), BrefeldinA (BFA; 50 mM stock in DMSO; Invitrogen; working concentration of 25 µM). Control treatments contained an equivalent amount of solvent. For testing NAA inhibition on BFA-induced internalization the conditions were: 60 min with 25 µM BFA; or 30 min pretreatment with 10 µM NAA, followed by 60 min co-treatment of NAA/BFA; or first a 30 min pretreatment with 25 µM GR24, then another 30 min pretreatment with NAA/GR24 (or a simultaneous pretreatment with GR24/NAA for 30 min), followed by concomitant GR24/NAA/BFA treatment for 60 min.

In situ expression and localization analysis

In *Arabidopsis*, whole-mount immunolocalization was performed as described (Sauer and Friml, 2010). Antibodies were diluted as follows: 1:1000 for rabbit anti-PIN1 and 1:600 for CY-3 (Sigma) conjugated anti-rabbit secondary antibody (Paciorek et al., 2005).

Drug Application and Experimental Conditions for the auxin metabolomics profiling

For the metabolomics profiling the seedlings were germinated on a mash for 6 days on ½ MS medium. Then they were transferred to a freshly prepared plate, containing ½ MS medium, supplemented with 50 µM GR24 or a control plate, containing the same amount of acetone (as the GR24 was dissolved in acetone). The treatment was done for 12h or 24h and there

were 3 biological replicates (3 different plates) with around 100 seedlings of each genotype. The root tips or the shoots were cutted and carefully collected in a 20 µl drop of water, which was placed on the edge of an Eppendorf tube and the samples were immediately frozen into liquid nitrogen and late shipped on dry ice for further analysis. The same procedure was repeated for the cotyledons.

Strigolactone root assay

For the strigolactone root assay, the seedlings were germinated on a GR24 or acetone (of the same volume) containing plate. The seedlings were grown for 8 days under the usual conditions. The plates were scanned and the primary root lengths and the density of lateral roots was measured.

Grafting experiments

For the grafting experiments, the seedlings were grown on a mash for 5 days. Under sterile conditions, the hypocotyl was cutted and then the different parts were reconnected. The regeneration of the tissue was evaluated and quantified in the following days. The emerging adventitious roots were removed.

3.8 Reference

Adamowski, M. and Friml, J. (2015). PIN-dependent auxin transport: action, regulation, and evolution. *Plant Cell* **27**: 20–32.

Agusti, J., Herold, S., Schwarz, M., Sanchez, P., Ljung, K., Dun, E.A., Brewer, P.B., Beveridge, C.A., Sieberer, T., Sehr, E.M., and Greb, T. (2011). Strigolactone signaling is required for auxin-dependent stimulation of secondary growth in plants. *Proc. Natl. Acad. Sci.* **108**: 20242 LP – 20247.

Akiyama, K., Matsuzaki, K., and Hayashi, H. (2005). Plant sesquiterpenes induce hyphal branching in arbuscular mycorrhizal fungi. *Nature* **435**: 824–827.

Balla, J., Kalousek, P., Reinöhl, V., Friml, J., and Procházka, S. (2011). Competitive canalization of PIN-dependent auxin flow from axillary buds controls pea bud outgrowth. *Plant J.* **65**: 571–577.

- Benjamins, R., Quint, A., Weijers, D., Hooykaas, P., and Offringa, R.** (2001). The PINOID protein kinase regulates organ development in *Arabidopsis* by enhancing polar auxin transport. *Development* **128**: 4057 LP – 4067.
- Benkova, E., Michniewicz, M., Sauer, M., Teichmann, T., and Pflanz, M.** (2003). Local, Efflux-Dependent Auxin Gradients as a Common Module for Plant Organ Formation. *Development* **130**: 591–602.
- Bennett, T. and Leyser, O.** (2014). Strigolactone signalling: standing on the shoulders of DWARFs. *Curr. Opin. Plant Biol.* **22**: 7–13.
- Bennett, T., Liang, Y., Seale, M., Ward, S., Müller, D., and Leyser, O.** (2016). Strigolactone regulates shoot development through a core signalling pathway. *Biol. Open* **5**: 1806 LP – 1820.
- Bhalerao, R.P., Eklöf, J., Ljung, K., Marchant, A., Bennett, M., and Sandberg, G.** (2002). Shoot-derived auxin is essential for early lateral root emergence in *Arabidopsis* seedlings. *Plant J.* **29**: 325–332.
- Booker, J., Sieberer, T., Wright, W., Williamson, L., Willett, B., Stirnberg, P., Turnbull, C., Srinivasan, M., Goddard, P., and Leyser, O.** (2005). MAX1 Encodes a Cytochrome P450 Family Member that Acts Downstream of MAX3/4 to Produce a Carotenoid-Derived Branch-Inhibiting Hormone. *Dev. Cell* **8**: 443–449.
- Brewer, P.B., Dun, E.A., Ferguson, B.J., Rameau, C., and Beveridge, C.A.** (2009). Strigolactone acts downstream of auxin to regulate bud outgrowth in pea and *Arabidopsis*. *Plant Physiol.* **150**: 482–493.
- Camp, P.J. and Randall, D.D.** (1985). Purification and Characterization of the Pea Chloroplast Pyruvate Dehydrogenase Complex : A Source of Acetyl-CoA and NADH for Fatty Acid Biosynthesis. *Plant Physiol.* **77**: 571–577.
- Casimiro, I., Beeckman, T., Graham, N., Bhalerao, R., Zhang, H., Casero, P., Sandberg, G., and Bennett, M.J.** (2003). Dissecting *Arabidopsis* lateral root development. *Trends Plant Sci.* **8**: 165–171.
- Casimiro, I., Marchant, A., Bhalerao, R.P., Beeckman, T., Dhooge, S., Swarup, R., Graham, N., Inzé, D., Sandberg, G., Casero, P.J., and Bennett, M.** (2001). Auxin transport promotes *Arabidopsis* lateral root initiation. *Plant Cell* **13**: 843–852.
- Cheng, Y., Dai, X., and Zhao, Y.** (2006). Auxin biosynthesis by the YUCCA flavin monooxygenases controls the formation of floral organs and vascular tissues in

Arabidopsis. *Genes Dev.* **20**: 1790–1799.

Christensen, S.K., Dagenais, N., Chory, J., and Weigel, D. (2000). Regulation of Auxin Response by the Protein Kinase PINOID. *Cell* **100**: 469–478.

Cook, C.E., Whichard, L.P., Turner, B., Wall, M.E., and Egley, G.H. (1966). Germination of Witchweed (*Striga lutea* Lour.): Isolation and Properties of a Potent Stimulant. *Science* (80-). **154**: 1189 LP – 1190.

Crawford, S., Shinohara, N., Sieberer, T., Williamson, L., George, G., Hepworth, J., Müller, D., Domagalska, M.A., and Leyser, O. (2010). Strigolactones enhance competition between shoot branches by dampening auxin transport. *Development* **137**: 2905 LP – 2913.

Dai, M. et al. (2012). A PP6-Type Phosphatase Holoenzyme Directly Regulates PIN Phosphorylation and Auxin Efflux in *Arabidopsis*. *Plant Cell* **24**: 2497 LP – 2514.

Dhonukshe, P., Aniento, F., Hwang, I., Robinson, D.G., Mravec, J., Stierhof, Y.-D., and Friml, J. (2007). Clathrin-Mediated Constitutive Endocytosis of PIN Auxin Efflux Carriers in *Arabidopsis*. *Curr. Biol.* **17**: 520–527.

Ding, Z., Galván-Ampudia, C.S., Demarsy, E., Łangowski, Ł., Kleine-Vehn, J., Fan, Y., Morita, M.T., Tasaka, M., Fankhauser, C., Offringa, R., and Friml, J. (2011). Light-mediated polarization of the PIN3 auxin transporter for the phototropic response in *Arabidopsis*. *Nat. Cell Biol.* **13**: 447.

Du, Y., Tejos, R., Beck, M., Himschoot, E., Li, H., Robatzek, S., Vanneste, S., and Friml, J. (2013). Salicylic acid interferes with clathrin-mediated endocytic protein trafficking. *Proc. Natl. Acad. Sci. U. S. A.* **110**: 7946–7951.

Dubrovsky, J.G., Sauer, M., Napsucialy-Mendivil, S., Ivanchenko, M.G., Friml, J., Shishkova, S., Celenza, J., and Benková, E. (2008). Auxin acts as a local morphogenetic trigger to specify lateral root founder cells. *Proc. Natl. Acad. Sci. U. S. A.* **105**: 8790–8794.

Flematti, G.R., Ghisalberti, E.L., Dixon, K.W., and Trengove, R.D. (2004). A Compound from Smoke That Promotes Seed Germination. *Science* (80-). **305**: 977 LP – 977.

Flematti, G.R., Waters, M.T., Scaffidi, A., Merritt, D.J., Ghisalberti, E.L., Dixon, K.W., and Smith, S.M. (2013). Karrikin and Cyanohydrin Smoke Signals Provide Clues to New Endogenous Plant Signaling Compounds. *Mol. Plant* **6**: 29–37.

Friml, J. et al. (2004). A PINOID-Dependent Binary Switch in Apical-Basal PIN Polar Targeting

- Kleine-Vehn, J., Łangowski, Ł., Wiśniewska, J., Dhonukshe, P., Brewer, P.B., and Friml, J.** (2008b). Cellular and Molecular Requirements for Polar PIN Targeting and Transcytosis in Plants. *Mol. Plant* **1**: 1056–1066.
- Koga, J.** (1995). Structure and function of indolepyruvate decarboxylase, a key enzyme in indole-3-acetic acid biosynthesis. *Biochim. Biophys. Acta - Protein Struct. Mol. Enzymol.* **1249**: 1–13.
- Koltai, H.** (2015). Cellular events of strigolactone signalling and their crosstalk with auxin in roots. *J. Exp. Bot.* **66**: 4855–4861.
- Koltai, H., LekKala, S.P., Bhattacharya, C., Mayzlish-Gati, E., Resnick, N., Winer, S., Dor, E., Yoneyama, K., Yoneyama, K., Hershenhorn, J., Joel, D.M., and Kapulnik, Y.** (2010). A tomato strigolactone-impaired mutant displays aberrant shoot morphology and plant interactions. *J. Exp. Bot.* **61**: 1739–1749.
- Kowalczyk, M. and Sandberg, G.** (2001). Quantitative analysis of indole-3-acetic acid metabolites in Arabidopsis. *Plant Physiol.* **127**: 1845–1853.
- Kulkarni, M.G., Sparg, S.G., Light, M.E., and Van Staden, J.** (2006). Stimulation of Rice (*Oryza sativa* L.) Seedling Vigour by Smoke-water and Butenolide. *J. Agron. Crop Sci.* **192**: 395–398.
- LeClere, S., Rampey, R.A., and Bartel, B.** (2004). IAR4, a gene required for auxin conjugate sensitivity in Arabidopsis, encodes a pyruvate dehydrogenase E1 α homolog. *Plant Physiol.* **135**: 989–999.
- Lernmark, U. and Gardestrom, P.** (1994). Distribution of Pyruvate Dehydrogenase Complex Activities between Chloroplasts and Mitochondria from Leaves of Different Species. *Plant Physiol.* **106**: 1633–1638.
- Ljung, K.** (2013). Auxin metabolism and homeostasis during plant development. *Development* **140**: 943 LP – 950.
- Lopez-Obando, M., Ligerot, Y., Bonhomme, S., Boyer, F.-D., and Rameau, C.** (2015). Strigolactone biosynthesis and signaling in plant development. *Development* **142**: 3615 LP – 3619.
- Lucas, M., Guédon, Y., Jay-Allemand, C., Godin, C., and Laplaze, L.** (2008). An Auxin Transport-Based Model of Root Branching in Arabidopsis thaliana. *PLoS One* **3**: e3673.
- Ludwig-Müller, J.** (2011). Auxin conjugates: their role for plant development and in the evolution of land plants. *J. Exp. Bot.* **62**: 1757–1773.

- Luethy, M.H., Miernyk, J.A., and Randall, D.D.** (1995). The mitochondrial pyruvate dehydrogenase complex: nucleotide and deduced amino-acid sequences of a cDNA encoding the *Arabidopsis thaliana* E1 α -subunit. *Gene* **164**: 251–254.
- Magnus, E.M., Dommerholt, F.J., De Jong, R.L.P., and Zwanenburg, B.** (1992). Improved synthesis of strigol analog GR24 and evaluation of the biological activity of its diastereomers. *J. Agric. Food Chem.* **40**: 1230–1235.
- Mano, Y. and Nemoto, K.** (2012). The pathway of auxin biosynthesis in plants. *J. Exp. Bot.* **63**: 2853–2872.
- Marhavý, P., Duclercq, J., Weller, B., Feraru, E., Bielach, A., Offringa, R., Friml, J., Schwechheimer, C., Murphy, A., and Benková, E.** (2014). Cytokinin Controls Polarity of PIN1-Dependent Auxin Transport during Lateral Root Organogenesis. *Curr. Biol.* **24**: 1031–1037.
- Matusova, R., Rani, K., Verstappen, F.W.A., Franssen, M.C.R., Beale, M.H., and Bouwmeester, H.J.** (2005). The strigolactone germination stimulants of the plant-parasitic *Striga* and *Orobancha* spp. are derived from the carotenoid pathway. *Plant Physiol.* **139**: 920–934.
- Mayzlish-Gati, E. et al.** (2012). Strigolactones are involved in root response to low phosphate conditions in *Arabidopsis*. *Plant Physiol.* **160**: 1329–1341.
- Michniewicz, M. et al.** (2007). Antagonistic Regulation of PIN Phosphorylation by PP2A and PINOID Directs Auxin Flux. *Cell* **130**: 1044–1056.
- Mooney, B.P., Miernyk, J.A., and Randall, D.D.** (2002). THE COMPLEX FATE OF α -KETOACIDS. *Annu. Rev. Plant Biol.* **53**: 357–375.
- Moorhead, G.B.G., Trinkle-Mulcahy, L., and Ulke-Lemée, A.** (2007). Emerging roles of nuclear protein phosphatases. *Nat. Rev. Mol. Cell Biol.* **8**: 234.
- Nelson, D.C., Flematti, G.R., Ghisalberti, E.L., Dixon, K.W., and Smith, S.M.** (2012). Regulation of Seed Germination and Seedling Growth by Chemical Signals from Burning Vegetation. *Annu. Rev. Plant Biol.* **63**: 107–130.
- Nelson, D.C., Flematti, G.R., Riseborough, J.-A., Ghisalberti, E.L., Dixon, K.W., and Smith, S.M.** (2010). Karrikins enhance light responses during germination and seedling development in *Arabidopsis thaliana*; *Proc. Natl. Acad. Sci.* **107**: 7095 LP – 7100.
- Nelson, D.C., Riseborough, J.-A., Flematti, G.R., Stevens, J., Ghisalberti, E.L., Dixon, K.W.,**

- and Smith, S.M.** (2009). Karrikins discovered in smoke trigger Arabidopsis seed germination by a mechanism requiring gibberellic acid synthesis and light. *Plant Physiol.* **149**: 863–873.
- Novák, O., Pěncík, A., and Ljung, K.** (2014). Identification and Profiling of Auxin and Auxin Metabolites BT - Auxin and Its Role in Plant Development. In E. Zažímalová, J. Petrášek, and E. Benková, eds (Springer Vienna: Vienna), pp. 39–60.
- Ostin, A., Kowalczyk, M., Bhalerao, R.P., and Sandberg, G.** (1998). Metabolism of indole-3-acetic acid in Arabidopsis. *Plant Physiol.* **118**: 285–296.
- Paciorek, T., Zažímalová, E., Ruthardt, N., Petrášek, J., Stierhof, Y.-D., Kleine-Vehn, J., Morris, D.A., Emans, N., Jürgens, G., Geldner, N., and Friml, J.** (2005). Auxin inhibits endocytosis and promotes its own efflux from cells. *Nature* **435**: 1251–1256.
- Pencík, A. et al.** (2013). Regulation of auxin homeostasis and gradients in Arabidopsis roots through the formation of the indole-3-acetic acid catabolite 2-oxindole-3-acetic acid. *Plant Cell* **25**: 3858–3870.
- Pencík, A., Casanova-Sáez, R., Pilarová, V., Žukauskaite, A., Pinto, R., Micol, J.L., Ljung, K., and Novák, O.** (2018). Ultra-rapid auxin metabolite profiling for high-throughput mutant screening in Arabidopsis. *J. Exp. Bot.* **69**: 2569–2579.
- Porfírio, S., Gomes da Silva, M.D.R., Peixe, A., Cabrita, M.J., and Azadi, P.** (2016). Current analytical methods for plant auxin quantification – A review. *Anal. Chim. Acta* **902**: 8–21.
- Prát, T., Hajný, J., Grunewald, W., Vasileva, M., Molnár, G., Tejos, R., Schmid, M., Sauer, M., and Friml, J.** (2018). WRKY23 is a component of the transcriptional network mediating auxin feedback on PIN polarity. *PLOS Genet.* **14**: e1007177.
- Prusinkiewicz, P., Crawford, S., Smith, R.S., Ljung, K., Bennett, T., Ongaro, V., and Leyser, O.** (2009). Control of bud activation by an auxin transport switch. *Proc. Natl. Acad. Sci. U. S. A.* **106**: 17431–17436.
- Quint, M., Barkawi, L.S., Fan, K.-T., Cohen, J.D., and Gray, W.M.** (2009). Arabidopsis IAR4 modulates auxin response by regulating auxin homeostasis. *Plant Physiol.* **150**: 748–758.
- Rakusová, H., Gallego-Bartolomé, J., Vanstraelen, M., Robert, H.S., Alabadí, D., Blázquez, M.A., Benková, E., and Friml, J.** (2011). Polarization of PIN3-dependent auxin transport for hypocotyl gravitropic response in Arabidopsis thaliana. *Plant J.* **67**: 817–826.
- Randall, D.D., Miernyk, J.A., David, N.R., Gemel, J., and Luethy University of Missouri, Columbia, Missouri 65211 (USA)), M.H. (Interdisciplinary P.G.** (1996). Regulation of leaf

- mitochondrial pyruvate dehydrogenase complex activity by reversible phosphorylation.
- Rashotte, A.M., DeLong, A., and Muday, G.K.** (2001). Genetic and chemical reductions in protein phosphatase activity alter auxin transport, gravity response, and lateral root growth. *Plant Cell* **13**: 1683–1697.
- Rasmussen, A., Hosseini, S.A., Hajirezaei, M.-R., Druge, U., and Geelen, D.** (2014). Adventitious rooting declines with the vegetative to reproductive switch and involves a changed auxin homeostasis. *J. Exp. Bot.* **66**: 1437–1452.
- Ruyter-Spira, C., Kohlen, W., Charnikhova, T., van Zeijl, A., van Bezouwen, L., de Ruijter, N., Cardoso, C., Lopez-Raez, J.A., Matusova, R., Bours, R., Verstappen, F., and Bouwmeester, H.** (2011). Physiological effects of the synthetic strigolactone analog GR24 on root system architecture in Arabidopsis: another belowground role for strigolactones? *Plant Physiol.* **155**: 721–734.
- Sabatini, S., Beis, D., Wolkenfelt, H., Murfett, J., Guilfoyle, T., Malamy, J., Benfey, P., Leyser, O., Bechtold, N., Weisbeek, P., and Scheres, B.** (1999). An Auxin-Dependent Distal Organizer of Pattern and Polarity in the Arabidopsis Root. *Cell* **99**: 463–472.
- Sachs, T.** (2000). Integrating Cellular and Organismic Aspects of Vascular Differentiation. *Plant Cell Physiol.* **41**: 649–656.
- Sachs, T.** (1981). The Control of the Patterned Differentiation of Vascular Tissues. In H.W.B.T.-A. in B.R. Woolhouse, ed (Academic Press), pp. 151–262.
- Salanenka, Y., Verstraeten, I., Löffke, C., Tabata, K., Naramoto, S., Glanc, M., and Friml, J.** (2018). Gibberellin DELLA signaling targets the retromer complex to redirect protein trafficking to the plasma membrane. *Proc. Natl. Acad. Sci. U. S. A.* **115**: 3716–3721.
- Sang, D. et al.** (2014). Strigolactones regulate rice tiller angle by attenuating shoot gravitropism through inhibiting auxin biosynthesis. *Proc. Natl. Acad. Sci.* **111**: 11199 LP – 11204.
- Sauer, M., Balla, J., Luschnig, C., Wisniewska, J., Reinöhl, V., Friml, J., and Benková, E.** (2006). Canalization of auxin flow by Aux/IAA-ARF-dependent feedback regulation of PIN polarity. *Genes Dev.* **20**: 2902–2911.
- Sauer, M. and Friml, J.** (2010). Immunolocalization of Proteins in Plants. In *Plant Developmental Biology: Methods and Protocols*, L. Hennig and C. Köhler, eds (Humana Press: Totowa, NJ), pp. 253–263.
- Scarpella, E., Marcos, D., Friml, J., and Berleth, T.** (2006). Control of leaf vascular patterning

- by polar auxin transport. *Genes Dev.* **20**: 1015–1027.
- Schlereth, A., Möller, B., Liu, W., Kientz, M., Flipse, J., Rademacher, E.H., Schmid, M., Jürgens, G., and Weijers, D.** (2010). MONOPTEROS controls embryonic root initiation by regulating a mobile transcription factor. *Nature* **464**: 913.
- Shinohara, N., Taylor, C., and Leyser, O.** (2013). Strigolactone Can Promote or Inhibit Shoot Branching by Triggering Rapid Depletion of the Auxin Efflux Protein PIN1 from the Plasma Membrane. *PLOS Biol.* **11**: e1001474.
- De Smet, I.** (2012). Lateral root initiation: one step at a time. *New Phytol.* **193**: 867–873.
- Sorefan, K., Booker, J., Haurogné, K., Goussot, M., Bainbridge, K., Foo, E., Chatfield, S., Ward, S., Beveridge, C., Rameau, C., and Leyser, O.** (2003). MAX4 and RMS1 are orthologous dioxygenase-like genes that regulate shoot branching in Arabidopsis and pea. *Genes Dev.* **17**: 1469–1474.
- Sorefan, K., Girin, T., Liljegren, S.J., Ljung, K., Robles, P., Galván-Ampudia, C.S., Offringa, R., Friml, J., Yanofsky, M.F., and Østergaard, L.** (2009). A regulated auxin minimum is required for seed dispersal in Arabidopsis. *Nature* **459**: 583.
- Soundappan, I., Bennett, T., Morffy, N., Liang, Y., Stanga, J.P., Abbas, A., Leyser, O., and Nelson, D.C.** (2015). SMAX1-LIKE/D53 Family Members Enable Distinct MAX2-Dependent Responses to Strigolactones and Karrikins in Arabidopsis. *Plant Cell* **27**: 3143–3159.
- van Staden, J., Sparg, S.G., Kulkarni, M.G., and Light, M.E.** (2006). Post-germination effects of the smoke-derived compound 3-methyl-2H-furo[2,3-c]pyran-2-one, and its potential as a preconditioning agent. *F. Crop. Res.* **98**: 98–105.
- Stanga, J.P., Smith, S.M., Briggs, W.R., and Nelson, D.C.** (2013). SUPPRESSOR OF MORE AXILLARY GROWTH2 1 controls seed germination and seedling development in Arabidopsis. *Plant Physiol.* **163**: 318–330.
- Tam, Y.Y., Epstein, E., and Normanly, J.** (2000). Characterization of auxin conjugates in Arabidopsis. Low steady-state levels of indole-3-acetyl-aspartate, indole-3-acetyl-glutamate, and indole-3-acetyl-glucose. *Plant Physiol.* **123**: 589–596.
- Tarkowská, D., Novák, O., Floková, K., Tarkowski, P., Turečková, V., Grúz, J., Rolčík, J., and Strnad, M.** (2014). Quo vadis plant hormone analysis? *Planta* **240**: 55–76.
- Terol, J., Bagues, M., Carrasco, P., Pérez-Alonso, M., and Paricio, N.** (2002). Molecular characterization and evolution of the protein phosphatase 2A B' regulatory subunit

- family in plants. *Plant Physiol.* **129**: 808–822.
- Turnbull, C.G.N., Booker, J.P., and Leyser, H.M.O.** (2002). Micrografting techniques for testing long-distance signalling in *Arabidopsis*. *Plant J.* **32**: 255–262.
- Umehara, M., Hanada, A., Yoshida, S., Akiyama, K., Arite, T., Takeda-Kamiya, N., Magome, H., Kamiya, Y., Shirasu, K., Yoneyama, K., Kyojuka, J., and Yamaguchi, S.** (2008). Inhibition of shoot branching by new terpenoid plant hormones. *Nature* **455**: 195.
- Waldie, T., McCulloch, H., and Leyser, O.** (2014). Strigolactones and the control of plant development: lessons from shoot branching. *Plant J.* **79**: 607–622.
- Waters, M.T., Nelson, D.C., Scaffidi, A., Flematti, G.R., Sun, Y.K., Dixon, K.W., and Smith, S.M.** (2012). Specialisation within the DWARF14 protein family confers distinct responses to karrikins and strigolactones in *Arabidopsis*. *Development* **139**: 1285 LP – 1295.
- Waters, M.T., Scaffidi, A., Sun, Y.K., Flematti, G.R., and Smith, S.M.** (2014). The karrikin response system of *Arabidopsis*. *Plant J.* **79**: 623–631.
- Willige, B.C., Isono, E., Richter, R., Zourelidou, M., and Schwechheimer, C.** (2011). Gibberellin regulates PIN-FORMED abundance and is required for auxin transport-dependent growth and development in *Arabidopsis thaliana*. *Plant Cell* **23**: 2184–2195.
- Wiśniewska, J., Xu, J., Seifertová, D., Brewer, P.B., Růžička, K., Blilou, I., Rouquié, D., Benková, E., Scheres, B., and Friml, J.** (2006). Polar PIN Localization Directs Auxin Flow in Plants. *Science* (80-.). **312**: 883 LP – 883.
- WOODWARD, A.W. and BARTEL, B.** (2005). Auxin: Regulation, Action, and Interaction. *Ann. Bot.* **95**: 707–735.
- Zhang, J., Nodzynski, T., Pencík, A., Rolcík, J., and Friml, J.** (2010). PIN phosphorylation is sufficient to mediate PIN polarity and direct auxin transport. *Proc. Natl. Acad. Sci. U. S. A.* **107**: 918–922.

4 Endosidin 9 (ES9) and Endosidin 9-17 (ES9-17) are small molecules, inhibitors of clathrin-mediated endocytosis

4.1 Introduction

In eukaryotic cells the clathrin-mediated endocytosis (CME) is a conserved and essential cellular trafficking mechanism (McMahon and Boucrot, 2011). It is a major route for the uptake of plasma membrane proteins and molecules from the extracellular environment. In plants, there are machineries and molecules, which are important for the CME such as clathrin, the adaptor protein complex-2 (AP-2), the dynamins and the TPLATE adaptor complex (TPC) (Baisa et al., 2013; Gadeyne et al., 2014). For the study of the endomembrane trafficking processes in the model organism *Arabidopsis thaliana*, one can use classical genetic approaches, but this method is often limited by the gene redundancy or by the mutant lethality (Zwiewka and Friml, 2012). Moreover, highly dynamic processes such as endomembrane trafficking are difficult to be approached at the protein level and a possible solution for that might be the implementation of small molecules, which have an immediate effect and alter the protein function (Hicks and Raikhel, 2012).

In the past years, the molecule tyrphostinA23 (TyrA23), which is a tyrosine-like small molecule, was developed as a substrate for mammalian tyrosine kinases but has been regularly used as an inhibitor of CME (Yaish et al., 1988). The mechanism of action of the molecule was through its ability to interfere with the interaction between the tyrosine-based internalization motifs and the medium subunit of the clathrin associated adaptor complex AP-2 (Crump et al., 1998; Banbury et al., 2003). Recent data showed that TyrA23 inhibits the formation of flagellin 22(flg22)-elicited reactive oxygen species formation, which shows that TyrA23 affects CME, but also other cellular processes (Smith et al., 2014). There are also other known CME inhibitors established in mammalian and yeast model systems such as the dynamin inhibitor dynasore, which targets the clathrin terminal domain, but has an effect also on the clathrin-independent endocytosis (Macia et al., 2006; McCluskey et al., 2013; Willox et al., 2014; Park et al., 2013). In addition, there is also the dynasore-based series of small molecules, called Dyngo, which is affecting the dynamin function (McCluskey et al., 2013). Another small-molecule inhibitor of CME is pitstop2, which has as a target the N-terminal

domain (nTD) of the CHC (von Kleist et al., 2011). Additional example of a compound, inhibitor of CME, is the natural product ikarugamycin, which has undefined mechanism of action (Elkin et al., 2016). Most of these molecules have not been thoroughly tested for their effects in plants.

In our papers, we identified Endosidin 9 (ES9) and Endosidin 9-17 from a collection of small molecules with the property to affect endomembrane trafficking (Dejonghe et al., 2016, 2019). ES9 is a small molecule inhibitor of clathrin-mediated endocytosis in *Arabidopsis thaliana*, HeLa cells and *Drosophila melanogaster*. We showed that this molecule uncouples mitochondrial oxidative phosphorylation, which is a property, shown also for TyrA23. The action of both molecules is through acidification of the cytoplasm caused by uncoupling proton gradients, which has an essential effect on energy metabolism, pH homeostasis and dynamic processes in the cells, such as clathrin-mediated endocytosis. The acidification was the reason for the increase in the lifetime of clathrin and the associated adaptors, which led to the reduction of the phosphatidylinositol 4,5-bisphosphate (PI(4,5)P₂), which is the reason for the inhibition of the formation of clathrin-coated pits. Additionally, we characterized the mode of action of a non-protonophoric improved analogue of ES9 - ES9-17, which is more specific and binds to the clathrin heavy chain. Both compounds, ES9 and ES9-17, have enlarged the options on molecules, which could be implemented to inhibit CME or design even better inhibitors of clathrin-mediated endocytosis in different model systems.

4.2 Results

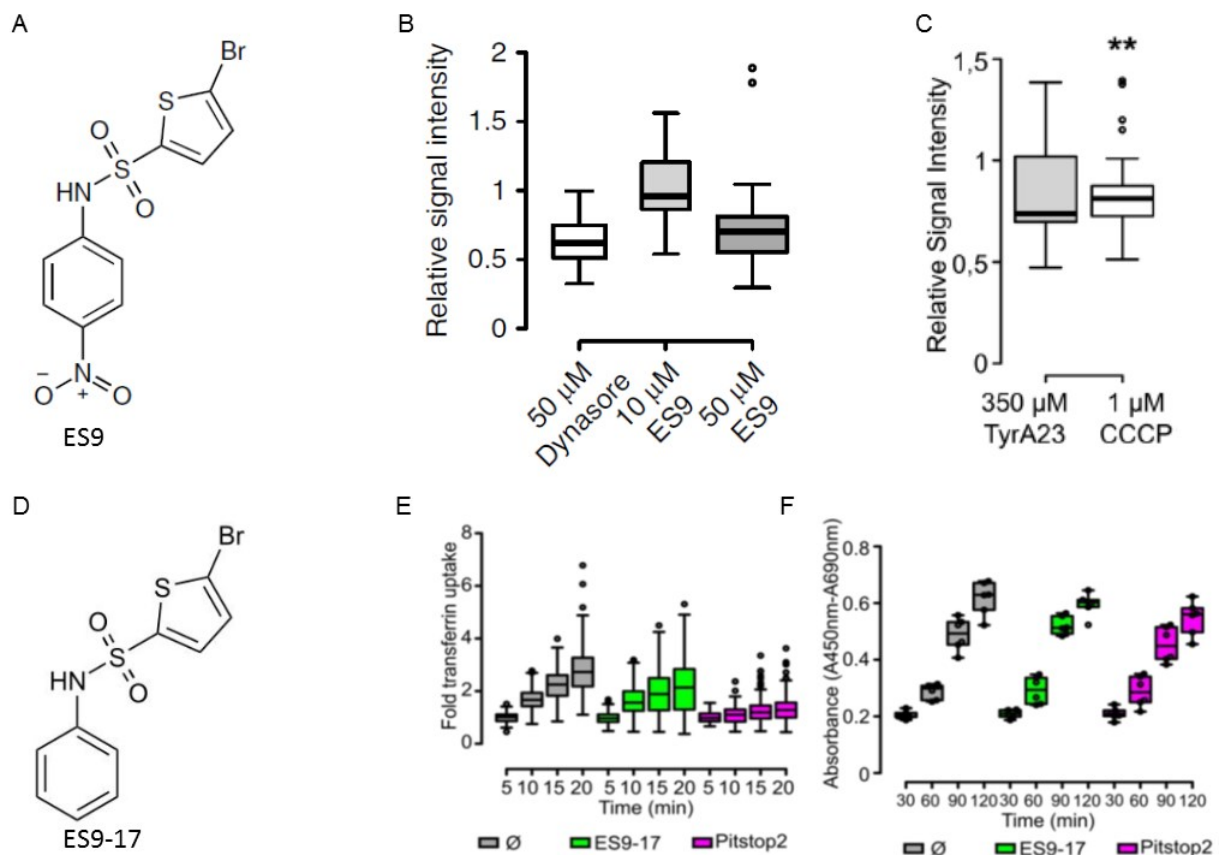


Figure 1: ES9 and ES9-17 as small molecules, inhibitors of clathrin-mediated endocytosis. (A) Chemical structure of ES9. **(B)** Boxplot representation of transferrin uptake in HeLa cells after 20 min in the presence of 50 μM dynasore and 10 or 50 μM ES9. The signal intensity is plotted relative to mock (DMSO) and shows a concentration dependent inhibition of uptake by ES9. Center lines show the medians; box limits indicate the 25th and 75th percentiles as determined by R software; whiskers extend 1.5 times the interquartile range from the 25th and 75th percentiles; outliers are represented by dots. The box width is relative to sample size ($n=35$, 29, and 61 cells). **(C)** Boxplot representation of transferrin uptake in HeLa cells in the presence of 1 μM carbonyl cyanide *m*-chlorophenyl hydrazine (CCCP) and 350 μM tyrphostin A23 (TyrA23) relative to mock (DMSO), $n=28$ and 25 cells respectively. **(D)** Structure of ES9-17. **(E)** Transferrin uptake in HeLa cells, relative to the first time point, in the presence of DMSO (\emptyset), ES9-17 (30 μM), and Pitstop2 (20 μM) at 5 to 20 min. At least 65 cells were quantified for four biological repeats. **(F)** WST-1 cell proliferation assay indicating metabolically active HeLa cells upon treatment with DMSO (\emptyset), ES9-17 (30 μM), and Pitstop2 (20 μM). Individual data points are plotted for two biological repeats.

To study the effect of the small molecules ES9 and ES9-17 we used an assay, where we did Live Cell Imaging on the uptake of fluorescently labelled transferrin into HeLa cells (Figure 1). We quantified the intracellular mean grey value for a time period of 20 min after the application of the clathrin-mediated endocytosis marker (Figure 1B, 1C and 1E). We compared the different treatments to the mock situation and we made our conclusions on the function of the small molecules. We did also a cell proliferation assay to verify that the effect of the compounds is not due to cytotoxicity (Figure 1F).

4.3 Discussion and conclusions

The small molecule ES9 impairs clathrin-mediated endocytosis in *Arabidopsis thaliana*, HeLa cells and *Drosophila* neurons (Dejonghe et al., 2016). Similarly, TyrA23, also decreased the cellular ATP levels and both molecules showed effects as CCCP on mitochondrial respiration, uncoupled oxidation and phosphorylation in isolated *Arabidopsis* mitochondria (Dejonghe et al., 2016). The small molecules ES9 and TyrA23 are uncouplers of mitochondrial oxidative phosphorylation, which causes cytoplasmic acidification and then due to these acidification there is a prolonged lifetime of clathrin and of the associated adaptors, which leads to a decrease in the phosphatidylinositol-4,5-biphosphate on the plasma membrane and due to this no clathrin pits can be formed (Dejonghe et al., 2016).

ES9-17 is another small molecule, which is a non-protonophoric analog of ES9, which binds CHC nTD and like this it impairs the clathrin-mediated endocytosis. ES9-17 can reduce the uptake of transferrin in HeLa cells at a concentration of 30 μ M ES9-17 for 20 min, but not to a degree, which was observed with 20 μ M Pitstop2. To verify that the inhibition of transferrin uptake was not due to the cytotoxicity of the compounds, we did a cell proliferation assay. In conclusion, ES9 and ES9-17 are another addition to the chemical toolbox for clathrin-mediated endocytosis inhibitors across different systems.

4.4 Material and Methods

HeLa cell cultures.

HeLa cells were grown in DMEM (Gibco, Life technologies), supplemented with 10% fetal calf serum (Gibco, Life Technologies) and 1% antibiotics (penicillin/streptomycin) (Gibco, Life Technologies), and maintained in a humidified incubator at 37°C under a 5% CO₂ atmosphere.

Live imaging of HeLa cells.

For the microscopy observation of living cells, HeLa cells were placed on a MatTek chamber and incubated overnight in a humidified incubator at 37°C and under a 5% CO₂ atmosphere to enable their attachment to the coverslip. All tested compounds were dissolved in DMSO and were diluted to the desired concentration in DMEM medium without fetal calf serum and without phenol red (Gibco, Life Technologies). To study the effect of different compounds on

endocytosis in HeLa cells, transferrin from human serum, Alexa Fluor 488 Conjugate (Life Technologies) was implemented. The cells were pre-treated with the compounds for 30 min at 37°C and a 5% CO₂ atmosphere, followed by the exchange of the medium with a fresh one, containing the same compound concentration and 25 µg ml⁻¹ fluorescently labelled transferrin. Imaging was done with a LSM 700 inverted confocal microscope (Zeiss) with a plan-apochromat 40x/1.2 water objective lens for a time period of up to 20 min after placing the transferrin-containing solution on the cells. The images were quantified in ImageJ by measuring the signal intensity of the mock-treated (between 0.01% [v/v] and 0.7% [v/v] DMSO) cells and the signal intensity of the compound-treated cells.

Cell viability assay. For the WST-1 assay, HeLa cells were grown in a 96-well plate and incubated with the compounds for 30 min, followed by the addition of 10 µl WST-1 reagent (Sigma-Aldrich) to 100 µl of medium. Absorbance was measured at 450 nm versus that at the 690 nm reference by means of a plate reader.

4.5 Reference

Adamowski, M., Narasimhan, M., Kania, U., Glanc, M., De Jaeger, G., and Friml, J. (2018). A Functional Study of AUXILIN-LIKE1 and 2, Two Putative Clathrin Uncoating Factors in Arabidopsis. *Plant Cell* **30**: 700 LP – 716.

Baisa, G.A., Mayers, J.R., and Bednarek, S.Y. (2013). Budding and braking news about clathrin-mediated endocytosis. *Curr. Opin. Plant Biol.* **16**: 718–725.

Banbury, D.N., Oakley, J.D., Sessions, R.B., and Banting, G. (2003). Tyrphostin A23 Inhibits Internalization of the Transferrin Receptor by Perturbing the Interaction between Tyrosine Motifs and the Medium Chain Subunit of the AP-2 Adaptor Complex. *J. Biol. Chem.* **278**: 12022–12028.

Crump, C.M., Williams, J.L., Stephens, D.J., and Banting, G. (1998). Inhibition of the Interaction between Tyrosine-based Motifs and the Medium Chain Subunit of the AP-2 Adaptor Complex by Specific Tyrphostins. *J. Biol. Chem.* **273**: 28073–28077.

Dejonghe, W. et al. (2019). Disruption of endocytosis through chemical inhibition of clathrin heavy chain function. *Nat. Chem. Biol.* **15**: 641–649.

Dejonghe, W. et al. (2016). Mitochondrial uncouplers inhibit clathrin-mediated endocytosis

- largely through cytoplasmic acidification. *Nat. Commun.* **7**: 11710.
- Dhonukshe, P., Aniento, F., Hwang, I., Robinson, D.G., Mravec, J., Stierhof, Y.-D., and Friml, J.** (2007). Clathrin-Mediated Constitutive Endocytosis of PIN Auxin Efflux Carriers in Arabidopsis. *Curr. Biol.* **17**: 520–527.
- Elkin, S.R., Oswald, N.W., Reed, D.K., Mettlen, M., MacMillan, J.B., and Schmid, S.L.** (2016). Ikarugamycin: A Natural Product Inhibitor of Clathrin-Mediated Endocytosis. *Traffic* **17**: 1139–1149.
- Gadeyne, A. et al.** (2014). The TPLATE Adaptor Complex Drives Clathrin-Mediated Endocytosis in Plants. *Cell* **156**: 691–704.
- Hicks, G.R. and Raikhel, N. V** (2012). Small Molecules Present Large Opportunities in Plant Biology. *Annu. Rev. Plant Biol.* **63**: 261–282.
- Kitakura, S., Vanneste, S., Robert, S., Löffke, C., Teichmann, T., Tanaka, H., and Friml, J.** (2011). Clathrin mediates endocytosis and polar distribution of PIN auxin transporters in Arabidopsis. *Plant Cell* **23**: 1920–1931.
- Macia, E., Ehrlich, M., Massol, R., Boucrot, E., Brunner, C., and Kirchhausen, T.** (2006). Dynasore, a Cell-Permeable Inhibitor of Dynamin. *Dev. Cell* **10**: 839–850.
- McCluskey, A. et al.** (2013). Building a better dynasore: the dyngo compounds potently inhibit dynamin and endocytosis. *Traffic* **14**: 1272–1289.
- McMahon, H.T. and Boucrot, E.** (2011). Molecular mechanism and physiological functions of clathrin-mediated endocytosis. *Nat. Rev. Mol. Cell Biol.* **12**: 517.
- Park, R.J., Shen, H., Liu, L., Liu, X., Ferguson, S.M., and De Camilli, P.** (2013). Dynamin triple knockout cells reveal off target effects of commonly used dynamin inhibitors. *J. Cell Sci.* **126**: 5305–5312.
- Reynolds, G.D., Wang, C., Pan, J., and Bednarek, S.Y.** (2018). Inroads into Internalization: Five Years of Endocytic Exploration. *Plant Physiol.* **176**: 208 LP – 218.
- Smith, J.M., Salamango, D.J., Leslie, M.E., Collins, C.A., and Heese, A.** (2014). Sensitivity to Flg22 Is Modulated by Ligand-Induced Degradation and de Novo Synthesis of the Endogenous Flagellin-Receptor FLAGELLIN-SENSING2. *Plant Physiol.* **164**: 440 LP – 454.
- von Kleist, L. et al.** (2011). Role of the Clathrin Terminal Domain in Regulating Coated Pit Dynamics Revealed by Small Molecule Inhibition. *Cell* **146**: 471–484.
- Willox, A.K., Sahraoui, Y.M.E., and Royle, S.J.** (2014). Non-specificity of Pitstop 2 in clathrin-mediated endocytosis. *Biol. Open* **3**: 326–331.

- Yaish, P., Gazit, A., Gilon, C., and Levitzki, A.** (1988). Blocking of EGF-dependent cell proliferation by EGF receptor kinase inhibitors. *Science* (80-.). **242**: 933 LP – 935.
- Zwiewka, M. and Friml, J.** (2012). Fluorescence imaging-based forward genetic screens to identify trafficking regulators in plants. *Front. Plant Sci.* **3**: 97.

5 General conclusions, discussion and perspectives

The endomembrane trafficking, besides the well-known cellular house-keeping functions, also mediates responses to the environmental changes and different developmental processes. The plant cell has trafficking machineries, which support a large spectrum of processes such as signal mediation, metabolite transport, organelle mobility, communication and cell proliferation. In *Arabidopsis thaliana*, the auxin influx and efflux carriers have been identified, which act at the plasma membrane and are important for the directional flow of this phytohormone (Grunewald and Friml, 2010). Through the trafficking of the auxin efflux carriers from the PIN family, many of the auxin related processes are regulated, which is crucial for the subcellular auxin homeostasis and also for the cell-to-cell directional transport (Grunewald and Friml, 2010). Moreover, the intracellular endomembrane trafficking is regulated by different mechanisms, where an important role play the small GTPases, which act as molecular switches of different processes due to their ability to bind or hydrolyze guanosine triphosphate (GTP). The cellular transport machineries are studied for many years, but still there are many uncharacterized molecular pathways, which is an interesting research topic to further characterize and identify novel membrane trafficking factors.

This PhD thesis is focused on endomembrane trafficking in *Arabidopsis thaliana*. I have characterized an additional component of intracellular membrane trafficking, which helps the plant to survive better and to adapt to inhibited ARF-GEF mechanisms. For this, we identified a mutant in a morphology based screen for plants growing and surviving better than the parental line in the presence of the fungal toxin BFA. On the other hand, it shows higher sensitivity on a cellular level as after washout or long incubation with BFA there are remaining BFA bodies. I combined pharmacological treatment and marker studies in order to characterize the role of the BAR1/SACSIN protein.

Next, in order to achieve better understanding of the regulation of the intracellular trafficking and PIN polarity, I studied the effect of strigolactones on the PIN internalization and also the role of phosphorylation in the strigolactones regulation of auxin feedback on PIN internalization. With my experiments and observations I confirmed that strigolactones have the property to moderate the polar auxin transport. We also report that the inhibitory effect of auxin on the cellular internalization of PINs is counteracted by SLs. As the effect of auxin on the inhibition of internalization is a requirement for increased PAT and also for the

canalization process, when strigolactones are applied into the system, then it becomes less likely to induce canalization related growth responses.

Last, but not least, with the aim to further characterize and understand the clathrin-mediated endocytosis process, I participated in a collaboration, where we characterized the role of two small molecules, which inhibit the FM4-64 uptake in *Arabidopsis thaliana*. ES9 acts as a chemical uncoupler of proton gradients, with important implications on energy metabolism, pH homeostasis and dynamic processes in the cell, including CME and mimics also the known CME inhibitor Tyrphostin A23. An analogue of ES9 – ES9-17 was identified which retained the ability to inhibit CME, yet lacked characteristics of an uncoupler. It proved to be more specific compared to ES9, and was found to bind to clathrin heavy chain.

In the next paragraphs, I will make general conclusions and I will discuss the research I did and also the future perspectives by suggesting experiments for further investigations.

5.1 SACSIN mediates adaptation of plant cells to ARF-GEF inhibition

We designed a morphology based screen on an EMS treated *PIN1pro::PIN1-GFP* expressing *Arabidopsis* population to select mutants, which have an insensitive phenotype to the vesicle trafficking inhibitor BFA, and show abnormal PIN1-GFP accumulation after long treatment with this compound. Among them, we identified *bar1* (*bfa altered response 1*), which is a recessive mutant and survives and develops better on a BFA containing *in vitro* cultures on solid medium compared to the parental *PIN1pro::PIN1-GFP* line. In addition, by using protein prediction tools, we observed a homology of the encoded protein to the human SACSIN. In humans, mutations in the *SACS* gene lead to ARSACS, which is a neurodegenerative disease, which cause is a defect in the mitochondria fission. In comparison, in plants, the SACSIN protein is present in the very early diverging species like green algae, ferns and moss, which suggests that the protein has an important and preserved role, which might be responsible for the adaptation to the changing environment. In addition, the protein prediction suggests that due to the presence of the 90-like ATPase domains, one of the putative roles of SACSIN is to direct folding through ATP-dependent mechanisms (Powers and Balch, 2013). Moreover, together with the presence of a C3HC4-type RING finger domain, the protein is prone to many interactions and bindings to other proteins, but also to participate in the protein homeostasis

network, where the SACSIN protein may play an important role as a component of the degradation machinery and proteostasis (Powers and Balch, 2013).

The plasma membrane of eukaryotic cells is an essential functional hub between the cell and the surrounding environment (Sigismund et al., 2012). At the cell surface, a crucial role play the regulated retrieval of transporters and receptors – from the plasma membrane (endocytosis) and then their delivery back by exocytosis, where the process in plants is known as constitutive endocytic recycling (Geldner et al., 2001). This mechanism is regulated by a vesicle budding regulator GNOM ARF-GEF, which is sensitive to a fungal toxin BFA (Geldner et al., 2001). The ARF proteins are known to perform their function in subcellular trafficking and their activity switches between the inactive (GDP) and the active (GTP) bound state (Geldner et al., 2003). There are evidences for the involvement of them in the subcellular trafficking of the PIN1 protein, where by implementing BFA as a pharmacological tool to study the vesicle trafficking process, the endocytic recycling of this protein was observed (Geldner et al., 2001, 2003; Richter et al., 2007; Tanaka et al., 2009). Moreover, the inhibition of the ARF protein function results in different trafficking defects defined by the intracellular accumulation of plasma membrane cargos (Lee et al., 2002). If there are defects in the endocytic recycling of the PIN1 protein, this would disrupt the polar auxin transport, which is required in developmental situations such as formation of lateral roots or vasculature system development (Geldner et al., 2004). We show that the *sacsin* morphology phenotype is characterized by a more complex vasculature system, which is evidence for a defect in the trafficking of the PIN1 protein and which suggests a role of SACSIN in auxin transport related processes. Additionally, the gravitropic response depends on the correct PIN2 polarity (Wiśniewska et al., 2006). There were no gravitropism defects and or altered PIN2 localization after immunolocalization studies in the epidermis cells of the *sacsin* root. The experiments in nondisturbed conditions were designed to verify, if SACSIN has any detectable trafficking defects. Our observations of the fluorescent recovery after photobleaching (FRAP) showed no significant difference in FRAP of *PIN1pro::PIN1-GFP* and *bar1-2* mutant, suggesting that the PIN1 trafficking defects are not caused by reduced PIN1 secretion or recycling. This results are consistent with our observations for the β -estradiol inducible PIN1-RFP line and for the *PIN2::PIN2-Dendra* line. Additionally, in the absence of BFA there was no effect on the vacuolar targeting of PIN2-GFP or defects in the endocytosis after performing FM4-64 uptake experiments. These results show that we cannot detect a role of SACSIN in normal trafficking,

but the mutation has a specific effect on BFA reactions, pronounced as higher sensitivity to this compound. It has a strong impact on the intracellular trafficking as well as plant growth and development (Geldner et al., 2001). We did a visual inspection and a quantitative analysis of the PIN1 and PIN2 proteins and also of the TGN marker VHAa1-GFP after treatments with BFA. Our analysis after immunolocalization of both PIN proteins and life imaging of the VHAa1-GFP protein revealed that there is the remaining BFA bodies after washout, but also after long incubation with BFA, which sustain in the cells of the mutant. In conclusion, the *sacsin* mutation has a specific effect on BFA reactions, both in the seedling growth and in the cellular reactions of the endomembrane system, observable by aggregation and dissolution of the BFA body. Interestingly, while the growth reaction is clearly resistance, the cellular reactions appears as oversensitivity or inability to recover.

In *Arabidopsis thaliana* there are distinct ARF-GEFs dependent apical and basal targeting machineries. In addition to its general function in plasma membrane to endosome and back trafficking for polar and non-polar cargoes, GNOM plays an essential role in the basal targeting of the PIN proteins, whereas apical targeting is independent of GNOM and possibly requires BFA-resistant ARF-GEFs (Kleine-Vehn et al., 2008). To identify the role of SACSIN in this process, we used the weak *gnom* allele – *gnom^{R5}* where there is increased targeting of PIN1 to the apical side, which illustrates an altered affinity of PIN1 for the apical targeting pathway (Kleine-Vehn et al., 2008). By analysing of our results we confirmed that pharmacological or genetic inhibition of the GNOM ARF-GEF is sufficient to recruit basal cargoes into the apical pathway. Interestingly, after long treatment with BFA, there is a partial apicalization of the PIN1 protein not only in wild type, but also in *sacsin*, however in *gnom^{R5}* the PIN1 protein is apicalized in all of the observed cells. As previously noted after long treatment with BFA, when the SACSIN protein is not participating in the whole machinery, then there is a trafficking defect from the BFA body to the apical side of the cells, pronounced in remaining BFA body aggregates in the cells. Moreover, we observe the pattern of apicalization also for *gnom^{R5}* in *sacsin* background, but additionally there is a defect in the trafficking machinery, observed as remaining BFA bodies in the cells after the prolonged BFA treatment. It seems that the aggregation or lack of aggregation of PIN1 in the body is a distinct phenomenon from its apico-basal sorting, which is unlike previous interpretations, where we rather concluded that the PIN1 has to leave the body to go apical instead.

In *Arabidopsis thaliana* there are eight genes, which encode Sec7 domain proteins. As previously identified, there are two BFA-insensitive ARF-GEFs – *gnl1* and *big3* (Richter et al., 2007, 2014). Indeed, *big3* was epistatic to *sacsin* as it was not germinating on a BFA containing *in vitro* cultures on solid medium. In addition, after the long treatment with BFA there were abnormally sized and shaped bodies in *big3* and in *big3 sacs**in*, which leads to the conclusion that *big3* is epistatic to *sacsin* and both genes participate in the same trafficking pathway. The protein-protein interaction is important to predict the protein function (Rao et al., 2014). The resulting phenotypes in a plant are based on the interactions between genes and proteins. By using computational tools, one can study the genetic interaction between two genes by implementing the already constructed networks. Moreover, by the application of clustering algorithms, different gene expressions can be analysed and grouped together, according to the bioinformatics data of their expression levels. As a result, the gene expression can help to elucidate the functional relationship between different genes. Based on previous research, the genes, which are co-expressed are more prone to interact with each other than the proteins, encoded by genes belonging to different clusters (Grigoriev and Biotech, 2001). By using bioinformatics tools, we identified that *SACSIN* is co-expressed with *BIG*, which is a regulator of auxin transport (Paciorek et al., 2005). The *BIG*-deficient mutant *doc1*, allelic to *tir3*, has less basipetal auxin transport through the body and as a result there are less lateral roots (Gil et al., 2001) and they require higher concentrations of auxin in order to block the PIN1 endocytosis upon the implementation of BFA as a vesicle trafficking inhibitor (Paciorek et al., 2005). On the other hand, *sacsin* has a slightly increased number of lateral roots and a better survival on a BFA *in vitro* cultures on solid medium. We examined the *SACSIN-BIG* genetic interaction to elucidate its role in protein trafficking. We show that there were additive effects, where *sacsin* gives better growth and *big* gives worse growth and the double mutant is in between. Furthermore, when treated for long time with BFA, in *sacsin* there are the remaining BFA aggregates in the cells, however in wild type and *doc1* there are less remaining cellular aggregates. Moreover, the cell phenotype of the double mutant looks like *sacsin* regarding the defective transcytosis, where the BFA bodies remain in the cells after long treatment with the vesicle trafficking inhibitor. Together, these results indicate that *sacsin* and *big* might function in the same trafficking pathway, but with opposite activities. As *sacsin* has more lateral roots and *big* less, then it might be that in *sacsin* there is higher

basipetal auxin transport through the stem and root, where *big* is compensating with exactly the opposite phenotype.

In these project we reveal an important novel insight into the intracellular trafficking mechanisms in *Arabidopsis thaliana*. We show that in this model organism morphology based forward genetics with BFA as a tool to identify mutant candidates is a feasible approach for novel components in endomembrane trafficking processes. By screening for mutants with a better growth and development on a BFA containing *in vitro* cultures on solid medium, we identified SACSIN. This protein is important for the plant to survive and grow better in the conditions of impaired BFA sensitive trafficking processes.

Taken together, SACSIN has a role in multiple GNOM regulated trafficking processes, which are pronounced as a prolonged recovery of the BFA bodies after a washout, where the Golgi apparatus and TGNs aggregate for longer and also after the long BFA treatment, whereas in *sacsin* background the cells are not able to dissolve the aggregated BFA body.

In summary, we have demonstrated that the interference with the function of SACSIN had a strong impact on the plant growth, survival and architecture in an artificial situation like the growth on a BFA containing *in vitro* cultures on solid medium.

5.2 Strigolactone interferes with auxin feedback on PIN internalization

The canalization hypothesis proposes a feedback effect of auxin on the polar localization of the auxin efflux carriers and consequently on the directionality of the auxin transport (Sauer et al., 2006). Another player in the establishment of many developmental processes is the phytohormone strigolactone, which also participates in the regulation of the polar auxin transport and canalization (Shinohara et al., 2013). As auxin reduces the internalization of the PIN proteins, when under the influence of strigolactone, it becomes less likely that canalization related growth responses are induced and the polar auxin transport is reduced (Shinohara et al., 2013).

To examine through which signalling pathway the effect of strigolactone occurs, we used the primary root of *Arabidopsis thaliana* as a model system. The PIN1 protein there is localized to the basal side of the stele cells (Kleine-Vehn et al., 2008). We studied the localization of this marker after application of NAA and/or strigolactone in the presence of BFA, which we used

as a tool to study the vesicle trafficking processes. Our results show that the inhibitory effect of GR24 on auxin-mediated PIN lateralization was impaired in *max2* when compared to wild type. Additionally, the receptor mutant *d14* showed less sensitivity to GR24 with respect of counteracting NAA action on PIN endocytic trafficking. These results suggest that the synthetic GR24 interferes with auxin-mediated feedback on PIN internalization through the D14 receptor and MAX2-dependent pathway and it negatively regulates the process of canalization, but also regulates the auxin mediated polarization of the PIN transporters.

5.3 Role of phosphorylation in the strigolactone regulation of auxin feedback on PIN internalization

Through the alteration of the cycling of the PIN proteins between the plasma membrane and the endomembrane system, which influences the abundance of PIN proteins on the plasma membrane, the flow of auxin through tissues can be regulated, which has a developmental effect (Prusinkiewicz et al., 2009). It was shown that one of the effects of GR24 is to reduce the basipetal auxin transport (Prusinkiewicz et al., 2009). Strigolactones regulate the auxin feedback on PIN internalization which has an effect on the canalization properties (Sachs, 2000; Sauer et al., 2006). On the other hand, there are the Ser/Thr protein kinase PINOID (PID) and the protein phosphatase 2A (PP2A), which also regulate the PIN localization (Kleine-Vehn et al., 2009). They act on the phosphorylation status of the PIN proteins, thus determining the apical or basal PIN targeting (Friml et al., 2004; Michniewicz et al., 2007). Previous research reported a role for PP2AAs (PP2AA1/RCN1, A2, and A3 proteins) in regulating PIN phosphorylation, polar localization and auxin transport (Rashotte et al., 2001; Michniewicz et al., 2007). They can participate in the assembly of both PP2A and PP6 holoenzymes (Dai et al., 2012). The last one is formed by *FyPPs*, *SAL* genes, and *PP2AAs*, which can physically interact with a subset of PIN proteins and the strength of their interaction is regulated by the phosphorylation status of the PIN proteins (Dai et al., 2012). This holoenzyme consists of the three subunits (regulatory subunits A and B and a catalytic subunit C) and it plays a major role in regulating PIN phosphorylation, auxin transport, polar targeting and diverse plant developmental processes (Dai et al., 2012). PP6-mediated dephosphorylation promotes basal targeting of PIN proteins, while PID-dependent phosphorylation promotes apical PIN localization and regulates polar auxin transport and plant development. *FyPP1* and *FyPP3*

genes function as the catalytic subunit of PP6 and are required for proper polar localization to the basal side of the stele cells and loss of their activity leads to a basal-to-apical shift in the PIN polar targeting (Dai et al., 2012). However, there was still no evidence for a role of putative catalytic subunits of PP2A (PP2AC) in the regulation of the PIN protein phosphorylation and auxin transport (Dai et al., 2012). The *Arabidopsis* genome contains five genes encoding the putative C subunits of PP2A (PP2Ac1-5), and presumably these genes have redundant functions in regulating plant development (Dai et al., 2012). *Moreover*, there were no significant phenotypic changes in *sal1* and *sal4* (we tested only those; regulatory subunit B) single mutant seedlings compared with Col-0, indicating that there is probably functional redundancy (Dai et al., 2012). For our experiments we also used *F1DN* (*35S::YFP-FyPP1^{DB1N}/Col-0*; hereafter, *F1DN*) and *F3DN* (*35S::YFP-FyPP3^{DB1N}/Col-0*; hereafter, *F3DN*) seedlings, which have drastic phenotypic changes, suggesting that PP6 is the primary phosphatase that regulates auxin transport-dependent plant developmental processes (Dai et al., 2012).

We were interested to characterize the role of phosphorylation in the strigolactone regulation of auxin feedback on PIN internalization. We did PIN1 protein immunolocalization after NAA and/or GR24 treatment, where we implemented BFA as a tool to visualize the vesicle trafficking processes. We tested whether *FyPP1*, *FyPP3*, *f1f3*, *SAL4* and *PP2AAs* are required for proper PIN1 localization and for this we did PIN1 immunolocalization after those treatments. In Col-0 roots, PIN1 is localized to the basal side of the stele cells, whereas in *f1f3*, *F1DN* and *F3DN* roots, there is a switch from the basal to the apical side in the vasculature cells of the untreated roots (Dai et al., 2012). Unfortunately, there are technical shortcomings, pronounced in the reproducibility and fluctuating tendencies when comparing our observations from the experiments on the different mutants. In our observations we get a reduction of the PIN1 internalization after GR/NAA/BFA treatment in the cases of *35S::FyPP1-GFP* and also in the dominant negative line *F1DN*, which makes any conclusions difficult. Additionally, we noticed less sensitivity of *SAL4* to GR24 with respect of counteracting NAA action on PIN endocytic trafficking. These results suggest that the synthetic GR24 interferes with auxin mediated feedback on PIN internalization where *SAL4* has a crucial role. Our conclusion from the performed experiments is that the phosphorylation might be directly or indirectly involved in the strigolactone regulation of auxin feedback on PIN internalization.

5.4 MAX2-dependence of strigolactone-mediated root growth inhibition

Strigolactone and auxin define the root architecture in a concentration-dependent manner. Both hormones act in a regulated feedback circuit as strigolactones alter the amount and transport of auxin. Strigolactone effect on the primary root growth is accompanied by a GR24 concentration dependent change. Previous research showed that *Arabidopsis* plants, grown in the presence of low levels of GR24 (1,25 and 2,5 μM) have an increase in the primary root length (Ruyter-Spira et al., 2011), which I could not observe in my experiments. The lower concentrations of GR24 lead to an increase in the auxin levels, which has an effect on the primary root length (Ruyter-Spira et al., 2011). At high concentrations of strigolactone these levels of auxin are reduced, which reduces the primary root length, but also the whole seedling appearance is affected and this could be due to general toxicity of the treatment (Ruyter-Spira et al., 2011).

Additionally, GR24 reduced the lateral root density, which is also a process, dependent on different auxin fluxes (Lucas et al., 2008). The lateral root development is stimulated by the auxin amounts in the root tip (Casimiro et al., 2003), which is delivered there by polar auxin transport from the aerial parts (Bhalerao et al., 2002). Auxin is delivered into the developing lateral root through the repolarization of the PIN1 protein, which permits lateral root influx (Ruyter-Spira et al., 2011). GR24 modulates this process by reducing the auxin levels in the aerial parts and then the amount of auxin, which reaches the LR, is not sufficient respectively (Ruyter-Spira et al., 2011).

Our results show that the application of strigolactones affects both primary root length and lateral root density. GR24 has an effect on the inhibition of the primary root length of wild type at low concentrations and also on the primary root length of *max2-1* at higher concentrations. Moreover, the action of strigolactones on the inhibition of lateral root development is MAX2-dependent as *max2* is showing a resistance in the density of lateral roots compared to the control. The response upon GR24 treatment is mediated through a modulation of local auxin levels and is therefore dependent on the auxin status and on the sensitivity of the plant. GR24 is a synthetic strigolactone and is a mixture of two stereoisomers (Mangnus et al., 1992), which could have different effect on the root development. To confirm the findings, experiments with natural strigolactones should be performed.

5.5 Putative regulator of PIN polarity identified by means of forward genetics screen using strigolactone analogue GR24

To characterize the role of strigolactone on the free IAA in *Arabidopsis thaliana*, we investigated the auxin-related metabolomics profiling after treatment with 50 μ M GR24 for 12 or 24h in the root tip and in the shoot. The application of strigolactone leads to elevation in the amount of free IAA in wild type. Moreover, we wanted to experimentally observe, if the mutation in the At5G50850 gene, coding for pyruvate dehydrogenase E1- β subunit (PD E1- β), or the mutation in the *max2* gene, have an effect on the levels of auxin conjugates. Unfortunately, there were no reproducible and repetitive trends in the amounts of conjugates in the mock and after strigolactone treatment. There were technical shortcomings in the sampling and in the analysis, nevertheless, there is a tendency that GR24 increases the levels of free auxin/IAA.

5.6 Endosidin 9 (ES9) and Endosidin 9-17 (ES9-17) are small molecules, inhibitors of clathrin-mediated endocytosis

In the model organism *Arabidopsis thaliana* the internalization of plasma membrane proteins and extracellular cargos happens through clathrin-mediated endocytosis (Reynolds et al., 2018). When characterizing the phenotype of mutants with defective clathrin-mediated endocytosis function, there is either a lethal phenotype or there is only a mild phenotype due to gene redundancy (Kitakura et al., 2011). In addition, there is also the option of inducible systems to interfere with CME, those targeting clathrin or auxillin or using small interfering RNA-mediated depletion of adaptor proteins (Gadeyne et al., 2014; Dhonukshe et al., 2007; Adamowski et al., 2018). The negative aspects of these approaches are connected with silencing, low gene induction efficiency and the longer time needed to deplete existing protein complexes. Positive aspect is that the applied effect of blocking the clathrin-mediated endocytosis can be reversed (Hicks and Raikhel, 2012).

The identified small molecule ES9 inhibits CME in *Arabidopsis thaliana*, HeLa cells and *Drosophila* neurons (Dejonghe et al., 2016). It has an influence on the energy metabolism in all those model organisms similar to the established inhibitors of the ATP production. Similarly, TyrA23, also decreased the cellular ATP levels and both molecules showed effects

as CCCP on mitochondrial respiration, uncoupled oxidation and phosphorylation in isolated *Arabidopsis* mitochondria (Dejonghe et al., 2016).

The ES9 non-protonophoric analog ES9-17 lacks a nitro group, which was electrostatically interacting with Arg64, and this is the reason why this new analog binds CHC nTD in a different orientation and affinity than ES9. ES9-17 can reduce the uptake of transferrin in HeLa cells at a concentration of 30 μ M ES9-17 for 20 min, but not to a degree, which was observed with 20 μ M Pitstop2. To verify that the inhibition of transferrin uptake was not due to the cytotoxicity of the compounds, we did a cell proliferation assay. In addition, in *Arabidopsis thaliana* Pitstop2 did not block FM4-64 uptake when applied for 30 min at 30 μ M concentration and it also failed to inhibit clathrin-mediated endocytosis. These results might be due to the amino acid differences between human and *Arabidopsis* CHC since the binding pocket of Pitstop2 in hCHC1 is well characterized.

In conclusion, ES9 and ES9-17 are another addition to the chemical toolbox for CME inhibitors across different systems. The property to selectively inhibit the CHC1 or CHC2 action will help to further characterize endomembrane trafficking mechanisms in plants and other model systems.

5.7 Reference

- Bhalerao, R.P., Eklöf, J., Ljung, K., Marchant, A., Bennett, M., and Sandberg, G.** (2002). Shoot-derived auxin is essential for early lateral root emergence in *Arabidopsis* seedlings. *Plant J.* **29**: 325–332.
- Casimiro, I., Beeckman, T., Graham, N., Bhalerao, R., Zhang, H., Casero, P., Sandberg, G., and Bennett, M.J.** (2003). Dissecting *Arabidopsis* lateral root development. *Trends Plant Sci.* **8**: 165–171.
- Dai, M. et al.** (2012). A PP6-Type Phosphatase Holoenzyme Directly Regulates PIN Phosphorylation and Auxin Efflux in *Arabidopsis*. *Plant Cell* **24**: 2497 LP – 2514.
- Dejonghe, W. et al.** (2019). Disruption of endocytosis through chemical inhibition of clathrin heavy chain function. *Nat. Chem. Biol.* **15**: 641–649.
- Dejonghe, W. et al.** (2016). Mitochondrial uncouplers inhibit clathrin-mediated endocytosis

largely through cytoplasmic acidification. *Nat. Commun.* **7**: 11710.

Friml, J. et al. (2004). A PINOID-Dependent Binary Switch in Apical-Basal PIN Polar Targeting Directs Auxin Efflux. *Science* (80-.). **306**: 862 LP – 865.

Geldner, N., Anders, N., Wolters, H., Keicher, J., Kornberger, W., Muller, P., Delbarre, A., Ueda, T., Nakano, A., and Jürgens, G. (2003). The Arabidopsis GNOM ARF-GEF Mediates Endosomal Recycling, Auxin Transport, and Auxin-Dependent Plant Growth. *Cell* **112**: 219–230.

Geldner, N., Friml, J., Stierhof, Y.-D., Jürgens, G., and Palme, K. (2001). Auxin transport inhibitors block PIN1 cycling and vesicle trafficking. *Nature* **413**: 425–428.

Geldner, N., Richter, S., Vieten, A., Marquardt, S., Torres-Ruiz, R.A., Mayer, U., and Jürgens, G. (2004). Partial loss-of-function alleles reveal a role for GNOM in auxin transport-related, post-embryonic development of Arabidopsis. *Development* **131**: 389–400.

Gil, P., Dewey, E., Friml, J., Zhao, Y., Snowden, K.C., Putterill, J., Palme, K., Estelle, M., and Chory, J. (2001). BIG: a calossin-like protein required for polar auxin transport in Arabidopsis. *Genes Dev.* **15**: 1985–1997.

Grigoriev, A. and Biotech, G.P.C. (2001). A relationship between gene expression and protein interactions on the proteome scale : analysis of the bacteriophage T7 and the yeast *Saccharomyces cerevisiae*. **29**: 3513–3519.

Grunewald, W. and Friml, J. (2010). The march of the PINs: developmental plasticity by dynamic polar targeting in plant cells. *EMBO J.* **29**: 2700–2714.

Kleine-Vehn, J., Dhonukshe, P., Sauer, M., Brewer, P.B., Wiśniewska, J., Paciorek, T., Benková, E., and Friml, J. (2008). ARF GEF-Dependent Transcytosis and Polar Delivery of PIN Auxin Carriers in Arabidopsis. *Curr. Biol.* **18**: 526–531.

Kleine-Vehn, J., Huang, F., Naramoto, S., Zhang, J., Michniewicz, M., Offringa, R., and Friml, J. (2009). PIN Auxin Efflux Carrier Polarity Is Regulated by PINOID Kinase-Mediated Recruitment into GNOM-Independent Trafficking in *Arabidopsis*. *Plant Cell* **21**: 3839 LP – 3849.

Lee, M.H., Min, M.K., Lee, Y.J., Jin, J.B., Shin, D.H., Kim, D.H., Lee, K.-H., and Hwang, I. (2002). ADP-ribosylation factor 1 of Arabidopsis plays a critical role in intracellular trafficking and maintenance of endoplasmic reticulum morphology in Arabidopsis. *Plant Physiol.* **129**: 1507–1520.

Lucas, M., Guédon, Y., Jay-Allemand, C., Godin, C., and Laplaze, L. (2008). An Auxin

- Transport-Based Model of Root Branching in *Arabidopsis thaliana*. *PLoS One* **3**: e3673.
- Mangnus, E.M., Dommerholt, F.J., De Jong, R.L.P., and Zwanenburg, B.** (1992). Improved synthesis of strigol analog GR24 and evaluation of the biological activity of its diastereomers. *J. Agric. Food Chem.* **40**: 1230–1235.
- Michniewicz, M. et al.** (2007). Antagonistic Regulation of PIN Phosphorylation by PP2A and PINOID Directs Auxin Flux. *Cell* **130**: 1044–1056.
- Paciorek, T., Zažímalová, E., Ruthardt, N., Petrášek, J., Stierhof, Y.-D., Kleine-Vehn, J., Morris, D.A., Emans, N., Jürgens, G., Geldner, N., and Friml, J.** (2005). Auxin inhibits endocytosis and promotes its own efflux from cells. *Nature* **435**: 1251–1256.
- Powers, E.T. and Balch, W.E.** (2013). Diversity in the origins of proteostasis networks--a driver for protein function in evolution. *Nat. Rev. Mol. Cell Biol.* **14**: 237–248.
- Prusinkiewicz, P., Crawford, S., Smith, R.S., Ljung, K., Bennett, T., Ongaro, V., and Leyser, O.** (2009). Control of bud activation by an auxin transport switch. *Proc. Natl. Acad. Sci. U. S. A.* **106**: 17431–17436.
- Rao, V.S., Srinivas, K., Sujini, G.N., and Kumar, G.N.S.** (2014). Protein-protein interaction detection: methods and analysis. *Int. J. Proteomics* **2014**: 147648.
- Rashotte, A.M., DeLong, A., and Muday, G.K.** (2001). Genetic and chemical reductions in protein phosphatase activity alter auxin transport, gravity response, and lateral root growth. *Plant Cell* **13**: 1683–1697.
- Reynolds, G.D., Wang, C., Pan, J., and Bednarek, S.Y.** (2018). Inroads into Internalization: Five Years of Endocytic Exploration. *Plant Physiol.* **176**: 208 LP – 218.
- Richter, S., Geldner, N., Schrader, J., Wolters, H., Stierhof, Y.D., Rios, G., Koncz, C., Robinson, D.G., and Jürgens, G.** (2007). Functional diversification of closely related ARF-GEFs in protein secretion and recycling. *Nature* **448**: 488–492.
- Richter, S., Kientz, M., Brumm, S., Nielsen, M.E., Park, M., Gavidia, R., Krause, C., Voss, U., Beckmann, H., Mayer, U., Stierhof, Y.-D., and Jürgens, G.** (2014). Delivery of endocytosed proteins to the cell–division plane requires change of pathway from recycling to secretion. *Elife* **3**: 1–16.
- Ruyter-Spira, C., Kohlen, W., Charnikhova, T., van Zeijl, A., van Bezouwen, L., de Ruijter, N., Cardoso, C., Lopez-Raez, J.A., Matusova, R., Bours, R., Verstappen, F., and Bouwmeester, H.** (2011). Physiological effects of the synthetic strigolactone analog GR24 on root system architecture in *Arabidopsis*: another belowground role for

strigolactones? *Plant Physiol.* **155**: 721–734.

Sachs, T. (2000). Integrating Cellular and Organismic Aspects of Vascular Differentiation. *Plant Cell Physiol.* **41**: 649–656.

Sauer, M., Balla, J., Luschig, C., Wisniewska, J., Reinöhl, V., Friml, J., and Benková, E. (2006). Canalization of auxin flow by Aux/IAA-ARF-dependent feedback regulation of PIN polarity. *Genes Dev.* **20**: 2902–2911.

Shinohara, N., Taylor, C., and Leyser, O. (2013). Strigolactone Can Promote or Inhibit Shoot Branching by Triggering Rapid Depletion of the Auxin Efflux Protein PIN1 from the Plasma Membrane. *PLOS Biol.* **11**: e1001474.

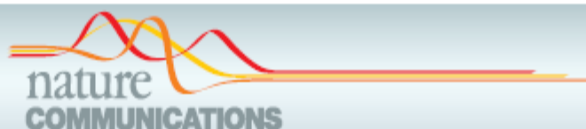
Sigmund, S., Confalonieri, S., Ciliberto, A., Polo, S., Scita, G., and Di Fiore, P.P. (2012). Endocytosis and signaling: cell logistics shape the eukaryotic cell plan. *Physiol. Rev.* **92**: 273–366.

Tanaka, H., Kitakura, S., De Rycke, R., De Groodt, R., and Friml, J. (2009). Fluorescence Imaging-Based Screen Identifies ARF GEF Component of Early Endosomal Trafficking. *Curr. Biol.* **19**: 391–397.

Wiśniewska, J., Xu, J., Seifertová, D., Brewer, P.B., Růžička, K., Blilou, I., Rouquié, D., Benková, E., Scheres, B., and Friml, J. (2006). Polar PIN Localization Directs Auxin Flow in Plants. *Science* (80-.). **312**: 883 LP – 883.

6 Appendix

6.1 Appendix A



ARTICLE

Received 17 Jul 2015 | Accepted 21 Apr 2016 | Published 8 Jun 2016

DOI: 10.1038/ncomms11710

OPEN

Mitochondrial uncouplers inhibit clathrin-mediated endocytosis largely through cytoplasmic acidification

Wim Dejonghe^{1,2}, Sabine Kuenen^{3,4}, Evelien Mylle^{1,2}, Mina Vasileva⁵, Olivier Keech⁶, Corrado Viotti⁷, Jef Swerts^{3,4}, Matyáš Fendrych⁵, Fausto Andres Ortiz-Morea^{1,2}, Kiril Mishev^{1,2}, Simon Delang⁸, Stefan Scholl⁸, Xavier Zarza⁹, Mareike Heilmann¹⁰, Jiorgos Kourelis^{9,†}, Jaroslaw Kasproicz^{3,4}, Le Son Long Nguyen¹¹, Andrzej Drozdzecki¹¹, Isabelle Van Houtte^{1,2}, Anna-Mária Szatmári^{1,2}, Mateusz Majda¹², Gary Baisa¹³, Sebastian York Bednarek¹³, Stéphanie Robert¹², Dominique Audenaert¹¹, Christa Testerink⁹, Teun Munnik⁹, Daniël Van Damme^{1,2}, Ingo Heilmann¹⁰, Karin Schumacher⁸, Johan Winne¹⁴, Jiří Friml⁵, Patrik Verstreken^{3,4} & Eugenia Russinova^{1,2}

ATP production requires the establishment of an electrochemical proton gradient across the inner mitochondrial membrane. Mitochondrial uncouplers dissipate this proton gradient and disrupt numerous cellular processes, including vesicular trafficking, mainly through energy depletion. Here we show that Endosidin9 (ES9), a novel mitochondrial uncoupler, is a potent inhibitor of clathrin-mediated endocytosis (CME) in different systems and that ES9 induces inhibition of CME not because of its effect on cellular ATP, but rather due to its protonophore activity that leads to cytoplasm acidification. We show that the known tyrosine kinase inhibitor tyrphostinA23, which is routinely used to block CME, displays similar properties, thus questioning its use as a specific inhibitor of cargo recognition by the AP-2 adaptor complex via tyrosine motif-based endocytosis signals. Furthermore, we show that cytoplasm acidification dramatically affects the dynamics and recruitment of clathrin and associated adaptors, and leads to reduction of phosphatidylinositol 4,5-bisphosphate from the plasma membrane.

¹Department of Plant Systems Biology, VIB, 9052 Gent, Belgium. ²Department of Plant Biotechnology and Bioinformatics, Ghent University, 9052 Gent, Belgium. ³VIB Center for the Biology of Disease, Laboratory of Neuronal Communication, 3000 Leuven, Belgium. ⁴Department for Human Genetics, and Leuven Institute for Neurodegenerative Diseases, KU Leuven, 3000 Leuven, Belgium. ⁵Institute of Science and Technology Austria, 3400 Klosterneuburg, Austria. ⁶Department of Plant Physiology, Umeå Plant Science Centre, Umeå University, 90187 Umeå, Sweden. ⁷Department of Plant Physiology, Institute of Biochemistry and Biology, University of Potsdam, 14476 Potsdam, Germany. ⁸Developmental Biology of Plants, Centre for Organismal Studies, Heidelberg University, 69120 Heidelberg, Germany. ⁹Department of Plant Cell Biology, Swammerdam Institute for Life Sciences, University of Amsterdam, 1090 GE Amsterdam, The Netherlands. ¹⁰Department of Cellular Biochemistry, Institute for Biochemistry and Biotechnology, Martin-Luther-University, 06120 Halle, Germany. ¹¹Compound Screening Facility, VIB, 9052 Ghent, Belgium. ¹²Department of Forest Genetics and Plant Physiology, Umeå Plant Science Centre, Swedish University of Agricultural Sciences, 90183 Umeå, Sweden. ¹³Department of Biochemistry, University of Wisconsin-Madison, Madison, Wisconsin 53706, USA. ¹⁴Laboratory for Organic Synthesis, Department of Organic and Macromolecular Chemistry, Ghent University, 9000 Ghent, Belgium. † Present address: The Plant Chemetics Laboratory, Department of Plant Sciences, University of Oxford, Oxford OX1 3RB, UK. Correspondence and requests for materials should be addressed to E.R. (email: eurus@psb.vib-ugent.be).

Clathrin-mediated endocytosis (CME) is a major pathway for the uptake of extracellular and plasma membrane material in all eukaryotic cells¹. CME is critical for the ability of cells to respond to environmental changes, including pathogen entry, synaptic vesicle turn-over, and the constitutive or regulated internalization of membrane-bound receptors and their ligands, which in turn might influence signalling outputs¹. In plant cells, CME depends on an evolutionarily conserved core machinery that, in addition to clathrin, comprises the adaptor protein complex-2 (AP-2) and dynamins as well as the newly discovered TPLATE adaptor complex (TPC)^{2,3}. Mainly classical genetic approaches have contributed to our current understanding about the mechanisms of CME in yeast, metazoans, and plants^{1,3}. In addition, chemical genetics also has the potential to facilitate studies of CME by providing small molecule effectors that can interfere with CME in a conditional manner⁴. An example of such a CME inhibitor is tyrphostinA23 (TyrA23). TyrA23 is a tyrosine-like small molecule originally developed as a substrate-competitive inhibitor of mammalian tyrosine kinases⁵. Subsequently, TyrA23 was found to inhibit CME, presumably through its ability to interfere with the interaction between the tyrosine-based internalization motifs present in different endocytic cargos and the medium subunit of the clathrin-associated adaptor complex AP-2 (refs 6,7). TyrA23 was mainly exploited as a CME inhibitor in plant cells by many researchers, including us (Supplementary Data 1), despite the fact that its mode of action has never been well characterized in this system. Recent studies have shown that TyrA23 inhibits flagellin 22 (flg22)-elicited reactive oxygen species formation⁸, indicating that TyrA23, affects not only CME but also other biochemical and/or cellular processes. Besides TyrA23, other chemical tools have been utilized to study the endocytosis in mammalian and yeast systems, such as the dynamin inhibitor dynasore⁹ and the pitstops¹⁰ that target the clathrin terminal domain, but these small molecules also display off-target effects, including inhibition of clathrin-independent endocytosis^{11–14}. Although dynasore has been used as a CME inhibitor in plants¹⁵, reports on the activity of other CME inhibitory compounds in plant cells are still lacking.

Here, we identified and characterized Endosidin9 (ES9), a small molecule inhibitor of CME in *Arabidopsis thaliana* and *Drosophila melanogaster*. We reveal that this molecule uncouples mitochondrial oxidative phosphorylation, a mode of action that is shared with TyrA23. We demonstrate that the effects of ES9 and TyrA23 on CME are not dependent on mitochondrial dysfunction and ATP depletion, but rather on their uncoupling activity at other membranes, leading to acidification of the cytoplasm. Acidification, but not plasma membrane depolarization, caused a dramatic increase in the lifetimes of clathrin and associated adaptors and led to a reduction of the phosphatidylinositol 4,5-bisphosphate (PI(4,5)P₂), thereby most likely inhibiting clathrin-coated pits formation.

Results

ES9 blocks CME in different systems. To identify chemical inhibitors of CME, we analysed a set of 123 small molecules that had previously been selected as endomembrane trafficking modifiers in a screen for inhibitors of pollen germination and pollen tube growth¹⁶ of tobacco (*Nicotiana tabacum*). From this set of small molecules we identified ES9 (Fig. 1a) based on its ability to inhibit the uptake of the lipophilic styryl endocytic tracer dye *N*-(3-triethylammoniumpropyl)-4-(6-(4-(diethylamino)phenyl)hexatrienyl)pyridinium dibromide (FM4-64)¹⁷ in *Arabidopsis* root epidermal cells with half-maximal inhibitory concentration (IC₅₀) of 5 μM (Fig. 1b; Supplementary Fig. 1a). To rule out that the ES9 effect was not limited to FM4-64,

we tested whether ES9 blocked the uptake of the fluorescently labelled Alexa fluor 674 castasterone (AFCS) analogue that binds the brassinosteroid receptor and undergoes CME¹⁸. In the absence of ES9, AFCS (20 μM, 30 min pulse, 20 min chase) was found to traffic to the vacuole in *Arabidopsis* root cells, but in the presence of ES9, AFCS was not internalized, indicating that its effect was not limited to FM dyes (Supplementary Fig. 1b).

To examine whether ES9 had the potential to act as a general inhibitor of CME, we assessed if ES9 interfered with the synaptic vesicle formation in *Drosophila* neurons and with the uptake of transferrin in HeLa cells, two clathrin-dependent processes^{1,19,20}. As a model synapse we used the *Drosophila* third instar neuromuscular junction (NMJ), where nerves were stimulated for 5 min with 90 mM KCl to enhance endocytosis and exocytosis^{19,20} in the presence of FM1-43, a dye that becomes internalized in newly formed vesicles upon nerve stimulation. Treatment with ES9 (10 μM, 30 min) did not block the uptake of FM1-43, but induced its accumulation into large membranous structures (Supplementary Fig. 1c). Transmission electron microscopy (TEM) studies confirmed the formation of abnormal membrane inclusions and the lack of normal-sized synaptic vesicles after ES9 application (Supplementary Fig. 1d), a phenotype reminiscent of acute loss of clathrin heavy chain (CHC)¹⁹, or dynamin²⁰ functions. To support this observation, we assessed the localization of the CME machinery before or after stimulation of NMJs in the presence of ES9 (10 μM, 30 min). Visualization of CHC (Fig. 1c) and the plasma membrane clathrin-associated AP-2 complex (Supplementary Fig. 1e) by super resolution immunofluorescence revealed that, after nerve stimulation, ES9 prevented their recruitment from the bouton centre to the periphery, where vesicles are endocytosed, a phenotype also observed when either dynamin or CHC were impaired^{19,20}. Similarly, the localization, but not the cellular levels of PI(4,5)P₂, was affected following ES9 treatment (Supplementary Fig. 1f,g). Finally, ES9 inhibited the uptake of transferrin in HeLa cells, a hallmark CME tracer¹, to an extent comparable to that of the known inhibitor dynasore⁹ when used at a high concentration (50 μM, 20 min) (Fig. 1d). Altogether these data show that ES9 was able to affect clathrin-dependent processes in different model systems.

ES9 arrests the dynamics of CME and membrane trafficking.

As ES9 inhibited several clathrin-dependent processes, we tested its effect on the dynamic recruitment of the CME machinery. The dynamic behaviour of TPLATE muniscin-like fused to green fluorescent protein (GFP) (TML-GFP), a subunit of the CME adaptor TPC³, was evaluated in *Arabidopsis* root cells after ES9 treatment and compared with the effect of the known CME inhibitor TyrA23 (Supplementary Data 1). An approximate average dwell time of 20 s was observed for TML-GFP in the plasma membrane in control conditions, including treatments with either dimethyl sulfoxide (DMSO) or the inactive TyrA23 analogue TyrA51 (50 μM; Fig. 2a,b; Supplementary Data 1). However, for seedlings treated with 10 μM ES9 or 50 μM TyrA23, the TML-GFP-labelled foci at the plasma membrane appeared stationary, often with a lifetime exceeding several minutes (Fig. 2a,b). The loss of dynamic behaviour occurred rapidly, as images were acquired 3–5 min after the start of the treatments. ES9 also inhibited the dynamic behaviour of another TPC subunit, TPLATE-GFP³, the AP-2 complex subunits AP2A1-GFP²¹, AP2M-GFP²², and AP2S-GFP²³, and clathrin represented by clathrin light chain 1 (CLC1)-GFP, CLC2-GFP, CLC3-GFP and CHC1-GFP, but notably did not impair recruitment and only slightly increased the lifetime of the red fluorescent protein (RFP)-dynamin-related protein1A (DRP1A)²⁴ at the plasma membrane (Fig. 2c; Supplementary Fig. 3a).

ES9 also affected the PI(4,5)P₂ component involved in CME, which was visualized with the 2xPH^{PLC} (P24Y) marker²⁵. Following application with ES9 (10 μM, 30 min) P24Y localized mainly to the cytoplasm, in contrast to its predominant plasma

membrane localization under control conditions, whereas phosphatidylinositol 4-phosphate (PI4P) maintained its plasma membrane localization, as illustrated by the 2xPH^{FAPP1} (P21Y)²⁵ marker (Supplementary Fig. 2a,e). The reduced plasma

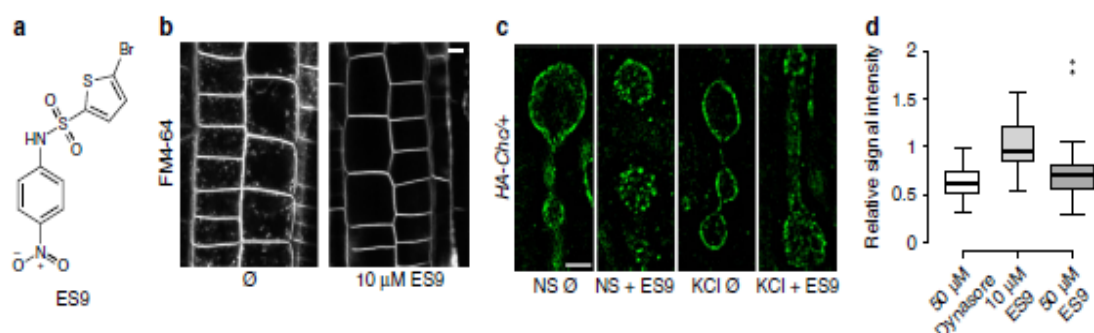


Figure 1 | ES9 inhibits CME in different systems. (a) Chemical structure of ES9. (b) Strongly reduced FM4-64 uptake (2 μM, 30 min) in *Arabidopsis* root cells in the presence of ES9 (10 μM) when compared with mock treatment (DMSO, 0). (c) Super resolution immunofluorescence images of boutons of the neuromuscular junction (NMJ) in third instar *Drosophila* larvae positive for HA-tagged clathrin heavy chain (HA-CHC) comparing mock with 10 μM ES9 (30 min), in both non-stimulated (NS) or 90 mM KCl-stimulated NMJs to induce uptake. (d) Boxplot representation of transferrin uptake in HeLa cells after 20 min in the presence of 50 μM dynasore and 10 or 50 μM ES9. The signal intensity is plotted relative to mock (DMSO) and shows a concentration-dependent inhibition of uptake by ES9. Center lines show the medians; box limits indicate the 25th and 75th percentiles as determined by R software; whiskers extend 1.5 times the interquartile range from the 25th and 75th percentiles; outliers are represented by dots. The box width is relative to sample size ($n=35$, 29, and 61 cells). Scale bars, 5 μm in b; 2 μm in c.

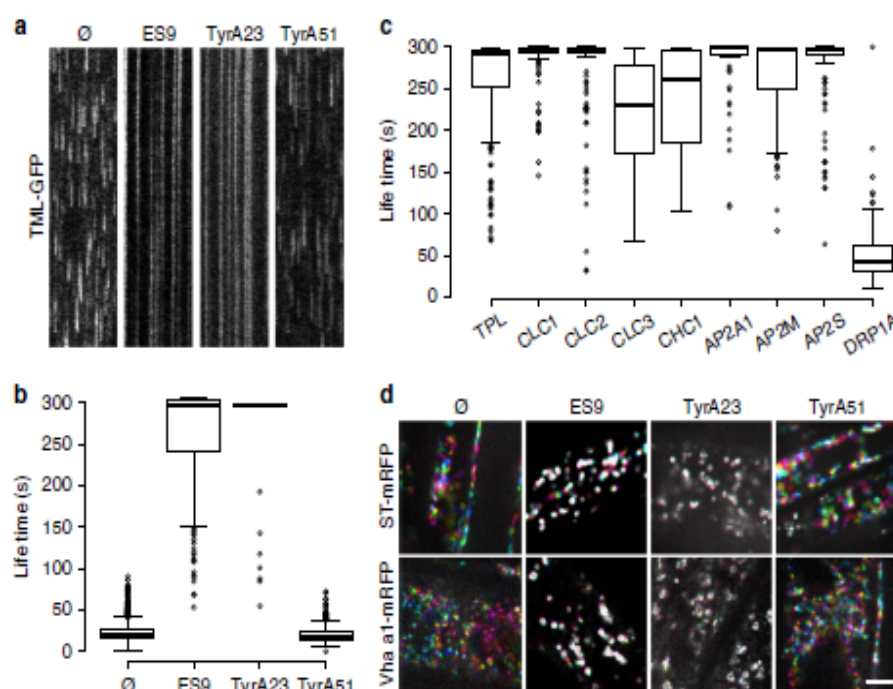


Figure 2 | ES9 inhibits CME dynamics and organelle movement in the cytoplasm. (a) Kymographs representing a line trace (horizontal axis) over a time period (vertical axis, 5 min), taken from the respective spinning disc movies (2 fs^{-1}) of *Arabidopsis* root cells and illustrating the life times of endocytic spots labelled by TML-GFP for the control treatment (DMSO, 0), 10 μM ES9, 50 μM tyrphostinA23 (TyrA23), and 50 μM TyrA51. (b) Boxplot representation of measured endocytic spot life times. $n=1646$, 171, 121, and 868 measurements. (c) Boxplot representation of kymograph-based life time of foci at the plasma membrane in the presence of 10 μM ES9 for green fluorescent protein (GFP)-tagged TPLATE, clathrin light chain (CLC), clathrin heavy chain (CHC), the adaptor protein complex-2 (AP-2), represented by the AP2A1, AP2M, and AP2S subunits, and the dynamin DRP1A. $n=204$, 125, 142, 243, 60, 150, 176, 121, and 247 measurements. (d) Visualization of the Golgi (ST-mRFP) and the trans-Golgi network (TGN, VHA- α -mRFP) in *Arabidopsis* root cells treated with 10 μM ES9, 50 μM TyrA23, 50 μM TyrA51, and mock (DMSO, 0) (5 min). Images are composed of six differentially coloured images taken with a 10-s interval. Movement is illustrated by the presence of the different colours, whereas white indicates static compartments. Boxplot centre lines show the medians; box limits indicate the 25th and 75th percentiles as determined by R software; whiskers extend 1.5 times the interquartile range from the 25th and 75th percentiles; outliers are represented by dots. Scale bar, 5 μm.

membrane recruitment of the PI(4,5)P₂ biosensor was correlated with a decrease in PI(4,5)P₂ levels after ES9 treatment (Supplementary Fig. 2b,c).

We next tested whether treatments with ES9 and TyrA23 would compromise the motility of Golgi and *trans*-Golgi network (TGN)/early endosome (EE) compartments, and the actin-cytoskeleton dynamics. When seedlings expressing Golgi (ST-mRFP)²⁶ and TGN/EE (VHA-al-mRFP)²⁷ markers were treated with ES9 (10 μM) or TyrA23 (50 μM), their dynamic behaviour was compromised after 3–10 min when compared with the control treatments with either TyrA51 (50 μM) or DMSO (Fig. 2d). Inhibition of the dynamic behaviour probably explains the observation that co-application of ES9 or TyrA23 with Brefeldin A (BFA), an inhibitor of the BFA-sensitive ADP-ribosylation factors guanine nucleotide exchange factors (ARF-GEFs)²⁸, prevented the formation of the BFA body (Supplementary Fig. 3b). Moreover, 10 μM ES9 treatment inhibited actin-cytoskeleton dynamics after 10 min, as visualized by the actin binding domain (ABD)-GFP²⁹ (Supplementary Fig. 3c). These results indicate that ES9 and TyrA23 affected the dynamics and recruitment of essential CME components at the plasma membrane, thereby hindering endocytosis, as well as affecting Golgi, TGN/EE, and actin dynamics, reflected in the inhibition of BFA body formation.

ES9 affects energy production. As CME is an energy-dependent process¹ and ATP depletion has been shown to severely reduce CME in mammalian cells^{30,31}, the capacity of ES9 to affect cellular ATP was assessed in dark-grown *Arabidopsis* PSB-D cell cultures. The ATP production inhibitors, antimycin A (AA)³² and oligomycin³³, which interfere with mitochondrial function, and the protonophore, carbonyl cyanide *m*-chlorophenyl hydrazone (CCCP)³⁴ were included as positive controls, whereas TyrA23 and TyrA51 were used as putative negative controls. ES9 (10 μM) induced a rapid initial depletion of ATP to ~50% cellular ATP after 2 min treatment. The ATP concentration decreased further, reaching a base line of ~10% remaining ATP when compared with mock treatment (Fig. 3a). Interestingly, 50 μM TyrA23, but not TyrA51, was also found to induce a reduction in the cellular ATP, in this case of ~75% after 2 min, subsequently stabilizing at ~10% residual ATP when compared with the mock control (Fig. 3a). The trends of ATP depletion profiles of ES9 and TyrA23 were similar to those of AA (20 μM) and CCCP (1 μM), but differed from that of oligomycin (10 μM) (Fig. 3a), of which the ATP content decrease occurred more gradually. To establish whether the observed ATP depletion resulted from acute cytotoxic effects of the compounds, we assessed the viability of PSB-D cells treated with the various compounds by staining with the viability tracer fluorescein diacetate (FDA)³⁵. In all cases, the FDA profiles increased similarly to the control treatment (Supplementary Fig. 4a). These results suggest that the impact of ES9 and TyrA23 on ATP production was not due to an acute loss in cell viability.

As PSB-D cell cultures were grown in the dark, the mitochondria-derived ATP represented the main cellular ATP source. To test the hypothesis that ES9 and TyrA23 alter mitochondrial functions, we isolated mitochondria from *Arabidopsis* leaves and performed a series of respiratory measurements *ex cellulo*. Mock treatment did not affect the mitochondrial electron transport chain (mETC), because high respiratory control ratios were maintained (Supplementary Fig. 4b). Addition of CCCP (1 μM) led to a characteristically rapid and transient increase in the respiratory rate as well as to a clear uncoupling between oxidative and phosphorylation reactions within the mETC, as shown by the respiratory control

ratio drop in spite of an ADP addition. Even at low concentrations, ES9 (1 μM) and TyrA23 (5 μM), but not TyrA51 (5 μM), had an effect similar to that of CCCP on respiratory properties (Supplementary Fig. 4c). The dissipation of the mitochondrial membrane potential in the presence of ES9 and TyrA23 was confirmed *in vivo* in cells of the early differentiation zone of *Arabidopsis* roots with the MitoTracker Red CM-H2XRos dye that stains mitochondria in live cells depending on their membrane potential³⁶. The mitochondrial labelling was not affected after mock (DMSO) and TyrA51 treatments (50 μM, 30 min) (Fig. 3b), whereas in cells treated for the same time with CCCP (1 μM), ES9 (10 μM), AA (20 μM), or TyrA23 (50 μM) labelling of mitochondria was not detected (Fig. 3b), implying that the electron transport was uncoupled or inhibited.

The ability of ES9 to deplete ATP was also evaluated in *Drosophila* and in human Jurkat cells (Supplementary Fig. 4d,e). Similar to *Arabidopsis*, ES9 (10 μM) depleted ATP in *Drosophila* S2 cell cultures like CCCP (10 μM), TyrA23 (50 μM), and AA (50 μM), as well as the otherwise considered inactive analogue TyrA51 (50 μM) (Supplementary Fig. 4d). ATP was also depleted by ES9 (50 μM, 3 h) in Jurkat cells grown in the presence of glucose or galactose to account for the Crabtree effect³⁷ (Supplementary Fig. 4e). Notably, 50 μM of the known dynamin inhibitor dynasore⁹ did not affect ATP concentrations, whereas TyrA23 and TyrA51 at 350 μM had the strongest effect in this system. In agreement, TEM studies revealed swollen mitochondria in synaptic boutons in *Drosophila* after ES9 treatment (10 μM, 30 min) (Supplementary Fig. 1d) and neuronal mitochondria labelling with tetramethylrhodamine ethyl ester (TMRE)³⁸ was greatly impaired in the presence of ES9 (10 μM, 30 min) and CCCP (10 μM, 30 min), confirming disruption of the mitochondrial function (Fig. 3c; Supplementary Fig. 4f). Taken together, the above results show that ES9, as well as TyrA23, are potent mitochondrial uncouplers in different systems.

ATP depletion does not immediately block CME. In metazoans, AA, oligomycin, and mitochondrial depolarization with CCCP have been linked to CME inhibition mainly through a metabolic block^{30,39,40}. In agreement, a reduction in transferrin internalization in HeLa cells (Supplementary Fig. 5a) and in FM1-43 uptake in stimulated boutons in *Drosophila* (Supplementary Fig. 5b,c) was observed after CCCP and TyrA23 applications. To investigate whether the ES9- and TyrA23-induced CME inhibition was triggered by ATP depletion, we evaluated the effect of CCCP, AA, and oligomycin on endocytosis in *Arabidopsis*, given that the CME inhibitors ES9 and TyrA23 also depleted cellular ATP. Similar to ES9 and TyrA23, CCCP (1 μM, 30 min) induced a complete inhibition of FM4-64 uptake with an IC₅₀ of 0.61 μM, compared with a IC₅₀ of 36 μM for TyrA23 (Supplementary Fig. 5d–g). In contrast, the inhibition of FM4-64 uptake, as measured from the plasma membrane/cytoplasmic signal intensity ratio, was only slightly affected when FM4-64 was co-applied with AA (50 μM, 30 min) or added after pre-treatment with oligomycin (50 μM, 30 min) and imaged after an additional 30 min (Supplementary Fig. 5d,e). In cells pre-treated with oligomycin, the ATP levels were similar to those treated with AA, CCCP and ES9 (Fig. 3a), indicating that ATP depletion alone is not sufficient to completely block FM4-64 uptake in plant cells. Consistently, AA treatment increased the lifetime of the TML-labelled foci in the plasma membrane, but did not block their dynamics, whereas the effect of CCCP resembled that of ES9 and TyrA23 (Fig. 2a,b; Supplementary Fig. 5h,i). Similar to the effects of ES9 and TyrA23, treatment with CCCP (1 μM) also compromised the

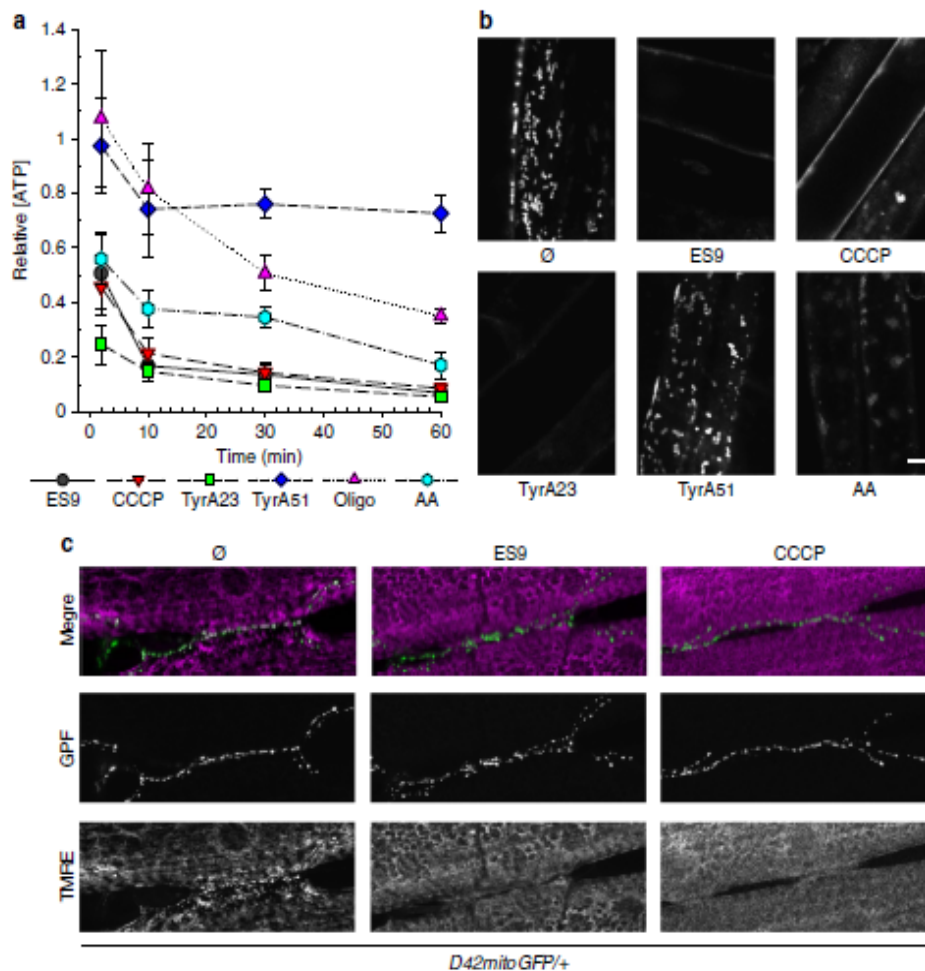


Figure 3 | ES9 is a mitochondrial uncoupler. (a) ATP measurements in the presence of 10 μ M ES9, 1 μ M carbonyl cyanide *m*-chlorophenyl hydrazine (CCCP), 50 μ M tyrphostinA23 (TyrA23), 50 μ M TyrA51, 20 μ M antimycin A (AA), and 10 μ M oligomycin (Oligo), showing various degrees of ATP depletion relative to mock treatment. Results were combined from three independent experiments. Error bars, s.e.m. (b) Confocal images of labelled mitochondria in *Arabidopsis* root cells (250 nM MitoTracker Red CM-H2XRos) in the presence of 10 μ M ES9, 1 μ M CCCP, 50 μ M TyrA23, 50 μ M TyrA51, 20 μ M AA, and the mock (DMSO, \emptyset) for 30 min. The absence of mitochondrial staining implies that the electron transport is uncoupled or inhibited. (c) Tetramethylrhodamine ethyl ester (TMRE) labelling of D42mitoGFP positive mitochondria in *Drosophila* neuromuscular junctions compared to mock (1% DMSO (v/v) in HL-3 medium, 15 min) with 10 μ M ES9 (30 min pre-treatment, 15 min treatment) and 10 μ M CCCP (15 min). Reduced TMRE staining points to disruption of the mitochondrial function and reveal more depolarized mitochondria. Scale bars, 5 μ m.

movement of the TGN/EE and blocked BFA body formation (Fig. 2d; Supplementary Fig. 3b,d). However, when seedlings expressing the Golgi (ST-mRFP) or the TGN/EE (VHA-a1-mRFP) markers were treated with AA (20 μ M), TGN/EE showed a dynamic behaviour comparable to that of the control, whereas the Golgi moved slower than the mock-treated sample (Supplementary Fig. 3d). In summary, these results show that although ATP depletion significantly reduced the dynamics of the CME machinery and the Golgi and TGN/EE movements in *Arabidopsis* cells, it was not the primary cause of the observed fast CME inhibition by ES9.

Cytoplasmic acidification inhibits CME in *Arabidopsis*. The difference in phenotypes between AA and oligomycin relative to CCCP, TyrA23, and ES9 led us to hypothesize that TyrA23 and ES9 might act similarly to CCCP as general protonophores,

thereby uncoupling proton gradients throughout the entire cell and resulting in the acidification of the cytoplasm⁴¹. To test this hypothesis, *Arabidopsis* seedlings were pre-incubated with Lyso Tracker Red DND 99, a dye that labels acidic compartments⁴² for 30 min before treatment with the various compounds. Mock treatment (DMSO) (Supplementary Fig. 5j) and treatments with 50 μ M TyrA51 or 20 μ M AA for 30 min had no effect on the Lyso Tracker Red DND 99 staining relative to untreated cells (Fig. 4a). However, addition of CCCP (1 μ M), ES9 (10 μ M) or TyrA23 (50 μ M) for 30 min resulted in a substantial increase of cytoplasmic Lyso Tracker Red DND 99 labelling (Fig. 4a), suggesting a change in proton concentration throughout the cell, possibly as a consequence of proton gradient dissipation over the tonoplast and the plasma membrane. Therefore, we measured the pH in the vacuole and the cytoplasm of root cells in the presence of the small molecules. By using a pH-GFP cytoplasmic marker⁴³, a significant acidification of the cytoplasm was observed for

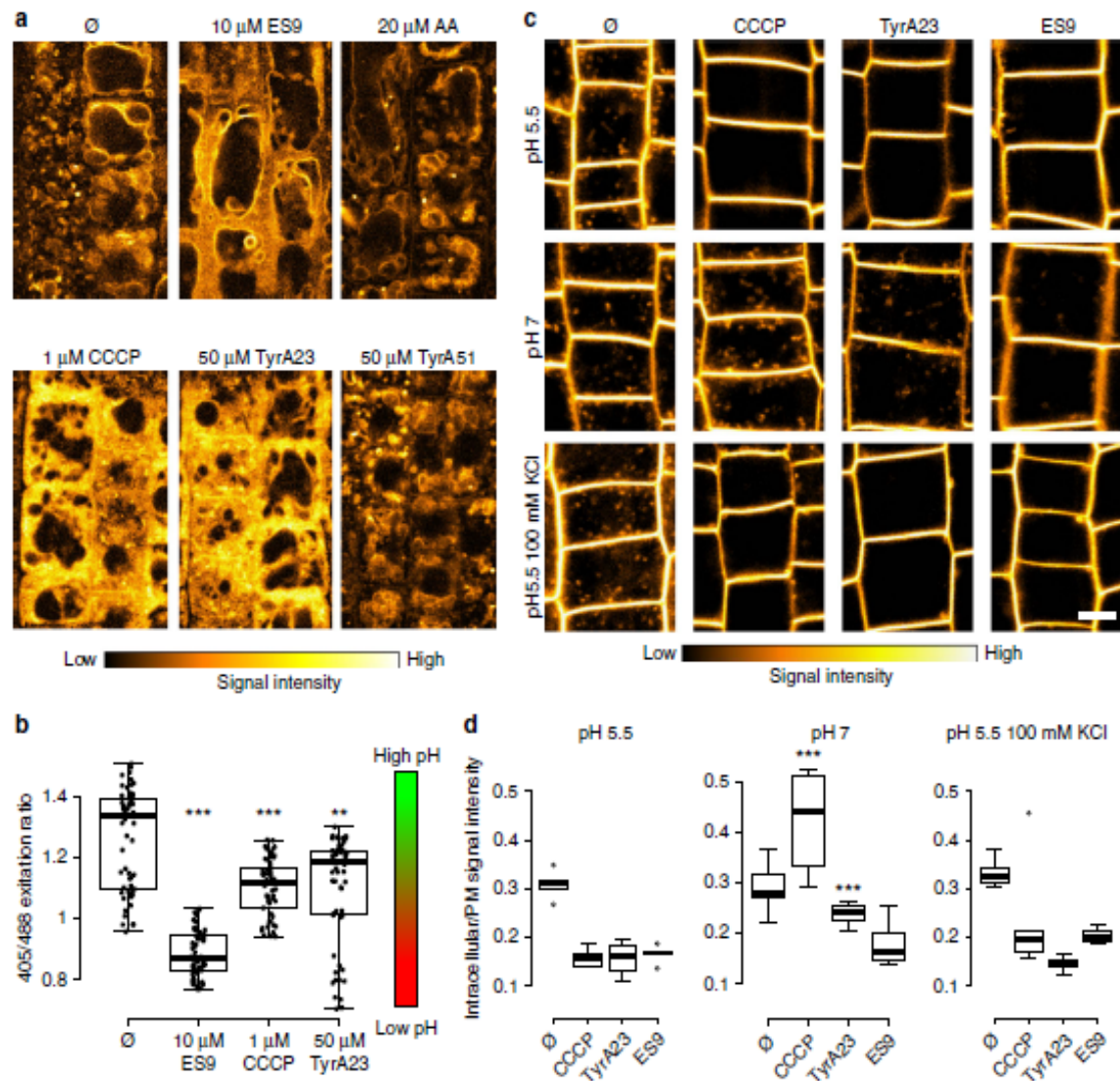


Figure 4 | Cytoplasmic acidification inhibits CME. (a) Confocal images of *Arabidopsis* root cells stained with Lyso Tracker Red DND 99 (30 min) followed by an additional 30 min in the presence of DMSO (\emptyset), ES9, antimycin A (AA), carbonyl cyanide *m*-chlorophenyl hydrazine (CCCP), typhostinA23 (TyrA23), and TyrA51. The presence of ES9, CCCP and TyrA23 relocalized the dye from the tonoplast to the cytoplasm (b) Boxplot representation of cytoplasmic pH measurements using pH-GFP in the presence of 10 μ M ES9, 50 μ M TyrA23, and 1 μ M CCCP, showing cytoplasmic acidification after treatment. $n = 59, 60, 54,$ and 61 seedlings respectively. Individual data points are represented. (c) Confocal images comparing FM4-64 uptake (30 min) at pH 5.5, pH 7, or pH 5.5 and 100 mM KCl in the presence of mock (DMSO, \emptyset), 1 μ M CCCP, 50 μ M TyrA23, and 10 μ M ES9. (d) Quantification of the FM4-64 signal intensity under the different conditions in c. Values represent the ratio of cytoplasmic/plasma membrane signal intensity. Stars indicate significance compared to the corresponding treatment at pH 5.5. ** $P < 0.01$ and *** $P < 0.001$ with a Kruskal-Wallis analysis of variance (ANOVA) on Ranks. The boxplot centre lines show the medians; box limits indicate the 25th and 75th percentiles as determined by R software; whiskers extend 1.5 times the interquartile range from the 25th and 75th percentiles; outliers are represented by dots. For each condition five to seven seedlings were measured. Scale bars, 5 μ m.

10 μ M ES9, 1 μ M CCCP, and 50 μ M TyrA23 (Fig. 4b), whereas the vacuolar pH was less affected in the presence of the same small molecules and considerably less affected than the positive controls, such as concanamycinA (ConcA) treatment and the genetic removal of the V-type proton pump in the *vha-a2vha-a3* double mutant⁴⁴ (Supplementary Fig. 5k). Given that the vacuolar pH showed only a modest increase, we hypothesized that cytoplasmic acidification could be attributed to the influx of extracellular protons from the acidic apoplast across the plasma membrane, where the main uncoupling activity of the compounds might occur. A prediction based on this model is

that acidification of the cytoplasm and inhibition of CME would be prevented by increasing the pH of the apoplast. Therefore, FM4-64 uptake in the presence of the various compounds was evaluated in seedlings incubated in alkaline growth medium (pH 7). Increasing the pH of the incubation medium from 5.5 to 7 had no effect on FM4-64 internalization (30 min) (Fig. 4c,d). In contrast, the ability of CCCP (1 μ M, 30 min) or TyrA23 (50 μ M, 30 min) to block FM4-64 uptake into cells was inhibited in seedlings incubated in media with a pH > 6.5 (Fig. 4c,d; Supplementary Fig. 6g). Intriguingly ES9 treatment (10 μ M, 30 min) at pH 7 remained sufficient to inhibit FM4-64 uptake

(Fig. 4c,d), suggesting that besides acidification, ES9 probably has additional effects on the process of CME.

As protonophores induce movement of protons across the cell membranes, they also cause a change in the plasma membrane potential⁴¹. We next addressed the question of whether plasma membrane depolarization caused by the protonophores impaired CME. For this experiment the membrane potential was dissipated by applying potassium ions (K^+) or valinomycin (Val)⁴⁵, an ionophore that binds K^+ and facilitates their transfer across lipid bilayers. To monitor the plasma membrane potential we used the voltage-sensitive fluorescent dye bis-(1,3-dibutylbarbituric acid)-trimethine oxonol (DiBAC4(3))⁴⁶. When bound to depolarized membranes this dye exhibits an enhanced fluorescence and conversely hyperpolarization is indicated by a decrease in fluorescence. Medium supplemented with 100 mM KCl was effective in depolarizing the plasma membrane in the epidermis of *Arabidopsis* roots as detected by DiBAC4(3) staining (Supplementary Fig. 6a) without causing cytoplasmic acidification, as estimated by the pH-GFP marker⁴³ and the Lyso Tracker Red DND 99 (Supplementary Fig. 6a,b). Application of 10 μ M Val also did not affect the cytoplasmic pH (Supplementary Fig. 6d,e), but failed to produce reliable DiBAC4(3) staining in *Arabidopsis* root epidermal cells, despite a clear phenotype apparent from the transmitted light images (Supplementary Fig. 6c). Val (10 μ M, 30 min) and 100 mM KCl application failed to inhibit FM4-64 uptake (Fig. 4c,d; Supplementary Fig. 6c), yet Val abolished staining of mitochondria with MitoTracker Red CM-H2XRos, indicative of its action as ionophore across cellular membranes (Supplementary Fig. 6f). Correspondingly, all three protonophores CCCP, TyrA23, and ES9 inhibited FM4-64 uptake in the presence of 100 mM KCl (Fig. 4c,d) at pH 5.5. Increasing pH gradually in the presence of 100 mM KCl delayed, but did not prevent, FM4-64 uptake in the presence of TyrA23 and CCCP (Supplementary Fig. 6g). Both CCCP and TyrA23 inhibited FM4-64 uptake at medium pH < 6.5 with or without the presence of 100 mM KCl (Fig. 4c; Supplementary Fig. 6g).

Altogether these data suggest that the very fast CME block by the protonophores is not due to energy depletion, or dissipation of membrane potential, but largely to cytoplasmic acidification.

Discussion

Here, we have identified and characterized the primary mode of action of a small molecule ES9, which inhibits CME in *Arabidopsis*, HeLa cells and *Drosophila* neurons. ES9 affected energy metabolism in all systems in the same manner as the known ATP production inhibitors. Surprisingly TyrA23, a known CME inhibitor (Supplementary Data 1), also reduced the cellular ATP levels. Both ES9 and TyrA23 displayed similar effects as CCCP on mitochondrial respiration and uncoupled oxidation and phosphorylation in isolated *Arabidopsis* mitochondria. Likewise, treatments with ES9 or TyrA23 affected the staining of several mitochondrial dyes *in vivo*, indicating that they might depolarize the mitochondrial membranes in different systems. The similarities in phenotypes exhibited by ES9, TyrA23, and CCCP suggested that these compounds have similar mode of action that differs from other mitochondrial inhibitors, such as AA or oligomycin. Indeed, whereas AA and oligomycin are specific inhibitors of ATP production^{32,33}, CCCP is a known protonophore and non-specific ATP production inhibitor, because it also depolarizes other membranes in the cell⁴¹. As ES9 and TyrA23 mimicked the CCCP action in almost all aspects tested, it might reasonably be presumed that ES9 and TyrA23 also act as protonophores, an assumption supported by the chemical characteristics of each compound. Like CCCP, both ES9 and TyrA23 are weak acids (sulfonamide and phenol, respectively)

that can dissociate into a proton and a stabilized, lipophilic anionic form at physiological pH, thus fitting the classical biochemical description of uncouplers (Supplementary Fig. 7). Although TyrA23 is quite hydrophilic relative to other uncouplers, its anionic form is probably stabilized by an intramolecular hydrogen bond, a known chemical feature in uncouplers that further increases anion lipophilicity, and thus, membrane permeability⁴⁷. In contrast, the TyrA51 analogue, which does not inhibit CME in plant cells, is more hydrophilic, which may explain its apparent less pronounced effects on mitochondrial function and cytoplasmic acidification.

Because ATP is required for CME in mammalian cells³¹, ES9 and TyrA23 might efficiently block CME through ATP depletion. However, although oligomycin and AA both reduced cellular ATP in *Arabidopsis* suspension cell cultures, they did not block endocytosis in root cells to the same extent as ES9 or TyrA23. Previously, a < 5% reduction in ATP content with AA has been shown to be sufficient to prevent endocytosis of the epidermal growth factor and the translocation of β -adrenergic receptors³⁰. It is possible that the length of treatments with the metabolic inhibitors in root cells used in our study did not reduce efficiently the ATP levels to concentrations low enough to block endocytosis. However, in yeast cells, depletion of ATP to 1–3% of the normal level did not inhibit CME, but affected vacuolar transport⁴⁸, suggesting that different eukaryotic systems may have different ATP requirements for CME. Moreover, the inhibitory effects of ES9 and TyrA23 on CME were rapid (< 1–3 min) and faster than the observed drop in ATP level, implying that the endocytosis block induced by these compounds cannot be attributed to ATP depletion alone. This conclusion is consistent with the observations in *Drosophila*, in which defects in mitochondrial function and reduction in ATP levels have no clear implications in synaptic vesicle recycling except under intense stimulation of neurons to mobilize reserve pool vesicles⁴⁰. In agreement, the mitochondrial uncoupler CCCP, like oligomycin and AA, reduced the FMI-43 dye uptake but it did not result in the accumulation of huge membrane inclusions as seen when the CHC¹⁹ or dynamin²⁰ functions are impaired.

Our data show that cytoplasmic acidification (pH < 6.5), but not dissipated plasma membrane potential, is the primary cause for CME inhibition in plant cells triggered by the protonophores. In mammalian systems, acidification of the cytoplasm with weak acids strongly reduces CME of transferrin and the epidermal growth factor but has little effect on the uptake of some toxins and fluid phase endocytosis^{45,49}. Mitochondrial uncouplers of oxidative phosphorylation are also weak acids that, due to their ability to cross membranes in both their protonated and unprotonated form, should be much more effective in perturbing cytoplasmic pH than weak acids that cross a membrane mainly in their protonated form. Indeed, uncouplers like CCCP have activity at other membranes, leading to cell acidification and cytotoxicity^{41,50,51}. Protonophore uncouplers are commonly used to alter the pH of the endocytic vesicles and lysosomes in mammalian cells^{41,52}. In contrast, the use of protonophore uncouplers to study CME is less frequent because the effects of these compounds across different experimental systems are variable and, thus, more difficult to interpret. Whereas CCCP blocks clathrin-dependent transferrin-mediated iron uptake in reticulocytes⁴⁹, CCCP has no impact on the internalization of fluorescein isothiocyanate-dextran in yeast cells⁴⁸. A possible explanation for the differential effects of protonophore uncouplers on CME might be the difference in cellular environments of the various experimental systems, as supported by our observations that the pH of the incubation media influenced the effect of the uncouplers on the CME. Accordingly, the cytoplasmic pH measurements in *Arabidopsis*

suggest that the main proton flow into the cytoplasm is established over the plasma membrane, although we cannot rule out a contribution from the vacuole and other organelles. Hence, protonophores are expected to induce more drastic effects in *Arabidopsis* than in mammalian systems, because the pH of the growth medium differs by more than one pH unit. Interestingly, an increase in pH of the extracellular environment has been shown to reduce the protonophore action of carbonyl cyanide-*p*-trifluoromethoxyphenylhydrazone⁵⁰, a small molecule uncoupler similar to CCCP, at the plasma membrane⁴¹, corresponding to the observed limitation of CCCP to inhibit FM4-64 uptake at neutral pH in plant cells (Fig. 4c,d). Further evidence in support of the cell-wide effects of CCCP, ES9, and TyrA23, is the inability of the mitochondrial electron transport chain inhibitor AA⁵² to inhibit FM4-64 uptake, to block Golgi and TGN/EE dynamics, as well as to cause cytoplasmic acidification. Acidification of the cytoplasm in mammalian cells did not reduce the number of clathrin-coated pits at the cell surface but interfered with the budding of clathrin-coated vesicles from the plasma membrane as well as from the TGN^{45,53}. Interestingly, it has been proposed that cytoplasmic acidification is required to induce the curvature of the clathrin lattice⁵⁴. Whether acidification of the plant cell cytoplasm has a similar effect on the clathrin lattice structure remains to be determined. Ultrastructural analysis of high-pressure frozen and freeze-substituted *Arabidopsis* root cells treated with CCCP and ES9 did not reveal any detectable morphological changes in either the plasma membrane, the mitochondria, or the number of clathrin-coated pits, although clathrin-coated pits are scarcely detected in these tissues⁵⁵ (ES9 treatment: 1 clathrin-coated pit/87 μ m plasma membrane; DMSO control: 1 clathrin-coated pit/117 μ m of plasma membrane) (Supplementary Fig. 8a,b). Experiments in living plant cells indicated that cytosolic acidification dramatically impaired the dynamics of clathrin (CHC, CLC) and associated adaptor proteins (AP-2, TPC) but did not affect the dynamics of the dynamin-related protein, DRPA1. These observations support the hypothesis that, as in mammalian cells^{45,53}, cytoplasmic acidification may possibly impair the scission of clathrin-coated pits in plants. In addition to inhibiting CME dynamics the protonophores, but not the membrane dissipation agents, caused a reduction in PI(4,5)P₂ levels as detected by the PI(4,5)P₂ biosensor and direct measurement of the phosphoinositides (Supplementary Fig. 2). The loss of PI(4,5)P₂ upon protonophores application correlated with a strong *in vitro* pH dependency of the two PI(4,5)P₂-forming enzymes from *Arabidopsis*, PIP5K1 and PIP5K2 kinases (Supplementary Fig. 2d), which have been demonstrated to control CME in *Arabidopsis* root cells⁵⁶. In this context we cannot exclude that ATP depletion also affected the activation of the lipid kinases because treatment with AA in time course experiments also reduced PI(4,5)P₂ levels (Supplementary Fig. 2c). As PI(4,5)P₂ is an important lipid-binding partner of endocytic proteins in animals⁵⁷, and is required for CME in plants⁵⁶, we can speculate that a reduction in PI(4,5)P₂ levels will prevent further recruitment of the CME machinery. Similarly, in mammalian cells, it was shown that the depletion of PI(4,5)P₂ resulted in a loss of clathrin-coat components from the plasma membrane⁵⁸.

Overall our data support a protonophore-induced inhibition of endocytosis by ES9 and TyrA23. However, the ES9 activities differed from the general protonophore effects in terms of synaptic vesicle recycling in *Drosophila*, where the phenotype triggered by ES9 resembled defects in clathrin or dynamin functions^{19,20}. The inhibitory effect of ES9 on FM4-64 uptake at more alkaline apoplasmic pH was retained, suggesting that, besides acidification, ES9 might also inhibit endocytosis through direct interaction with the CME machinery. This however remains to be

determined. Our ultrastructural analysis of compound-treated *Arabidopsis* root cells revealed that both ES9 and CCCP induced morphological alterations of the Golgi apparatus and the TGN/EE (Supplementary Fig. 8c) similar to the reported effects of CCCP in mammalian cells^{59,60}. Interestingly, only the ES9 treatment induced the formation of Golgi-endoplasmic reticulum (ER) hybrid compartments (Supplementary Fig. 8c), indicative of a non-functional coat protein I trafficking⁶¹. This observation again points towards targets of ES9 that are independent from its proton gradient uncoupling activity.

To date, TyrA23 is the most commonly used CME inhibitor in plants (Supplementary Data 1). This is probably because other inhibitors of this process in mammalian cells, such as dynasore, do not appear to function very efficiently in plants. Given our results on the protonophoric characteristics of TyrA23, the data obtained with this inhibitor in plant cells should be evaluated in light of an acidification-induced block of endocytosis, rather than interference between cargo and adaptor molecules. The general endocytosis block caused by TyrA23 also argues against the latter. TyrA23 still might affect cargo recruitment by AP-2 in mammalian cells, but in plants the essential biochemical proof is still lacking, as subtle differences in amino acid composition and tertiary or quaternary AP-2 structure might compromise TyrA23 binding. Nonetheless, additional effects of TyrA23 on inhibition of CME through cargo recognition cannot be excluded at this point. However, the protonophore activity of TyrA23 overrides any specificity at the level of cargo recruitment by AP-2, because cytoplasmic acidification impairs CME severely. Unless a TyrA23 analogue is developed that cannot dissipate proton gradients and can still interfere with cargo recruitment, the use of TyrA23 to specifically inhibit cargo recruitment to AP-2 should be avoided, at least in plants.

Methods

Plant material and growth conditions. *Arabidopsis thaliana* (L.) Heynh. (accession Columbia-0 [Col-0]) seedlings and other lines were stratified for 2 days at 4 °C and grown vertically on agar plates containing half-strength Murashige and Skoog (½ MS) medium supplemented with 1% (w/v) sucrose for 5 days at 22 °C in a 16-h light/8-h dark cycle, prior to use. *Arabidopsis* seedlings were used as control or for labelling of mitochondria and acidic compartments. The following marker lines were used: pTML-TML-GFP/*tml-1* (ref. 3), pPLATE-TPLATE-GFP/*plate* (TPL-GFP)³, pCLC1-CLC1-GFP/Col-0, pCLC2-CLC2-GFP/Col-0, pCLC3-CLC3-GFP/Col-0, pRPS5A-CHC1-GFP/Col-0, p35S-AP2A1-GFP/Col-0 (ref. 21), pAP2M-AP2M-GFP/*ap2m22*, pAP2S-AP2S-GFP/*ap2s23*, mRFP-DRP1A⁵⁴, ST-mRFP²⁵, VHA-a1-mRFP²⁷, P24Y²⁵ and P21Y²⁵, GFP-VAMP727 (ref. 62), and ABD2-GFP (ref. 29).

Expression of GFP-tagged CHC1 and CLC in *Arabidopsis*. Entry clones pDONRRP4-1R_RPSSA²¹, pDONRRP2R-P3_GFPstop, and pDONR211 entry of CHC1 (At3g11130) were used together with pK7m34GW in multi-site Gateway reactions (Life Technologies) to yield the pRPS5A-CHC1-GFP construct. For cloning in pDONR211, the CHC1 was amplified with primers CHC1fw and CHC1rev-nostop. To generate the pCLC2-CLC2-GFP construct, a genomic fragment containing CLC2 (At2g20760) and ~1.2 kb of DNA upstream of the putative ATG start site of CLC2 was amplified by PCR with the bacterial artificial chromosome (BAC) DNA P5H14 as a template and *Nsi*I-forward and *Sac*I-reverse primers. The PCR product pCLC2-CLC2 was cloned into pGEM-T EASY (Promega) by site-directed mutagenesis (New England Biolabs). On the resulting construct (pSB1107), the adenosine of the putative ATG start site of At2g20770, which is located within the 1.2 kb CLC2 upstream sequence, was deleted and transcribed on the opposite strand of CLC2. The resulting construct (pSB1109) was digested with *Nsi*I and *Sac*I and sub-cloned into the *Pst*I-*Sac*I sites of the plant expression vector pSB384 (ref. 63) to generate pSB1112. The construct containing the C-terminally GFP-tagged CLC1 (At2g40060) (pCLC1-CLC1-GFP) had been described previously⁶⁴. To generate the pCLC3-CLC3-GFP construct, a genomic fragment containing CLC3 (At3g51890) and ~1.5 kb of DNA upstream of the putative CLC3 start site, was PCR amplified with Col0 genomic DNA as a template and *Sac*I-forward and *Sac*I-reverse primers. The pCLC3-CLC3 PCR product was cloned into pGEM-T Easy (Promega) for DNA sequence analysis. The resulting construct (pSB1399) was sub-cloned as *Sac*I-*Sac*I fragment into the *Pst*I-*Sac*I restriction sites of pSB384 to generate pSB1404. The pCLC-CLC-GFP and pRPS5A-CHC1-GFP constructs were transformed into *Arabidopsis* (accession

Col-0) wild type plants by the *Agrobacterium tumefaciens*-mediated floral dip method⁶⁵. The pCLC-CLC-GFP and pRPSSA-CHC1-GFP transgenic plants were selected by growth on ½ MS agar (0.6% [w/v]) plates containing 50 mg ml⁻¹ kanamycin. Primers used during the cloning procedures are listed in Supplementary Table 1.

Chemical treatments and imaging in *Arabidopsis*. TyphostinA23, typhostinA51, oligomycin, anisomycin, carbonyl cyanide 3-chlorophenylhydrazone, brefeldin A, valinomycin, Bis(1,3-dibutylbarbituric acid) trimethine oxonol (DiBAC4(3)) and fluorescein diacetate (all from Sigma-Aldrich) were dissolved in DMSO (Sigma-Aldrich), except oligomycin and valinomycin in ethanol. ES9 was acquired through Chembridge (<http://www.chembridge.com/>). Endocytosis was visualized with application of 2 μM N-(3-triethylammoniumpropyl)-4-(6-(4-(diethylamino)phenyl)hexatrienyl)pyridinium dibromide (FM4-64, Life Technologies). For staining of mitochondria, seedlings were first treated for 30 min in 1/4 MS (a 1:1 dilution of ½ MS with water) with the respective small molecules. Subsequently, seedlings were transferred to liquid 1/4 MS with 250 nM MitoTracker Red CM-H2XRos (Molecular Probes, Life Technologies) and the respective small molecules for an additional 30 min. Similarly, acidic compartments were labelled with Lyso Tracker Red DND 99 (Molecular Probes, Life Technologies) by treating seedlings with 250 nM Lyso Tracker Red DND 99 in liquid 1/4 MS for 30 min. The small molecule treatment started by addition of the small molecule at the respective concentration to seedlings in the solution-containing Lyso Tracker Red DND 99 for another 30 min. Seedlings were stained with DiBAC4(3) (10 μM) for 30 min together with the respective treatments. Seedlings were imaged on an FV10 ASW confocal laser scanning microscope (Olympus) with a 60× water immersion lens (numerical aperture [NA] 1.2) and 3× digital zoom. Endocytic foci *in vivo* were measured with an Ultra View Vox Spinning disc confocal imaging system (PerkinElmer) running on the Velocity software package mounted on an Eclipse Ti inverted microscope (Nikon) with a Plan Apo Lambda 100× oil NA 1.45 corrected lens and third-generation perfect focus system (PFSIII) for Z-drift compensation. Time series were acquired at two time points per second intervals for 5 min. Excitation was done with a solid-state 488 nm DPSS laser (50 mW) and images were acquired with an Imagem C9100-13 512 × 512 back-illuminated (16 × 16 μm pixel size) electron microscopy charge-coupled device camera (Hamamatsu Photonics). Images were processed with the ImageJ software packages (Fiji). For kymographs, background was subtracted with a rolling ball radius of 50 pixels and a walking average of 2 was applied. Kymographs were generated with a line thickness of 3. Images were converted to 8-bit in ImageJ for FM4-64 signal intensity measurements. Regions of interest (ROIs) were selected based on the plasma membrane or cytosol localization. Histograms listing all intensity values per ROI were generated and the averages of the 100 most intense pixels were used for calculations.

ATP measurements. Wild type PSB-D *Arabidopsis* cell cultures were used and maintained as described before⁶⁶. Three-day-old cell cultures were diluted 100 times and mixed thoroughly before distribution of 95 μl in 96-well plates. Subsequently, 5 μl of a 1/50 dilution of the small molecule stock solution (× 1,000) in MS medium with Minimal Organics medium was added to cells (final dilution of × 1,000) with a Freedom EVO robot (Tecan). ATP levels were detected by addition of 80 μl of the ATPlite 1step Luminescence Assay System (PerkinElmer) after incubation of cells in the presence of small molecules for the indicated time. Fluorescence was measured with an EnVision 2104 Multilabel Reader (PerkinElmer) with the Wallac EnVision manager software package. ATP lite luminescence was detected with the ultra-sensitive luminescence technology. FDA stock solution (2% [w/v] FDA in acetone) was diluted 100× in target medium and 5 μl was added to 95 μl cell culture. Fluorescence was detected with an excitation at 485 nm (band width 14 nm) and emission at 535 nm (band width 25 nm). The same procedure applied for the *Drosophila* Schneider 2 (S2) cell suspension cultures that were maintained in Sf-900 II serum-free medium (Gibco) at 25 °C without CO₂ and distributed in 96-well plates for analysis (95 μl, 25,000 cells). The Jurkat cells were maintained at 37 °C and 5% CO₂ in RPMI1640 (Gibco) medium and distributed in a similar manner as the S2 cells.

Measurement of respiratory control ratios. Mitochondria from *Arabidopsis* leaves were isolated following the previously described method A⁶⁷. Briefly, 5 g of leaves were ground with a mortar and a pestle, filtered through a 20 μm nylon net, and crude mitochondria were concentrated with differential centrifugations. Mitochondria were kept on ice prior to respiratory measurements. Respiration was measured accordingly⁶⁷ with a Clark-type oxygen electrode (Hansatech) at 25 °C and recorded with a sekonic SS-250F recorder. Dioxygen concentration in air-saturated water was established at 240 μM and a final volume of only 0.5 ml was used in the cuvette. A mix of malate/glutamate (0.1 M/1 M) was chosen as substrate for the mETC and was injected to a final dilution of 1/100. Mitochondrial respiration was stimulated by injection of ADP (10 mM) to a final dilution of 1/100. TyrA23, TyrA51, and GCCP were solubilized with DMSO and measurements of only 5 μl DMSO injected at the beginning, the middle, and at the end of the treatments were used as controls. Independent extractions were repeated 4–6 times with consistent results. Traces shown are actual traces obtained with the recorder, scanned, and digitalized.

Phospholipid level determination in *Arabidopsis*. Phospholipid levels were measured as described⁶⁸. Briefly, 7-day-old seedlings grown on 1% (w/v) agar plates containing ½ MS medium supplemented with 0.5% (w/v) sucrose, 0.1% (v/v) 2-(*N*-morpholino)ethane sulfonic acid (MES) and pH 5.7 (KOH), were used for the experiment. Three seedlings per sample were metabolically labelled by flotation overnight in continuous light in 200 μl 2.5 mM MES buffer pH 5.7 (KOH) and 1 mM KCl, containing 10 μCi of carrier-free [³²P] PO₄³⁻. Seedlings were treated by addition of 200 μl MES buffer with double concentrations of the various inhibitors or DMSO as control. Treatments were stopped at the indicated times by adding 5% (v/v) perchloric acid. The lipids were extracted and analysed by thin-layer chromatography⁶⁸. Radioactivity was visualized and quantified by phosphorimaging (Typhoon FLA 7000; GE Healthcare). Each treatment was done 3–6 times and repeated twice independently. Lipids levels were normalized with the radioactivity signal of the total lipid sample. N-fold change and corresponding fractional standard deviation were calculated by setting the respective control treatment to 1. Statistical differences between treatments were calculated by performing independent samples *t*-tests in IBM SPSS Statistics (version 21).

PIP5K1 and PIP5K2 protein expression and enrichment. PIP5K1 and PIP5K2 were recombinantly expressed as maltose-binding protein (MBP) fusions from pMALc5g plasmids (New England Biolabs, Ipswich, MA, USA) in *Escherichia coli* Rosetta2 cells. Starter cultures in 50 ml of 2YT media were inoculated with single colonies and grown at 30 °C overnight with shaking at 200 r.p.m. Expression cultures were inoculated at an OD₆₀₀ of 0.1 and grown in 300 ml of 2YT media (1.6% [w/v] peptone, 1% [w/v] yeast extract, 0.5% [w/v] NaCl) in baffled flasks at 37 °C with shaking at 95 r.p.m. MBP-PIP5K1 expression was induced with 1 mM isopropyl-1-thio-β-D-galactopyranoside (IPTG) at an OD₆₀₀ of 1.5; MBP-PIP5K2 expression was induced with IPTG at an OD₆₀₀ of 0.7. After induction the cultures were shaken at 28 °C and 95 r.p.m. for 4 h. Cells were subsequently harvested by centrifugation for 20 min at 10,000g. Bacterial pellets were resuspended in 40 ml of 20 mM Tris-HCl, pH 7.5, 200 mM NaCl, 1 mM EDTA (buffer A), containing protease inhibitor cocktail (Sigma-Aldrich) and 1 mg ml⁻¹ lysozyme (Serva Electrophoresis). After incubation on ice for 1 h, cells were further disrupted using a french-press (Gaulin, APV Homogeniser GmbH) at 1,200 bar. Membrane particles were removed by centrifugation for 20 min at 20,000g and 4 °C and the supernatant was kept cold during enzyme purification. MBP-PIP5K1 and MBP-PIP5K2 were enriched with an akta-protein purification system (akta FPLC, GE Healthcare Life Sciences). Lysates were applied with a flow rate of 1 ml min⁻¹ onto a 5 ml MBP-Trap column (GE Healthcare Life Sciences) equilibrated with buffer A. The column was washed with buffer A. Bound protein was eluted with 10 mM maltose in buffer A at a flow rate of 1 ml min⁻¹.

In vitro test for PI4P 5-kinase activity. MBP-PIP5K1 and MBP-PIP5K2 activities were tested with 1 μg of enriched protein. To assay for pH-dependent lipid kinase activity, a three-component system buffer of 50 mM acetic acid, 50 mM MES and 100 mM Tris was used. The pH of the buffer was adjusted with HCl or NaOH by one-unit increments from pH 3 to 10. After incubation at room temperature for 1 h, lipid products were extracted as previously described⁶⁹. The extracted lipids were dried, redissolved in 20 μl chloroform, and were then separated by thin-layer chromatography using silica 60 plates (Merck) and chloroform:methanol:ammonium hydroxide:water (45:45:11; v/v/v/v) as developing solvent. Radiolabelled lipids were visualized by exposing a phosphorimager screen (BAS-MP 2040s, Fuji) and the extent of ³²P-incorporation was quantified by phosphorimaging (BAS-1500).

TEM of *Arabidopsis* root tips. *Arabidopsis* root tips from 5-day-old seedlings were submerged in 200 mM sucrose, 10 mM trehalose, and 10 mM Tris buffer, pH 6.6 (ref. 70), transferred into planchettes (3.0 × 0.5 mm, Al, type A and B; Leica Microsystems) and frozen in a high-pressure freezer HPM100 (Leica Microsystems). Freeze substitution was done in a EM APS2 unit (Leica Microsystems) in dry acetone supplemented with 0.4% (v/v) uranyl acetate at -85 °C for 16 h, followed by 5 h warm-up to -50 °C. After washing with 100% (v/v) ethanol for 60 min, samples were infiltrated and embedded in Lowicryl HM20 resin at -50 °C (intermediate steps of 30, 50, 70% HM20 in ethanol, 1 h each). The resin was polymerized with ultraviolet light for 3 days in the freeze substitution unit. Ultrathin sections were cut on a ultramicrotome UC7 (Leica Microsystems) and post-stained with aqueous uranyl acetate/lead citrate. Sections were examined by JEM 1230 (JEOL) or CM100 (Philips) transmission electron microscopes, both operating at 80 kV. Micrographs were recorded with a MSC 600CW (Gatan) digital camera or by scanning negatives (MACO EM films TYP S, 6.5 × 9 cm, ES 206) with a Perfection V750 Pro system (Epson).

pH measurements. For cytosolic pH measurements, 4-day-old UB10:pH-GFP plants⁴³ were transferred to 2 ml of liquid ½ MS (pH 5.5, 2.15 g l⁻¹ MS salts, 0.5 g l⁻¹ MES) for 30 min with the indicated drugs or mock (DMSO). Imaging was done with a 700 confocal microscope (Zeiss) with a Plan-Apochromat 20 × /0.8 M27 objective lens. pH-GFP was excited by 405 and 488 nm diode lasers and the emission was collected separately between 500 and 555 nm. The images were evaluated in ImageJ (Fiji) by measuring intensities of both channels in six circular

ROIs per root meristematic zone. Vacuolar pH was measured as described before⁴⁴ for a 2-h incubation with the indicated small molecules.

Statistical tests and generation of graphs. All statistical tests and graphs other than boxplots were performed and generated using SigmaPlot 13. Boxplots were generated with the online tool BoxPlotR (<http://boxplot.tyerslab.com/>) from the Tyers and Rappalber laboratories.

Drosophila genetics. Fly stocks were maintained on standard maize meal and molasses medium and were obtained from the Bloomington Drosophila Stock Center (Indiana University) or from the Leuven Institute for Neurodegenerative Disease (Leuven, Belgium)²⁰.

FM1-43 uptake assay and immunohistochemistry in Drosophila. FM1-43 labelling was done as described⁷¹. Third-instar wild type larvae were dissected in HL-3 and, before a stimulation protocol, flies were incubated for 30 min in HL-3 supplemented with and without 10 μ M ES9 or for 10 min in HL-3 supplemented with 10 μ M CCCP or mock (1% [v/v] DMSO). Next, neurons were stimulated for 5 min in HL-3 with 90 mM KCl and 1.5 mM CaCl₂ in the presence of FM1-43 (4 μ M) (Life Technologies) with or without small molecules. After labelling, the preparation was washed several times with HL-3 supplemented with or without small molecules. Images were captured with a confocal microscope (A1R, Nikon) with a 60 \times (NA 1.0) water dipping lens and a 4 \times zoom. The bouton FM1-43 intensity was quantified with ImageJ and corrected for background labelling in the muscles. Immunohistochemistry was performed as described²⁰. Larvae were treated in a similar fashion as for the FM1-43 dye uptake assay without the presence of FM1-43. Not-stimulated animals were bated in HL-3 without small molecules. The treated flies were fixed and stained with primary antibodies. Alexa 555-conjugated secondary antibodies or Alexa 488-conjugated secondary antibodies (Life Technologies) were used at 1:1,000. Larvae expressing HA-tagged CHC (HA-Chc⁺) were stained with a mouse anti-HA antibody (Covance) at 1:500 and rabbit anti- α -adaplin antibody⁷² at 1:200 (gift from M. González-Gaitán) and Alexa 555-conjugated secondary antibodies. Larvae expressing PLC δ 1-PH-GFP under the control of the neuronal nSybGAL4 promoter (PLC δ 1-PH-GFP, nSybGAL4/nSybGAL4)⁷³ to visualize the localization of PI(4,5)P₂ were not double stained. Super-resolution structural illumination microscopy images were acquired on a microscope (Elyra S.1; Carl Zeiss) with a 63 \times (NA 1.4) oil lens and three rotations at room temperature. The acquired images were processed and stored with the ZEN 2011 software (Carl Zeiss).

Phosphatidylinositol analysis in Drosophila NMJs. Third-instar larvae expressing PLC δ 1-PH-GFP under the control of the neuronal nSybGAL4 promoter (PLC δ 1-PH-GFP, nSybGAL4/nSybGAL4) were used to analyse the levels of PI(4,5)P₂ in the NMJ⁷³. Larvae were treated in a similar fashion as for the FM1-43 dye uptake assay without the presence of FM1-43. Not-stimulated animals were bated in HL-3 without small molecules. Next, the treated animals were imaged. Images were captured with a confocal microscope (A1R, Nikon) with a 60 \times (NA 1.0) water dipping lens and a 4 \times zoom. The average GFP intensity in synaptic boutons of the NMJ were quantified with ImageJ and corrected for background signals.

TEM of Drosophila synaptic boutons of the NMJs. TEM experiments were performed as described²⁰. First, third-instar wild type larvae were dissected in HL-3 and, prior to a stimulation protocol, flies were incubated for 30 min in HL-3 supplemented with and without 10 μ M ES9. Next, neurons were stimulated for 5 min in HL-3 with 60 mM KCl and 1.5 mM CaCl₂ with or without small molecules. After labelling, the preparation was washed several times with HL-3 supplemented with or without small molecules. Next, the samples were fixed in 4% paraformaldehyde and 1% glutaraldehyde in 0.1 M Na-Cacodylate buffer (pH 7.4) for 2 h at room temperature and subsequently kept in the fridge overnight. Next, the fixed fillets were washed four times for 15 min in a glass recipient with 0.1 M Na-Cacodylate, pH 7.4 and subsequently osmicated with 2% osmium (OsO₄/Na-Cacodylate buffer) on ice for 2 h. Subsequently, samples were washed with chilled 0.1 M Na-Cacodylate buffer for 15 min followed by a 15 min wash with ddH₂O. After the washing step with ddH₂O, samples were stained with 2% uranyl-acetate and again washed with ddH₂O before dehydration. After dehydration with an ethanol series samples were placed in propylene oxide for twice 10 min and embedded in Agar 100 (Laborimpex, Agar Scientific). Ultrathin sections (70 nm) were cut on an EM UC7 ultratome (Leica), collected on grids (Laborimpex, Agar Scientific), coated with Butvar, and imaged with a JEM 1400 transmission electron microscope (JEOL). Images were acquired at 80 kV with an 11 mega-pixel bottom-mounted camera (Quemesa, Olympus) and ITEM5.2 Software (Olympus) at \times 10k and \times 20k zooms.

TMRE labelling in Drosophila. TMRE was used to label the mitochondrial membrane potential as described³⁰. Third-instar larvae with mitochondria in motor neurons labelled with mitoGFP (D42mitoGFP/+) were dissected in

HL-3 and incubated for 30 min in HL-3 supplemented with and without 10 μ M ES9. Subsequently, larvae were treated for 15 min with HL-3 medium supplemented with 50 nM TMRE (Abcam) and the appropriate small molecule at room temperature. For CCCP treatment, larvae were incubated for 15 min in HL-3 supplemented with 50 mM TMRE and 10 μ M CCCP or mock (1% [v/v] DMSO). Fillets were washed with HL-3 and the appropriate small molecule and images were captured by confocal microscopy (A1R, Nikon) with a 60 \times (NA 1.0) water dipping lens. The TMRE labelling intensity was quantified with ImageJ. First, 32-bit image of the mitoGFP channel was thresholded to select the mitochondria of the NMJ. Subsequently, the TMRE labelling intensity was measured in that region.

HeLa cell cultures. HeLa cells were grown in DMEM (Gibco, Life technologies), supplemented with 10% fetal calf serum (Gibco, Life Technologies) and 1% antibiotics (penicillin/streptomycin) (Gibco, Life Technologies), and maintained in a humidified incubator at 37 °C under a 5% CO₂ atmosphere.

Live imaging of HeLa cells. For the microscopy observation of living cells, HeLa cells were placed on a Maffek chamber and incubated overnight in a humidified incubator at 37 °C and under a 5% CO₂ atmosphere to enable their attachment to the coverslip. All tested compounds were dissolved in DMSO and were diluted to the desired concentration in DMEM medium without fetal calf serum and without phenol red (Gibco, Life Technologies). To study the effect of different compounds on endocytosis in HeLa cells, transferrin from human serum, Alexa Fluor 488 Conjugate (Life Technologies) was implemented. The cells were pre-treated with the compounds for 30 min at 37 °C and a 5% CO₂ atmosphere, followed by the exchange of the medium with a fresh one, containing the same compound concentration and 25 μ g ml⁻¹ fluorescently labelled transferrin. Imaging was done with a LSM 700 inverted confocal microscope (Zeiss) with a plan-apochromat 40 \times /1.2 water objective lens for a time period of up to 20 min after placing the transferrin-containing solution on the cells. The images were quantified in ImageJ by measuring the signal intensity of the mock-treated (between 0.01% [v/v] and 0.7% [v/v] DMSO) cells and the signal intensity of the compound-treated cells.

Data availability. The authors declare that all data supporting the findings of this study are available within the article and its Supplementary Information files.

References

- McMahon, H. T. & Boucrot, E. Molecular mechanism and physiological functions of clathrin-mediated endocytosis. *Nat. Rev. Mol. Cell Biol.* **12**, 517–533 (2011).
- Baias, G. A., Mayers, J. R. & Bednarek, S. Y. Budding and braking news about clathrin-mediated endocytosis. *Curr. Opin. Plant Biol.* **16**, 718–725 (2013).
- Gadeyne, A. et al. The TPLATE adaptor complex drives clathrin-mediated endocytosis in plants. *Cell* **156**, 691–704 (2014).
- Hicks, G. R. & Raich, N. V. Small molecules present large opportunities in plant biology. *Annu. Rev. Plant Biol.* **63**, 261–282 (2012).
- Yaish, P., Gazit, A., Gilon, C. & Levitzki, A. Blocking of EGF-dependent cell proliferation by EGF receptor kinase inhibitors. *Science* **242**, 933–935 (1988).
- Crump, C. M., Williams, J. L., Stephens, D. J. & Banting, G. Inhibition of the interaction between tyrosine-based motifs and the medium chain subunit of the AP-2 adaptor complex by specific tyrrhostins. *J. Biol. Chem.* **273**, 28073–28077 (1998).
- Banbury, D. N., Oakley, J. D., Sessions, R. B. & Banting, G. Tyrrhostin A23 inhibits internalization of the transferrin receptor by perturbing the interaction between tyrosine motifs and the medium chain subunit of the AP-2 adaptor complex. *J. Biol. Chem.* **278**, 12022–12028 (2003).
- Smith, J. M., Salamango, D. J., Leslie, M. E., Collins, C. A. & Heese, A. Sensitivity to flg22 is modulated by ligand-induced degradation and de novo synthesis of the endogenous flagellin-receptor FLAGELLIN-SENSING2. *Plant Physiol.* **164**, 440–454 (2014).
- Macia, E. et al. Dynasore, a cell-permeable inhibitor of dynamin. *Dev. Cell* **10**, 839–850 (2006).
- von Kleist, I. et al. Role of the clathrin terminal domain in regulating coated pit dynamics revealed by small molecule inhibition. *Cell* **146**, 471–484 (2011).
- McChuskey, A. et al. Building a better dynasore: the dyngo compounds potently inhibit dynamin and endocytosis. *Traffic* **14**, 1272–1289 (2013).
- Willcox, A. K., Sahnouni, Y. M. E. & Royle, S. J. Non-specificity of Pitstop 2 in clathrin-mediated endocytosis. *Biol. Open* **3**, 326–331 (2014).
- Park, R. J. et al. Dynamin triple knockout cells reveal off target effects of commonly used dynamin inhibitors. *J. Cell Sci.* **126**, 5305–5312 (2013).
- Stahlschmidt, W., Robertson, M. J., Robinson, P. J., McChuskey, A. & Haucke, V. Clathrin terminal domain-ligand interactions regulate sorting of mannose 6-phosphate receptors mediated by AP-1 and GGA adaptors. *J. Biol. Chem.* **289**, 4906–4918 (2014).
- Sharfman, M. et al. Endosomal signaling of the tomato leucine-rich repeat receptor-like protein LeEix2. *Plant J.* **68**, 413–423 (2011).

16. Drakakaki, G. *et al.* Clusters of bioactive compounds target dynamic endomembrane networks *in vivo*. *Proc. Natl Acad. Sci. USA* **108**, 17850–17855 (2011).
17. Jeřínková, A. *et al.* Probing plant membranes with FM dyes: tracking, dragging or blocking? *Plant J* **61**, 883–892 (2010).
18. Irani, N. G. *et al.* Fluorescent castasterone reveals BR11 signaling from the plasma membrane. *Nat. Chem. Biol.* **8**, 583–589 (2012).
19. Kasprówsz, J. *et al.* Inactivation of dathrin heavy chain inhibits synaptic recycling but allows bulk membrane uptake. *J. Cell Biol.* **182**, 1007–1016 (2008).
20. Kasprówsz, J., Kluenen, S., Swerts, J., Miskiewicz, K. & Verstreken, P. Dynamin photoinactivation blocks Clathrin and α -adaptin recruitment and induces bulk membrane retrieval. *J. Cell Biol.* **204**, 1141–1156 (2014).
21. Di Rubbo, S. *et al.* The dathrin adaptor complex AP-2 mediates endocytosis of brassinosteroid insensitive1 in *Arabidopsis*. *Plant Cell* **25**, 2986–2997 (2013).
22. Yamaoka, S. *et al.* Identification and dynamics of *Arabidopsis* adaptor protein-2 complex and its involvement in floral organ development. *Plant Cell* **25**, 2958–2969 (2013).
23. Fan, L. *et al.* Dynamic analysis of *Arabidopsis* AP2 σ subunit reveals a key role in dathrin-mediated endocytosis and plant development. *Development* **140**, 3826–3837 (2013).
24. Mravec, J. *et al.* Cell plate restricted association of DRP1A and PIN proteins is required for cell polarity establishment in *Arabidopsis*. *Curr. Biol.* **21**, 1055–1060 (2011).
25. Simon, M. L. A. *et al.* A multi-colour/multi-affinity marker set to visualize phosphoinositide dynamics in *Arabidopsis*. *Plant J* **77**, 322–337 (2014).
26. Teh, O. K. & Moore, I. An ARF-GEF acting at the Golgi and in selective endocytosis in polarized plant cells. *Nature* **448**, 493–496 (2007).
27. Dettmer, J., Hong-Hermesdorf, A., Stierhof, Y.-D. & Schumacher, K. Vacuolar H⁺-ATPase activity is required for endocytic and secretory trafficking in *Arabidopsis*. *Plant Cell* **18**, 715–730 (2006).
28. Geldner, N., Priml, J., Stierhof, Y.-D., Jürgens, G. & Palme, K. Auxin transport inhibitors block PIN1 cycling and vesicle trafficking. *Nature* **413**, 425–428 (2001).
29. Wang, Y.-S., Yoo, C.-M. & Bancalor, E. B. Improved imaging of actin filaments in transgenic *Arabidopsis* plants expressing a green fluorescent protein fusion to the C- and N-termini of the fimbrin actin-binding domain 2. *New Phytol.* **177**, 525–536 (2008).
30. Liao, J.-F. & Perkins, J. P. Differential effects of antimycin A on endocytosis and exocytosis of transferrin also are observed for internalization and externalization of β -adrenergic receptors. *Mol. Pharmacol.* **44**, 364–370 (1993).
31. Schmid, S. L. & Carter, L. L. ATP is required for receptor-mediated endocytosis in intact cells. *J. Cell Biol.* **111**, 2307–2318 (1990).
32. Potter, V. R. & Reif, A. E. Inhibition of an electron transport component by antimycin A. *J. Biol. Chem.* **194**, 287–297 (1952).
33. Hong, S. & Pedersen, P. L. ATP synthase and the actions of inhibitors utilized to study its roles in human health, disease, and other scientific areas. *Microbiol. Mol. Biol. Rev.* **72**, 590–641 (2008).
34. Heytler, P. G. Uncoupling of oxidative phosphorylation by carbonyl cyanide phenylhydrazones. I. Some characteristics of *m*-Cl-CCP action on mitochondria and chloroplasts. *Biochemistry* **2**, 357–361 (1963).
35. Clarke, J. M., Gillings, M. R., Altavilla, N. & Beattie, A. J. Potential problems with fluorescein diacetate assays of cell viability when testing natural products for antimicrobial activity. *J. Microbiol. Methods* **46**, 261–267 (2001).
36. Poot, M. *et al.* Analysis of mitochondrial morphology and function with novel fixable fluorescent stains. *J. Histochem. Cytochem.* **44**, 1363–1372 (1996).
37. Marroquin, L. D., Hynes, J., Dykens, J. A., Jamieson, J. D. & Will, Y. Circumventing the Crabtree effect: replacing media glucose with galactose increases susceptibility of HepG2 cells to mitochondrial toxicants. *Toxicol. Sci.* **97**, 539–547 (2007).
38. Slabbaert, J. R. *et al.* Shawn, the *Drosophila* homolog of SLC25A39/40, is a mitochondrial carrier that promotes neuronal survival. *J. Neurosci.* **36**, 1914–1929 (2016).
39. Qian, Z. M. & Morgan, E. H. Effect of metabolic inhibitors on uptake of non-transferrin-bound iron by reticulocytes. *Biochim. Biophys. Acta* **1073**, 456–462 (1991).
40. Verstreken, P. *et al.* Synaptic mitochondria are critical for mobilization of reserve pool vesicles at *Drosophila* neuromuscular junctions. *Neuron* **47**, 365–378 (2005).
41. Budder, K. J. & Vaughan-Jones, R. D. Effects of mitochondrial uncouplers on intracellular calcium, pH and membrane potential in rat carotid body type I cells. *J. Physiol.* **513**, 819–833 (1998).
42. Dolman, N. J., Kilgore, J. A. & Davidson, M. W. A review of reagents for fluorescence microscopy of cellular compartments and structures, Part I: BacMam labeling and reagents for vesicular structures. *Curr. Protoc. Cytom.* **65**, 12.30.1–12.30.27 (2013).
43. Fendrych, M. *et al.* Programmed cell death controlled by ANAC033/SOMBRERO determines root cap organ size in *Arabidopsis*. *Curr. Biol.* **24**, 931–940 (2014).
44. Krebs, M. *et al.* *Arabidopsis* V-ATPase activity at the tonoplast is required for efficient nutrient storage but not for sodium accumulation. *Proc. Natl Acad. Sci. USA* **107**, 3251–3256 (2010).
45. Sandvig, K., Olsnes, S., Petersen, O. W. & van Deurs, B. Acidification of the cytosol inhibits endocytosis from coated pits. *J. Cell Biol.* **105**, 679–689 (1987).
46. Konrad, K. R. & Hedrich, R. The use of voltage-sensitive dyes to monitor signal-induced changes in membrane potential-ABA triggered membrane depolarization in guard cells. *Plant J* **55**, 161–173 (2008).
47. Terada, H. Uncouplers of oxidative phosphorylation. *Environ. Health Perspect* **87**, 213–218 (1990).
48. Makarov, M. & Nevalainen, L. T. Transport of a fluorescent macromolecule via endosomes to the vacuole in *Saccharomyces cerevisiae*. *J. Cell Biol.* **104**, 67–75 (1987).
49. Thorstensen, K. Hepatocytes and reticulocytes have different mechanisms for the uptake of iron from transferrin. *J. Biol. Chem.* **263**, 16837–16841 (1988).
50. Park, K.-S. *et al.* FCCP depolarizes plasma membrane potential by activating proton and Na⁺ currents in bovine aortic endothelial cells. *Pflügers Arch.* **443**, 344–352 (2002).
51. Bagar, T., Altenbach, K., Read, N. D. & Benčina, M. Live-cell imaging and measurement of intracellular pH in filamentous fungi using a genetically encoded ratiometric probe. *Eukaryot. Cell* **8**, 703–712 (2009).
52. Maxfield, F. R. Weak bases and ionophores rapidly and reversibly raise the pH of endocytic vesicles in cultured mouse fibroblasts. *J. Cell Biol.* **95**, 676–681 (1982).
53. Hansen, S. H., Sandvig, K. & van Deurs, B. Clathrin and HA2 adaptors: effects of potassium depletion, hypertonic medium, and cytosol acidification. *J. Cell Biol.* **121**, 61–72 (1993).
54. Heuser, J. Effects of cytoplasmic acidification on clathrin lattice morphology. *J. Cell Biol.* **108**, 401–411 (1989).
55. Robinson, D. G. & Hillmer, S. In *The Plant Plasma Membrane* (eds Larsson, C. & Möller, I. M.) 233–255 (Springer-Verlag, 1990).
56. Ischebeck, T. *et al.* Phosphatidylinositol 4,5-bisphosphate influences PIN polarization by controlling dathrin-mediated membrane trafficking in *Arabidopsis*. *Plant Cell* **25**, 4894–4911 (2013).
57. Posor, Y., Eichhorn-Grünig, M. & Hauke, V. Phosphoinositides in endocytosis. *Biochim. Biophys. Acta* **1851**, 794–804 (2015).
58. Zencu, R. *et al.* Loss of endocytic clathrin-coated pits upon acute depletion of phosphatidylinositol 4,5-bisphosphate. *Proc. Natl Acad. Sci. USA* **104**, 3793–3798 (2007).
59. Burkhardt, J. K., Hester, S. & Argon, Y. The glycoprotein of VSV accumulates in a distal Golgi compartment in the presence of CCCP. *J. Cell Sci.* **92**, 643–654 (1989).
60. Burkhardt, J. K. & Argon, Y. Intracellular transport of the glycoprotein of VSV is inhibited by CCCP at a late stage of post-translational processing. *J. Cell Sci.* **92**, 633–642 (1989).
61. Richter, S. *et al.* Functional diversification of closely related ARF-GEFs in protein secretion and recycling. *Nature* **448**, 488–492 (2007).
62. Ebine, K. *et al.* A SNARE complex unique to seed plants is required for protein storage vacuole biogenesis and seed development of *Arabidopsis thaliana*. *Plant Cell* **20**, 3006–3021 (2008).
63. Kang, B.-H., Busse, J. S. & Bednarek, S. Y. Members of the *Arabidopsis* dynamin-like gene family, ADL1, are essential for plant cytokinesis and polarized cell growth. *Plant Cell* **15**, 899–913 (2003).
64. Konopka, C. A. & Bednarek, S. Y. Variable-angle epifluorescence microscopy: a new way to look at protein dynamics in the plant cell cortex. *Plant J.* **53**, 186–196 (2008).
65. Clough, S. J. & Bent, A. F. Floral dip: a simplified method for *Agrobacterium*-mediated transformation of *Arabidopsis thaliana*. *Plant J.* **16**, 735–743 (1998).
66. Van Leeene, J. *et al.* A tandem affinity purification-based technology platform to study the cell cycle interactome in *Arabidopsis thaliana*. *Mol. Cell. Proteomics* **6**, 1226–1238 (2007).
67. Keech, O., Diazgremel, P. & Gardeström, P. Preparation of leaf mitochondria from *Arabidopsis thaliana*. *Physiol. Plant.* **124**, 403–409 (2005).
68. Munnik, T. & Zarza, X. Analyzing plant signaling phospholipids through ³²P-labeling and TLC. *Methods Mol. Biol.* **1009**, 3–15 (2013).
69. Im, Y. J., Brglez, L., Dieck, C., Perera, I. Y. & Boss, W. F. Phosphatidylinositol 4-kinase and phosphatidylinositol 4-phosphate 5-kinase assays. *Methods Mol. Biol.* **1009**, 163–174 (2013).
70. Hillmer, S., Viotti, C. & Robinson, D. G. An improved procedure for low temperature embedding of high pressure frozen and freeze-substituted plant tissues resulting in excellent structural preservation and contrast. *J. Microsc.* **247**, 43–47 (2012).

71. Verstreken, P., Ohyama, T. & Bellen, H. J. FM 1-43 labeling of synaptic vesicle pools at the *Drosophila* neuromuscular junction. *Methods Mol. Biol.* **440**, 349–369 (2008).
72. González-Gaitán, M. & Jäckle, H. Role of *Drosophila* alpha-adaptin in presynaptic vesicle recycling. *Cell* **88**, 767–776 (1997).
73. Khuong, T. M., Habets, R. L., Slabbaert, J. R. & Verstreken, P. WASP is activated by phosphatidylinositol-4,5-bisphosphate to restrict synapse growth in a pathway parallel to bone morphogenetic protein signaling. *Proc. Natl Acad. Sci. USA* **107**, 17379–17384 (2010).

Acknowledgements

We thank Yvon Jaillais, Ikuko Hara-Nishimura, Akihiko Nakano, Takashi Ueda and Jintong Lin for providing materials, Natasha Raikhel, Glenn Hicks, Steffen Vanneste, and Ricardo Tejos for useful suggestions, Patrick Callaerts for providing S2 *Drosophila* cell cultures, Michael Stüttgen for providing HeLa cells, Annick Bleyers for literature searches, VIB Bio Imaging Core for help with imaging conditions and Martine De Cock for help in preparing the article. This work was supported by the Agency for Innovation by Science and Technology for a pre-doctoral fellowship to W.D.; the Research fund KU Leuven (GOA), a Methusalem grant of the Flemish government and VIB to S.K., J.K. and P.V.; by the Netherlands Organisation for Scientific Research (NWO) for ALW grants 846.11.002 (C.T.) and 867.15.020 (T.M.); the European Research Council (project ERC-2011-StG-20101109 PSDP) (to J.F.); a European Research Council (ERC) Starting Grant (grant 260678) (to P.V.), the Research Foundation-Flanders (grants G.0747.09, G094011 and G093511) (to P.V.), the Hercules Foundation, an Interuniversity Attraction Poles Poles Program, initiated by the Belgian State, Science Policy Office (to P.V.), the Swedish Vetenskapsrådet grant to O.K., the Ghent University 'Bijzonder Onderzoek Fonds' (BOF) for a predoctoral fellowship to F.A.O.-M., the Research Foundation-Flanders (FWO) to K.M. and E.R.

Author contributions

W.D., A.-M.S., S.R. and E.R. initiated the work and designed the experiments; W.D. carried out all experiments in *Arabidopsis*. S.K., J.K. J.S. and P.V. contributed *Drosophila* experiments; M.V. and J.F. contributed the HeLa cells assays; W.D., F.A.O.-M., K.M., E.M., and D.V.D. did imaging and data analysis. M.M. produced preliminary data; O.K. performed respiratory measurements; C.V. did the TEM work in *Arabidopsis*; M.F., J.F., S.D., S.S. and K.S. contributed to the pH measurements; X.Z., J.K. C.T. and T.M. measured phospholipids; G.B., I.V.H., and S.B. did cloning and generated *Arabidopsis* transgenic lines; L.S.L.N., A.D., W.D. and D.A. did ATP measurements; J.W. contributed chemistry expertise; M.H. and I.H. contributed the PIP5K1 and PIP5K2 data; W.D. and E.R. wrote the manuscript. All authors revised the manuscript.

Additional information

Supplementary Information accompanies this paper at <http://www.nature.com/naturecommunications>

Competing financial interests: The authors declare no competing financial interests.

Reprints and permission information is available online at <http://npg.nature.com/reprintsandpermissions/>

How to cite this article: Dejonghe, W. et al. Mitochondrial uncouplers inhibit clathrin-mediated endocytosis largely through cytoplasmic acidification. *Nat. Commun.* **7**:11710 doi: 10.1038/ncomms11710 (2016).



This work is licensed under a Creative Commons Attribution 4.0 International License. The images or other third party material in this article are included in the article's Creative Commons license, unless indicated otherwise in the credit line; if the material is not included under the Creative Commons license, users will need to obtain permission from the license holder to reproduce the material. To view a copy of this license, visit <http://creativecommons.org/licenses/by/4.0/>

RESEARCH ARTICLE

WRKY23 is a component of the transcriptional network mediating auxin feedback on PIN polarity

Tomáš Prát¹*, Jakub Hajný^{1,2}*, Wim Grunewald³, Mina Vasileva¹, Gergely Molnár¹, Ricardo Tejos^{3,4}, Markus Schmid^{5,6}, Michael Sauer⁷, Jiří Friml¹ †

1 Institute of Science and Technology (IST), Klosterneuburg, Austria, **2** Laboratory of Growth Regulators, Palacký University, Olomouc, Czech Republic, **3** Department of Plant Biotechnology and Bioinformatics, Ghent University and Center for Plant Systems Biology, VIB, Ghent, Belgium, **4** Facultad de Recursos Naturales Renovables, Universidad Arturo Prat, Iquique, Chile, **5** Department of Molecular Biology, Max Planck Institute for Developmental Biology, Tübingen, Germany, **6** Department of Plant Physiology, Umeå Plant Science Centre, Umeå University, Umeå, Sweden, **7** Department of Plant Physiology, University of Potsdam, Potsdam, Germany

* These authors contributed equally to this work.

† jiri.friml@ist.ac.at



OPEN ACCESS

Citation: Prát T, Hajný J, Grunewald W, Vasileva M, Molnár G, Tejos R, et al. (2018) WRKY23 is a component of the transcriptional network mediating auxin feedback on PIN polarity. *PLoS Genet* 14(1): e1007177. <https://doi.org/10.1371/journal.pgen.1007177>

Editor: Lucia Strader, Washington University in St. Louis, UNITED STATES

Received: November 16, 2016

Accepted: December 29, 2017

Published: January 29, 2018

Copyright: © 2018 Prát et al. This is an open access article distributed under the terms of the [Creative Commons Attribution License](https://creativecommons.org/licenses/by/4.0/), which permits unrestricted use, distribution, and reproduction in any medium, provided the original author and source are credited.

Data Availability Statement: Raw microarray data from this article can be found in the EMBL ArrayExpress repository under accession number E-MEXP-3283. All other relevant data are within the paper and its Supporting Information files.

Funding: This work was supported by the European Research Council (project ERC-2011-StG-201101109-PSDF). WG was a postdoctoral fellow of the Research Foundation Flanders. The funders had no role in study design, data collection

Abstract

Auxin is unique among plant hormones due to its directional transport that is mediated by the polarly distributed PIN auxin transporters at the plasma membrane. The canalization hypothesis proposes that the auxin feedback on its polar flow is a crucial, plant-specific mechanism mediating multiple self-organizing developmental processes. Here, we used the auxin effect on the PIN polar localization in *Arabidopsis thaliana* roots as a proxy for the auxin feedback on the PIN polarity during canalization. We performed microarray experiments to find regulators of this process that act downstream of auxin. We identified genes that were transcriptionally regulated by auxin in an AXR3/IAA17- and ARF7/ARF19-dependent manner. Besides the known components of the PIN polarity, such as PID and PIP5K kinases, a number of potential new regulators were detected, among which the WRKY23 transcription factor, which was characterized in more detail. Gain- and loss-of-function mutants confirmed a role for WRKY23 in mediating the auxin effect on the PIN polarity. Accordingly, processes requiring auxin-mediated PIN polarity rearrangements, such as vascular tissue development during leaf venation, showed a higher WRKY23 expression and required the WRKY23 activity. Our results provide initial insights into the auxin transcriptional network acting upstream of PIN polarization and, potentially, canalization-mediated plant development.

Author summary

The plant hormone auxin belongs to the major plant-specific developmental regulators. It mediates or modifies almost all aspects of plant life. One of the fascinating features of the auxin action is its directional movement between cells, whose direction can be regulated

and analysis, decision to publish, or preparation of the manuscript.

Competing interests: The authors have declared that no competing interests exist.

by auxin signaling itself. This plant-specific feedback regulation has been proposed decades ago and allows for the self-organizing formation of distinct auxin channels shown to be crucial for processes, such as the regular pattern formation of leaf venation, organ formation, and regeneration of plant tissues. Despite the prominent importance of this so-called auxin canalization process, the insight into the underlying molecular mechanism is very limited. Here, we identified a number of genes that are transcriptionally regulated and act downstream of the auxin signaling to mediate the auxin feedback on the polarized auxin transport. One of them is the *WRKY23* transcription factor that has previously been unsuspected to play a role in this process. Our work provides the first insights into the transcriptional regulation of the auxin canalization and opens multiple avenues to further study this crucial process.

Introduction

The phytohormone auxin plays a key role in many aspects of a plant's life cycle. A unique attribute of auxin is its polarized, intercellular movement that depends, among other components, on the polarly localized PIN-FORMED (PIN) auxin exporters [1–3]. The so-called canalization hypothesis proposes that auxin acts also as a cue in the establishment of new polarity axes during the polarization of tissues by the formation of self-organizing patterns due to the formation of narrow auxin transport channels driven by the polarized auxin carriers from an initially broad domain of auxin-transporting cells [4–6]. Canalization has been implied to mediate multiple key plant developmental processes, including formation of new vasculature [7], regeneration after wounding [8, 9], and competitive control of apical dominance [10–12]. Whereas the molecular details of canalization are largely unknown, the key constituents are (i) the feedback regulation of the auxin transport directionality by auxin and (ii) the gradual concentrating and narrowing of auxin channels [4]. The auxin feedback on the transport directionality can be realized by the auxin impact on the PIN polarity [8] and might be related to an auxin effect on clathrin-mediated internalization of PIN proteins [13, 14], but the connection is still unclear [15]. Presumably, this feedback regulation of the PIN repolarization also plays a role in the establishment of the embryonic apical-basal axis [16, 17], during organogenesis [18], and termination of shoot bending responses [19].

Auxin feedback on the PIN polarity can be experimentally approximated by PIN polarity rearrangements after auxin treatment of *Arabidopsis thaliana* roots. Under standard conditions, PIN1 is localized at the basal (root-ward) sides of endodermal and pericycle cells and cells of the vascular tissue [20], whereas PIN2 exhibits a basal polarity in the young cortex cells, but an apical (shoot-ward) polarity in epidermal cells [21, 22]. After treatment with auxin, PIN1 changes from predominantly basal to also inner-lateral in endodermal and pericycle cells, whereas PIN2 undergoes a localization shift from the basal to also outer-lateral side of cortex cells [8]. The exact molecular mechanism and biological significance of this effect is unclear, but it has so far successfully served as easy, experimentally tractable proxy for auxin feedback on PIN polarity [8]. It depends on the transcriptional SCF^{TIR1}-Aux/IAA-ARF auxin signalling pathway [23]. In brief, upon auxin binding to the TIR1/AFB receptor family, transcriptional repressors and co-receptors of the Aux/IAA class are degraded, in turn releasing auxin response transcription activators of the ARF family [24, 25].

In a heat-shock (HS)-inducible *HS::axr3-1* line expressing a mutated, nondegradable version of the IAA17 transcriptional repressor [25, 26], as well as in the *arf7 arf19* double mutant defective for these two functionally redundant transcriptional activators expressed in primary

roots [27], auxin is no longer effective in mediating PIN polarity rearrangements in the root meristem [8]. These results suggest that transcriptional auxin signalling regulates the cellular abundance of so far unknown regulators, which, in turn, modify subcellular sorting or trafficking pathways and other polarity determinants, ultimately leading to changes in the polar PIN distribution.

In this work, we carried out an expression profiling experiment in *Arabidopsis* roots to identify potential regulators of the PIN polarity that are transcriptionally regulated by auxin signalling. We identified several novel regulators and characterized in more detail the transcription factor WRKY23 and its role in auxin-mediated PIN polarization, thus providing initial insights into a molecular mechanism of the auxin feedback on the directional auxin flow—one of the key prerequisites of canalization.

Results

Microarray-based identification of components mediating auxin impact on PIN polarity

The rationale behind the microarray approach was to search for genes that were (i) regulated by auxin in roots under conditions when auxin changes PIN polarity and (ii) their auxin regulation is mediated by the IAA17 (AXR3) transcriptional repressor. First, to look for auxin-induced genes, we matched data from NAA-treated and untreated heat-shocked wild type (WT) Columbia-0 (Col-0) control seedlings and found 523 auxin-induced genes, with a minimum of two-fold difference. As in the *HS:axr3-1* line under the same conditions auxin fails to induce PIN polarity changes (Fig 1A and 1B) [8], we compared heat-shocked and auxin-treated Col-0 seedlings to similarly handled *HS:axr3-1* seedlings, expressing the auxin-resistant version of IAA17 (AXR3) and we identified 667 genes (Fig 1C). The overlap of this set with the 523 auxin-induced genes yielded 245 genes induced by auxin and regulated downstream of IAA17 (S1 Table), including *PATELLIN2* and *PATELLIN6* that encode phosphatidylinositol transfer proteins, concomitantly characterized to be crucial for the regulation of embryo and seedling patterning in *Arabidopsis* [28]. Further comparison with published microarray data on *arf7 arf19* mutant seedlings [29], which are also ineffective in rearranging the PIN polarity [8], yielded a final list of 125 genes (S2 Table), of which some had previously been found to be involved in PIN polarity regulation, including the AGC3 kinase PINOID (PID), and its homologs WAG1 and WAG2 are known to phosphorylate PIN proteins [30], contributing to the control of their polar distribution [31–33]. Nevertheless, overexpression of *PID* was shown to be dominant over the auxin-induced PIN lateralization [8]. Another identified candidate with a known role in the PIN polar distribution was the phosphatidylinositol-4-phosphate 5 kinase PIP5K1. This protein, together with its close homolog PIP5K2, is enriched on basal and apical membrane domains and they are required for PIN trafficking [34, 35] and localization [36, 37]. Other candidates for polarity determinants include several previously known players in auxin-mediated plant development, such as RUL1, a leucine-rich repeat receptor-like kinase regulating cambium formation, a process linked to PIN polarity control [38].

Auxin-dependent PIN lateralization in the root meristem requires a rather prolonged auxin treatment [8], hinting at the involvement of a whole cascade of transcriptional processes. Therefore, we looked for additional auxin-induced transcription factor (TF) genes, which, based on their analogous behaviour in similar experiments and on their known functions, would be potential candidates for having a role in auxin-mediated development. The list of candidates contains e.g. *MINI ZINC FINGER1* (*MIF1*), affecting auxin responses during ectopic meristem formation [39], but also *WRKY23*. *WRKY* genes belong to a plant-specific

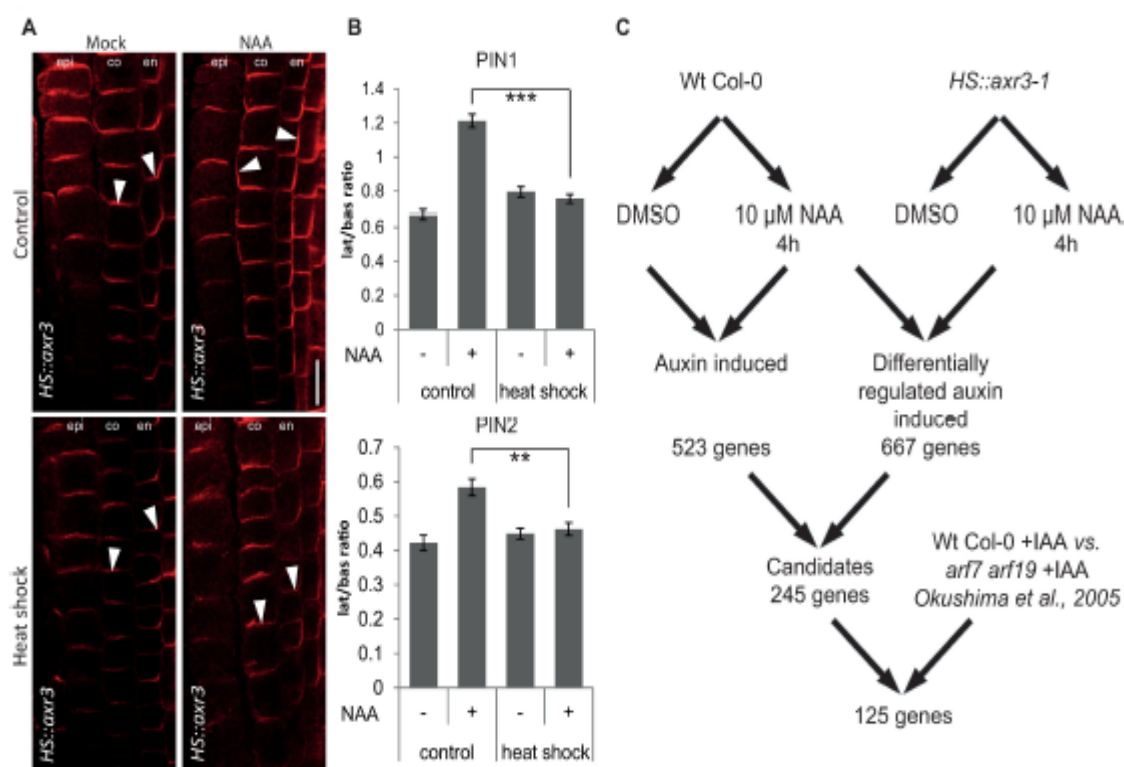


Fig 1. Putative transcriptional components of the auxin-mediated PIN polarization. (A) Simultaneous immunolocalization of PIN1 and PIN2 in *HS::axr3-1* plants. Heat shock-induced overexpression of *axr3-1* abolishes lateral PIN relocation after auxin (4 h, 10 μM NAA) treatment, confirming dependence on the SCF^{TR1}-Aux/IAA-ARF signalling pathway. Arrowheads highlight representative examples of PIN localization in the respective tissues and treatments (PIN1 in endodermis and PIN2 in cortex). Bar = 10 μm. epi, epidermis; co, cortex; en, endodermis. (B) Quantitative evaluation of (A), confirming reduced auxin-dependent relocation of PIN1 (top) and PIN2 (bottom) in the induced *HS::axr3-1* line. Graph shows mean ratio of lateral-to-basal signal intensity of PIN1 in endodermal and PIN2 in cortex cells. Error bars indicate standard error. A One-Way ANOVA test compared marked sets of data. (** $p < 0.01$; *** $p < 0.0001$; $n > 35$ cells corresponding to a minimum of 10 roots per treatment and experiment were imaged under comparable conditions). Experiments were carried out at least 3 times; one representative experiment is presented. (C) Scheme of the microarray experiment and analysis strategy.

<https://doi.org/10.1371/journal.pgen.1007177.g001>

family of 72 TFs in *Arabidopsis*, typically associated with plant defense processes and plant-pathogen interactions [40]. These genes were named by a shared sequence motif of 60 amino acids containing a conserved domain of seven invariant amino acids (WRKYGQK) [41]. The WRKYGQK motif provides a high binding preference and contacts a 6-bp DNA sequence element—the W-box (/TTGACT/C) contained in target gene promoters [40, 42]. Distinct WRKY TFs have distinct selective binding preferences to certain W-box variants [43]. The role of WRKY23 has been established in plant defence processes during plant-nematode interactions, but also in auxin transport regulation by flavonol biosynthesis that affects root and embryo development. In *Arabidopsis* embryos, the WRKY23 expression attenuates both auxin-dependent and auxin-independent signalling pathways toward stem cell specification [44–46]. In addition, WRKY23 is unique within its gene family, because none of the other WRKY genes in these experimental conditions was responsive to auxin and, thus, present in the gene selection (S2 Table). In this work, we focused on one of the transcription factors fulfilling our selection criteria, and investigated the role of WRKY23-dependent transcriptional regulation in auxin-dependent PIN repolarization.

WRKY23 expression is regulated by auxin signalling

First, we confirmed and analysed the auxin regulation of *WRKY23* expression. Promoters of auxin-inducible genes typically contain tandem-localized auxin response elements (AuxREs) that are recognised by auxin response factors (ARFs) [47, 48]. ARFs dimerize to act as molecular callipers and provide specificity to the auxin-dependent gene regulation by measuring the distance of AuxREs in the element pair at the promoter [48]. The length of the intergenic region between the 3'-UTR of the previous gene *UPBEAT* (*UPB*; *At2g47270*) and the 5'-UTR of *WRKY23* (*At2g47260*) is 4.5 kbp. The predicted 2.4-kbp *WRKY23* promoter by the AGRIS tool [49] contains 10 AuxRE and AuxRE-like sites and the extended promoter of 3.2 kbp used for native promoter fusion construct [44] contains two additional AuxRE sites (Fig 2A). Such a density of auxin-regulatory sequences in the promoter makes direct regulation by ARF-dependent auxin signalling a plausible scenario.

In accordance with these results, we found that *WRKY23* is auxin inducible in a dose- and time-dependent manner. When we treated *Arabidopsis* seedlings with 100 nM NAA for 4 h, the *WRKY23* transcription increased 2-fold, and 1 μ M NAA led to a 6-fold increase (Fig 2B). Time response experiments at the consensus concentration of 10 μ M NAA used in PIN lateralization experiments [8] revealed that the *WRKY23* transcription starts to increase approximately after 1.5 h of auxin treatment with a stronger increase after between 2 and 4 h (Fig 2C). This relatively slow auxin-mediated transcriptional regulation of *WRKY23* is well within the time frame for the auxin-mediated PIN lateralization that also occurs strongly only after 4 h [8]. The dependence on the auxin signalling was further supported by the compromised *WRKY23* auxin inducibility in the *HS:axr3-1* and *arf7 arf19* mutants (Fig 2D and 2E). These results show that the *WRKY23* transcription depends on the SCF^{TR1}-Aux/IAA-ARF auxin signalling pathway and confirm *WRKY23* as a candidate regulator of auxin-mediated PIN polarization.

A transgenic line harbouring the *uidA* reporter gene (or GUS-coding gene) under the control of a 3.2-kb upstream sequence from *WRKY23* (*WRKY23::GUS*), whose expression pattern has previously been confirmed by in situ hybridization [44, 45], revealed that auxin induces the ectopic expression of *WRKY23* in root tissues, partly overlapping with root regions, in which the PIN lateralization can be observed (S1G and S1H Fig). Without auxin treatment, the expression pattern of *WRKY23* partially overlaps with the *DR5* auxin response reporter (S1G and S1I Fig) and auxin distribution as revealed by anti-IAA immunolocalization [44, 45, 50]. Previously, *WRKY23* has been shown to be expressed in all apical cells of an octant stage embryo and at heart stage to be detected in both the root and the shoot stem cell niches (S1D and S1E Fig) [46], possibly indicating that *WRKY23* has—besides its role in root development—also a function in shoot development. We found *WRKY23::GUS* expression in pollen grains (S1C Fig), the shoot apical meristem (SAM) (S1A Fig and Fig 2F), as well as at the hydathodes of cotyledons (S1F Fig), coinciding with known auxin response maxima [51]. Sectioning the SAM revealed specific *WRKY23* expression in the L1, L2, and L3 layers (S1A Fig). *WRKY23* promoter activity was prominently associated with the vascular tissues of flowers, cotyledons, and leaves (S1B and S1F Fig and Fig 2G). Notably, the *WRKY23* expression mirrored the pattern of developing leaf vasculature with the highest expression in cells adjacent to the differentiated xylem (Fig 2G) and were detected in a venation-like pattern even before any morphological changes typical for the differentiated vasculature were visible (Fig 2F and 2G). In the previous, external auxin source-mediated canalization experiments in pea stems, the PIN channels were preceding the formation of vasculature and later the differentiated xylem formed adjacent to the PIN channels [11]. Thus, the *WRKY23* expression pattern in

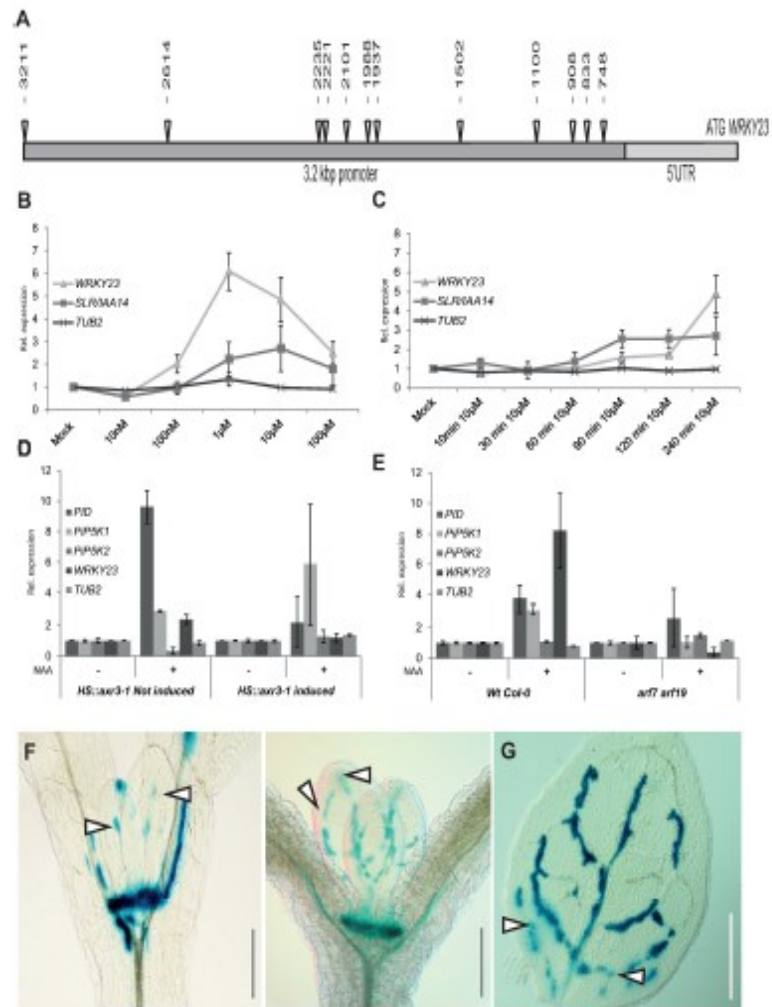


Fig 2. WRKY23 acts downstream of the Aux/IAA—ARF auxin pathway and marks developing vasculature. (A) Schematic depiction of WRKY23 promoter; AuxRE and AuxRE-like response elements are shown as triangles (B and C) WRKY23 transcript levels depend on auxin dose and treatment time. qRT-PCR analysis of WRKY23 expression after a 4 h treatment with different concentrations of NAA (B) and after different treatment times with 10 μM NAA (C). TUB2 and SLR/IAA14 are shown as negative and positive controls, respectively. Values represent relative fold change of expression. Error bars represent standard deviation (see [Materials and Methods](#) for detailed description). (D and E) WRKY23 expression depends on the SCF^{TR1}-Aux/IAA-ARF signalling pathway. qRT-PCR confirmation of the microarray experiment showing the expression of WRKY23 and genes previously connected to PIN polarity in *HS:aux3-1* (D), and in *arf7 arf19* double mutant plants (E). Values represent relative fold change. Error bars indicate standard deviation (see [Materials and Methods](#) for detailed description). (F, G) Expression of WRKY23::GUS in the shoot apical meristem (SAM) and in the presumptive leaf vasculature (G). Besides strong activity in the SAM, GUS staining overlaps with, and partly precedes, the appearance of differentiating vascular strands in young leaves. Two representative plants in consecutive developmental stages are shown. Patchy expression of WRKY23::GUS in the vasculature of young developing true leaves (G). Arrowheads in F and G depict areas with GUS activity presumably coinciding with future vascular strands that are not morphologically discernible yet.

<https://doi.org/10.1371/journal.pgen.1007177.g002>

Arabidopsis largely overlaps with presumptive PIN channels being consistent with a role of WRKY23 in venation patterning of leaves—a process regulated by the polarized auxin transport [51, 52].

In summary, the presence of auxin-responsive elements in the promoter, the auxin-inducibility of the *WRKY23* expression together with its dependence on AXR3, ARF7 and ARF19 activities indicate that the *WRKY23* transcription is regulated by Aux/IAA- and ARF-dependent auxin signalling. In addition, the association of the *WRKY23* expression with developing vasculature is consistent with a possible involvement of *WRKY23* in the auxin-mediated PIN polarization process.

WRKY23 gain-of-function leads to PIN1 and PIN2 lateralization

Next, we tested whether an altered *WRKY23* expression or activity affected the auxin regulation of the PIN1 and PIN2 protein localization. A strong constitutive overexpression of *WRKY23* was obtained by means of a GAL4-VP16-UAS transactivation system (*RPS5A*>>*WRKY23*) [45, 46, 53]. The 35S promoter-driven *WRKY23* line (35S:*WRKY23*) as well as also 35S promoter-driven dexamethasone-glucocorticoid (DEX/GR) receptor system (35S:*WRKY23-GR*) were used for constitutive overexpression, eventually, with inducible nuclear localization [45, 46]. Constitutive overexpression of *WRKY23* had an impact on the PIN2 but not PIN1 polarity. It caused the PIN2 lateralization in root cortex cells, to some extent mimicking the application of auxin (Fig 3A and 3B). Subsequent treatment with NAA further increased lateralization of PIN2 in cortex cells and caused increased lateralization of PIN1 as compared to wild type (Fig 3A and 3B and S2C and S2D Fig). An inducible *WRKY23* gain-of-function line had a similar effect: seedlings of a 35S:*WRKY23-GR* line treated with DEX to induce *WRKY23-GR* translocation to the nucleus, resulted in PIN2 but not PIN1 lateralization in the cortex cells. Again, additional NAA treatment had an additive effect on PIN2 lateralization and caused a stronger PIN1 lateralization than as seen in the wild type (S3C and S3D Fig and S2C and S2D Fig).

Thus, both constitutive and inducible *WRKY23* gain-of-function consistently led to PIN2 lateralization and increased the auxin-mediated PIN1 and PIN2 lateralization.

Repression of WRKY23 activity abolishes the auxin effect on the PIN2 polarization

In complementary experiments, we tested the downregulation effect of the *WRKY23* function. The large *WRKY* family of homologous proteins has an extensive functional redundancy among individual members [54]. As the functional compensation of *wrky23* loss-of-function by other members was likely, given the large size of the *WRKY* gene family, we used a dominant-negative approach with the chimeric repressor silencing technology [55]. This technology is based on a translational fusion of an activating TF with the repressor domain SRDX, thus inhibiting the expression of target genes. The transactivation activity of *WRKY23* had previously been verified in a tobacco transient expression assay, in which the activating or repressing potential of the TF fused to GAL4 had been checked in the presence of a *UAS:Luciferase* construct [45].

Plants expressing *WRKY23-SRDX* under both the native and constitutive promoters showed a clear auxin insensitivity in PIN2 lateralization, namely the auxin treatment did not lead to lateralization when compared to the controls (S3A and S3B Fig). Notably, PIN1 lateralization did not change visibly after NAA treatment (S2C and S2D Fig).

wrky23 partial loss-of-function mutants are defective in auxin impact on the PIN polarity

To investigate intrafamily redundancy and to assess specifically the role of *WRKY23* on the auxin effect on the PIN polarity, we isolated two T-DNA insertional mutants in the *WRKY23*

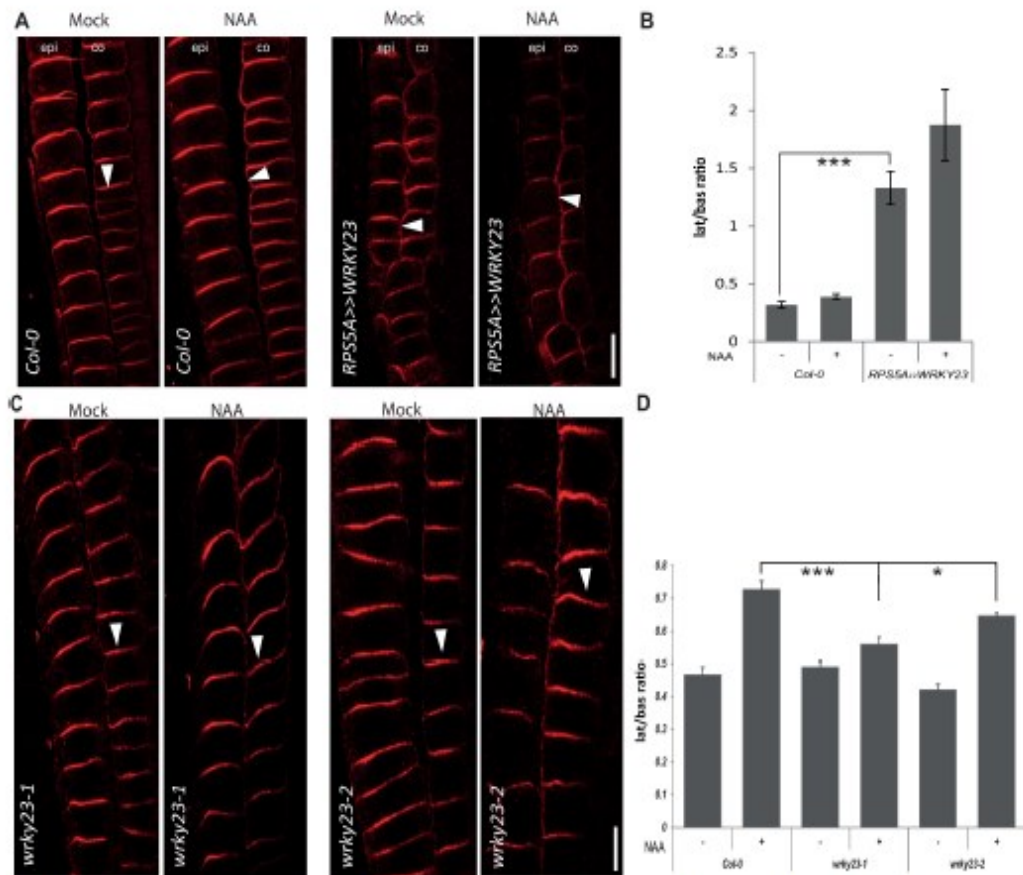


Fig 3. WRKY23 is required for auxin-mediated PIN lateralization in the root. (A) Immunolocalization analysis of PIN2 without or after NAA (4 h, 10 μ M) treatment in WT Col-0 and *RPS5A>>WRKY23*. Arrowheads highlight PIN2 polarity. epi, epidermis; co, cortex. (B) Quantitative evaluation of (A) showing mean ratio of PIN2 lateral-to-basal signal intensity in cortex cells. Note that PIN2 lateralization in *RPS5A>>WRKY23* roots is increased even without auxin that still remains effective. Error bars indicate standard error. A One-Way ANOVA test compared marked sets of data (***) $p < 0.0001$; $n > 35$ cells corresponding to a minimum of 10 roots per treatment and experiment were imaged under comparable conditions). (C) Immunolocalization analysis of PIN2 without or with NAA treatment in WT Col-0 and *wrky23* mutants. Arrowheads highlight representative examples of PIN2 polarity in the epi, epidermis; co, cortex. (D) Quantitative evaluation of the experiment in (C) showing mean ratio of PIN2 lateral-to-basal signal intensity in endodermal. Error bars indicate standard error. A One-Way ANOVA test compared marked sets of data (* $p < 0.05$; *** $p < 0.001$; $n > 100$ cells corresponding to a minimum of 10 roots per treatment and experiment were imaged under comparable conditions). Experiments were carried out 3 times; one representative experiment is presented).

<https://doi.org/10.1371/journal.pgen.1007177.g003>

locus, designated *wrky23-1* and *wrky23-2* (Fig 4A). The quantitative reverse transcription-polymerase chain reaction (qRT-PCR) analysis revealed that both alleles are knock-downs, *wrky23-1* having more downregulated expression (Fig 4B).

Similarly to the *WRKY23-SRDX* lines, both *wrky23* mutant alleles showed a reduced PIN2 lateralization response to auxin treatment and, additionally, also reduced PIN1 lateralization. Specifically, following the NAA treatment, the PIN1 and PIN2 lateralization in root endodermal cells was diminished in the *wrky23-2* weaker knock-down and, even more so, in the stronger *wrky23-1* allele (S2A and S2B Fig and Fig 3C and 3D). The observed opposite effects of *WRKY23* gain- and loss-of-function on the PIN lateralization suggested that *WRKY23* plays an important role in the auxin-mediated PIN polarity rearrangements.

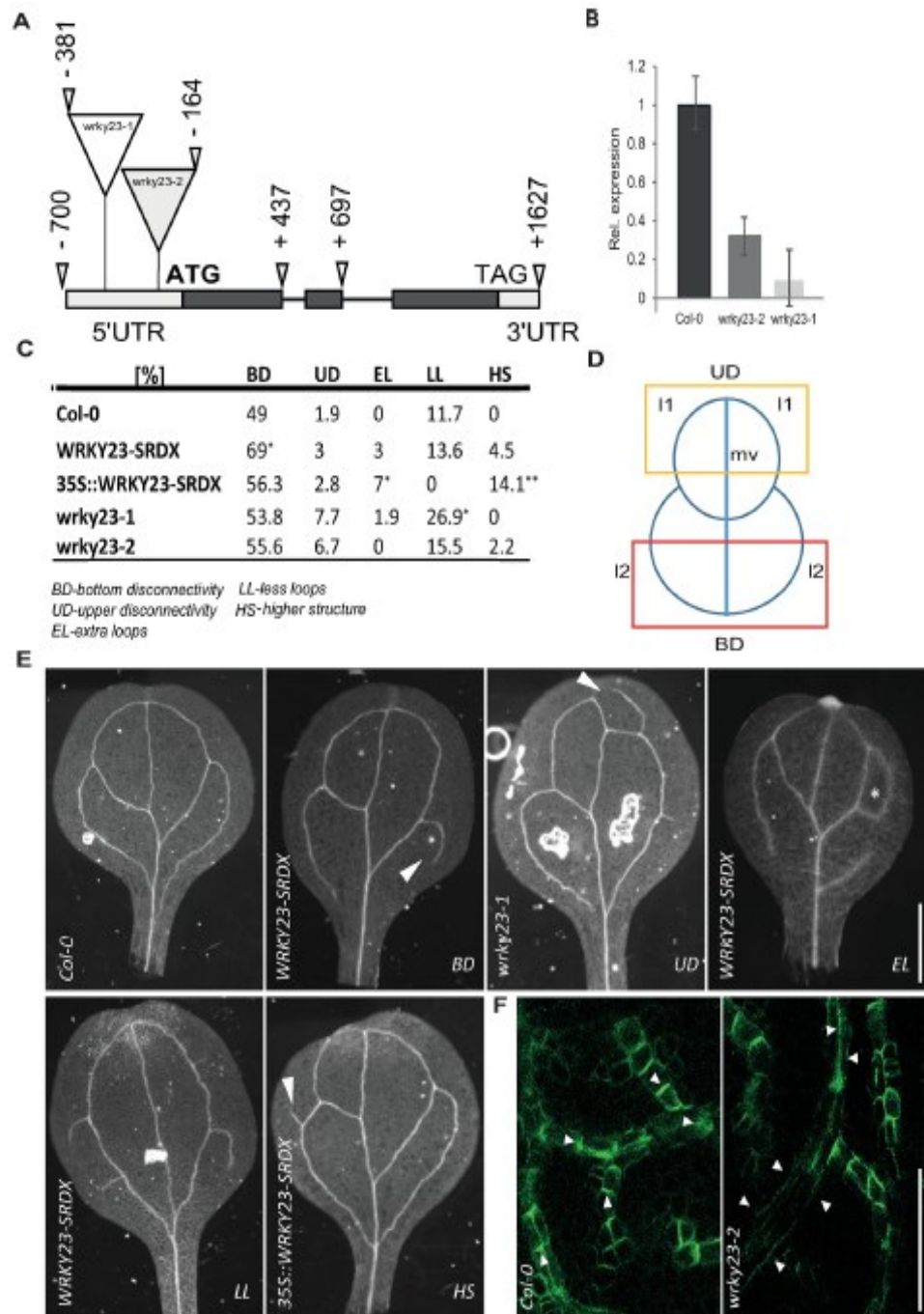


Fig 4. Isolation and characterization of wrky23 mutants. (A) Schematic representation of the WRKY23 locus. Exons are represented by boxes, while introns are shown as lines. Coding regions are filled with dark grey. Exact locations of the T-DNA insertions are depicted. (B) qRT-PCR analysis of WRKY23 expression in the isolated mutant lines. Relative expression values are normalized to the level detected in WT Col-0. See Materials and Methods for more details. (C) Evaluation of cotyledon vasculature defects in WRKY23-SRDX, 35S::WRKY23-SRDX and wrky23 mutants. A One-Way ANOVA test compared marked sets of data (* $p < 0.05$; *** $p < 0.001$; $n > 50$ cotyledons). (D) Schematic representation of cotyledon vasculature pattern. I1, first loop; I2, second loop; mv, midvein. Yellow and red box delineate UD and BD zone of evaluating. (E) Representative images of analysed vasculature defects. (F) Representative images of immunolocalization analysis of PIN1 in developing young first leaves. In the WT, PIN1 shows typical polarization, whereas in wrky23-2 mutant this polarization is abolished. At least 50 leaves per genotype were analysed.

<https://doi.org/10.1371/journal.pgen.1007177.g004>

WRKY23 plays a role in PIN polarization during venation patterning

The importance of a tight PIN polarity regulation for directional auxin fluxes and plant growth and development has been demonstrated previously [2, 3]. Therefore, we analysed the phenotypes related to PIN polarity or auxin transport in transgenic lines with an altered expression or activity of *WRKY23*. 35S::*WRKY23* overexpressing plants show growth retardation and root meristem patterning defects [45]. Also, dominant negative lines showed severe defects in lateral root organogenesis [45]. Both *WRKY23-SRDX* and 35S::*WRKY23* lines had shorter roots than those of Col-0 (S4A Fig) and *WRKY23-SRDX* showed defects in gravitropism, similar to those observed in the auxin transport mutant *pin2/eir1* [56, 57]. Notably, native promoter-driven *WRKY23-SRDX* displayed a significant increase in lateral root density (S4B Fig). Notably, none of these phenotypical defects, including root meristem disorganization, root growth inhibition, and lateral root development alteration, were observed in the *wrky23* mutant alleles (S4A and S4B Fig), suggesting that these more pleiotropic defects are not related to the *WRKY23* action specifically, but they could reflect a broader role of the *WRKY* gene family in plant development.

The canalization hypothesis proposed that the leaf venation pattern depends on the auxin feedback on the PIN polarity [58]. We analysed several features of vascular defects in cotyledons—bottom disconnectivity of I2 vein loops (BD), upper disconnectivity of I1 vein loops (UD), extra loops (EL), less loops (LL) and appearance of higher order structures (HS) (Fig 4C–4E). In plants expressing *WRKY23::WRKY23-SRDX* and 35S::*WRKY23-SRDX*, we observed vasculature patterning defects manifested by increased incidence in BD, HS and EL. On the other hand, both *wrky23-1* and *wrky23-2* mutant alleles showed more defects in UD and LL (Fig 4C).

Next, we tested the PIN1 polarity during vascular tissue development by means of anti-PIN1 antibody staining on young first leaves. In the WT leaves, the staining revealed a pronounced PIN1 polarization along the basipetal (rootward) direction (S4C Fig). In the 35S::*WRKY23* and *WRKY23-SRDX* lines, the typical PIN1 polarity was partly or completely abolished in some veins or their parts (S4C Fig). Similar PIN1 polarity defects were also found in *wrky23-1* and *wrky23-2* lines (Fig 4F and S4C Fig). The venation defects might be interpreted in terms of defective canalization (as suggested by the PIN1 polarity defects), although the venation defects differ somewhat from defects induced by auxin transport inhibition [51, 52]. This observation indicates that interference with the PIN polarization does not have the same consequence as inhibition of PIN auxin transport activity.

In summary, our genetic analysis revealed that from the numerous functions of the *WRKY* family in the regulation of plant development [45, 46], *WRKY23* is more specifically involved in auxin-mediated PIN polarity rearrangements and leaf venation patterning.

Discussion

Classical experiments have led to the formulation of the so-called canalization hypothesis that proposes an auxin feedback on the auxin transport and consequent formation of auxin channels as a central element of multiple self-organizing developmental processes; in particular formation and regeneration of vasculature [7]. In canalization, the auxin transport through an initially homogeneous tissue follows a self-organizing pattern, leading from initially broad fields of auxin-transporting cells to eventually a narrow transport channel, consequently establishing the position of future vascular veins [6]. This hypothesis [4, 5] is further supported by successful modelling efforts based on the concerted cellular polarization via a feedback mechanism, by which auxin influences the directionality of its own flow by polarity rearrangement of auxin carriers [6, 15, 59–62]. Most of these models rely on hypothetical propositions, such as

auxin flux sensors or direct cell-to-cell communication, giving testimony of our lack of understanding how canalization works mechanistically. However, the auxin impact on the PIN polarization has been experimentally demonstrated in different contexts and this effect has been shown to rely on the transcriptional gene expression activation through auxin signalling [8, 9, 11, 19].

Our transcriptional profiling experiments on auxin-dependent PIN rearrangements in *Arabidopsis* roots provide insight into the transcriptional reprogramming during auxin-mediated PIN polarity rearrangements and identify potential downstream molecular components in this process, including established PIN polarity regulators, such as PID, PIP5K, and PATELLINS [28, 30, 37, 63], validating the soundness of the experimental concept. Among a number of novel components awaiting further characterization, we also found the transcriptional activator WRKY23.

WRKY23 is an auxin-responsive gene. The local upregulation of the WRKY23 expression following the auxin application is consistent with a possible involvement in the PIN repolarization process. The WRKY23 transcription is induced by auxin in a dose- and time-dependent manner and it is reminiscent of the expression pattern of the *DR5rev* auxin signalling reporter. Notably, WRKY genes are traditionally known to be involved in defensive processes in plants. More and more, this limited functional spectrum has been broadened by studies uncovering the involvement of these TFs in developmental and physiological processes other than plant defense [45, 46, 64, 65]. In the case of WRKY23, besides a role in plant-nematode interaction with subsequent activation of auxin responses, participation in auxin transport through flavonol synthesis in the root as well as a function in a *mp/bdl*-dependent pathway in embryo development have been demonstrated [44–46].

We show that WRKY23 is a crucial factor required for auxin-mediated PIN polarity rearrangements, because gain-of-function and dominant-negative WRKY23 lines as well as *wrky23* mutants were strongly affected in this process. These defects at the cellular level revealed by the exogenous auxin application appears to be developmentally relevant, because *wrky23* mutants are defective also in the PIN1 polarization process during vascular tissue formation of leaf venation and consequently in vascular tissue formation. Notably, increased PIN2 but not PIN1 lateralization in the WRKY23 overexpression lines and PIN2 but not PIN1 insensitivity to auxin treatment in WRKY23-SRDX lines indicate a partly diverging mechanism controlling PIN1 and PIN2 relocation. This is consistent with reported differences in PIN1 and PIN2 trafficking mechanisms [66].

Our results also suggest that WRKY23 is a critical player in auxin feedback on PIN polar localization. As a TF, WRKY23 is probably not directly involved in regulating localization of transmembrane proteins, such as PIN proteins. Instead, this work opens avenues for future studies revealing the WRKY23-dependent transcriptional network. The identification of WRKY23 and its role in the auxin feedback on the PIN polarity along with other established PIN polarity regulators proves that our transcriptomics dataset can be mined in the future to identify additional regulators. Ultimately, it will provide insights into the molecular mechanism of this key aspect of the canalization-dependent regulation of plant development.

Materials and methods

Plant material and growth conditions

All *Arabidopsis thaliana* (L.) Heynh. lines were in Columbia-0 (Col-0) background. The insertional mutants *wrky23-1* (SALK_003943) and *wrky23-2* (SALK_38289) were obtained from NASC and genotyped with the primers listed in S3 Table. The *arf7 arf19* double mutant and the *HS:axr3-1* transgenic line have been described previously [26, 29] as well as the *DR5::GUS*

[18] and *PIN1-GFP* [67]. For *RPS5A*>>*WRKY23* analyses, the F1 generation of a *RPS5A::GALAVP16* [53] × *UAS::WRKY23* [45] cross was analysed and compared with the F1 generations from the *UAS::WRKY23* × WT Col-0 and *RPS5A::GALAVP16* × WT Col-0 crosses. *WRKY23::GUS*, 35S::*WRKY23-GR*, 35S::*WRKY23*, *WRKY23::WRKY23-SRDX*, and 35S::*WRKY23-SRDX* have been described previously [44, 45]. Seeds were surface-sterilized overnight by chlorine gas, sown on solid *Arabidopsis* medium (AM+; half-strength MS basal salts, 1% [w/v] sucrose, and 0.8% [w/v] phytoagar, pH 5.7), and stratified at 4°C for at least 2 days prior to transfer to a growth room with a 16-h light/8-h dark regime at 21°C. The seedlings were grown vertically for 4 or 6 days, depending on the assay.

Arabidopsis seedlings were treated with auxin or chemicals in liquid AM+ at 21°C in a growth room with the following concentrations and times: for α -naphthaleneacetic acid (NAA; Sigma-Aldrich) at 10 μ M for 4 h; dexamethasone (DEX; Sigma-Aldrich) 10 μ M for 24 h. Mock treatments were done with equivalent amounts of DMSO.

Microarray analysis

Wild type Col-0 and *HS::axr3-1* seeds were grown vertically on AM+ plates for 5 days. We applied a 40 min heat shock at 37°C to the seedlings, followed by a 1.5-h recovery at normal growth temperature. Subsequently, the seedlings were transferred to liquid AM+ and treated with 10 μ M NAA or DMSO for 4 h. Afterward, the lower third of 100–130 roots from each treatment was cut off, frozen in liquid N₂. RNA was extracted with the RNeasy mini kit (Qiagen). Probes were prepared and hybridized to the *Arabidopsis* ATH1–121501 gene expression array (Affymetrix) as described [68]. Expression data for Col-0, *HS::axr3-1*, both NAA and mock treated, had been deposited under the ArrayExpress number E-MEXP-3283. Expression profiling data for *arf7 arf19* (ArrayExpress: E-GEOD-627) have been published previously [29]. Raw data were pairwise analyzed with the logit-t algorithm [69] with a cutoff of $p = 0.05$.

RNA extraction, cDNA synthesis, and quantitative RT-PCR and analysis

RNA extraction, cDNA synthesis, and quantitative (q)RT-PCR were done as described [37]. Selected candidate gene transcript levels were quantified with qRT-PCR with specific primer pairs, designed with Primer-BLAST (<http://www.ncbi.nlm.nih.gov/tools/primer-blast/>). Transcript levels were normalized to *GAMMA-TUBULIN 2* (*TUB2*; AT5G05620), which was constitutively expressed and auxin independent across samples. All PCRs were run in three biological replicates per three technical repeats. The data were processed with a qRT-PCR analysis software (Frederik Coppens, Ghent University-VIB, Ghent, Belgium). Primers used in this study are listed in the S3 Table.

Whole-mount *in situ* immunolocalization, microscopy, and quantitative PIN relocation analysis

PIN immunolocalizations of primary roots and young leaves were carried out as described [70]. The antibodies were used as follows: anti-PIN1, 1:1000 [13] and anti-PIN2, 1:1000 [71]. For primary roots, the secondary goat anti-rabbit antibody coupled to Cy3 (Sigma-Aldrich) was diluted 1:600. For young leaves, the secondary goat anti-rabbit antibody coupled to Alexa Fluor 488 (Sigma-Aldrich) was diluted 1:600. For confocal microscopy, a Zeiss LSM 700 confocal microscope was used. The PIN relocation was quantitatively analysed as described [8], at least 3 experiments were performed for each observation. Note that the absolute levels of the PIN lateralization index may vary between individual experiments (depending on the anti-PIN signal strength), but the relative differences are always consistent.

Phenotypic analysis

All measurements were done with ImageJ (<http://rsb.info.nih.gov/ij>). For the root length analysis 6-day-old seedlings were scanned and root lengths were measured. For the lateral roots analysis 10-day-old seedlings were scanned and lateral root density was calculated from ratio number of LR/root length.

Histological analyses and microscopy

To detect β -glucuronidase (GUS) activity, seedlings were incubated in reaction buffer containing 0.1 M sodium phosphate buffer (pH 7), 1 mM ferricyanide, 1 mM ferrocyanide, 0.1% Triton X-100, and 1 mg/ml X-Gluc for 2 h in the dark at 37°C. Afterward, chlorophyll was removed by destaining in 70% ethanol and seedlings were cleared.

Tissues (seedlings and cotyledons) were cleared in a solution containing 4% HCl and 20% methanol for 15 min at 65°C, followed by a 15-min incubation in 7% NaOH and 70% ethanol at room temperature. Next, seedlings were rehydrated by successive incubations in 70%, 50%, 25%, and 10% ethanol for 5 min, followed by incubation in a solution containing 25% glycerol and 5% ethanol. Finally, seedlings were mounted in 50% glycerol and monitored by differential interference contrast microscopy DIC (Olympus BX53) or a stereomicroscope (Olympus SZX16).

Supporting information

S1 Fig. Pattern of GUS expression in WRKY23::GUS plants. (A) SAM section showing specific WRKY23 expression in the L1, L2, and L3 layers. (B) WRKY23 expression in the pistil vasculature. (C) Anther showing WRKY23::GUS activity in pollen (inset). (D) GUS staining of WRKY23::GUS embryos showing promoter activity in all apical cells of an early globular embryo. (E) GUS activity in the SAM and RAM of an early torpedo stage embryo. (F) Cotyledon showing GUS staining at the hydathode (h) and in the vasculature. (G–J) WRKY23 promoter activation by auxin treatment. G and H: Expression pattern of WRKY23::GUS in the root changes following 6 h of auxin treatment. GUS staining becomes generally stronger and additionally expressed in the meristematic and transition zones of the root tip/arrowhead. I and J: DR5::GUS activity under the same experimental conditions as in (G–H). (PDF)

S2 Fig. Polarity of PIN1 in WRKY23 transgenic lines. (A and B) Immunolocalization of PIN1 in *wrky23* mutants and *arf7/19* lines revealing reduced lateralization of PIN1. Arrowheads highlight PIN1 polarity. en, endodermis; per, pericycle. Graph shows mean ratio of lateral-to-basal signal intensity of PIN1 in endodermal cells. Error bars indicate standard error. A One-Way ANOVA test compared marked sets of data (***) $p < 0.0001$; $n > 60$ cells corresponding to a minimum of 10 roots per treatment and per experiment imaged under comparable conditions). Experiments were carried out at least 3 times; one representative experiment is shown. (C) Immunolocalization of PIN1 in dominant-negative WRKY23-SRDX plants driven by native promoter and overexpression lines - 35S::WRKY23, 35S::WRKY23-GR. WT Col-0 was used as a control. Arrowheads highlight PIN1 polarity in endodermal cells. en, endodermis; per, pericycle. Bar = 10 μ m. (D) Quantitative evaluation of (C) showing mean ratio of lateral-to-basal signal intensity of PIN1 in cortex cells. Error bars indicate standard error. A One-Way ANOVA test compared marked sets of data (***) $p < 0.0001$; $n > 60$ cells corresponding to a minimum of 10 roots per treatment and per experiment were imaged under comparable conditions). Experiments were carried out at least 3 times; one representative

experiment is shown.

(PDF)

S3 Fig. Polarity of PIN2 in WRKY23 transgenic lines. (A) Immunolocalization of PIN2 in dominant-negative WRKY23-SRDX plants driven by native and constitutive promoter. WT Col-0 was used as a control (see Fig 3A and quantification in S3B). Arrowheads highlight PIN2 polarity in cortex cells. epi, epidermis; co, cortex. Bar = 10 μ m. (B) Quantitative evaluation of (A) showing mean ratio of lateral-to-basal signal intensity of PIN2 in cortex cells. Error bars indicate standard error. A One-Way ANOVA test compared marked sets of data (** $p < 0.0001$; $n > 70$ cells corresponding to a minimum of 10 roots per treatment and per experiment were imaged under comparable conditions). Experiments were carried out at least 3 times; one representative experiment is shown.

(C) Immunolocalization of PIN2 in DEX-inducible 35S::WRKY23-GR plants treated with DEX and/or NAA. WT Col-0 was used as control (see quantification in S3D). Arrowheads highlight PIN2 polarity in cortex cells. epi, epidermis; co, cortex. Bar = 10 μ m. (D) Graph showing mean ratio of lateral-to-basal signal intensity of PIN2 in cortex cells. Induced 35S::WRKY23-GR roots show slightly more PIN2 lateralization without auxin that is apparently more effective to increase PIN2 lateralization in this line than the controls. Error bars indicate standard error. A One-Way ANOVA test compared marked sets of data (** $p < 0.0001$, * $p < 0.05$; $n > 35$ cells corresponding to a minimum of 10 roots per treatment and per experiment were imaged under comparable conditions). Experiments were carried out at least 3 times; one representative experiment is shown.

(PDF)

S4 Fig. Phenotype defects in WRKY23 transgenic lines and wrky23 mutants. (A) Primary root length of 6-day-old transgenic lines and wrky23 mutants. Central lines show median values; box limits indicate the 25th and 75th percentiles as determined by the R software; whiskers extend 1.5 times the interquartile range from the 25th and 75th percentiles. Significance was determined by two-tailed equal T-test between Col-0 and other lines; (** $p < 0.001$); $n > 60$ roots per line. (B) Lateral root density in plants with impaired WRKY23 function. WRKY-SRDX denotes WRKY23::WRKY23-SRDX. Box plot properties and statistical analysis are as in (A). $n > 80$ roots per line. (C) Immunolocalization analysis of PIN1 in developing true leaves. In the WT, PIN1 shows typical polarization towards the leaf base, whereas in WRKY23 transgenic lines and wrky23 mutants this polarization of some branches is abolished. Arrowheads highlights defective PIN1 polarization in vasculature. At least 50 leaves per genotype were analysed. (D) Quantitative evaluation of (C) showing percentage of abolished PIN1 polarity. At least 50 branches per genotype were analysed.

(PDF)

S1 Table. Candidate genes from the microarray experiment. (A) Venn diagram representing gene overlay of microarray experiments. Dataset of auxin-regulated genes in WT Col-0 seedlings was overlaid with a second set of genes acquired from the comparison of auxin-treated WT Col-0 and heat-shock-induced auxin-treated HS::axr3-1 lines. Overlap of these genes yielded a list of 245. (B) List of the 245 genes. Gene model descriptions are depicted as they appear in the TAIR database.

(PDF)

S2 Table. Narrowed-down list of candidate genes from the microarray experiments. (A) Venn diagram representing gene overlay of microarray experiments. Datasets of genes differentially regulated in HS::axr3-1 compared to auxin-regulated genes in WT Col-0 were overlaid with a third set of genes that are no longer auxin regulated in the arf7 arf19 background [29].

Overlap of all three microarrays gave 125 genes. (B) List of the 125 overlapping genes containing putative polarity regulators. Gene model descriptions are depicted as they appear in the TAIR database.

(PDF)

S3 Table. List of PCR primers used.

(PDF)

Acknowledgments

We thank D. Weigel for support with microarray analysis; F. Coppens for assistance with the qRT-PCR analysis and M. De Cock and M. Abas for help in preparing the manuscript. We gratefully acknowledge the Nottingham Arabidopsis Stock Center (NASC) for providing mutant lines. This work was supported by the European Research Council (project ERC-2011-StG 20101109-PSDP). WG was a postdoctoral fellow of the Research Foundation Flanders.

Author Contributions

Conceptualization: Tomáš Prát, Wim Grunewald, Michael Sauer, Jiří Friml.

Data curation: Tomáš Prát, Jakub Hajný, Wim Grunewald, Mina Vasileva, Gergely Molnár, Ricardo Tejos, Markus Schmid, Michael Sauer, Jiří Friml.

Formal analysis: Tomáš Prát, Jakub Hajný, Wim Grunewald, Gergely Molnár, Ricardo Tejos, Michael Sauer, Jiří Friml.

Investigation: Tomáš Prát, Jakub Hajný, Wim Grunewald, Mina Vasileva, Gergely Molnár, Ricardo Tejos, Markus Schmid, Michael Sauer, Jiří Friml.

Methodology: Tomáš Prát, Jakub Hajný, Wim Grunewald, Michael Sauer, Jiří Friml.

Writing – original draft: Tomáš Prát, Gergely Molnár, Michael Sauer, Jiří Friml.

References

1. Patrášek J, Mravec J, Bouchard R, Blakeslee JJ, Abas M, Seifertová D, et al. PIN proteins perform a rate-limiting function in cellular auxin efflux. *Science*. 2006; 312: 914–918. <https://doi.org/10.1126/science.1123542> PMID: 16601150
2. Wiśniewska J, Xu J, Seifertová D, Brewer PB, Růžička K, Billou I, et al. Polar PIN localization directs auxin flow in plants. *Science*. 2006; 312: 883. <https://doi.org/10.1126/science.1121356> PMID: 16601151
3. Adamowski M, Friml J. PIN-dependent auxin transport: action, regulation, and evolution. *Plant Cell*. 2015; 27: 20–32. <https://doi.org/10.1105/tpc.114.134874> PMID: 25604445
4. Sachs T. The induction of transport channels by auxin. *Planta*. 1975; 127: 201–206. <https://doi.org/10.1007/BF00380716> PMID: 24430469
5. Sachs T. Cellular interactions in tissue and organ development. *Symp Soc Exp Biol*. 1986; 40: 181–210. PMID: 3544302
6. Bennett T, Hines G, Leyser O. Canalization: what the flux? *Trends Genet*. 2014; 30: 41–48. <https://doi.org/10.1016/j.tig.2013.11.001> PMID: 24296041
7. Berleth T, Sachs T. Plant morphogenesis: long-distance coordination and local patterning. *Curr Opin Plant Biol*. 2001; 4: 57–62. PMID: 11163169
8. Sauer M, Balla J, Luschig C, Wiśniewska J, Reinöhl V, Friml J, Benková E. Canalization of auxin flow by Aux/IAA-ARF-dependent feedback regulation of PIN polarity. *Genes Dev*. 2006; 20: 2902–2911. <https://doi.org/10.1101/gad.390806> PMID: 17043314
9. Mazur E, Benková E, Friml J. Vascular cambium regeneration and vessel formation in wounded inflorescence stems of Arabidopsis. *Sci Rep*. 2016; 6: 33754. <https://doi.org/10.1038/srep33754> PMID: 27649687

10. Booker J, Chatfield S, Leyser O. Auxin acts in xylem-associated or medullary cells to mediate apical dominance. *Plant Cell*. 2003; 15: 495–507. <https://doi.org/10.1105/tpc.007542> PMID: 12566587
11. Balla J, Kalousek P, Reinöhl V, Friml J, Procházková S. Competitive canalization of PIN-dependent auxin flow from axillary buds controls pea bud outgrowth. *Plant J*. 2011; 65: 571–577. <https://doi.org/10.1111/j.1365-3113.2010.04443.x> PMID: 21219506
12. Bennett T, Hines G, van Rongen M, Waldie T, Sawchuk MG, Scarpella E, Ljung K, Leyser O. Connective auxin transport in the shoot facilitates communication between shoot apices. *PLoS Biol*. 2016; 14: e1002446. <https://doi.org/10.1371/journal.pbio.1002446> PMID: 27119525
13. Paciorek T, Zažímalová E, Ruthardt N, Petrášek J, Šterhof Y-D, Kleine-Vehn J, et al. Auxin inhibits endocytosis and promotes its own efflux from cells. *Nature*. 2005; 435: 1251–1256. <https://doi.org/10.1038/nature03633> PMID: 15988527
14. Robert S, Kleine-Vehn J, Barbez E, Sauer M, Paciorek T, Baster P, et al. ABP1 mediates auxin inhibition of clathrin-dependent endocytosis in *Arabidopsis*. *Cell*. 2010; 143: 111–121. <https://doi.org/10.1016/j.cell.2010.09.027> PMID: 20887896
15. Wabnick K, Kleine-Vehn J, Balla J, Sauer M, Naramoto S, Reinöhl V, et al. Emergence of tissue polarization from synergy of intracellular and extracellular auxin signaling. *Mol Syst Biol*. 2010; 6: 447. <https://doi.org/10.1038/msb.2010.103> PMID: 21179019
16. Robert HS, Grones P, Stepanova AN, Robles LM, Lokerse AS, Alonso JM, et al. Local auxin sources orient the apical-basal axis in *Arabidopsis* embryos. *Curr Biol*. 2013; 23: 2506–2512. <https://doi.org/10.1016/j.cub.2013.09.039> PMID: 24291089
17. Wabnick K, Robert HS, Smith RS, Friml J. Modeling framework for the establishment of the apical-basal embryonic axis in plants. *Curr Biol*. 2013; 23: 2513–2518. <https://doi.org/10.1016/j.cub.2013.10.038> PMID: 24291090
18. Benková E, Michniewicz M, Sauer M, Teichmann T, Seifertová D, Jürgens G, Friml J. Local, efflux-dependent auxin gradients as a common module for plant organ formation. *Cell*. 2003; 115: 591–602. PMID: 14651850
19. Rakusová H, Abbas M, Han H, Song S, Robert HS, Friml J. Termination of shoot gravitropic responses by auxin feedback on PIN3 polarity. *Curr Biol*. 2016; 26: 3026–3032. <https://doi.org/10.1016/j.cub.2016.08.067> PMID: 27773568
20. Friml J, Benková E, Billou I, Wiśniewska J, Hamann T, Ljung K, et al. AtPIN4 mediates sink-driven auxin gradients and root patterning in *Arabidopsis*. *Cell*. 2002; 108: 661–673. PMID: 11893337
21. Müller A, Guan C, Gälweiler L, Tänzler P, Huijser P, Marchant A, et al. *AtPIN2* defines a locus of *Arabidopsis* for root gravitropism control. *EMBO J*. 1998; 17: 6903–6911. <https://doi.org/10.1093/emboj/17.23.6903> PMID: 9843496
22. Kleine-Vehn J, Leitner J, Zwiewka M, Sauer M, Abas L, Luschig C, Friml J. Differential degradation of PIN2 auxin efflux carrier by retromer-dependent vacuolar targeting. *Proc Natl Acad Sci USA*. 2008; 105: 17812–17817. <https://doi.org/10.1073/pnas.0808073105> PMID: 19004783
23. Chapman EJ, Estelle M. Mechanism of auxin-regulated gene expression in plants. *Annu Rev Genet*. 2009; 43: 265–285. <https://doi.org/10.1146/annurev-genet-102108-134148> PMID: 19686081
24. Grones P, Friml J. Auxin transporters and binding proteins at a glance. *J Cell Sci*. 2015; 128: 1–7. <https://doi.org/10.1242/jcs.159418> PMID: 25556248
25. Salehin M, Bagchi R, Estelle M. SCF^{TIR1/AFB}-based auxin perception: mechanism and role in plant growth and development. *Plant Cell*. 2015; 27: 9–19. <https://doi.org/10.1105/tpc.114.133744> PMID: 25604443
26. Knox K, Grierson CS, Leyser O. *AXR3* and *SHY2* interact to regulate root hair development. *Development*. 2003; 130: 5769–5777. <https://doi.org/10.1242/dev.00659> PMID: 14534134
27. Wilmoth JC, Wang S, Tiwari SB, Joshi AD, Hagen G, Guilfoyle TJ, et al. NPH4/ARF7 and ARF19 promote leaf expansion and auxin-induced lateral root formation. *Plant J*. 2005; 43: 118–130. <https://doi.org/10.1111/j.1365-3113.2005.02432.x> PMID: 15960621
28. Tejos R, Rodríguez-Furlán C, Adamowski M, Sauer M, Norambuena L, Friml J. PATELLINS are regulators of auxin-mediated PIN1 relocation and plant development in *Arabidopsis thaliana*. *J Cell Sci*. 2017; in press (<https://doi.org/10.1242/jcs.204198>) PMID: 28687624
29. Okushima Y, Overvoorde PJ, Arima K, Alonso JM, Chan A, Chang C, et al. Functional genomic analysis of the *AUXIN RESPONSE FACTOR* gene family members in *Arabidopsis thaliana*: unique and overlapping functions of *ARF7* and *ARF19*. *Plant Cell*. 2005; 17: 444–463. <https://doi.org/10.1105/tpc.104.028316> PMID: 15659631
30. Michniewicz M, Zago MK, Abas L, Weijers D, Schweighofer A, Meskiene I, et al. Antagonistic regulation of PIN phosphorylation by PP2A and PINOID directs auxin flux. *Cell*. 2007; 130: 1044–1056. <https://doi.org/10.1016/j.cell.2007.07.033> PMID: 17889649

Disruption of endocytosis through chemical inhibition of clathrin heavy chain function

Wim Dejonghe^{1,2,16,17}, Isha Sharma^{1,2,17}, Bram Denoo³, Steven De Munck^{4,5}, Qing Lu^{1,2}, Kiril Mishev^{1,2,6}, Haydar Bulut⁷, Evellen Mylle^{1,2}, Riet De Rycke^{1,2,8}, Mina Vasileva⁹, Daniel V. Savatin^{1,2}, Wim Nerinckx^{10,11}, An Staes^{10,12}, Andrzej Drozdzecki^{13,14}, Dominique Audenaert^{13,14}, Klaas Yperman^{1,2}, Annemieke Madder³, Jifri Friml¹⁵, Daniël Van Damme^{1,2}, Kris Gevaert^{10,12}, Volker Haucke¹⁵, Savvas N. Savvides^{1,2,5}, Johan Winne³ and Eugenia Russinova^{1,2*}

Clathrin-mediated endocytosis (CME) is a highly conserved and essential cellular process in eukaryotic cells, but its dynamic and vital nature makes it challenging to study using classical genetics tools. In contrast, although small molecules can acutely and reversibly perturb CME, the few chemical CME inhibitors that have been applied to plants are either ineffective or show undesirable side effects. Here, we identify the previously described endosidin9 (ES9) as an inhibitor of clathrin heavy chain (CHC) function in both *Arabidopsis* and human cells through affinity-based target isolation, in vitro binding studies and X-ray crystallography. Moreover, we present a chemically improved ES9 analog, ES9-17, which lacks the undesirable side effects of ES9 while retaining the ability to target CHC. ES9 and ES9-17 have expanded the chemical toolbox used to probe CHC function, and present chemical scaffolds for further design of more specific and potent CHC inhibitors across different systems.

Clathrin-mediated endocytosis (CME) is a major route for internalization of plasma membrane proteins and molecules from the extracellular environment^{1,2}, but its dynamic and essential nature makes it difficult to dissect using classical genetics approaches. Chemical inhibitors of endocytosis are an attractive alternative to the current methods available for disrupting protein functions. However, despite the extensive structural and biochemical knowledge about CME in eukaryotic cells³, the development of chemicals that interfere with this process is still at a relatively early stage. To date, a few small molecules have been shown to target the CME machinery in mammalian, yeast or plant systems⁴. Among the most commonly used small-molecule CME inhibitors in mammalian systems are Pitstop2 (ref. 5), targeting the N-terminal domain (NTD) of the CHC, Dynasore⁶ and the Dynasore-based series of small molecules called Dyngo⁷, the latter pair affecting the dynamin function. A natural product, Ikarugamycin, has recently been used to inhibit CME in different systems, but neither its potency nor specificity toward CME has been extensively examined⁸. As none of the above-mentioned molecules displayed consistent effects in plant cells, the plant cell biology has taken advantage of tyrphostin A23, a CME-inhibiting small molecule⁹. However, tyrphostin A23 has recently been described as a protonophore in *Arabidopsis thaliana*, and its inhibition of endocytosis was shown to occur through non-specific cytoplasmic acidification⁹. Therefore, CME research in plants

would benefit from novel, potent small-molecule inhibitors that dissect endocytosis to improve our understanding of the many physiological processes that rely on it.

Previously, ES9 (1) was characterized as an endocytosis inhibitor in different model systems⁹. Although ES9 is a protonophore, its interference with CME did not originate solely from cytoplasmic acidification. In *Drosophila melanogaster*, ES9 blocked synaptic vesicle recycling, mimicking the phenotypes in mutants defective in clathrin or dynamin functions whereas in *Arabidopsis*, ES9 was found to retain its ability to inhibit endocytosis at an increased apoplastic pH⁹. These results suggested that, despite its protonophore activity, ES9 may directly interfere with proteins involved in CME. Here, we demonstrated that ES9 binds the NTD of the *Arabidopsis* clathrin heavy chain (CHC). Further structure activity relation (SAR) analysis identified a non-protonophoric ES9 analog with a similar mode of action, as confirmed by cellular thermal shift assay (CETSA)¹⁰ and drug affinity-responsive target stability (DARTS)¹¹. Altogether, we expand the current chemical toolbox for CME inhibition and present promising scaffolds for further development of chemical probes targeting CHC across different systems. For further information on ES9 and other agents featured in this article, see the sections at the end of the article titled Synthetic functions. In the main text, these agents are flagged as numerals within parentheses and are cross-linked to the appropriate section(s).

¹Department of Plant Biotechnology and Bioinformatics, Ghent University, Ghent, Belgium. ²Center for Plant Systems Biology, VIB, Ghent, Belgium.

³Department of Organic and Macromolecular Chemistry, Ghent University, Ghent, Belgium. ⁴Unit for Structural Biology, Department of Biochemistry and Microbiology, Ghent University, Ghent, Belgium. ⁵Unit for Structural Biology, Center for Inflammation Research, VIB, Ghent, Belgium. ⁶Institute of Plant Physiology and Genetics, Bulgarian Academy of Sciences, Sofia, Bulgaria. ⁷Department of Biology, Chemistry and Pharmacy, Freie Universität Berlin, Berlin, Germany. ⁸Ghent University Expertise Centre for Transmission Electron Microscopy and VIB Biomaging Core, Ghent, Belgium. ⁹Institute of Science and Technology, Klosterneuburg, Austria. ¹⁰Center for Medical Biotechnology, VIB, Ghent, Belgium. ¹¹Department of Biochemistry and Microbiology, Ghent University, Ghent, Belgium. ¹²Department of Biomolecular Medicine, Ghent University, Ghent, Belgium. ¹³VIB Screening Core, Ghent, Belgium. ¹⁴Expertise Centre for Bioassay Development and Screening, Ghent University, Ghent, Belgium. ¹⁵Department of Molecular Pharmacology and Cell Biology, Leibniz Research Institute for Molecular Pharmacology, Berlin, Germany. ¹⁶Present address: Department of Botany and Plant Sciences, Institute of Integrative Genome Biology, University of California, Riverside, CA, USA. ¹⁷These authors contributed equally: Wim Dejonghe, Isha Sharma. *e-mail: eurus@psb.vib-ugent.be

Results

ES9 targets identified through affinity purification. Despite unspecific inhibition of endocytosis due to protonophore activity, a possibility remained that ES9 inhibits CME through a direct interaction with its machinery⁹. To explore this option, we performed a SAR analysis of ES9 to identify a suitable position for derivatization with a linker-biotin tag to facilitate affinity-based target identification (Supplementary Fig. 1a and Supplementary Note 1). A small collection of commercially available and in-house-synthesized ES9 analogs were investigated for their ability to inhibit the uptake of the lipophilic styryl endocytic tracer dye *N*-(3-triethylammoniumpropyl)-4-(6-(4-(diethylamino) phenyl) hexatrienyl)pyridinium dibromide (FM4-64)¹² in *Arabidopsis* root epidermal cells (Supplementary Fig. 1a–c). The partial structures or possible hydrolysis products ES9-3 (2) and ES9-7 (3) lacked activity in this endocytosis inhibition assay. Similarly, methylation of the acidic sulfonamide (NH) position of ES9-6 (4) resulted in FM4-64 uptake and, thus, loss of activity. Replacement of the bulky bromine substituent on the thiophene ring by a hydrogen atom produced a simplified analog ES9-2 (5) that retained activity, suggesting a suitable anchoring place for a linker-biotin moiety. Replacement of the thiophene ring per se by its phenyl biosister delivered the active phenylsulfonamide analog ES9-8 (6) that readily allowed further derivatization of the bromine-occupied position. A hydroxyl-terminated linker was introduced at this position, resulting in the analog ES9-9 (7) that indeed retained its activity in the endocytosis inhibition assay. Next, a biotin tag was added to generate a biotin-coupled variant of the active ES9-9, named ES9-10 (8). However, ES9-10 lost the ability to inhibit FM4-64 uptake, probably because it was prevented from entering the cell by either the biotin moiety requiring transport¹³ or the cell wall. A linker-biotin probe without the ES9 moiety, ES9-13 (9) (Supplementary Fig. 1a–c), was used as a negative control.

To identify potential targets of ES9, we performed an affinity purification followed by mass spectrometry using ES9-10 and ES9-13 and protein extracts from peripheral subunit-binding domain (PSB-D) wild-type (WT) *Arabidopsis* cell cultures. In total, three biological replicates were examined, each represented by three technical repeats. Proteins were listed based on the number of times identified and based on the number of peptide-to-spectrum matches (Supplementary Table 1). To reduce the number of putative ES9-10 interactors, we filtered the obtained data as previously described^{14,15}. Proteins bound to ES9-10 in more than one biological replicate and not identified in the ES9-13 pull-downs were considered, resulting in a list of 11 candidates. The top-ranking protein was the CHC1 isoform (AT3G11130), an essential CME component¹⁶, although the remainder of the identified proteins may represent ES9-10 protein targets of low abundance. Unexpectedly, the CHC2 isoform (AT3G08530) was found in both the ES9-10 and control affinity purifications.

ES9 binds CHC. We chose to further focus on CHC, because it has a well-described role in CME¹⁶. To validate the potential interaction between ES9 and CHC1 in *Arabidopsis*, we employed CETSA, which monitors target engagement based on small molecule-induced changes in the thermal stability of protein targets¹⁰. The CHC aggregation temperature (T_{agg}) was assessed through immunoblot analysis, detecting both *Arabidopsis* CHC isoforms CHC1 and CHC2. Thermal denaturation of CHC under control (dimethylsulfoxide (DMSO)) conditions indicated a T_{agg} of 45 ± 0.23 °C (mean \pm s.e.m.) (Fig. 1a). For isothermal dose-response fingerprinting (ITDRF_{CETSA}), the temperature was set at 46 °C to ensure a sufficient shift in the denaturation temperature, and the ES9 half-maximum effective concentration (EC_{50}) was determined to be 120.5 ± 1.09 μ M (mean \pm s.e.m.) (Supplementary Fig. 2a). In contrast, ATP synthase- β (ATP- β), used as a control,

was largely unaffected, even at high concentrations. To achieve sufficiently sized T_{agg} shifts, we used 250 μ M ES9, which generated a lower T_{agg} of 43.08 ± 0.29 °C (mean \pm s.e.m.) compared to the control (45.06 ± 0.23 °C, mean \pm s.e.m.), resulting in a T_{agg} shift of 2 °C (Fig. 1a). Thermal denaturation of the control proteins, tubulin and ATP- β , showed negligible T_{agg} shifts in the presence of either 250 μ M ES9 or vehicle (Fig. 1b and Supplementary Fig. 2b). Moreover, T_{agg} in the presence of the inactive ES9-6 (250 μ M) hardly differed from the control (44.49 ± 0.27 °C and 44.76 ± 0.47 °C, respectively) (mean \pm s.e.m.) (Supplementary Fig. 2c). The results obtained with CETSA were further corroborated by DARTS¹¹. In the presence of 250 μ M ES9, CHC was significantly protected from pronase digestion at 1:2,000 dilution when compared to DMSO-treated samples, which was not observed for the control protein ATP- β (Fig. 1c). Taken together, our data indicated that CHC is probably the target of ES9 in *Arabidopsis* cells.

ES9 binds the nTD of CHC. In an attempt to predict the CHC binding site of ES9, we docked ES9 to the only available structures of human CHC1 (hCHC1, Q00610) nTD in complex with either Pitstop1 (pdb 2XZG) or Pitstop2 (pdb 4G55)⁵. The prediction with pdb 4G55 suggested that the binding site for ES9 on *Arabidopsis* CHC1 might be the same as that for Pitstop2 in hCHC1 (Supplementary Fig. 3a). Residues Arg64, Phe91 and Gln89 in the binding site were set as flexible during docking and the first nine predicted positions were all similar, except for minor reorientations of the flexible residues. To confirm this prediction, the highly homologous β -propeller nTDs of the hCHC1 and the two *Arabidopsis* CHC1 and CHC2 isoforms (Supplementary Fig. 3b) were produced and the respective protein–ES9 interactions were analyzed in vitro by means of differential scanning fluorimetry. We detected a shift in the thermostability of the *Arabidopsis* CHC1 nTD, resulting in a change in its melting temperature (ΔT_m) (Fig. 1d and Supplementary Table 2). In contrast, the thermal denaturation curve for the inactive ES9-6 (160 μ M) overlapped with that of DMSO (Fig. 1d). Protein stability of the nTD in the presence of ES9 was similar for *Arabidopsis* CHC1, CHC2 and hCHC1 (Supplementary Fig. 2d,e and Supplementary Table 2). Altogether, our results demonstrate that ES9 binds to the nTD of CHC in both *Arabidopsis* and humans.

To understand the molecular basis of the ES9 interaction with the CHC nTD, we determined the structure of the hCHC1 nTD in complex with ES9 by protein X-ray crystallography (Fig. 2a). Crystals diffracted up to a resolution of 1.6 Å, and the structure was solved by molecular replacement with hCHC1 nTD as a search model (Supplementary Table 3). The hCHC1 nTD forms a seven-bladed β -propeller, each with four anti-parallel strands. The electron density for ES9 could be identified between the first and second blades (Fig. 2b). Modeling of ES9 into this electron density revealed that the ES9-binding site on the hCHC1 nTD overlaps with the binding site for the CME adaptor proteins harboring a clathrin box motif¹⁷. ES9 is positioned in the cavity formed by six amino acids (Arg64, Ile93, Phe91, Gln89, Leu82 and Ile66), which are conserved between *Arabidopsis* and human CHC nTDs (Supplementary Fig. 3b). The conformation of ES9 is stabilized by electrostatic interactions between its benzonitro moiety and Arg64, and between its thiophene group and the carboxyl oxygen of Ser67 (Fig. 2c,d). Thus, the crystal structure analysis corroborated the docking predictions that ES9 targets the nTD of CHC in a fashion similar to Pitstop2 (ref. 5).

Identification of non-protonophoric ES9 analogs. Although ES9 binds CHC, the protonophore activity of this small molecule⁹ limits its use as a specific CME inhibitor. With the aim of uncoupling the two ES9 activities, we carried out a focused SAR analysis to identify ES9 analogs that are not protonophores but retain the ability to inhibit FM4-64 uptake (Supplementary Fig. 4a and Supplementary

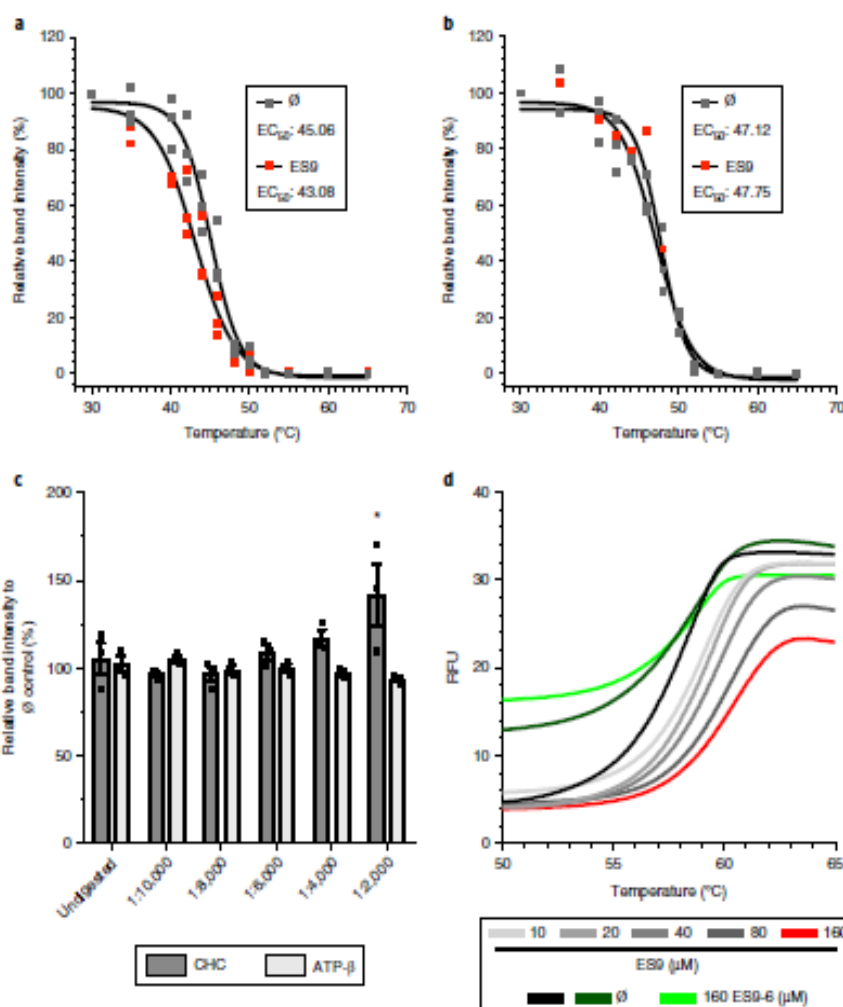


Fig. 1 | ES9 binds CHC. **a, b**, Thermal denaturation curves for endogenous CHC (**a**) and tubulin (**b**) in the presence of ES9 (250 μ M) or DMSO (indicated as \emptyset) for 30 min. Relative band intensities derived from immunoblot analysis were calculated based on the lowest temperature (30 $^{\circ}$ C). EC_{50} is shown on the graphs. Individual data points are plotted for $n=3$ biological independent experiments. For the uncropped blots, see Supplementary Fig. 9. **c**, Protein digestion for 30 min in the presence of pronase and ES9 (250 μ M) or DMSO (\emptyset) for CHC and ATP- β . An undigested sample was included as control. The relative band intensity from immunoblot analysis was calculated based on the DMSO control. Bars indicate the mean, and error bars indicate s.e.m. Individual data points are shown for $n=3$ biological independent experiments. $P=0.027$ for one-way analysis of variance (ANOVA); Dunnett's multiple comparisons test, $*P=0.04$ and compared to the undigested control. For the uncropped blots, see Supplementary Fig. 11. **d**, Changes in thermodynamic stability of the Arabidopsis CHC1 nTD in the presence of different concentrations of ES9 and the inactive analog ES9-6. Controls are respective to ES9 and ES9-6 treatments. The data shown are representative of $n=3$ independent experiments. RFU, relative fluorescence units.

Note 1). Since a weak acid that gives a delocalized anionic charge via electronic conjugation within a large hydrophobic compound is a known molecular architecture that allows protonophore activity, resulting in lipophilic anions³⁵, we attempted to influence the acidity of the sulfonamide of ES9. For several analogs with expected differences in acidity and/or charge delocalization, we assessed both FM4-64 uptake inhibition and the impact on the mitochondrial membrane potential as visualized with MitoTrackerTM in *Arabidopsis* root epidermal cells⁹ (Supplementary Fig. 4b–d). The *meta* position of the nitro group in ES9-29 (**10**) is expected to make the sulfonamide less acidic, while preserving specific contacts with target biomolecules. However, ES9-29 retained its protonophore activity indicating that it was still fairly acidic. Other substitutions on the phenyl ring in ES9-15 (**11**) and ES9-16 (**12**) led to loss of FM-64 uptake inhibition activity. Elimination of the nitro group in ES9

should have markedly shifted the equilibrium toward the protonated form by inhibiting resonance of the charge to the phenyl ring, but it could affect the binding affinities for biomolecular targets. In fact, we found that both ES9-14 (**13**) (Supplementary Fig. 4a) and ES9-17 (**14**) (Fig. 3a) remained active with respect to FM4-64 uptake inhibition and did not abolish MitoTracker staining of mitochondria (Supplementary Fig. 4b–d). Although ES9-17 inhibited FM4-64 uptake with an EC_{50} of 13 μ M (Fig. 3b), 30 μ M was used for further cellular analysis to ensure a substantial reduction in endocytosis (Fig. 3c). In addition, CME inhibition with ES9-17 proved to be reversible, as FM4-64 uptake was recovered after 120 min wash-out with control medium (Supplementary Fig. 4e).

To rule out that ES9-17 is a protonophore, we assessed its capacity to affect cellular ATP in dark-grown *Arabidopsis* PSB-D cell cultures when used at 30 μ M together with ES9 (10 μ M) and the inactive

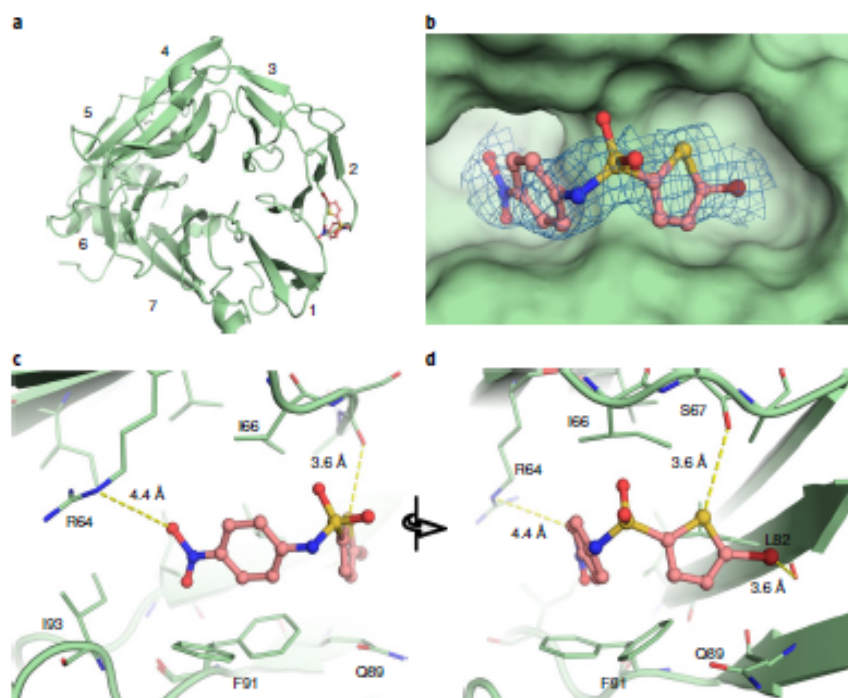


Fig. 2 | ES9 binds the terminal domain of CHC. **a**, The structure of the human CHC1 nTD (green) is shown in complex with ES9 (salmon). **b**, Omitted electron density ($2F_o - F_c$) of ES9, contoured at the 1σ level, is observed inside the hydrophobic clathrin box, which is located between the first and second blades of the nTD. **c**, The interaction distances between the nTD residues and ES9 are denoted by yellow dashes. The zoomed-in view of the benzonitro moiety of ES9 indicates that the oxygen of the nitro group interacts electrostatically with R64. **d**, A 60° -rotated view of ES9 focuses on the bromothiophene moiety. While the sulfur atom of the thiophene group is shown in close contact to the carboxyl oxygen of S67, the bromine atom forms a halogen bond with the carboxyl oxygen of L82.

analog ES9-6 ($50\mu\text{M}$). Neither ES9-17 nor ES9-6 depleted ATP, in contrast to ES9 (ref. ⁷) (Fig. 3d), while fluorescein diacetate fluorescence increased over time, indicating viable cells (Supplementary Fig. 5a). Previously ES9 was shown to acidify the cytoplasm, probably through dissipation of the proton gradients over the plasma membrane⁹. Therefore, we assessed whether ES9-17 would affect the cytoplasmic pH. *Arabidopsis* seedlings were pre-incubated with Lyso Tracker²⁰ to label acidic compartments, followed by 30 min incubation with DMSO, $10\mu\text{M}$ ES9 or $30\mu\text{M}$ ES9-17 (Fig. 3e). Unlike ES9, staining in the presence of ES9-17 did not differ from the control, indicating that cytoplasmic pH was not substantially altered. Furthermore, and different from ES9, application of ES9-17 did not compromise the motility of the actin cytoskeleton (Fimbrin-GFP)²¹, microtubules (GFP-MAP4)²², the Golgi (ST-mRFP)²³ and the *trans*-Golgi network/early endosome compartments (VHA-a1-GFP)²⁴ (Supplementary Fig. 5b–e).

ES9-17 is a CME inhibitor. To characterize the potential of ES9-17 as a CME inhibitor in *Arabidopsis*, we evaluated the internalization of two plasma membrane-localized proteins subjected to CME. Seedlings expressing the brassinosteroid receptor²⁵ BR INSENSITIVE1 (BR11) tagged to GFP (*BR11:BR11-GFP*)²⁶ were pretreated with cycloheximide (CHX) to reduce newly synthesized proteins, followed by treatment with DMSO or ES9-17 ($30\mu\text{M}$) for 30 min and then with $50\mu\text{M}$ Brefeldin A (BFA) and FM4-64 for 30 min. In the presence of ES9-17, BR11-GFP and FM4-64 failed to label BFA bodies (Fig. 4a), suggesting inhibition of uptake from the plasma membrane. The lack of BR11-GFP-labeled BFA bodies was not due to inhibited BFA body formation, because BFA bodies marked by the VHA-a1-GFP²⁴ were formed (Supplementary

Fig. 6a). Furthermore, fluorescently labeled Alexa Fluor674 castasterone (AFCS), which binds to BR11 and consequently enters the cell through CME²⁵, failed to stain the vacuole in root epidermal cells when applied together with $30\mu\text{M}$ ES9-17 to seedlings expressing BR11-GFP²⁶ (Supplementary Fig. 6b). To corroborate our findings with BR11, we examined the PEP RECEPTOR1 (PEPR1)²⁷. Elicitation of *Arabidopsis* root cells expressing *RPSSA:PEPR1-GFP* with 100nM Pep-1 after pretreatment with DMSO induced PEPR1-GFP endocytosis (Fig. 4b). However, elicitation with Pep-1 after pretreatment with $30\mu\text{M}$ ES9-17 did not cause PEPR1-GFP internalization (Fig. 4b), implying an inhibitory effect of ES9-17 on the CME-mediated PEPR1 uptake.

In an attempt to explain the impaired cargo internalization by ES9-17, we evaluated the dynamic behavior of clathrin light chain1 (CLC1)-GFP⁹, CHC1-GFP⁹ and one representative of the *Arabidopsis* CME adaptors, the TPLATE munc18-like (TML) subunit of the TPLATE complex²⁸ in the plasma membrane of *Arabidopsis* root epidermal cells. In the presence of DMSO, CLC1-GFP, CHC1-GFP and TML-GFP, foci had an average residence lifespan of 31.98, 44.62 and 36.72 s, respectively (Fig. 4c and Supplementary Fig. 6c,d). When seedlings were treated with $30\mu\text{M}$ ES9-17, the residence lifespan of CLC1, CHC1 and TML in the plasma membrane increased substantially, with an average of 73.99, 83.55 and 68.66 s, respectively.

Since ES9 was found to bind both *Arabidopsis* and human CHC, we assessed whether ES9-17 could inhibit transferrin uptake in HeLa cells, a well-known clathrin-mediated process². Treatment of HeLa cells with $30\mu\text{M}$ ES9-17 for 30 min appeared to reduce the uptake of transferrin, but not to the extent observed with $20\mu\text{M}$ Pitstop2 (Supplementary Fig. 7a). In parallel with the inhibitory treatments, cell proliferation assays ascertained that reduced

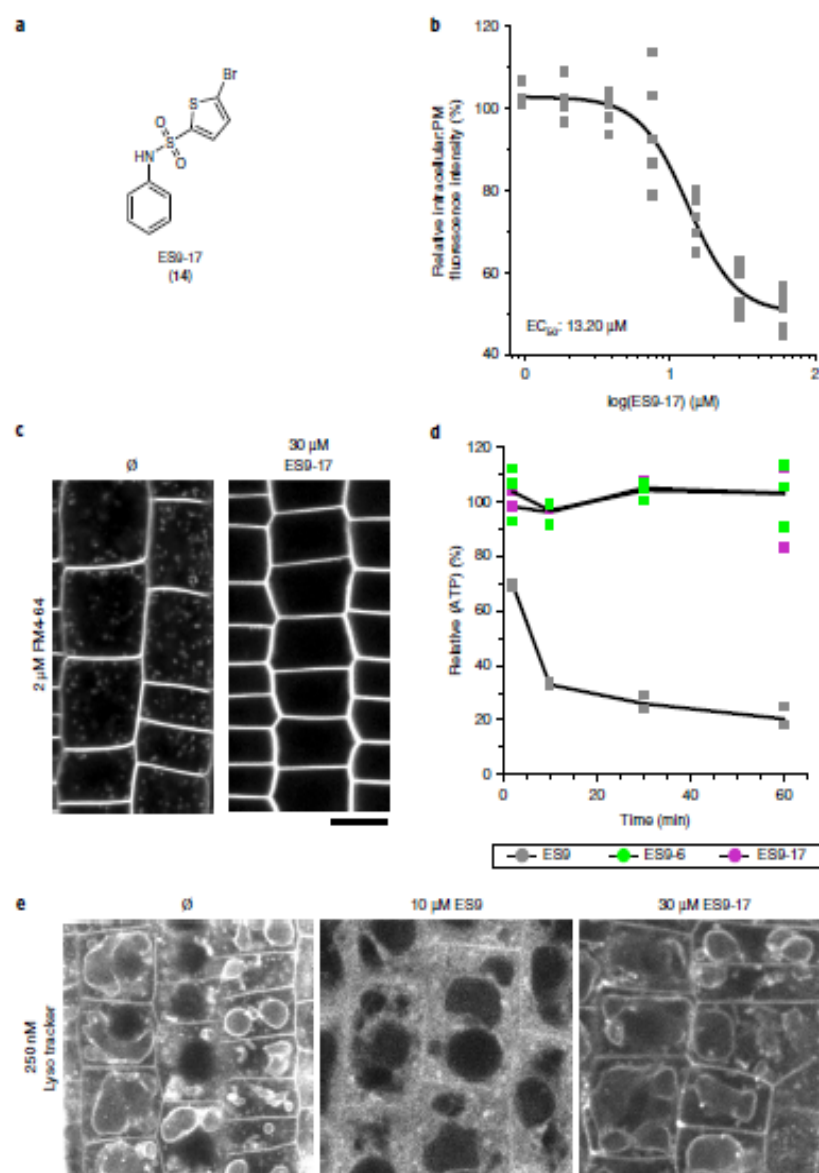


Fig. 3 | ES9-17 is not a protonophore. **a**, Structure of ES9-17 (**14**). **b**, Dose response of ES9-17-mediated FM4-64 uptake inhibition. The data are plotted as the ratio of the intracellular over the plasma membrane (PM) FM4-64 fluorescence intensity; EC_{50} is shown on the graph. At least three cells were measured per seedling, for $n=3$ seedlings. **c**, Strongly reduced FM4-64 uptake ($2\ \mu\text{M}$, 30 min) in *Arabidopsis* root epidermal cells in the presence of ES9-17 ($30\ \mu\text{M}$) when compared to the DMSO (indicated as \emptyset) control. The samples were pretreated with either ES9-17 ($30\ \mu\text{M}$) or DMSO for 30 min; $n=6$ seedlings. **d**, Measurements of ATP concentration in WT *Arabidopsis* PSB-D cell cultures treated for 30 min with ES9 ($10\ \mu\text{M}$), ES9-17 ($30\ \mu\text{M}$) and ES9-6 ($50\ \mu\text{M}$), showing the ATP concentrations relative to the DMSO control. Individual data points are plotted for $n=3$ biological replicates. **e**, Confocal images of *Arabidopsis* epidermal root cells stained with Lyso Tracker Red DND 99 (30 min) and treated additionally for 30 min with DMSO (\emptyset), ES9 ($10\ \mu\text{M}$) or ES9-17 ($30\ \mu\text{M}$). Scale bars, $10\ \mu\text{m}$. The experiments in **b**, **c** and **e** were repeated independently three, six and four times, respectively, with similar results.

transferrin uptake was not due to the cytotoxicity of the compounds (Supplementary Fig. 7b). In an effort to compare ES9-17 to Pitstop2, we sought to assess the activity of the latter in *Arabidopsis* but failed to detect CME inhibition. Pitstop2 did not block FM4-64 uptake when applied at $30\ \mu\text{M}$ for 30 min (Supplementary Fig. 7c), and similarly failed to inhibit internalization of BRI1-GFP in the presence of BFA (Supplementary Fig. 7d). Higher concentrations of Pitstop2 appeared to affect overall the FM4-64 fluorescence, but did not result in uptake inhibition (Supplementary Fig. 7e). Moreover,

the CETSA thermal denaturation curves for CHC and ATP- β in the presence of either DMSO or $250\ \mu\text{M}$ Pitstop2 were very similar. The T_{agg} values with DMSO and Pitstop2 for CHC were $44.57 \pm 0.29^\circ\text{C}$ and $44.50 \pm 0.34^\circ\text{C}$ (mean \pm s.e.m.), respectively, and for ATP- β were $55.03 \pm 1.41^\circ\text{C}$ and $54.63 \pm 1.05^\circ\text{C}$ (mean \pm s.e.m.), respectively (Supplementary Fig. 7f).

Taken together, ES9-17 impaired both the uptake of different endocytic cargoes and the dynamic behavior of core CME components. In addition, ES9-17 reduced transferrin uptake in HeLa cells,

albeit less so than Pitstop2, whereas Pitstop2 proved to be inactive in *Arabidopsis* with respect to CME inhibition.

ES9-17 targets CHC. Because ES9-17 inhibited several clathrin-dependent processes and ES9 was found to bind CHC, we hypothesized that CHC might also be the target of ES9-17. To test this hypothesis, we used CETSA and DARTS, as done for ES9. ITDRF_{CETSA} analysis at 46 °C indicated an EC₅₀ of 123.10 ± 1.13 μM (mean ± s.e.m.) for ES9-17 (Supplementary Fig. 8a). When lysates were treated with DMSO we observed a T_{50%} for CHC of 44.96 ± 0.2 °C (mean ± s.e.m.), whereas for 250 μM ES9-17 the T_{50%} was 42.71 ± 0.2 °C (mean ± s.e.m.), generating a T_{50%} shift of 2.2 °C, similar to ES9 (Fig. 5a). In contrast, ES9-17 failed to induce a shift in T_{50%} for tubulin and ATP-β (Fig. 5b and Supplementary Fig. 8b). These results were supported by DARTS assays using 250 μM ES9-17. At pronase concentrations of 1:6,000 and 1:4,000, two- and 1.5-fold stabilization were observed for CHC in ES9-17-treated cell lysates, respectively, whereas ATP-β (Fig. 5c), and selected TPLATE complex²⁸ and adaptor protein complex-2 subunits²⁹, were not stabilized (Supplementary Fig. 8c–e). To evaluate the specificity of ES9-17, we assessed its potential interaction with the coatomer subunit (AT4G34450, γ-COP), because this protein ranked second in the ES9 interactors list (Supplementary Table 1). The DARTS assay with ES9-17 failed to demonstrate sufficient protection of γ-COP (Supplementary Fig. 8f), demonstrating that ES9-17 does not bind γ-COP. Previously we observed that ES9 affects Golgi cisternal morphology and induces the formation of Golgi-endoplasmic reticulum hybrid compartments⁹ indicative of non-functional coat protein I (COPI) trafficking. Transmission electron microscopy (TEM) analysis of *Arabidopsis* Col-0 root tips treated with ES9-17 (30 μM) did not reveal striking morphological changes in the Golgi network and endoplasmic reticulum (Supplementary Fig. 8g), although occasionally ES9-17 appeared to induce enlarged multivesicular bodies (Supplementary Fig. 8g, white triangle). Altogether, our results showed that ES9-17 did not affect the COPI function in *Arabidopsis*.

To confirm the results obtained with ES9-17 in CETSA and DARTS assays, we assessed genetically whether ES9-17 interacts with CHC. Double-knockout mutant lines in CHC cannot be used, because CHC has an essential function¹⁶. Therefore, several single-mutant alleles for *CHC1* and *CHC2* (ref. ¹⁶) were examined. Primary root growth of 5-day-old *Arabidopsis* seedlings was inhibited with an EC₅₀ of 10 μM (Supplementary Fig. 8h); 12 μM ES9-17 was used to ensure sufficient root growth inhibition. Seedlings of mutant

lines *chc1-4* (Supplementary Fig. 8i), *chc2-1* and *chc2-2* (ref. ¹⁶) displayed a significantly increased sensitivity to ES9-17 compared to Col-0 seedlings (Fig. 5d). Root growth did not significantly vary for the different genotypes when grown under control conditions (Supplementary Fig. 8j). Collectively, the results obtained with CETSA, DARTS and the CHC mutants point toward CHC as a protein target of ES9-17 in *Arabidopsis*.

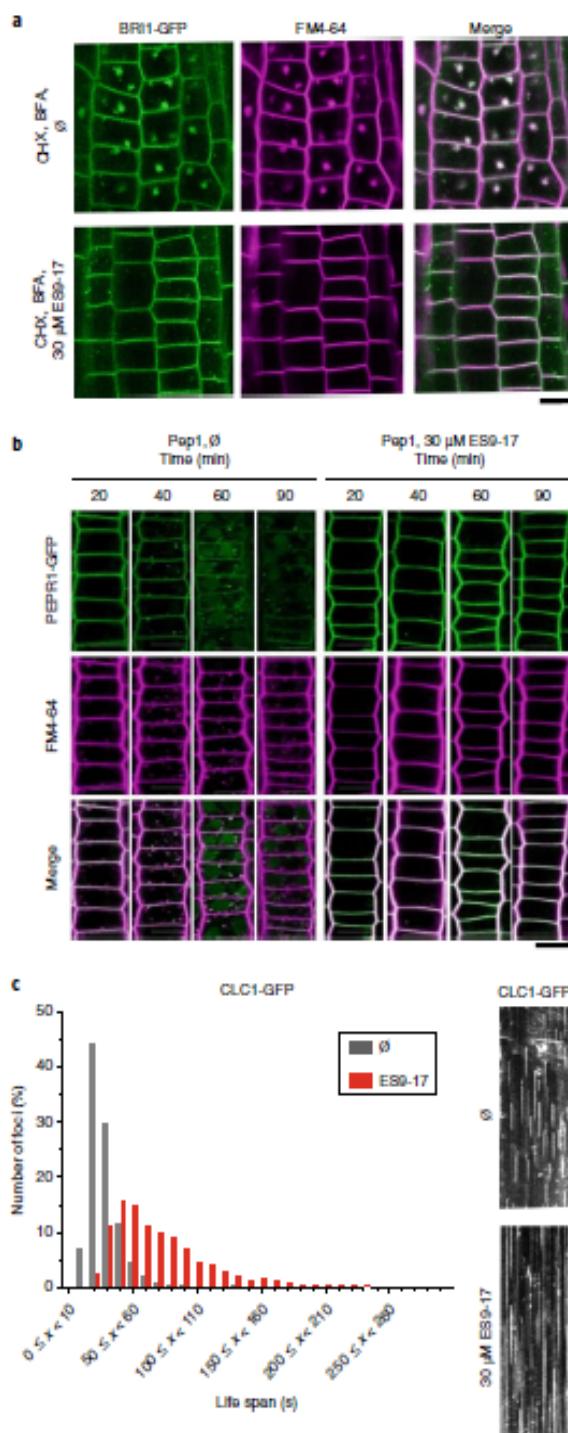


Fig. 4 | ES9-17 is a CME inhibitor. **a**, ES9-17 inhibited recruitment of the plasma membrane-localized BR11-GFP to the BFA body. Samples were pretreated with 50 μM CHX for 1 h and treated with either DMSO (indicated as 0) or ES9-17 (30 μM) for 30 min, followed by a combined application of FM4-64 (2 μM) and BFA (50 μM) for an additional 30 min in the presence of the inhibitor. Scale bar, 10 μm. **b**, Confocal images of *Arabidopsis* root epidermal cells expressing PEPRI-GFP. Seedlings were treated with ES9-17 (30 μM) or DMSO (0) for 30 min, followed by elicitation with 100 nM Pep-1. The internalization of PEPRI-GFP was followed until 90 min post elicitation. Scale bar, 20 μm. **c**, Histograms representing the measured endocytic foci lifespan of CLC1-GFP (*CLC1:CLC1-GFP/Col-0*) in the presence of ES9-17 (30 μM) or DMSO (0); $n = 1,276$ and 1,069 measurements from ten and four seedlings, respectively. Kymographs represent a line trace (horizontal axis), over a time period (vertical axis) taken from a time lapse (2 frames s⁻¹) of *Arabidopsis* root epidermal cells that illustrates the lifespan of endocytic foci labeled by CHC1-GFP. Scale bar, 10 s. The experiments in **a–c** were repeated independently three times with similar results. The life time distribution graph was generated by grouping the events into specific categories, annotated as, for example, 0 ≤ x < 10: the category holding those events with a life time (x) being larger or equal (≤) than 0 s and smaller (<) than 10 s.

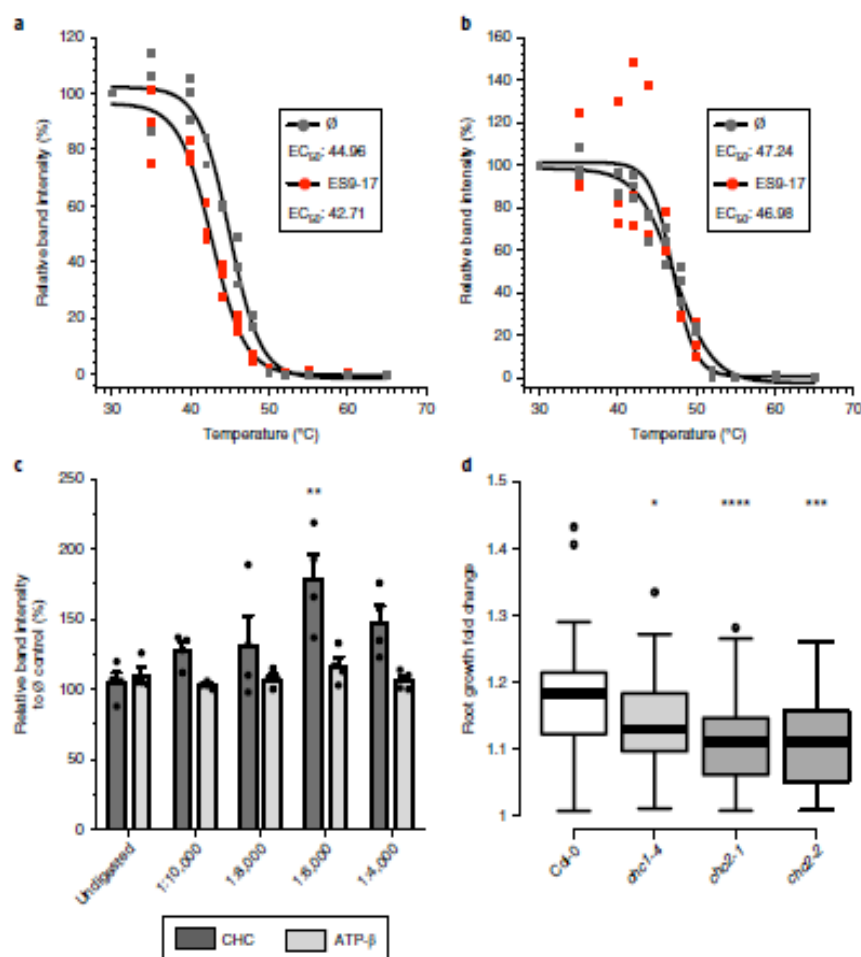


Fig. 5 | ES9-17 targets CHC. **a, b**, Thermal denaturation curves for endogenous CHC (**a**) and tubulin (**b**) in the presence of either ES9-17 (250 μ M) or DMSO (indicated as \emptyset) for 30 min. Relative band intensity from immunoblot analysis was calculated based on the lowest temperature (30 $^{\circ}$ C); EC₅₀ is shown on the graphs. Individual data points are plotted for $n=3$ biological independent experiments. For the uncropped blots, see Supplementary Fig. 9. **c**, Protein digestion for 30 min in the presence of pronase and ES9-17 (250 μ M) or DMSO (\emptyset) for CHC and ATP- β . An undigested sample was included as control. The relative band intensity from immunoblot analysis was calculated based on the DMSO control. Bars indicate the mean, and error bars indicate s.e.m. Individual data points are shown for $n=4$ biological independent experiments. $P=0.02$ for ANOVA, with a Dunnett's multiple comparisons test, ** $P=0.006$, and compared to the undigested control. For the uncropped blots, see Supplementary Fig. 12. **d**, Boxplot representation of the root growth fold change over 48 h for WT *Arabidopsis* Col-0 seedlings treated with ES9-17 (12 μ M). Center lines show the medians; box limits indicate the 25th and 75th percentiles as determined by R software and outliers are represented by dots; $n=80$ seedlings from three independent experiments. $P<0.0001$ for ANOVA, with a Dunnett's multiple comparisons test for which * $P=0.038$, *** $P=0.0002$ and **** $P<0.0001$.

Discussion

In plants, CME is among the pathways most studied for the internalization of plasma membrane and extracellular cargos¹. As loss-of-function CME mutants are frequently lethal or have no phenotypes because of gene redundancy¹⁶, methods to perturb CME are largely reliant on inducible expression of mutant forms of critical proteins involved in endocytosis, such as clathrin and auxilin^{30,31}, and small interfering RNA-mediated depletion of adaptor proteins²⁸. Drawbacks include low gene induction efficiency, silencing and the considerable time needed to deplete existing protein complexes (2–5 days). Meanwhile the cell may adapt and even alter its gene expression, without certitude that only CME is impacted. Prolonged loss of a protein, such as clathrin, might impair post-Golgi trafficking²² with potential defects in secretion and vacuolar targeting as a consequence. Therefore, application of small-molecule inhibitors of

CME combined with live-cell imaging can facilitate studies of the CME machinery. Attractive features of chemical inhibitors are that they can be applied acutely to reveal the direct blocking of a particular process, and that their effect is reversible²³.

Over the years, different small-molecule effectors of endosomal function in *Arabidopsis* have been described, including Secdin¹⁵ and several compounds from the endostatin series^{34–37}. Characterization of the CME inhibitor ES9 (ref. 7) identified it as a protonophore, causing ATP depletion and cytoplasmic acidification, a mode of action shared with the commonly used plant CME inhibitor tyrphostin A23. Therefore, in contrast to mammalian systems, in which the CME inhibitors Pistop2 and Dynasore are well established¹⁴, plants lack small molecules that specifically target CME. While Dynasore has been used as a CME inhibitor in plants²⁸, reports on the activity of Pistop2 in plant cells are lacking. Our results revealed that

Pitstop2 is inactive as a CME inhibitor in *Arabidopsis*, which can be rationalized using structural considerations based on a key amino acid difference between *Arabidopsis* and human CHC, and in light of the structurally characterized binding pocket of Pitstop2 in hCHC1. The hallmark of Pitstop2 binding to hCHC1 centers on the accommodation of its naphthalene ring by an evenly distributed cushion of β -branched residues (Ile52, Ile66, Ile80, Ile93 and Val50)⁵. However, *Arabidopsis* CHC1 and CHC2 display a Leu at position 80 (Supplementary Fig. 3b), which is expected to introduce steric hindrance that would prevent Pitstop2 binding.

Although chemically different from Pitstop2, ES9 targeted the nTD of CHC in a similar fashion, as revealed by the crystal structure of the hCHC1 nTD with ES9. Regardless, the usefulness of ES9 as a specific CME inhibitor is compromised by its protonophore characteristics. The non-protonophore analog ES9-17, however, lacks the nitro group of ES9 that establishes an electrostatic interaction with Arg64. As a consequence, ES9-17 might bind the CHC nTD in a different orientation and affinity than ES9 (Supplementary Fig. 3a). Nevertheless, ES9-17 inhibited the uptake of both FM4-64 and several CME cargoes in *Arabidopsis*, validating it as an inhibitor of endocytosis. Moreover, ES9-17 appeared more specific when compared to ES9, as the Golgi morphology in the presence of ES9-17 was not altered, unlike ES9, which induced substantial morphological changes in the Golgi⁹. These morphological changes are likely to have resulted from its protonophore characteristics and from targeting the γ -COP subunit of the coatamer complex, which ranked second after CHC1 in the ES9-10 affinity purification list.

Different *in vitro* target validation methods showed that ES9-17 behaves like ES9, strongly suggesting that the former also targets CHC to inhibit CME. Currently we can only speculate why the CETSA EC₅₀ differed from the FM4-64 inhibition EC₅₀ for both ES9 and ES9-17. Possibly, accessory proteins present in a biological context might have increased affinity but, equally, *in vitro* conditions might have increased the apparent EC₅₀ values. Furthermore, ES9 appeared to be able to inhibit FM4-64 uptake with a higher potency (EC₅₀ = 5.16 μ M)⁹ than that of ES9-17 (EC₅₀ = 13 μ M), probably due to being both a protonophore and a CHC inhibitor.

Identification of ES9-17 thus presents several new opportunities in the quest to understand clathrin-mediated trafficking. For example, ES9 and ES9-17 offer chemical scaffolds, different from the Pitstop family, to improve and identify more potent inhibitors of the CHC function. By doing so we would further increase our understanding of the molecular aspects of CHC function. As we established that ES9 binds the same pocket as Pitstop2, it is reasonable to assume that the mode of ES9 inhibition would be similar to that of Pitstop2, that is, interfering with the recruitment of accessory proteins harboring a clathrin box motif⁵. Furthermore, although the core function of CHC in CME is known, we have little understanding of the specific roles of CHC1 and CHC2 in *Arabidopsis*. Rendering either CHC1 or CHC2 insensitive to ES9-17, yet still biologically functional, might help to deconvolve their function. The ability to selectively inhibit the CHC1 or CHC2 function might help to highlight their different roles in the endomembrane system, or at the tissue and developmental levels. Taken together, because other CME inhibitors, including Pitstop2, lack activity in *Arabidopsis*, to our knowledge ES9-17 is the only probe allowing both dynamic and reversible inhibition of CME in *Arabidopsis*.

Online content

Any methods, additional references, Nature Research reporting summaries, source data, statements of data availability and associated accession codes are available at <https://doi.org/10.1038/s41589-019-0262-1>.

Received: 13 July 2018; Accepted: 4 March 2019;
Published online: 22 April 2019

References

- Reynolds, G. D., Wang, C., Pan, J. & Bednarek, S. Y. Inroads into internalization: five years of endocytic exploration. *Plant Physiol.* **176**, 208–218 (2018).
- Kaksonen, M. & Roux, A. Mechanisms of clathrin-mediated endocytosis. *Nat. Rev. Mol. Cell Biol.* **19**, 313–326 (2018).
- Mettlen, M., Chen, P.-H., Srinivasan, S., Danuser, G. & Schmid, S. L. Regulation of clathrin-mediated endocytosis. *Annu. Rev. Biochem.* **87**, 871–896 (2018).
- Mishev, K., Dejonghe, W. & Russtova, E. Small molecules for dissecting endomembrane trafficking: a cross-systems view. *Chem. Biol.* **20**, 475–486 (2013).
- von Kleist, L. et al. Role of the clathrin terminal domain in regulating coated pit dynamics revealed by small molecule inhibition. *Cell* **146**, 471–484 (2011).
- Macia, E. et al. Dynasore, a cell-permeable inhibitor of dynamin. *Dev. Cell* **10**, 839–850 (2006).
- McCluskey, A. et al. Building a better dynasore: the Dyngo compounds potently inhibit dynamin and endocytosis. *Traffic* **14**, 1272–1289 (2013).
- Elkin, S. R. et al. Ikarugamyctin: a natural product inhibitor of clathrin-mediated endocytosis. *Traffic* **17**, 1139–1149 (2016).
- Dejonghe, W. et al. Mitochondrial uncouplers inhibit clathrin-mediated endocytosis largely through cytoplasmic acidification. *Nat. Commun.* **7**, 11710 (2016).
- Jafari, R. et al. The cellular thermal shift assay for evaluating drug target interactions in cells. *Nat. Protoc.* **9**, 2100 (2014).
- Lomenick, B. et al. Target identification using drug affinity responsive target stability (DARTS). *Proc. Natl Acad. Sci. USA* **106**, 21984–21989 (2009).
- Jelinková, A. et al. Probing plant membranes with FM dyes: tracking, dragging or blocking? *Plant J.* **61**, 883–892 (2010).
- Ludwig, A., Stolz, J. & Sauer, N. Plant sucrose-H⁺ symporters mediate the transport of vitamin H. *Plant J.* **24**, 503–509 (2000).
- Van Leene, J. et al. An improved toolbox to unravel the plant cellular machinery by tandem affinity purification of *Arabidopsis* protein complexes. *Nat. Protoc.* **10**, 169–187 (2015).
- Mishev, K. et al. Nonselective chemical inhibition of Sec7 domain-containing ARF GTPase exchange factors. *Plant Cell* **30**, 2573–2593 (2018).
- Kitakura, S. et al. Clathrin mediates endocytosis and polar distribution of PIN auxin transporters in *Arabidopsis*. *Plant Cell* **23**, 1920–1931 (2011).
- Popova, N. V., Deyev, I. E. & Petrenko, A. G. Clathrin-mediated endocytosis and adaptor proteins. *Acta Naturae* **5**, 62–73 (2013).
- Ontzuka, S., Ikewaki, N. & Shiratsuki, S. A mechanism by which propofol induces cytotoxicity. *J. Drug Metab. Toxicol.* **8**, 230 (2017).
- Poot, M. et al. Analysis of mitochondrial morphology and function with novel fixable fluorescent stains. *J. Histochem. Cytochem.* **44**, 1363–1372 (1996).
- Dolman, N. J., Kilgore, J. A. & Davidson, M. W. A review of reagents for fluorescence microscopy of cellular compartments and structures, part I: BacMam labeling and reagents for vesicular structures. *Curr. Protoc. Cytom.* **65**, 12.30.1–12.30.27 (2013).
- Wang, Y.-S., Yoo, C.-M. & Blancaflor, E. B. Improved imaging of actin filaments in transgenic *Arabidopsis* plants expressing a green fluorescent protein fusion to the C- and N-terminal of the fibrin actin-binding domain 2. *New Phytol.* **177**, 525–536 (2008).
- Marc, J. et al. GFP-MAP4 reporter gene for visualizing cortical microtubule rearrangements in living epidermal cells. *Plant Cell* **10**, 1927–1940 (1998).
- Teh, O.-k. & Moore, I. An ARF-GEF acting at the Golgi and in selective endocytosis in polarized plant cells. *Nature* **448**, 493–496 (2007).
- Deitmer, J., Hong-Hermesdorf, A., Stierhof, Y.-D. & Schumacher, K. Vacuolar H⁺-ATPase activity is required for endocytic and secretory trafficking in *Arabidopsis*. *Plant Cell* **18**, 715–730 (2006).
- Irani, N. G. et al. Fluorescent castasterone reveals BR11 signaling from the plasma membrane. *Nat. Chem. Biol.* **8**, 583–589 (2012).
- Friedrichsen, D. M., Joazeiro, C. A. P., Li, J., Hunter, T. & Chory, J. Brassinosteroid-insensitive-1 is a ubiquitously expressed leucine-rich repeat receptor serine/threonine kinase. *Plant Physiol.* **123**, 1247–1255 (2000).
- Ortiz-Moreno, F. A. et al. Danger-associated peptide signaling in *Arabidopsis* requires clathrin. *Proc. Natl Acad. Sci. USA* **113**, 11028–11033 (2016).
- Gadeyne, A. et al. The TPLATE adaptor complex drives clathrin-mediated endocytosis in plants. *Cell* **156**, 691–704 (2014).
- Di Rubbo, S. et al. The clathrin adaptor complex AP-2 mediates endocytosis of brassinosteroid insensitive1 in *Arabidopsis*. *Plant Cell* **25**, 2986–2997 (2013).
- Dhonukshe, P. et al. Clathrin-mediated constitutive endocytosis of PIN auxin efflux carriers in *Arabidopsis*. *Curr. Biol.* **17**, 520–527 (2007).
- Adamowski, M. et al. A functional study of AUXILIN-LIKE1 and 2, two putative clathrin uncoating factors in *Arabidopsis*. *Plant Cell* **30**, 700–716 (2018).
- Robinson, D. G. & Pimpl, P. Clathrin and post-Golgi trafficking: a very complicated issue. *Trends Plant Sci.* **19**, 134–139 (2014).

33. Hicks, G. R. & Ratkheh, N. V. Small molecules present large opportunities in plant biology. *Annu. Rev. Plant Biol.* **63**, 261–282 (2012).
34. Drakakaki, G. et al. Clusters of bioactive compounds target dynamic endomembrane networks in vivo. *Proc. Natl Acad. Sci. USA* **108**, 17850–17855 (2011).
35. Zhang, C. et al. Endostatin targets conserved exocyst complex subunit EXO70 to inhibit exocytosis. *Proc. Natl Acad. Sci. USA* **113**, E41–E50 (2016).
36. Kania, U. et al. The inhibitor Endostatin 4 targets SEC7 domain-type ARF GTPase exchange factors and interferes with subcellular trafficking in eukaryotes. *Plant Cell* **30**, 2553–2572 (2018).
37. Li, R. et al. Different endomembrane trafficking pathways establish apical and basal polarities. *Plant Cell* **29**, 90–108 (2017).
38. Sharfman, M. et al. Endosomal signaling of the tomato leucine-rich repeat receptor-like protein LeE1x2. *Plant J.* **68**, 413–423 (2011).

Acknowledgements

We thank S. Vanneste for fruitful discussions, R. Kumar for providing the pDONR211-AP25 plasmid, D. Martínez Molina for help with the CETSA protocol and M. De Cock for help in preparing the manuscript. This work was supported by the Research Foundation-Flanders (project No. G022516N to E.R., project No. G009415N to D.V.D. and project No. G0E5718N to E.R. and J.E.); the European Research Council (ERC Co T-Rex, grant No. 682436 to D.V.D.); the Deutsche Forschungsgemeinschaft (No. TRR186/A08 to V.H.); the Agency for Innovation by Science and Technology for postdoctoral (K.M.) and predoctoral (W.D. and S.D.M.) fellowships; the China Science Council for a predoctoral fellowship (Q.L.); the joint research projects (Nos. VS.025.13N and VS.095.16N) within the framework of cooperation between the Research

Foundation-Flanders and the Bulgarian Academy of Sciences (K.M.); and the Belgian Science Policy Office for a postdoctoral fellowship to non-EU researchers (I.S.).

Author contributions

W.D. and E.R. initiated the work. W.D., I.S. and E.R. designed the experiments. W.D., I.S., B.D., A.M. and J.W. performed SAR. W.D., K.M., A.S. and K.G. performed affinity purification and MS analysis. H.B. and V.H. performed the X-ray crystallography. I.S., S.D.M. and S.N.S. performed the in vitro binding assay. W.N. did the molecular docking. W.D., I.S. and Q.L. performed CETSA. W.D., I.S. and Q.L. performed DARTS. W.D., I.S., E.M., D.V.S., and D.V.D. carried out the imaging and data analysis. I.S. performed the cloning and generated transgenic *Arabidopsis* cell cultures. W.D., I.S., A.D. and D.A. performed ATP measurements. M.V. and J.F. contributed to the HeLa cell assays. K.Y. generated the TPLATE antibody. Q.L. and R.D.R. performed TEM. W.D., I.S. and E.R. wrote the manuscript. All authors commented on the results and the manuscript.

Competing interests

The authors declare no competing interests.

Additional information

Supplementary information is available for this paper at <https://doi.org/10.1038/s41589-019-0262-1>.

Reprints and permissions information is available at www.nature.com/reprints.

Correspondence and requests for materials should be addressed to E.R.

Publisher's note: Springer Nature remains neutral with regard to jurisdictional claims in published maps and institutional affiliations.

© The Author(s), under exclusive licence to Springer Nature America, Inc. 2019

Methods

Plant materials and growth conditions. *Arabidopsis thaliana* (L.) Heynh. (accession Columbia-0 (Col-0)) seedlings and other lines were stratified for 2 days at 4 °C and grown on agar plates containing half-strength Murashige and Skoog (0.5 x MS) medium supplemented with 1% (w/v) sucrose for 5 days at 22 °C in a 16h/8h light/dark cycle. The *Arabidopsis* mutants and transgenic lines used were: *chc2-1* (ref. ¹⁹), *chc2-2* (ref. ¹⁹), *TML:TML-GFP/tml-1* (ref. ²⁰), *CLC1:CLC1-GFP/Col-0* (ref. ⁷), *RP55A:CHC1-GFP/Col-0* (ref. ⁷), *VHA-a1:VHA-a1-GFP/Col-0* (ref. ²¹), *35S:ST-mRFP/Col-0* (ref. ²²), *RP55A:PEPR1-GFP/pepr1pepr2* (ref. ²³), *BRI1:BRI1-GFP/Col-0* (ref. ²⁴), *35S:GFP-MAP4/Le²* and *35S:Pimbrin-GFP/Col-0* (ref. ²⁵). The transfer DNA (T-DNA) insertion line *chc1-4* (SALK_110063) was obtained from the Nottingham Arabidopsis Stock Centre and confirmed by PCR using the left primer (5'-CAAGTGACGCATCACAACATG-3'), the right primer (5'-ACCATTGCTCAAAACATACGC-3') and the T-DNA-specific primer LBA1 (5'-TGGTTTCACGTAGTGGCCATC-3') (Supplementary Fig. 8).

Generation of hemagglutinin-tagged AP2S and AP2M constructs and Arabidopsis PSB-D cell culture transformation. Entry clones *pDONRRP4-1R-RP55A*, *pDONRRP2R-P3-HAstop* and *pDONR211-AP2S* (AT1G47830) or *pDONR211-AP2M* (AT5G46630) were used with *pH7m34GW* in multi-site Gateway reactions (Life Technologies) to generate *RP55A:AP2S-HA* and *RP55A:AP2M-HA* expression constructs. These were used to transform PSB-D WT *Arabidopsis* cell cultures as previously described¹⁴.

Chemical treatments, chemical labeling and imaging in Arabidopsis. Analogs and ES9 were either acquired through Chembridge (<http://www.chembridge.com/>) or synthesized. These were dissolved in DMSO (Sigma-Aldrich) and 50 mM stocks were stored at -20 °C in glass vials. ES9-17 was freshly prepared from lyophilized powder (stored at -20 °C) before use. BFA and Pitstop2 (Sigma-Aldrich), CHX (Calbiochem), Lyso Tracker Red DND99 and MitoTracker Red CM-H2XRos (ThermoFisher Scientific) were dissolved in DMSO. Endocytosis was visualized with 2 μM FM4-64 (Life Technologies). Washout experiments involved 30 min pretreatment of seedlings in liquid >0.5 MS medium with ES9-17 (30 μM), followed by an additional 30 min treatment in the presence of FM4-64 (2 μM). Subsequent substitution of treatment medium by medium without treatment, but with FM4-64, constituted the washout. Seedlings were imaged at the indicated time points. The experiment was performed twice independently. Repeat 1 was washed with regular 0.5 x MS and FM4-64 (2 μM), while repeat 2 was washed with 0.5 x MS plus DMSO and FM4-64 (2 μM). Staining and imaging of mitochondria and acidic compartments in the seedlings treated with the small molecules were performed as described previously¹⁴. To visualize inhibition of GFP-tagged BRI1 (*BRI1:BRI1-GFP*)²⁶, *Arabidopsis* seedlings were pretreated for 1 h with 50 μM CHX, followed by treatments with either DMSO or ES9-17 (30 μM) for 30 min and then with 50 μM BFA and FM4-64 for 30 min. To observe the internalization of APCS²⁶, seedlings expressing BRI1-GFP were treated with ES9-17 for 30 min followed by 20 μM of AFCS for 20 min. Seedlings were then washed and observed microscopically for 20 min. To follow PEPR1-GFP internalization, seedlings expressing PEPR1-GFP were treated with either DMSO or ES9-17 for 30 min and FM4-64 (2 μM) was added for a further 15 min. Seedlings were then elicited with 100 nM Pep1 for 10 s, washed with medium in the presence of ES9-17 and imaged at different time points. Imaging for AFCS uptake and PEPR1 internalization was performed with a Leica SP8 confocal laser scanning microscope with a 40 x water-immersion lens. The lifespan of endocytic foci in seedlings was measured following treatment with either ES9-17 or DMSO for 30 min as described previously¹⁴. Seedlings expressing VHA-a1-GFP and ST-mRFP were treated with or without the drug for 30 min, followed by time lapse imaging at six time points for 90 s, at 10 s intervals. Images were taken with an Olympus FV10 ASW confocal laser scanning microscope with a 60 x water-immersion lens (numerical aperture 1.2) and 3 x digital zoom.

The cytoskeletal dynamics of *Arabidopsis* root cells with and without drug treatments were performed with a PerkinElmer spinning disk microscope using a 60 x water-corrected Plan Apo (numerical aperture 1.2) objective. Time lapse series were taken for either 12 min (five time points per minute (MAP4)) or 5 min (one time point per second (Pimbrin)). Images were processed with ImageJ version 1.52 (Fiji, <https://fiji.sc/>). For the MAP4 and Pimbrin superimposed multi-color images, the background was subtracted using a rolling ball radius of 50 pixels and a walking average of four was applied to the time series. Colored projections were generated by superimposing six different time points spread evenly over the duration of the acquisition. These six time points were merged using the merge channels tool of Fiji, where the gray channel was left blank. All experiments described for Pitstop2 in *Arabidopsis* were performed as described for ES9-17. For the quantification of the cytosolic/plasma membrane signal intensity ratio, non-saturated images were converted in ImageJ to 8-bit and regions of interest were selected based on the plasma membrane or cytosol localization. Histograms listing intensity values per region of interest were generated, and the averages of the 100 most intense pixels were used for calculations. Three cells were quantified per seedling and averaged.

ATP measurements. Fluorescein diacetate and ATP measurements in 3-day-old WT PSB-D *Arabidopsis* cell cultures were performed as described previously¹⁴.

Affinity purification with biotinylated small molecules. PSB-D WT cell cultures were harvested from the medium, flash-frozen in liquid nitrogen and ground with a Retsch MM400. Cell material was weighed and extraction buffer added (50 mM Tris-HCl, pH 8, 150 mM NaCl, 0.1% NP-40 (Sigma-Aldrich) with one tablet 10 ml⁻¹ cOmplete ULTRA protease inhibitor cocktail, EDTA-free (Roche) at a ratio of 2:1 (200 μl extraction buffer for 100 mg material)). Protein concentration was determined by the Bradford method (Quick start Bradford x1 Dye reagent (Bio-Rad)). Lysate was prepared by the removal of endogenous biotin, with Streptavidin Sepharose High Performance beads (GE Healthcare), hereafter referred to as beads). Washed beads (50 μl, washed three times with extraction buffer) were applied to 1 ml lysate and incubated at 4 °C for 1 h on a rotary wheel. A second batch of beads was washed three times with extraction buffer, and biotinylated small molecules (2 μl of 50 mM stock per 50 μl beads) were added with the final wash. The mixture was left at room temperature for 15 min, the supernatant of the final wash removed and transferred to 4 °C until further use. Supernatant constituting the biotin-cleared lysate was added to beads incubated with the biotinylated small molecules. This mixture was incubated for 2 h, or overnight at 4 °C on a rotary wheel, followed by centrifugation whereafter the mixture was spun down (4 °C), the supernatant removed and beads were washed three times (50 mM Tris-HCl, pH 8, 150 mM NaCl). Appropriate amounts of the lithium dodecyl sulfate (LDS) sample buffer (4 x LDS sample buffer supplemented with x10 sample-reducing agent (Novex, Life Technologies)) were added and samples were incubated for 10 min at 70 °C, followed by centrifugation at 18,000g for 2 min. The resulting supernatant was run on 4–12% Bis-Tris protein gels with MES buffer (NuPage Novex gels and buffer from Life technologies). Gels were stained with SYPRO Ruby protein gel stain (Molecular probes, Invitrogen), and stained gel regions were excised and cut into approximately three pieces before submission to liquid chromatography–tandem mass spectrometry (LC–MS/MS) analysis.

LC–MS/MS analysis. Gel pieces containing the proteins of interest were excised and transferred to Biopure Eppendorf tubes (Eppendorf AG). After two consecutive 15 min wash steps with water/acetonitrile (1/1, v/v) (both HPLC analytical, Mallinckrodt Baker B.V.), gel pieces were dried in a centrifugal vacuum concentrator, rehydrated in 10 μl of a 0.02 μg μl⁻¹ sequencing-grade modified trypsin stock solution (Promega Corporation) and submerged in freshly prepared solution of 50 mM ammonium bicarbonate. Overnight digestion at 37 °C was stopped by acidification with trifluoroacetic acid (TFA). After centrifugation (16,000g for 5 min), the peptide mixture was removed from the gel pieces, transferred to a new Eppendorf tube, dried in a centrifugal vacuum concentrator and redissolved in 20 μl of 0.1% (w/v) TFA in water/acetonitrile (98/2, v/v) (loading solvent). Next, 10 μl of the 20 μl peptide mixtures obtained were introduced into an LC–MS/MS system through an Ultimate 3000 RSLC nano LC (ThermoFisher Scientific) in-line connected to a QExactive mass spectrometer (ThermoFisher Scientific). Samples were first loaded on an in-house-made trapping column (100 μm internal diameter, 20 mm, 5 μm beads C18 Reprosil-HD, Dr. Matsch). After flushing from the trapping column, samples were loaded on an analytical column (75 μm internal diameter x 150 mm, 5 μm beads C18 Reprosil-HD, Dr. Matsch) and packed in the needle (PicoFrit SELF/PicoTip emitter, PFP360-75-15-N-5, New Objective). Peptides were loaded with loading solvent (0.1% (v/v) TFA in water/acetonitrile, 2/98 (v/v)) and separated with a linear gradient from 98% solvent A' (0.1% (v/v) formic acid in water) to 40% solvent B' (0.1% (v/v) formic acid in water/acetonitrile, 20/80 (v/v)) for 30 min at a flow rate of 300 nl min⁻¹, followed by a 5 min wash, reaching 99% solvent B'. Two packing and two analytical columns were configured in tandem liquid chromatography mode. The mass spectrometer was operated in data-dependent, positive-ionization mode, automatically switching between MS and MS/MS acquisition for the ten most abundant peaks in a given MS spectrum. The source voltage was 3.4 kV and the capillary temperature was 275 °C. One MS1 scan (*m/z* 400–2,000, AGC target 3 x 10⁶ ions, maximum ion injection time 80 ms) acquired at a resolution of 70,000 (at 200 *m/z*) was followed by up to ten MS/MS scans (resolution 17,500 at 200 *m/z*) of the most intense ions fulfilling predefined selection criteria (AGC target 5 x 10⁴ ions, maximum ion injection time 60 ms, isolation window 2 Da, fixed first mass 140 *m/z*, spectrum data type centroid, underfill ratio 2%, intensity threshold 1.7 x E4, exclusion of unassigned, 1, 5–8, >8 charged precursors, peptide match preferred, exclude isotopes on, dynamic exclusion time 20 s). The higher-energy collisional dissociation collision energy was set at 25% normalized collision energy, and the polydimethylcyclohexane background ion at 445.120025 Da was used for internal calibration (lock mass).

From the MS/MS data in each liquid chromatography run, Mascot generic files (mgf) were created with the Mascot Distiller software (version 2.4.3.3, Matrix Science). These peak lists were searched with the Mascot search engine and the Mascot Daemon interface (version 2.4, Matrix Science). Spectra were searched against the TAIR10 database. Variable modifications were set to pyroglutamate formation of amino-terminal glutamine, acetylation of the protein N-terminus, methionine oxidation and propanamide cysteine formation. Mass tolerance on precursor ions was set to ±10 ppm (with the Mascot C13 option set at 1), and on fragment ions to 20 millimass unit. The instrument setting was on ESI-QUAD. The enzyme was set to trypsin/P, allowing one missed cleavage, whereas cleavage was allowed also when lysine or arginine was followed by proline. Only peptides that

were ranked first and scored above the threshold score, set at 99% confidence, were withheld. All data were managed by *ms_limms* and analyzed with R (<http://www.R-project.org>) embedded in KNIME. The data were filtered by removing all peptides smaller than eight amino acids, and only those proteins containing at least two peptides in one of the experiments were used for data analysis.

CETSA. The protocol used is based on a previously published procedure⁴⁹ with minor adjustments. WT or transgenic *Arabidopsis* PSB-D cell cultures were harvested, flash-frozen in liquid nitrogen and ground with a Retsch MM400. Cell material was added at a ratio of 2:1 in extraction buffer (50 mM Tris-HCl, pH 7.6, 150 mM NaCl, 0.1% NP-40 with one tablet 10 ml⁻¹ cComplete ULTRA protease inhibitor cocktail, EDTA-free (Roche)). Samples were thawed on ice for 15 min followed by centrifugation for 30 min (18,000 g at 4 °C). Lysates were pooled per cell type, and protein concentration was determined by the Bradford method (Quick start Bradford ×1 Dye reagent (Bio-Rad)). Lysates were incubated with small molecules/DMSO for 30 min at room temperature on a rotary wheel, then aliquoted in 60 µl fractions in PCR tubes, treated for 2 min at 12 temperature points (30, 35, 40, 42, 44, 46, 48, 50, 52, 55, 60 and 65 °C) in a Bio-Rad thermal cycler, allowed to cool and centrifuged (18,000 g) for 30 min at 4 °C. The supernatant (50 µl) was processed for standard immunoblot analysis for protein detection. All antibodies were diluted in Tris buffered saline with Tween and 5% (w/v) skimmed milk. Anti-CHC (1:3,000, AS10 690 Agrisera) and anti-ATP-β (1:4,000, AS05085 Agrisera) were detected with horseradish peroxidase (HRP)-linked anti-rabbit IgG (1:10,000, GE Healthcare), anti-tubulin (1:15,000) with HRP-linked anti-mouse IgG (1:10,000, GE Healthcare), anti-TPLATE (1:1,000, custom-made BIOTEM, France) and HA with anti-HA-HRP (1:4,000, Abcam). Blots were developed with Western Lightning Plus-ECL, Enhanced Chemiluminescence Substrate (PerkinElmer) and imaged with a Bio-Rad ChemiDoc XRS+ molecular imager. Band intensities were measured with the Bio-Rad Image Lab software package (version 6.0.0 Build 25).

DARTS. The DARTS protocol was adopted as previously described^{51,52}. Lysates were prepared as described for CETSA, and were incubated with either ES9-17 or DMSO for 30 min at room temperature. After incubation, lysates were split into equal aliquots for pronase (Roche, No. 10165921001) digestion. Pronases were diluted from a 10 mg ml⁻¹ stock solution in distilled water. The 1:100 starting dilution of pronase was obtained by dissolving 12.5 µl pronase stock solution in 87.5 µl 1× tenascin-C buffer (500 mM Tris-HCl, pH 8, 500 mM NaCl, 100 mM CaCl₂, 10× stock) and was used for all subsequent dilutions, which were prepared with 1× tenascin-C buffer. Digestion (30 min) was started with 1 min intervals and stopped by the addition of the sample buffer at ×1 final concentration (4× LDS sample buffer with 10× sample-reducing agent; Novex, Life Technologies) in the same sequence as the digestion that had been started. Immunoblotting, protein detection and quantification were performed as described for CETSA. Anti-γ-COP (anti-Sec21p) (1:1,000, AS08327, Agrisera) was detected with anti-rabbit IgG and HRP-linked antibody (1:10,000, GE Healthcare).

Molecular docking. Water and all ligands of the human clathrin nTD crystal structure pdb-entry 4G55 in complex with Pttstop2 (ref. 7) were manually deleted from the pdb-text file. The emptied structure was locally minimized with GROMOS96 (43B1 parameter set)⁵³ implemented within the Swiss-PdbViewer⁵⁴, and polar hydrogens were added. The S9 ligand was drawn three-dimensionally with Avogadro version 1.1.1 (ref. 55) and was minimized with the MMFF94s force field⁵⁶. AutoDockTools version 1.5.4 suite⁵⁷ was used for pdbqt-format preparations of proteins and ligands. Dockings were done with AutoDock-Vina version 1.1.0 (ref. 58) with exhaustiveness set at 64; residues Arg64, Phe91 and Gln89 were set as flexible. The grid-box size was $x=20$, $y=22$ and $z=20$ Å, centered at $x=50.0$, $y=-10.2$ and $z=24.5$. PyMOL (Molecular Graphics System, version 1.7, Schrödinger, LLC) was used for visualization.

Cloning, expression and purification of human nTD CHC1 and *Arabidopsis* nTD CHC1/2. *Arabidopsis* nTD CHC1 (AT3G11130, residues 1–377), CHC2 (AT3G08530, residues 1–378) and human nTD CHC1 (Q00610, residues 1–363) were synthesized and cloned into the pGEX4T-1 vector and transformed into competent *Escherichia coli* BL21 (DE3) cells. Transformed cells were cultured in Luria-Bertani medium supplemented with carbenicillin (100 µg ml⁻¹) at 37 °C to an optical density of 0.6, and expression was induced with 1 mM isopropyl-1-β-D-thio-β-galactopyranoside. Cell cultures were maintained for 4 h at 37 °C. Next, cells were harvested by centrifugation at 6,000 g, resuspended in lysis buffer (10 mM Tris-HCl, pH 8.3, 500 mM NaCl, 10% (w/v) glycerol and 5 mM dithiothreitol) supplemented with protease inhibitors (Roche) and lysed by sonication. The proteins were purified by affinity purification using a GSTrap FF 1 ml column. The column was equilibrated with equilibration buffer (10 mM sodium phosphate buffer, 150 mM NaCl, pH 7.5) and the sample applied to the GSTrap column. The column was subsequently washed with equilibration buffer and the bound protein was eluted with the elution buffer (10 mM NaH₂PO₄, 150 mM NaCl, 10 mM reduced glutathione, pH 7.5) and collected in 1 ml aliquots. The glutathione-S-transferase (GST) tag was cleaved by overnight thrombin digest at 20 °C, and the sample was applied to a GSTrap column to remove the cleaved GST and uncleaved GST-CHC.

Flow-through was collected and further polished by size exclusion chromatography with a SD75 16/600 column (GE Healthcare) equilibrated with HEPES buffered saline (20 mM HEPES, pH 7.4, 150 mM NaCl). Protein concentration at absorbance 280 (A_{280}) was measured with a Nanodrop 1000 (ThermoFisher Scientific) and aliquots at a concentration of 2 mg ml⁻¹ were stored at –80 °C.

X-ray data collection. Purification and crystallization of nTD were performed as previously described⁵. X-ray data were collected at beamline BL14.2 at BESSY-II (Berlin, Germany) and processed in the X-ray spectrometer detector system and Xscale⁵⁹. Data collection statistics are shown in Supplementary Table 3. The phase problem was solved by molecular replacement with Phaser⁶⁰ using the 1.7 Å structure of nTD (PDB ID code 4G55) as a model. All water molecules and ligand atoms were omitted from the starting model. Refinement to 1.6 Å resolution was performed in PHENIX⁶¹. The structure file of ES9 was generated using the Dundee PRODRG2 server⁶² and manually fitted to the electron density. All structural figures were produced with PyMOL (Molecular Graphics System, version 1.7, Schrödinger, LLC)⁶³. The data were deposited in the Protein Data Bank (PDB), www.rcsb.org (PDB ID code 6E4L).

Differential scanning fluorimetry assay. For the differential scanning fluorimetry assay, the Light cycler 480, Real-time PCR system (Roche) was used as described previously⁶⁴. The nTD of human CHC1 and *Arabidopsis* CHC1 and CHC2 was diluted in a buffer containing 20 mM HEPES, pH 7.4 and 150 mM NaCl. Each well of a 96-well microplate contained 1.6 µM protein, 5× Sypro Orange (Invitrogen) and 2.5 µl of compound and buffer up to a total volume of 25 µl. Thermal scanning from 10 to 95 °C at 1.5 °C min⁻¹ was done with a real-time PCR set-up and the fluorescence intensity was measured every 10 s. The software Light cycler 480Sw 1.5.1 was utilized for calculation of melting temperature.

Transferrin uptake in HeLa cell cultures. Maintenance and imaging of HeLa cells for transferrin uptake was performed as described previously⁶.

Cell viability assay. For the WST-1 assay, HeLa cells were grown in a 96-well plate and incubated with the compounds for 30 min, followed by the addition of 10 µl WST-1 reagent (Sigma-Aldrich) to 100 µl of medium. Absorbance was measured at 450 nm versus that at the 690 nm reference by means of a plate reader.

Root growth assay. Seeds were sown on 0.5× MS solid medium, stratified for 2 days at 4 °C in the dark and placed vertically in the light. Five days after germination, seedlings were transferred to solid 0.5× MS medium without sucrose supplemented with 100 mM *D*-sorbitol with either ES9-17 or DMSO for 2 days, whereafter the plates were scanned and root growth was measured. Scanned images were processed and evaluated with ImageJ. Fold changes in root growth were measured as a ratio of root length at the start of treatment with either ES9-17 or DMSO to the root length at the end of treatment.

TEM. Five-day-old *A. thaliana* Col-0 seedlings, grown on solid 0.5× MS medium, were immersed in liquid 0.5× MS supplemented with either DMSO or ES9-17 for 30 min. Root tips were excised, immersed in 20% (w/v) BSA and frozen in a high-pressure freezer (Leica EM ICE, Leica Microsystems). Freeze substitution was performed with a Leica EM AFS (Leica Microsystems) in dry acetone containing 1% (w/v) OsO₄ and 0.5% glutaraldehyde for 4 days as follows: –90 °C for 54 h, 2 °C h⁻¹ increase for 15 h, –60 °C for 8 h, 2 °C h⁻¹ increase for 15 h and –30 °C for 8 h. Samples were slowly warmed to 4 °C, rinsed three times with acetone for 20 min each, infiltrated over 3 days at 4 °C in Spurr's resin and embedded in capsules. Samples were polymerized at 70 °C for 16 h. Ultra-thin sections were made using an ultra-microtome (Leica EM UC6) and post-stained in Leica EM AC20 for 40 min in uranyl acetate at 20 °C and for 10 min in lead stain at 20 °C. Sections were collected on formvar-coated copper slot grids. Grids were viewed with a JEM 1400plus transmission electron microscope (JEOL) operating at 60 kV.

Statistical tests and generation of graphs. Statistical tests and graphs, except boxplots, were generated with Graphpad Prism 6, version 8.0.1. Dose-response curves with a log-transformed x axis were generated using nonlinear regression with a log(inhibitor) versus response model, and setting a variable slope (four parameters) and top and bottom constraints to 1 and 0, respectively. Other dose-response and CETSA curves were generated with Boltzmann sigmoid equation with top and bottom constraints set to 1 and 0, respectively, where applicable. Boxplots were generated with the online tool BoxPlotR (<http://boxplot.tyreslab.com/>) from the Tyers and Rappsilber laboratories.

Reporting Summary. Further information on research design is available in the Nature Research Reporting Summary linked to this article.

Data availability

All accession codes supporting the findings of this study are available within the paper and its Supplementary Information. Structures are accessible under the PDB code 6E4L. There is no restriction on data availability.

References

39. Helsen, K. et al. *ms_lims*, a simple yet powerful open source laboratory information management system for MS-driven proteomics. *Proteomics* **10**, 1261–1264 (2010).
40. Scott, W. R. P. et al. The GROMOS biomolecular simulation program package. *J. Phys. Chem.* **103**, 3596–3607 (1999).
41. Guex, N. & Peitsch, M. C. SWISS-MODEL and the Swiss-Pdb Viewer: an environment for comparative protein modeling. *Electrophoresis* **18**, 2714–2723 (1997).
42. Hanwell, M. D. et al. Avogadro: an advanced semantic chemical editor, visualization, and analysis platform. *J. Cheminform.* **4**, 17 (2012).
43. Halgren, T. A. & MMFF, V. I. MMFF94s option for energy minimization studies. *J. Comput. Chem.* **20**, 720–729 (1999).
44. Sanner, M. F. Python: a programming language for software integration and development. *J. Mol. Graph. Model.* **17**, 57–61 (1999).
45. Troiti, O. & Olson, A. J. AutoDock Vina: improving the speed and accuracy of docking with a new scoring function, efficient optimization and multithreading. *J. Comput. Chem.* **31**, 455–461 (2010).
46. Kabsch, W. XDS. *Acta Crystallogr. D* **66**, 125–132 (2010).
47. McCoy, A. J. et al. Phaser crystallographic software. *J. Appl. Crystallogr.* **40**, 658–674 (2007).
48. Adams, P. D. et al. PHENIX: a comprehensive Python-based system for macromolecular structure solution. *Acta Crystallogr. D* **66**, 213–221 (2010).
49. Schüttelkopf, A. W. & van Aalten, D. M. PRODRG: a tool for high-throughput crystallography of protein-ligand complexes. *Acta Crystallogr. D* **60**, 1355–1363 (2004).
50. Huynh, K. & Parich, C. L. Analysis of protein stability and ligand interactions by thermal shift assay. *Curr. Protoc. Protein Sci.* **79**, 28.9.1–28.9.14 (2015).